Investigation into Peroxiredoxin and interactions in the Peroxiredoxin peroxide scavenging system

Submitted by

Paul Brian Charles James

to the University of Exeter as a thesis for the degree of Doctor of Philosophy in Biological Sciences

(September 2010)

I certify that all material in this thesis which is not my own work has been identified and that no material has previously been submitted and approved for the award of a degree by this or any other University.

Paul James

Abstract

Peroxiredoxins are a family of multifunctional enzymes that are able to protect the cell against oxidative stress. Peroxiredoxins form part of a recently discovered peroxide scavenging system along with thioredoxin, thioredoxin reductase and sulfiredoxin.

This study describes the purification of a recombinant human peroxiredoxin II from human erythrocytes. The original recombinant clone contained a point mutation at the fourth residue from glycine to valine and a number of problems were encountered with aggregation during purification. Reverting back to the original amino acid sequence allowed the protein to be purified and concentrated without aggregation, as well as leading to over-expression in the same oligomeric state as the native sample from blood.

This study also describes the over-expression and purification of the human peroxiredoxin II protein in the intermolecular disulfide form as well as the subsequent crystallisation and X-ray diffraction studies. The crystal structure for this form of the protein was obtained to 3.3 Å resolution revealing the peroxiredoxin to be in the decameric form. In addition conformational changes in the protein that are necessary for formation of the intermolecular disulfide between the peroxidatic (Cys52) and resolving cysteine (Cys172) have been observed. The structure also revealed that these movements did not interfere with the dimer:dimer interface as had been previously suggested. This then allows the disulfide to be seen within the decameric form of peroxiredoxin.

The production of covalent complexes formed between peroxiredoxin and sulfiredoxin, and peroxiredoxin and thioredoxin was also investigated. Complexes were stabilised by using DTNB to form a covalent bond between specific cysteine residues. The complex binding results from size exclusion chromatography showed that decameric peroxiredoxin bound to sulfiredoxin in a 1:5 ratio and decameric peroxiredoxin bound to thioredoxin in a 1:10 ratio.

Cloning, over-expression and purification of the selenocysteine containing enzyme thioredoxin reductase was achieved. A minimal selenocysteine insertion sequence was added to the 3’ end of the DNA sequence to drive selenocysteine insertion in place of the typical stop UGA codon. The activity of

this protein was found to be low but was greatly increased when co-expressed with a plasmid containing the *selA*, *selB* and *selC* genes. Although the activity of this co-expressed thioredoxin reductase was ~20% of the native enzyme activity, it was comparable to the activity of other recombinant forms of the enzyme.

These studies report the purification of all of the proteins necessary to reform the peroxiredoxin system and allow the production of a working assay for peroxiredoxin activity. Together with the first report for a structure of a decameric disulfide form of human peroxiredoxin II a greater insight into the peroxiredoxin system has been obtained.

Acknowledgements

I would like to thank Prof. Jenny Littlechild for all her support and encouragement throughout this PhD and my scientific career to date. I am very grateful to Dr. Michail Isupov for his help and advice with the crystallography performed in this work. I am also very grateful to Dr Kirsty Line for her continued support and patience throughout this project. I would also like to thank Dr. Andrew Shaw and Dr Robert Parker for their help with the SPR. I would also like to thank Prof. Willison and Heather Rada for giving me the chance to look at the interaction with PDCL3.

I would like to thank everybody from the Biocatalysis Centre both past and present that have helped me throughout this project. Especially Kirsty, Carrie, Anne Marie and Chris who were always available for scientific discussion or an extended tea into lunch break.

I would like to thank my family for their continued love and support. Finally I would like to thank Lizzy and Hannah for all their support and for always being on hand for a glass of wine, or a gin.

Abbreviations

3D	3-dimensional
APS	Ammonium persulfate
ATP	Adenosine triphosphate
BAM	Benzamidine
BASI	barley α-amylase/subtilisin inhibitor
BE	Adherent human colon carcinoma cells
CCP4	Collaborative computational project, number 4
DNA	Deoxyribonucleic acid
DTNB	5,5'-dithiobis-(2-nitrobenzoic acid)
DTT	Dithiothreitol
EC	Enzyme commission
EDC	1-Ethyl-3-[3-dimethylaminopropyl]carbodiimide
EDTA	Ethylenediaminetetraacetic acid
EM	Electron microscopy
ESI-MS	Electrospray ionization mass spectrometry
FAD	Flavin adenine dinucleotide
FFQ	Fast flow Q Sepharose
GF	Gel filtration
HEPES	N-(2-Hydroxyethyl)piperazine-N'-(2-ethanesulfonic acid)
His-tag	Poly histidine tag
IPTG	Isopropyl-1-thio-β-D-galactopyranoside
LB	Luria-Bertani
LDAO	Lauryldimethylamineoxide
MAD	Multiple-wavelength anomalous diffraction
MWCO	Molecular weight cut off
NADPH	Nicotinamide adenine dinucleotide phosphate
NHS	N-hydrocysulfosuccinimide
OD	Optical density
PAGE	Polyacrylamide gel electrophoresis
PCR	Polymerase chain reaction
PDB	Protein data bank
PEG	Polyethylene glycol

PLP2	Yeast phosducin-like protein 2
PMSF	Phenylmethanesulfonylfluoride
Prx	Peroxiredoxin
RMS	Root mean square
ROS	Reactive oxygen species
SAD	Single-wavelength anomalous diffraction
SAXS	Small angle X-ray scattering
SDS	Sodium dodecyl sulfate
SECIS	Selenocysteine insertion sequence
SLIM	Site-directed ligase independent mutagenesis
SOD	Superoxide dismutase
SPR	Surface plasmon resonance
Srx	Sulfiredoxin
TCEP	Tris(2-carboxyethyl)phosphine
TEMED	N,N,N',N'-Tetramethyl-1-,2-diaminomethane
T_M	Melting temperature
TNB	5-thiobis-(2-nitrobenzoic acid)
Tris-HCl	Tris (hydroxymethyl) aminomethane
Trx	Thioredoxin
TrxR	Thioredoxin reductase
UV	Ultraviolet

Table of Contents

List of Figures

List of Tables

List of Equations

1. Introduction

1.1. Reactive oxygen species

Reactive oxygen species (ROS) are products of normal metabolism and can be beneficial or harmful to cells and tissues depending on their concentration. In 1954 an idea was put forward that oxygen may be toxic to cells and that partially reduced forms of oxygen were responsible for this toxicity (Gerschman *et al*., 1954). The next breakthrough in the identification of ROS occurred when a weak electron paramagnetic resonance signal was attributed to the presence of oxygen free radicals in a number of lyophilized biological materials (Commoner *et al*., 1954). The next major leap forward came in the discovery of the antioxidant enzyme superoxide dismutase (SOD) which provided conclusive evidence for the presence and importance of the ROS in biological systems (McCord and Fridovich, 1969).

This research has lead to a huge number of papers that have shown biological systems are not only able to coexist with ROS but use them to their advantage for a number of biological processes. Reactive oxygen species are molecules containing oxygen that are highly reactive due to the presence of unpaired valence shell electrons that are highly reactive (Halliwell and Cross, 1994). The ROS can be split into two groups, the first is the O_2-derived free radicals, superoxide anion ($O_2^{\bullet -}$), hydroxyl ($HO^{\bullet}$), peroxyl ($RO_2^{\bullet}$) and alkoxyl ($RO^{\bullet}$) radicals. The second group are the O_2-derived non-radical species such as hydrogen peroxide (H_2O_2) (Halliwell and Cross, 1994).

ROS species can have beneficial effects on biological systems usually in low concentrations as they can take part in the cellular signalling and in the defence response to infectious agents (Valko *et al*., 2006). The harmful effects of ROS are discussed in much further detail throughout this introduction.

1.1.1. Superoxide anion

The superoxide anion ($O_2^{\bullet -}$) is generated by the reduction of molecular oxygen (O_2). A one electron addition to molecular oxygen is used to create this free radical species (equation 1.1) (Raha and Robinson, 2000). Although being a free radical the species is thought to be relatively unreactive as it is unable to penetrate lipid membranes and so is localized to the place in which it was produced. The superoxide anion is mainly produced in mammals in the

mitochondrial electron transport chain. The main locations of this in the mitochondria are at complex I, where superoxide is generated in the matrix, and complex III, where it is produced on both sides of the inner membrane (St-Pierre *et al*., 2002).

$O_2 + e^- \rightarrow O_2\bullet^-$

Equation 1.1. The formation of the superoxide anion by a one electron addition to molecular oxygen.

The major enzyme involved in the reduction of the superoxide anion is SOD. This enzyme catalyses the disproportionation of the superoxide anion to hydrogen peroxide and oxygen (equation 1.2).

$2\ O_2\bullet^- + 2H^+ \rightarrow H_2O_2 + O_2$

Equation 1.2. The formation of hydrogen peroxide from the superoxide anion using hydrogen ions.

1.1.2. Hydrogen peroxide

The major source of hydrogen peroxide in the cell is the dismutation of superoxide (equation 1.2). The major source of the latter is the electron transport chains and the nicotinamide adenine dinucleotide phosphate (NADPH) oxidases. Hydrogen peroxide is thought to be much more reactive than the superoxide anion because of its ability to move through biological membranes. Although hydrogen peroxide is thought to pass freely across biological membranes this movement is regulated by the lipid and protein composition of the membranes, as well as the presence of hydrogen peroxide carriers such as aquaporins (Bienert *et al*., 2007). Although it is not a radical species it does play a large role in radical formation, reacting to more reactive ROS such as the hypochlorous acid (HOCl) and the hydroxyl radical (HO•). H_2O_2 is known to be removed by at least three antioxidant systems; catalases (Alfonso-Prieto *et al*., 2009), glutathione peroxidases (Battin and Brumaghim, 2009) and the peroxiredoxins (Chae *et al*., 1999). Hydrogen peroxide is a very good electrophile and participates in substitution reactions.

1.1.3. Hydrogen peroxide redox signaling

Hydrogen peroxide is able to modify specific and important amino acid residues. These modifications are usually reversible and form the basis of their redox

signaling abilities. The redox signaling either occurs by the direct modification of amino acid residues or indirectly through the products of their reactions blocking important residues that will inhibit the protein function (Salemeen *et al*., 2003; van Montfort *et al*., 2003). Hydrogen peroxide has also been shown to induce conformational changes in target proteins that can also affect protein function (Storz *et al*., 1990).

1.1.4. The hydroxyl radical

The hydroxyl radical is thought to be the most reactive and therefore the most damaging of all the ROS. The hydroxyl radical is produced by the reduction of the hydrogen peroxide molecule which is catalyzed by the presence of metal ions such as iron (Fe^{2+}) and copper (Cu^{+}) in a reaction known as the Fenton reaction (equation 1.3) (Winterbourn, 1995).

$$H_2O_2 + Fe^{2+}/\ Cu^{+} \rightarrow HO\bullet + HO^{-} + Fe^{3+}/\ Cu^{2+}$$

Equation 1.3. The Fenton reaction. Hydrogen peroxide undergoes a redox reaction producing a hydroxyl anion and a hydroxyl free radical in the presence of a metal catalyst.

1.1.5. Sites of production of reactive oxygen species

Within the eukaryotic cell there are a number of different producers of reactive oxygen species with one of the major producers being the mitochondria. Of the total O_2 consumed by mitochondria 2% is converted to reactive oxygen species (Turrens, 2003). It is also the most common site for the dismutase of the superoxide anion and the breakdown of hydrogen peroxide in the Fenton reaction. Peroxisomes form the major source of cytosolic hydrogen peroxide. Peroxisomes are a single membrane organelle present in eukaryotic cells that play a major role in lipid metabolism and the metabolism of many other organic substrates (Wanders *et al*., 2010).

1.1.6. The human erythrocyte

Erythrocytes, or red blood cells, are the major means of transport for O_2 in the body, which they take up from the lungs and deliver while moving through capillaries (Engelhardt and Arnold, 1975). Erythrocytes are thought to be exposed to oxidative stress from a wide range of different sources. Erythrocytes are shown to possess large amounts of O_2 and haemoglobin as part of their function both of which are producers of the reactive oxygen species O_2^{-} and

H_2O_2 (Halliwell and Gutteridge, 1999 ; Alayash *et al*., 2001). Erythrocytes have a 120 day life span and are unable to produce new protein so they require an excellent antioxidant pathway to detoxify ROS before any damage can occur to the proteins contained within.

1.2. Antioxidant enzymes

Cells have developed a number of interacting enzyme networks for the detoxification of reactive oxygen species. The first reactive oxygen species metabolizing enzyme that was discovered was the previously discussed two metal-containing SOD (Dougherty *et al*., 1978). This enzyme is able to react two molecules of the superoxide anion together with two hydrogen ions converting them into molecular oxygen and hydrogen peroxide (Liochev and Fridovich, 2010) (equation 1.4).

Catalase, another antioxidant enzyme, contains a heme group and will catalyze the dismutation of hydrogen peroxide to water and molecular oxygen (Deisseroth and Dounce, 1970) (equation 1.5). Catalase can also remove other toxins by oxidising them along with hydrogen peroxide (equation 1.6).

$2H_2O_2 \rightarrow 2H_2O + O_2$

Equation 1.4. The dismutation of H_2O_2 to water and molecular oxygen.

$H_2O_2 + RH_2 \rightarrow R + 2H_2O$

Equation 1.5. The oxidation of toxins in a coupled reduction with hydrogen peroxide.

Glutathione peroxidases (GPx) are selenocysteine containing enzymes that have been found to detoxify organic hydroperoxides by their conversion to alcohols while forming a glutathione disulfide (equation 1.7) (Epp *et al*., 1983).

$ROOH + 2GSH \rightarrow ROH + GSSG + H_2O$

Equation 1.6. The conversion of hydroperoxides to alcohols using GPx

The system that this study focuses on is the peroxiredoxin system. The peroxiredoxin system contains a number of enzymes that interact to reduce peroxide substrates using redox active cysteine residues (Hofmann *et al*., 2002).

1.3. Oxidative stress

Oxidative stress arises from an imbalance between the reactive oxygen species mentioned and the systems in the cell designed to detoxify them. If the mechanism by which reactive oxygen species are removed break down then this can leave them available to attack and damage all the major groups of biomolecules (DNA, lipids and proteins).

Reactive oxygen species have been shown to have a number of different chemical modification affects on DNA such as DNA cleavage, protein-DNA cross links and the oxidation of purines (Marnett, 2000). If these alterations occur and the DNA repair proteins are not able to correct them this could lead to incorrect base pairing and the replication of “faulty” DNA. This has been identified as potentially one of the reasons why individuals that have a high exposure to oxidative stress show higher rates of cancer (Mates *et al*., 1999; Klaunig *et al*., 2010). Lipids are susceptible to peroxidation as their polyunsaturated fatty acid structures contain a number of double bonds that are highly reactive with free radicals (Niki, 2009). Proteins are also highly susceptible to reactive oxygen species attack, which often leaves them modified with the effects being anything from partial structural changes leaving the protein less active, to complete denaturation (Butterfield *et al*., 1998).

Oxidative stress is thought to play a role in the process of ageing (McArdle and Jackson, 2000) and in the process of diseases such as Alzheimers (Bonda *et al*., 2010), Parkinsons (Zhou *et al*., 2008), arthritis (Mapp *et al*., 1995), diabetes (Baynes and Thorpe, 1999) and multiple sclerosis (Gilgun-Sherki *et al*., 2004).

1.4. The biological redox chemistry of cysteine

Cysteine (Cys, C) is an amino acid that contains a side chain thiol (SH) group (figure 1.1). Cysteine can play an important role in the folding (and therefore structure) and stability of some proteins through the formation of disulfide bonds.

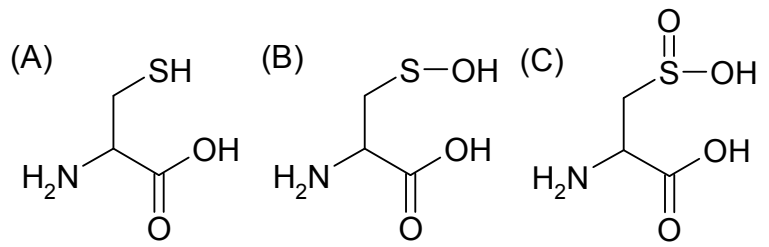

Figure 1.1. The chemical structure of the amino acid cysteine in the thiol (A), sulfenic acid (B) and sulfinic acid form (C).

The thiol group is important in the detection of hydrogen peroxide. The rate of reaction between the protein thiol group and hydrogen peroxide is very important in redox signalling. The two most important factors in the reactivity of the thiol group is the ability of the cysteine residue to be deprotonated to the thiolate anion (equation 1.8) and how accessible this thiol group is.

$$\text{Protein-S-H} \rightleftharpoons \text{Protein-S}^- + \text{H}^+$$

Equation 1.7. Deprotonation of a cysteine residue to form the thiolate group.

The cysteine residue thiol group is nucleophilic and has a p*K*a of 8.5. This p*K*a is close to neutral in the cell and so the thiol group is often seen in its reactive thiolate (S^-) form which is highly nucleophilic (Bulaj *et al*., 1998). The reactivity of the thiol group is highly linked to pH which shows the importance of the thiolate form in the reactivity of the cysteine residue (Jocelyn, 1972).

The structural environment in which the thiol group is located can also play a large role in the reactivity of the group (Friedman, 1973) as the environment will usually provide a positively charged residue to stabilize the negative charge on the thiol group. The structural environment will also play a large role in the accessibility of the thiolate anion.

As well as the thiol there are three other species involving the sulfur atom of the cysteine side chain that are of interest in this project, these are the sulfenic acid (R-SOH), sulfinic acid (R-S(O)OH) and the disulfide form (R-S-S-R). There is a switch in the oxidation state of sulfur between the thiol (-2), sulfenic acid (0) and sulfinic acid (+2) states.

1.4.1. Reaction of thiol with hydrogen peroxide

As discussed before the reaction of the thiol group usually proceeds through the thiolate ion produced depending on the environment of the cysteine residue. This thiolate ion is a highly reactive nucleophile and its oxidation reaction with hydrogen peroxide (H_2O_2) produces a sulfenic acid as well as a molecule of water (Jacob *et al*., 2004). Thiolate ion formation is not the only prerequisite for the reaction with H_2O_2; it was discovered by studying the rates of different thiol containing enzymes (Stone, 2004) that the reaction also requires residues around the active site cysteine that are able to stabilize the reaction intermediate (Tosatto *et al*., 2008).

$$\text{Protein-S}^- + H_2O_2 + H^+ \rightarrow \text{Protein-SOH} + H_2O$$

Equation 1.8. The oxidation reaction of a thiolate ion with H_2O_2 forming water and a sulfenic acid group.

1.4.2. Forming the disulfide state

Sulfenic acid is thought to be an unstable and highly reactive species that is heavily involved in redox signaling (Poole *et al*., 2004). If present with another thiol group the sulfenic acid form usually undergoes a rapid reaction forming a disulfide bond and a molecule of water (equation 1.9) (Allison, 1976).

$$\text{Protein-SOH} + \text{Protein'-SH} \rightarrow \text{Protein-S-S-Protein'} + H_2O$$

Equation 1.9. The reaction of the sulfenic acid with a thiol forming a disulfide bond and a molecule of water.

1.4.3. Forming the sulfinic acid state

It has been noted that the sulfenic acid form can be reduced back to the thiol form if treated with a reducing agent, but a delay in this treatment can cause the oxidation to become irreversible suggesting a switch from the sulfenic to the sulfinic acid form (equation 1.10) (Little and O'Brien, 1969).

$$\text{Protein-SOH} + H_2O_2 \rightarrow \text{Protein-S(O)OH} + H_2O$$

Equation 1.10. The hyper-oxidation reaction of the sulfenic acid with a molecule of H_2O_2 forming the sulfinic acid and a molecule of water.

1.5. Peroxiredoxin

Peroxiredoxins (Prxs) are a family of multi-functional enzymes that protect against oxidative stress (Hofmann *et al*., 2002). Prxs are antioxidant enzymes that use the redox active cysteine residues to reduce an O-O bond present in hydrogen peroxide and a range of organic hydroperoxides (ROOH) (Peshenko and Shichi, 2001. Prxs are located mainly in the cytosol but have also been found in mitochondria, chloroplasts and peroxisomes (Hofmann *et al*., 2002). This is expected as these are also the major sites of reactive oxygen species production. Prxs can be produced at very high levels and are found to be the third most abundant protein in erythrocytes (Moore *et al*., 1991), and in the top ten most produced proteins in *Escherichia coli (E. coli)* (Link *et al*., 1997). The protein is also thought to form between 0.1 and 0.8% of the total soluble protein in other types of mammalian cells (Chae *et al*., 1999).

The Prxs are a ubiquitous family of enzymes that have been identified in yeast (Morgan and Veal, 2007), plant (Dietz, 2003) and animal cells (Miranda-Vizuete *et al*., 2000) as well as in bacteria and archaea (Dubbs and Mongkolsuk, 2007) and have been seen to have increased levels of expression under oxidative stress conditions (Halliwell, 1999).

Prxs are split into two categories, the 1-Cys and 2-Cys Prx, based upon the number of redox active cysteines they possess. With further structural and mechanistic data available the 2-Cys Prx were then further split into two sub-classes, the typical and atypical 2-Cys Prx. The typical 2-Cys Prx are homodimers than contain two identical active sites (Hirotsu *et al*., 1999a; Schroder *et al*., 2000; Alphey *et al*., 2000). The atypical 2-Cys Prx are thought to behave in the same way but are functionally monomeric with the redox active cysteines located on the same protein (Seo *et al*., 2000). It is thought that all of the different classes of Prx have the same first step in the mechanism and it is the recycling of the oxidized sulfenic acid form back to the reduced thiol state that differs.

The peroxiredoxin system is a system of enzymes made up of Prx, thioredoxin, thioredoxin reductase and sulfiredoxin all of which will be talked about in this introduction. There have been six different sub forms of Prx (PrxI – VI) discovered in mammals. PrxI – IV are all typical 2-Cys Prx, PrxV is an atypical

2-Cys Prx and PrxVI is a 1-Cys Prx. The different sub forms of Prx differ in length (ranging from 198 – 271 amino acids), cellular location and the location on the human chromosome (Wood *et al*., 2003b). Prx I, II, III and V are reduced solely by thioredoxin (coupled with thioredoxin reductase and NADPH), Prx IV is able to use thioredoxin and glutathione where as Prx VI is only able to use glutathione.

Prxs have been shown to have catalytic efficiencies of ~10^7 M^{-1} s^{-1} (Akerman and Muller, 2005). This catalytic efficiency is comparable to those of catalase, heme peroxidase and selenium-containing glutathione reductase (Wood *et al*., 2003b).

1.5.1. Peroxiredoxin II from human erythrocytes

Peroxiredoxin II from human erythrocytes (hPrxII) (EC 1.11.1.15) was previously known as thioredoxin peroxidase B, natural killer enhancing factor-B (Shau *et al*., 1994)), thioredoxin-linked peroxidase (Cha and Kim, 1995) and is known to be the same as calpromotin (Moore *et al*., 1991) and torin (Harris and Naeem, 1981). The gene encoding PrxII is located on chromosome 19 (19p13.2).

hPrxII protein consists of 198 residues with a molecular weight of ~22 kDa (Moore and Shriver, 1994). hPrxII has been found to be the third most abundant protein in the erythrocytes and has a cellular concentration of ~5.5 mg/ml (Moore *et al*., 1991). hPrxII is a typical 2-Cys Prx containing two redox active cysteines. hPrxII is a functionally dimeric protein with the peroxidatic cysteine (Cys_P) and the resolving cysteine (Cys_R) being presented to the active site by different chains of the dimer (Schroder *et al*., 2000).

The PrxII has a wide range of different functions such as the reduction of hydrogen peroxide (Peskin *et al*., 2007) and its ability to act as a molecular chaperone. It also has a wide range of functions specific to the erythrocyte. The protein is able to activate the Gardos channels in the erythrocytes that help to increase the K^+ efflux from the red blood cell (Moore *et al*., 1991). The protein is also known to be an inhibitor of platelet-derived growth factor signalling (Lee *et al*., 2007).

hPrxII is thought to exist mainly in the reduced state under native conditions due to the reductive environment within the erythrocyte. hPrxII is shown to have a

high sensitivity to H_2O_2 and is shown to result in formation of the disulfide intermediate (Low *et al*., 2007). It is believed that the recycling of the disulfide intermediate is relatively slow in the erythrocyte due to the relatively low amounts of thioredoxin reductase present which can lead to the accumulation of disulfide hPrxII. PrxII is thought to be very important in the protection of the erythrocyte from H_2O_2 produced by haemoglobin as mice deficient in PrxII suffer from hemolytic anaemia (Low *et al*., 2008) whereas mice deficient in catalase or glutathione peroxidase do not (Johnson *et al*., 2000; Ho *et al*., 2004).

1.5.1.1. The structure of hPrxII

The crystal structure of the decameric hPrxII was solved to a resolution of 1.7 Å at the University of Exeter (Schroder *et al*., 2000).The monomeric structure can be split into two domains. Domain I (residues 2-169) consists of five α helices, two 3_{10} helices and an extended seven-stranded β sheet. The second domain is the C-terminal arm (residues 170-198) and is made up of one α helix. hPrxII contains a thioredoxin fold which consists of four β strands (β3, β4, β6 and β7) and four α helices (α1, α2, α4 and α5) (Schroder *et al*., 2000).

Figure 1.2. Cartoon representation of the monomeric unit from the decameric structure of hPrxII from human erythrocytes (PDB: 1QMV). The redox active cysteines are

shown in orange sticks with the loop regions shown in green, α helices shown in red and β sheets shown in yellow (figure created using PyMol DeLano Scientific).

hPrxII is thought to be functionally dimeric and the dimer within the decameric structure reveals an active site where the Cys_P and Cys_R are brought by different members of the homodimer and each dimer contains two redox active sites. The dimer has an ellipsoidal shape with dimensions 52 Å x 53 Å x 60 Å. The dimer interface buries 2109 $Å^2$ (21 %) of solvent-accessible surface area per monomer. The dimer is held together by hydrogen bonds and hydrophobic interactions between the C-terminal arm of one monomer and domain I of the other monomer.

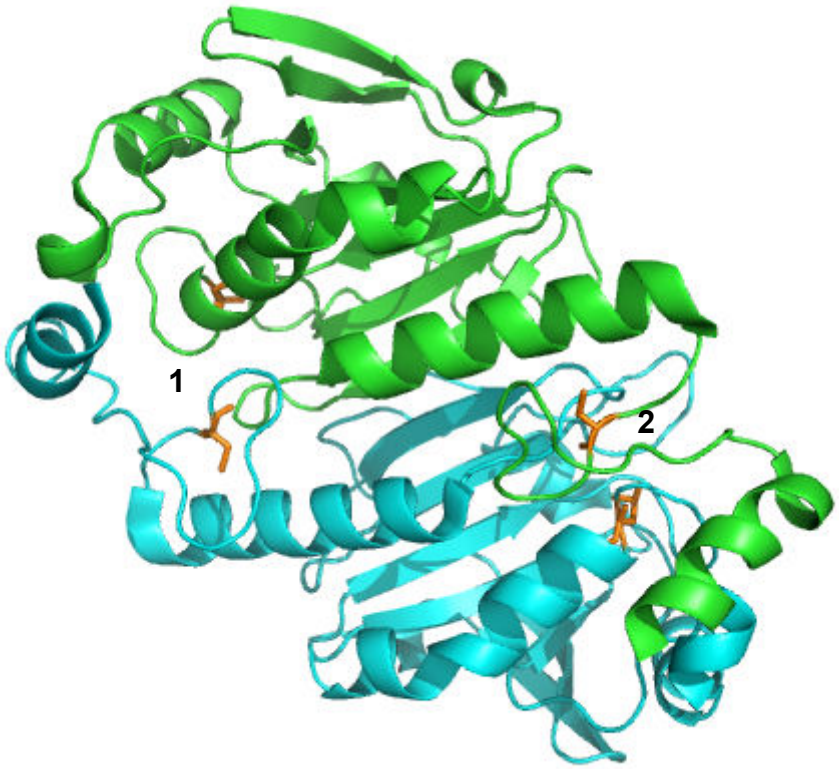

Figure 1.3. Cartoon representation of the homodimeric structure of hPrxII from human erythrocytes (PDB: 1QMV) with one monomer shown in green and the other shown in blue. The dimer contains two redox active sites indicated by the numbers 1 and 2. The redox active cysteines are shown in orange in stick mode (figure created using PyMol DeLano Scientific).

The crystal structure of hPrxII showed the protein to be in a decameric structure where five homodimers join together to form a toroid shape with point group symmetry 52 (Schroder *et al*., 2000) with a maximal diameter of ~130 Å, an

inside diameter of ~60 Å and thickness of ~50 Å. In the toroid shape there is an overall buried surface area of 2740 $Å^2$ per subunit which is 28% of the surface area. The decamer is held together by mainly hydrophobic interactions between residues Leu45, Phe47, Thr48, Phe81, Ala85, Val107 and Gly123. The decameric structure of this protein had been observed previously using electron microscopy (Harris *et al*., 1969).

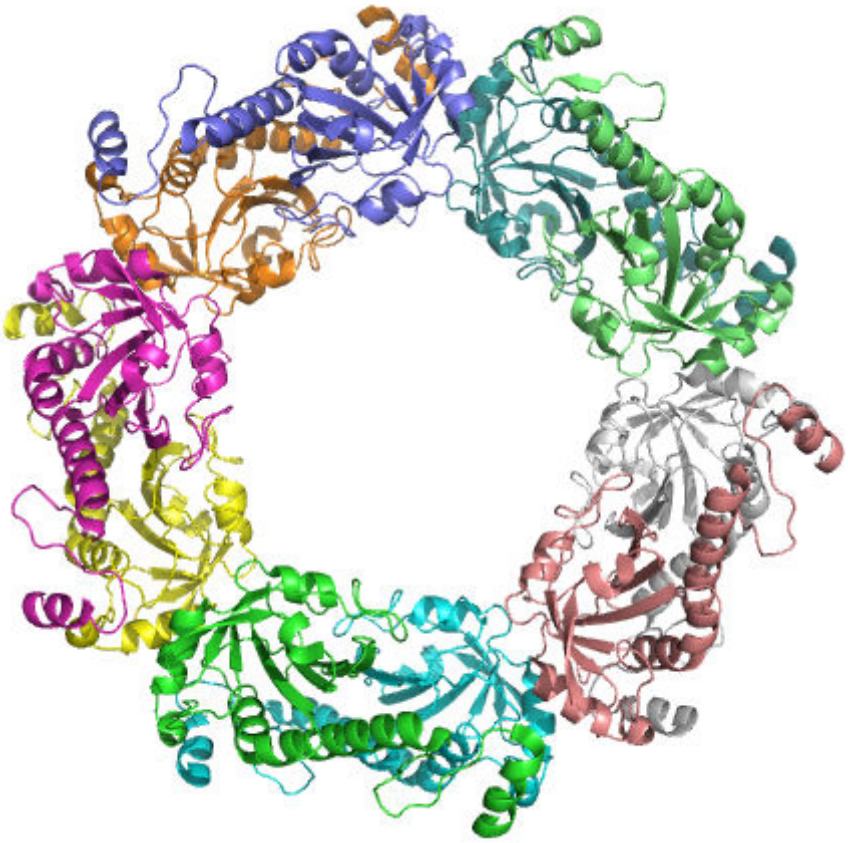

Figure 1.4. Cartoon representation of the decameric structure of hPrxII from human erythrocytes (PDB: 1QMV) with each individual chain within the 5 homodimers being shown in a different colour (figure created using PyMol DeLano Scientific).

1.5.1.2. The structure of the hPrxII active site

Within the homodimer there are two active sites. Each active site is made up of two redox active cysteines; the Cys_P is located on the N-terminus of one chain and the Cys_R which is located on the C-terminus of the other chain. In the crystal structure presented in Schroder *et al*., (2000) the Cys_P is shown to be in the hyper-oxidized sulfinic acid form that was thought to leave the protein inactive until the discovery of sulfiredoxin (Srx). The Cys_P is located in a hydrophobic pocket made up of residues Tyr43, Pro44, Thr48, Val50, Glu54,

Trp86, Arg127, Arg150 and Val171 from the other subunit (figure 1.5) and from these residues both Thr48 and Arg127 have been confirmed as essential for activity through mutagenetic studies (Montemartini *et al*., 1999; Flohe *et al*., 2002). The Arg127 residue is essential as it will lower the p*K*a of the Cys_P during the first step of the reaction mechanism (Montemartini *et al*., 1999).

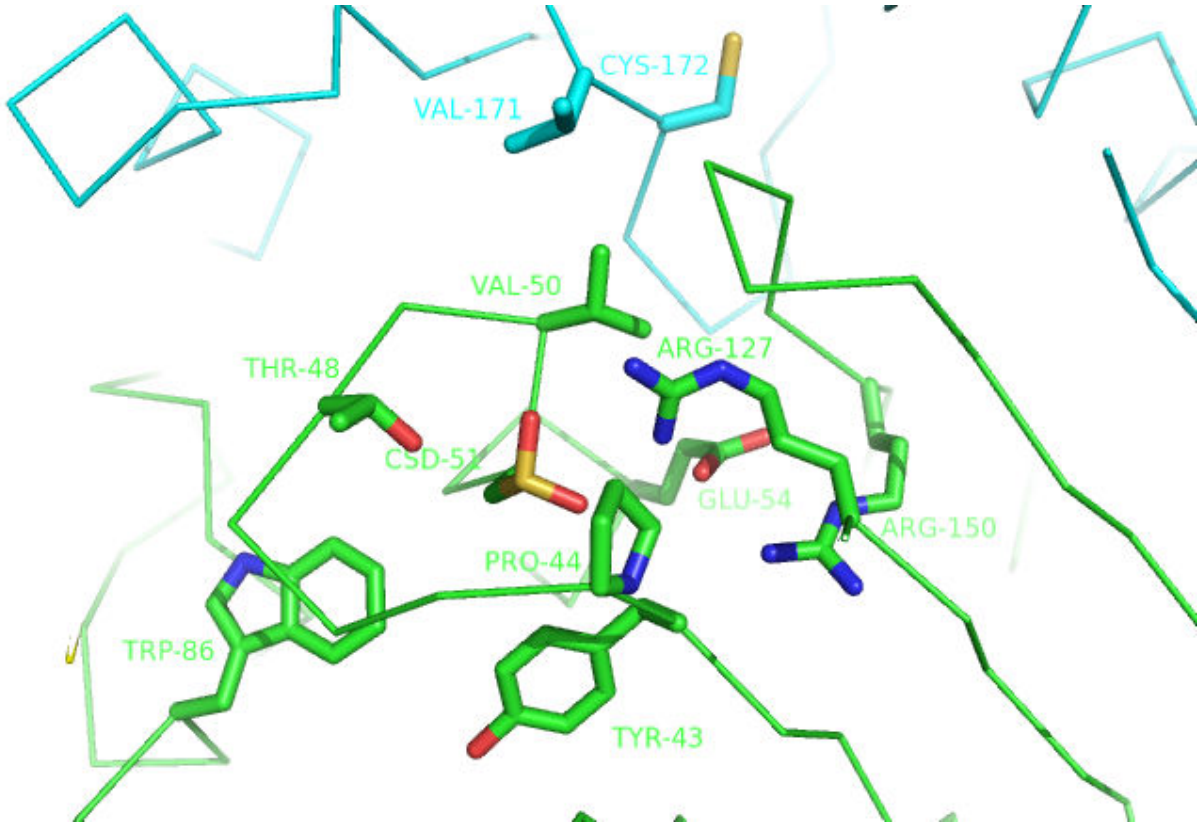

Figure 1.5. Ribbon and stick representation of the hydrophobic region around the active site Cys_P (CSD51) of hPrxII from human erythrocytes (PDB: 1QMV). The different subunits of the hPrxII homodimer are shown in green and cyan. The residues that form this hydrophobic region are *Tyr43*, **Pro44**, **Thr48**, **Val50**, **Glu54**, **Trp86**, **Arg127**, **Arg150** and *Val171* from the other subunit (the residues in bold sequence are conserved in all mammalian Prx sequences and the residues in italics are conserved only among the 2-Cys mammalian Prxs) (figure created using PyMol DeLano Scientific).

The Cys_R (Cys172) is located in an apolar environment that has limited solvent accessibility that could account for why the Cys_R does not undergo hyper-oxidation and is preserved in its thiol status. There is a ~10 Å gap between the Cys_P and the Cys_R which is too far away for an interaction between the two meaning there must be a structural rearrangement that must occur to allow the two to interact (Schroder *et al*., 2000).

1.5.1.3. The hPrxII catalytic cycle

The hPrxII catalytic cycle is made up of five different stages. The first step is the peroxidation of the Cys_P which involves the oxidation of the cysteine thiol to a cysteine sulfenic acid. The second step is the resolution of the sulfenic acid where the Cys_P and the Cys_R form an intermolecular disulfide bond. The last step of the normal catalytic cycle is the recycling of the intermolecular disulfide back to the reduced state with both redox active cysteines in the thiol form. The fourth and fifth step represent an abnormal part of the catalytic cycle. The second step of the reaction can be thought of as "slow" and the hold at this stage can be a factor in the Cys_P becoming hyper-oxidized to the sulfinic acid form (Wood *et al*., 2003b). This is the fourth step of the cycle. The fifth step of the catalytic cycle would involve the reduction of the hyper-oxidized form of the protein back to the oxidized form allowing the protein to re-enter the normal catalytic cycle (Jeong *et al*., 2006).

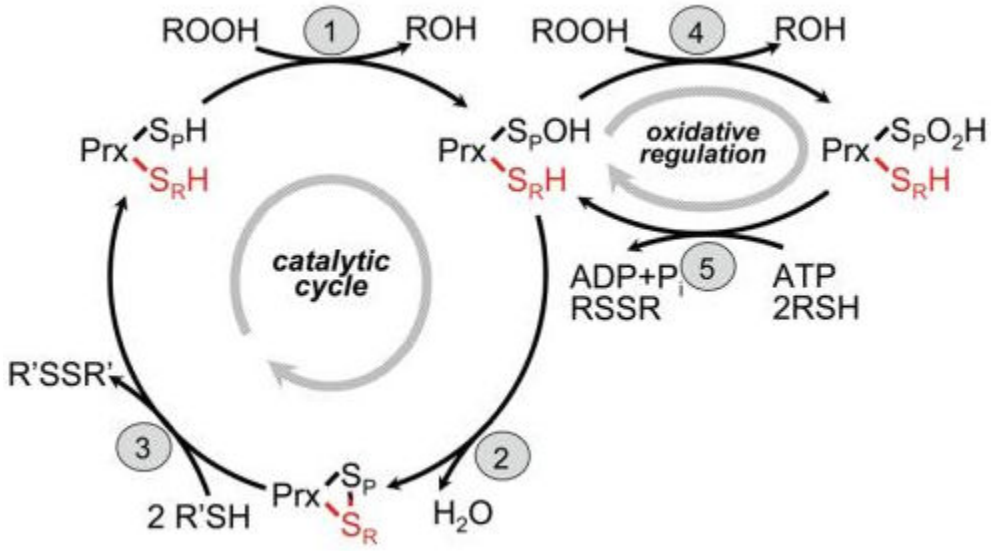

Figure 1.6. The five steps of the hPrxII catalytic cycle. The normal catalytic cycle is seen on the left hand side showing the peroxidation (step 1), the resolution (step 2) and the recycling (step 3). Hyper-oxidation of the Cys_P leads to a side catalytic cycle that shows the hyper-oxidation (step 4) and reduction of the sulfinic acid (step 5). Mechanism adapted from Hall *et al*., (2009).

In each reduction step of the catalytic cycle another protein is used to reduce hPrxII. Thioredoxin (Trx) is used to reduce the disulfide state back to the fully

reduced thiol state (Holmgren, 1985) and in the case of the hyper-oxidized sulfinic acid; sulfiredoxin is used to reduce the Cys_P back to the sulfenic acid form which can re-enter the normal catalytic cycle (Jeong *et al*., 2006).

1.5.1.4. The hPrxII mechanism

The mechanism for the 1st step of the catalytic cycle shown above is thought to be similar for all classes of PrxII. The Cys_P is able to form a stable thiolate anion due to the active site environment described above which then attacks the peroxide forming a cysteine sulfenic acid on Cys_P and an alcohol molecule is released (figure 1.7).

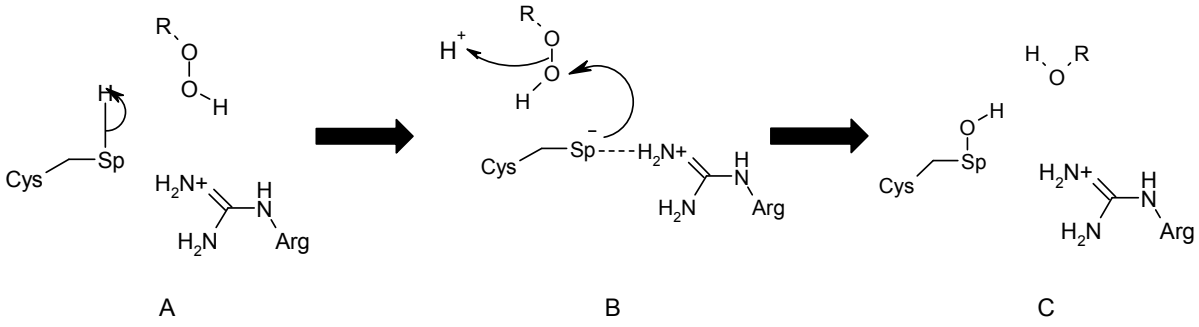

Figure 1.7. The mechanism of the 1st step or peroxidation reaction of hPrxII. Part A shows the formation of the thiolate anion that is stabilized by the presence of Arg127. Part B shows the attack of the thiolate anion of the peroxide substrate and the formation of the alcohol. Part C shows the sulfenic acid and alcohol (or water if the peroxide substrate is H_2O_2) products of the reaction. Mechanism recreated from Wood *et al*., (2003b).

1.5.1.5. The hyper-oxidation of Peroxiredoxin

Hyper-oxidation occurs due to a "slow" step in the reaction between the Cys_P and Cys_R (Wood *et al*., 2003b). One of the reasons for this is thought to be the YF and GGLG structural motif that sits above the active site (figure 1.8). The motif sits on a helix in the C-terminus and is thought to limit the ability of the C-terminus to unfold and allow the formation of the intermolecular disulfide (Schroder *et al*., 2000). This allows the protein to become overwhelmed by the peroxide substrate switching the redox state of the Cys_P (Wood *et al*., 2003a). The cysteine residue becomes hyper-oxidized converting it from the sulfenic acid form to the sulfinic acid form (Jacob *et al*., 2004). This YF structural motif contained within the C-terminal arm has been studied by mutagenesis and removal or lack of the motif shows a much reduced sensitivity to H_2O_2

suggesting it is required for hyper-oxidation to occur (Sayed and Williams, 2004). The sulfinic acid form has become very important in understanding the role of Prx to regulate redox signaling (Wood *et al*., 2003a).

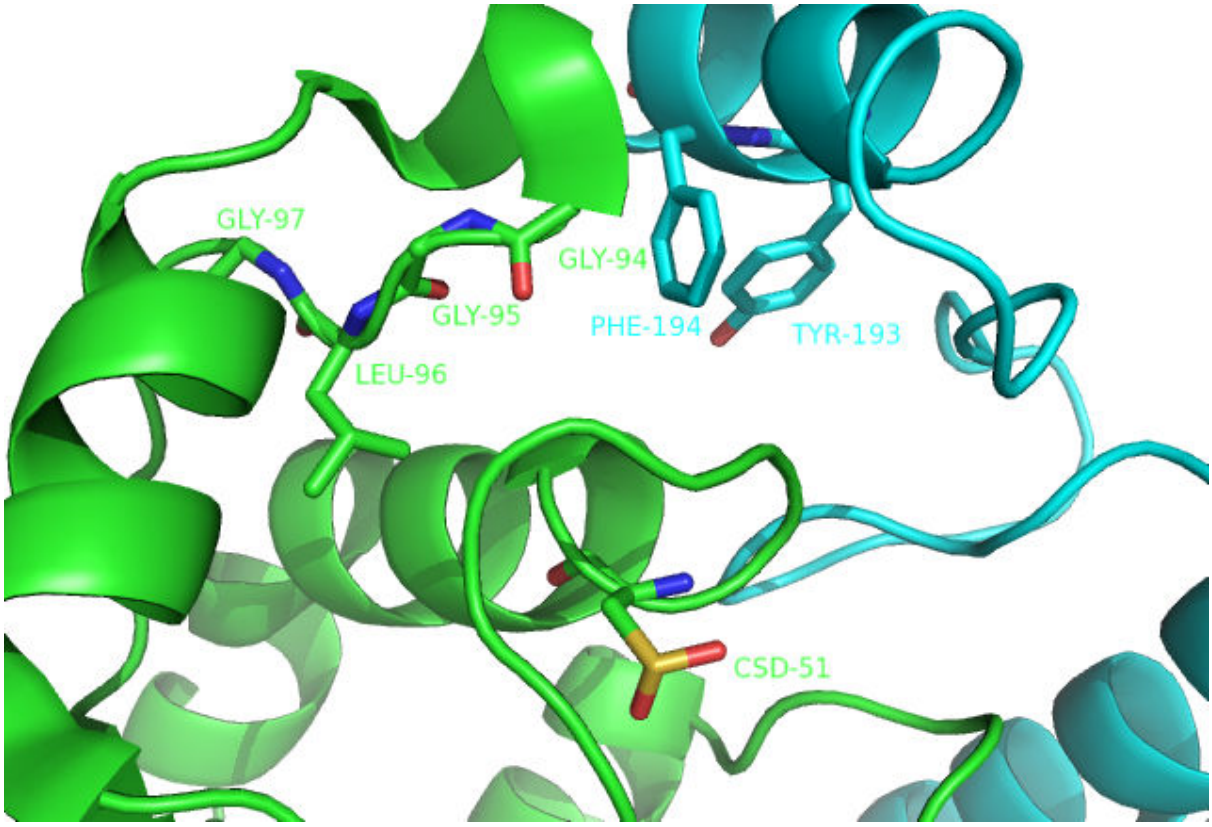

Figure 1.8. Cartoon representation of the GGLG and YF structural motifs that are believed to hinder the hPrxII (PDB: 1QMV) ability to allow it to form the disulfide state leading to hyper-oxidation of the cysteine residue (figure created using PyMol DeLano Scientific).

1.5.1.6. Oligomerisation of peroxiredoxin II

Although we know the proteins to be homodimeric there was evidence for the oligomerisation of the protein to the decameric form as early as the 1960's when Torin (now known to be hPrxII), a protein from human erythrocytes, showed complexes with tenfold symmetry when studied using transmission electron microscopy (TEM) (Harris, 1969; Harris *et al*., 2002). The decameric form seen in the TEM was confirmed by the crystal structure of hPrxII (Schroder *et al*., 2000). The decameric form has also been observed for Rat PrxI (Matsumura *et al*., 2008). Bovine PrxIII (Cao *et al*., 2005) can exist in a dodecameric form and when crystallised a novel structure was revealed. This

crystal structure showed dodecamers are interconnected forming a two-ring catenane (Cao *et al*., 2005).

This oligomerisation of the Prx is thought to be affected by a number of different factors. The oligomeric properties of the Prx have been studied using a number of different biophysical techniques such as gel filtration (Logan and Mayhew, 2000), dynamic light scattering (Wood *et al*., 2002a) and analytical ultracentrifugation (Schroder *et al*., 2000). The factors shown to affect the oligomeric state of the protein are ionic strength (Schroder, 1998), pH (Kristensen *et al*., 1999) and changes in the redox active cysteines (Wood *et al*., 2002). It has also been shown that the histidine (his) tag attached and used for purification may affect the oligomeric state of the protein. Size exclusion studies of the PrxIII protein showed that the presence of the poly histidine tag stabilized the formation of the dodecamer and may be a source of bias when working with recombinant Prxs (Cao *et al*., 2007).

It is believed that the change in oligomeric state of peroxiredoxins can link its redox state to its function. A study by Barrano-Medina *et al*., (2008) shows that formation of decameric Prx occurs at a critical concentration (1 – 2 μM) that is similar for a range of Prxs. It is believed that this critical concentration is not affected by the presence of any poly histidine tag. A study of Prx from pea (Bernier-Villamor *et al*., 2004) and barley (Konig *et al*., 2002; Konig *et al*., 2003) revealed that the decameric form of the protein is preferred under reducing conditions. The decameric form was also preferred when the pH was reduced (8.0 – 7.5), suggesting a protonatable amino acid could aid decamer formation (Barranco-Medina *et al*., 2009). The hPrxII decamer has been shown to break down at pH >7.8 and in the presence of high concentrations (2.5 M) of urea (Kristensen *et al*., 1999).

It is postulated in Schroder *et al*., (2000) that the intermolecular disulfide state would find it difficult to form or stay in the decameric structure due to the structural rearrangements that would need to take place for the disulfide to form. The interconversion between the oxidized (Matsumura *et al*., 2008) and the disulfide form of the rat PrxI (HBP23) (Hirotsu *et al*., 1999a) led to a breakdown from the decamer to the dimer (Matsumura *et al*., 2008) respectively and it is noted that this could also occur with the hPrxII (Schroder *et al*., 2000).

A further study by Alphey *et al.* (2000) postulated that the nucleophilic attack of Cys_R upon Cys_P would cause the structural rearrangements that break the decameric structure during disulfide formation.

It is believed that the dimer – decamer switch in Prx is dynamic and *in vivo* there is continuous interconversion between the species. Decameric Prxs have also been shown to aggregate together to form higher molecular weight forms (HMW). A dodecameric form of Prx has been observed and is believed to have a chaperone function (Moon *et al*., 2005) and their presence in the human erythrocyte has been postulated (Meissner *et al*., 2007).

1.5.1.7. Peroxiredoxin chaperone activity

A chaperone is a protein that helps to facilitate the correct folding of denatured and developing proteins (chaperonins) (Gatenby, 1992). Chaperones can also help to maintain proteins in their unfolded state during transportation (molecular chaperonins) (Hartl and Martin, 1995) as well as preventing the aggregation of certain proteins *in vivo* (Ellis and Minton, 2006). Many chaperones are expressed under cellular stress conditions such as high temperature (Ellis and van der Vies, 1991) and repair misfolded proteins. As discussed previously a HMW dodecamer of hPrxII was found to be a highly efficient chaperone protecting HeLa cells from H_2O_2 induced apoptosis (Moon *et al*., 2005). hPrxII is found only to be active as a chaperone when the oligomeric switch from decamer to dodecamer occurs. This is thought to occur as a response to high levels of H_2O_2 and could help to play a role in protecting the cell from apoptosis although the mechanism by which this occurs is not yet fully understood.

1.5.1.8. Peroxiredoxin cell signalling activity

One theory put forward to explain the hyper-oxidation of Prx to the sulfinic acid state is its ability to take part in cell signaling. It is already known that higher eukaryotic organisms are able to use higher concentrations of peroxide in the cell to mediate cell signalling (Rhee, 2006). The “floodgate” hypothesis put forward suggests that Prx is responsible for removing H_2O_2 before it is able to reach the peroxide sensitive targets. When the H_2O_2 concentation increases and Prx becomes hyperoxidised, the peroxide is able to break through the Prx barrier enabling the peroxide to interact with peroxide sensitive targets (Wood *et al*., 2003a). A second hypothesis suggests Prx is used as a measuring tool for

the amount of peroxide the cell is exposed to. In this theory hyperoxidised Prx is the oxidative stress signal and this signal can be turned off when the sulfinic acid is reduced and can be used to signal apoptosis (Jonsson and Lowther, 2007).

1.6. Sulfiredoxin

As part of the mode of action for PrxII the active site Cys_P can become hyper-oxidized to the cysteine sulfinic acid as part of the catalytic cycle. This sulfinic acid cannot be reduced by biological reductants and was thought to be an end point with Prx unable to be reduced (Hamann *et al*., 2002) until the discovery of sulfiredoxin (Srx). The protein was originally identified in *Saccharomyces cerevisisae* and was identified through a screen for hydrogen peroxide-induced genes (Biteau *et al*., 2003). In the Biteau *et al.* (2003) study it was discovered that the Srx mRNA levels were increased >200 fold 15 minutes after treatment with peroxide and that deletion of the gene resulted in a decreased tolerance to the peroxide treatment. There was also evidence of complex formation between yeast peroxiredoxin (Tsa1) and Srx and subsequent removal of the redox active cysteine of Srx resulted in loss of activity and complex formation. These complexes were also found to be sensitive to dithiothreitol (DTT) suggesting the production of a disulfide bond between the two enzymes. This study also showed that the reduction of the Prx by Srx requires the conserved cysteine residue on the Srx as well as adenosine triphosphate (ATP) and either Mg^{2+} or Mn^{2+} metal ions. The Srx sequence has been found to be conserved in a number of higher eukaryotes with the active site motif (GCHR) containing the redox active cysteine residue being highly conserved (Biteau *et al*., 2003).

1.6.1. Human sulfiredoxin

The human Srx (hSrx) has ~34% sequence identity to the original Srx from *S. cerevisisae*. In hSrx the active site motif contains a cysteine residue (Cys99) that is thought to be the redox active cysteine (Jeong *et al*., 2006). hSrx is 136 amino acids in length and has a molecular weight ~15 kDa.

1.6.1.1. Structure of hSrx

The crystal structure of Srx has been studied extensively and has been crystallized on its own (Jonsson *et al*., 2005) as well as in the presence of ATP and Mg^{2+} (Jonsson *et al*., 2008c), ADP (Jonsson *et al*., 2005) and PrxI (Jonsson

et al., 2008a). In these studies it is a truncated from of the protein (ET-Srx) that is able to form crystals with the all the residues up to residue 32 removed. This is probably due to this region having a high glycine content which is unstructured and flexible preventing crystallization (Jonsson *et al*., 2005). The original Srx structure was found to represent a new protein fold containing a core of five stranded mixed β-sheets surrounded by three α-helices (figure 1.9). It was found to contain a signature sequence that is able to bind a phosphate ion through hydrogen bonds (Phe96-Gly/Ser97-Gly98-Cys99-His100-Arg101). The hSrx has a concave shape that could leave it ideally suited to interacting with the convex surface of the hPrxII decamer (Jonsson *et al*., 2005).

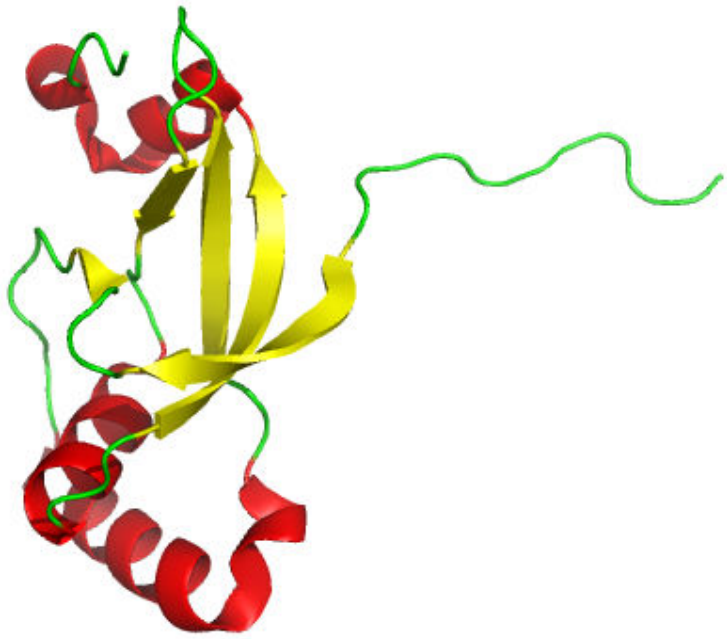

Figure 1.9. Cartoon representation of the crystal structure of hSrx (PDB: 1XW3), the five β-sheet strands (yellow) can be seen in the middle surrounded by the three α-helices (red) with the loop regions shown in green (figure created using PyMol DeLano Scientific).

1.6.1.2. hSrx mechanism

The Srx mechanism which has been confirmed by biochemical and structural analyses suggests that a structural rearrangement brings the ATP molecule that is bound to the nucleotide binding motif of Srx close to the Cys_P of Prx (Jonsson

et al., 2008c; Jonsson *et al*., 2008a).The γ-phosphate of ATP is attacked by the Cys_P sulfinic acid generating a phosphoryl ester intermediate. This intermediate is then attacked by the thiol on the redox active cysteine residue (Cys-99) to form a thiosulfinate bond between the Prx and Srx molecules (figure 1.10) (Roussel *et al*., 2008a; Jonsson *et al*., 2008d). The disulfide bond can then be reduced by another enzyme (glutathione (GSH) or thioredoxin) to allow the sulfenic acid form to be reincorporated into the normal hPrxII catalytic cycle (Woo *et al*., 2003).

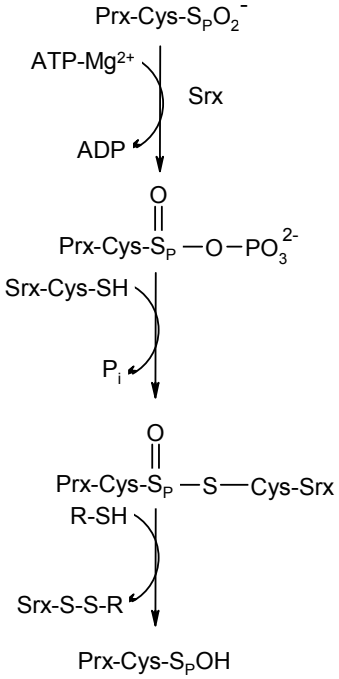

Figure 1.10. Mechanism of the reduction of the sulfinic acid Cys_P by hSrx. Step 1 shows the formation of a sulfinic acid phosphoryl ester intermediate as the ATP molecule is attacked. The Cys99 of Srx then attacks this intermediate forming a Prx-Srx thiosulfinate intermediate (mechanism recreated from Jonsson *et al*., (2008c).

1.6.2. The peroxiredoxin – sulfiredoxin interaction

A number of structural studies have been carried out to look at the interaction between the hyper-oxidized Prx and Srx molecules to study the structural rearrangements that would need to allow the Srx molecule to access and reduce the Cys_P (Jonsson *et al*., 2008a; Jonsson *et al*., 2009a). At the moment the structural studies have mainly been limited to PrxI which has a 77% sequence identity to PrxII as formation of stable complexes forming crystals between PrxII and hSrx have proved unsuccessful (Jonsson *et al*., 2008a).

The first crystal structure of PrxI in complex with Srx was formed using DTNB to form a disulfide bond between the Cys_P of PrxI (Cys52) and the redox active cysteine of hSrx (Cys99) (figure 1.11).

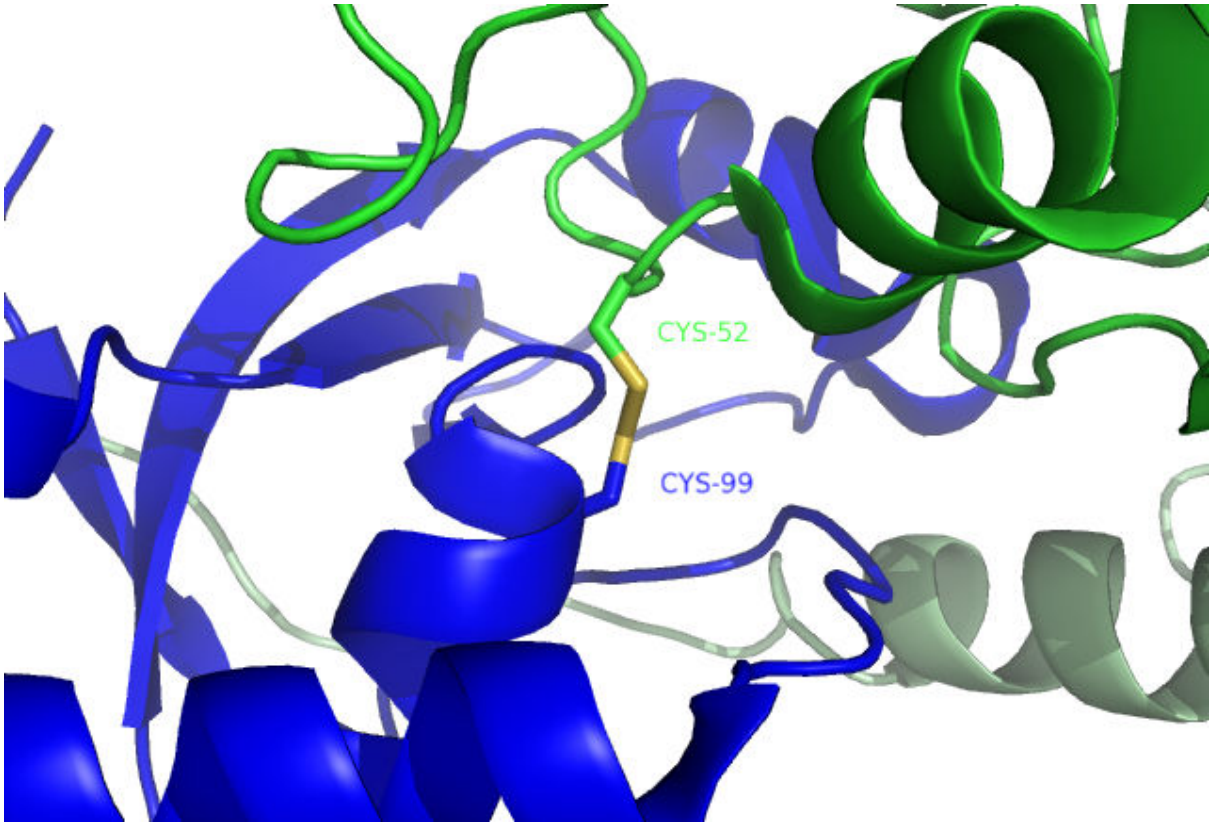

Figure 1.11. Cartoon and stick representation of the disulfide bond between the Cys_P of PrxI (Cys52) and the redox active cysteine of hSrx (Cys99) (PDB: 2RII). The PrxI chain a is shown in green, the PrxI chain b is shown in pale green, the Srx chain is shown in blue and the disulfide bond is shown in orange (due to the engineered nature of this bond we see a simple disulfide bond instead of the thiosulfinate bond we would expect to see in the native) (figure created using PyMol DeLano Scientific).

The complex was found to contain one PrxI dimer and two Srx monomers where the Srx was found between the active site of one PrxI chain and the C-terminal tail that had unfolded onto the non-catalytic backside surface of the Srx (Jonsson *et al*., 2008a) (figure 1.12). The binding was shown to take place between the C-terminal arm (residues 172-186) and a hydrophobic groove on the Srx molecule. It was suggested that this “embrace” was essential to allow the Srx molecule to be held in the correct orientation for catalysis as the active site interactions would not have been sufficient to hold it.

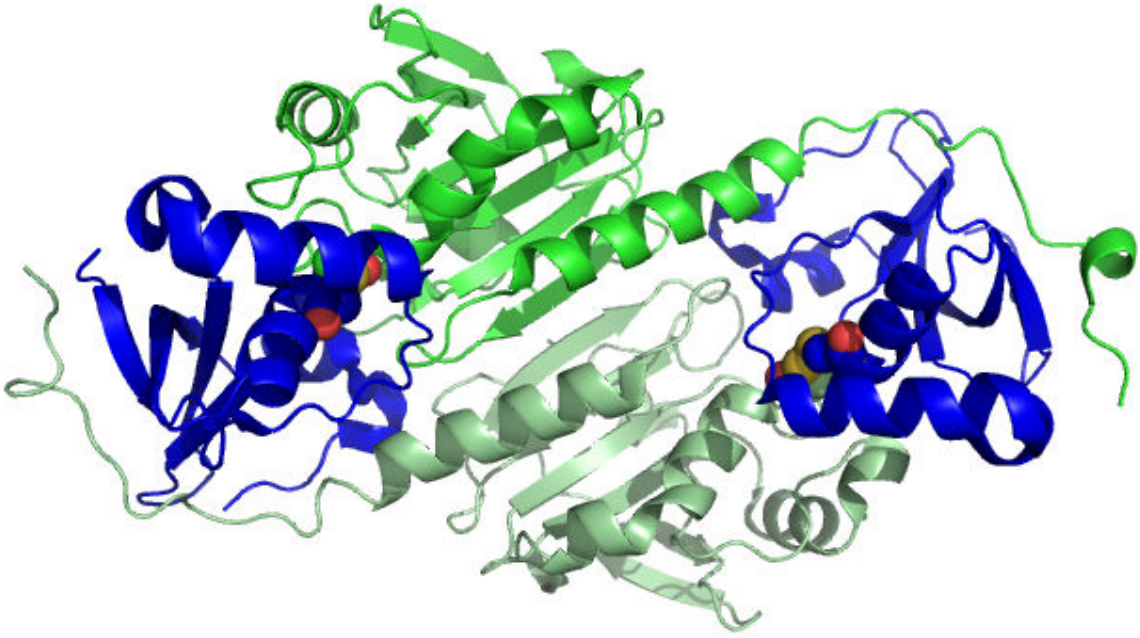

Figure 1.12. Cartoon representation of the complex formed between PrxI and Srx (PDB: 2RII) shows the C-terminal arm of the PrxI unfolded and interacting with the non-catalytic backside of the Srx molecule. The Srx monomers are shown in blue with the Prx dimer shown with chain a in green and chain b in light green, the disulfide bonds are shown as spheres (figure created using PyMol DeLano Scientific).

From the original hPrxII crystal structure it can be seen that the YF motif seen at the C-terminal end of the hPrxII chain must move when binding of the Srx molecules occurs, as the two species would try and occupy the same space. Unfortunately due to a poor electron density the YF motif is not observed in the PrxI-Srx complex but it must have moved to allow space for the hSrx to bind (Schroder *et al*., 2000; Jonsson *et al*., 2008a). Another important structural motif of the Prx-Srx complex is the GGLG motif that is thought to be important in ATP binding (Wood *et al*., 2003b; Jonsson *et al*., 2008b).

The second complex between peroxiredoxin and sulfiredoxin was formed to allow the study of the complex in the presence of ATP and Mg^{2+}. This crystal was formed by mutating out all of the cysteine residues including those that are needed for the redox reaction (leaving the proteins inactive) and by forming a covalent disulfide bond using DTNB, between two residues that are known to interact in the essential repair embrace (Jonsson *et al*., 2009a). This structure

revealed that the C-terminal arm embrace that was seen before provides a hydrophobic surface with which Phe50 (PrxI) can bind. This residue binding helps to unfold Prx allowing the ATP molecule to attack the hyper-oxidized Cys_P (Jonsson *et al*., 2009a). As yet there are still no crystal structures of an hPrxII-Srx complex.

A second PrxI-ET-Srx structure revealed the position of the co-factors that allow the reduction of the sulfenic acid to take place. As mentioned above the reduction of the sulfenic acid by sulfiredoxin requires the presence of ATP and Mg^{2+}. In the previous crystal structure the intermolecular disulfide formed meant that the ATP-Mg^{2+} was not seen. In this crystal structure the active site Cys residues have been mutated out and Cys residue introduced at the “backside” interface between hPrxI and ET-Srx. This structure reveals unfolding in the helix containing Cys_P allowing the packing of Phe50 (PrxI) into a hydrophobic pocket on Srx. This structural rearrangement positioned an oxygen atom of Asp52 (PrxI) within 4.3 Å of the γ-phosphate of ATP bound to Srx, which supports the phosphorylation of the Cys_P as the first step in the reaction between the two enzymes (Jonsson *et al*., 2009b).

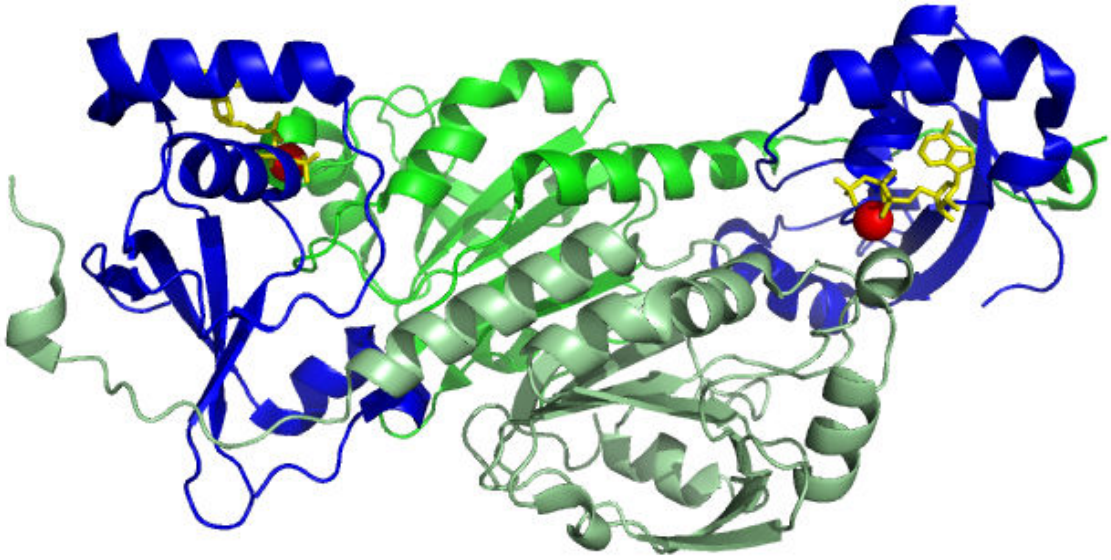

Figure 1.13. Cartoon representation of the PrxI-ET-Srx (PDB: 3HY2) complex showing the position of ATP (yellow stick) and Mg^{2+} (red sphere). The two subunits of the hPrxI homodimer are shown in green and pale green, with the Srx chains shown in blue (figure created using PyMol DeLano Scientific).

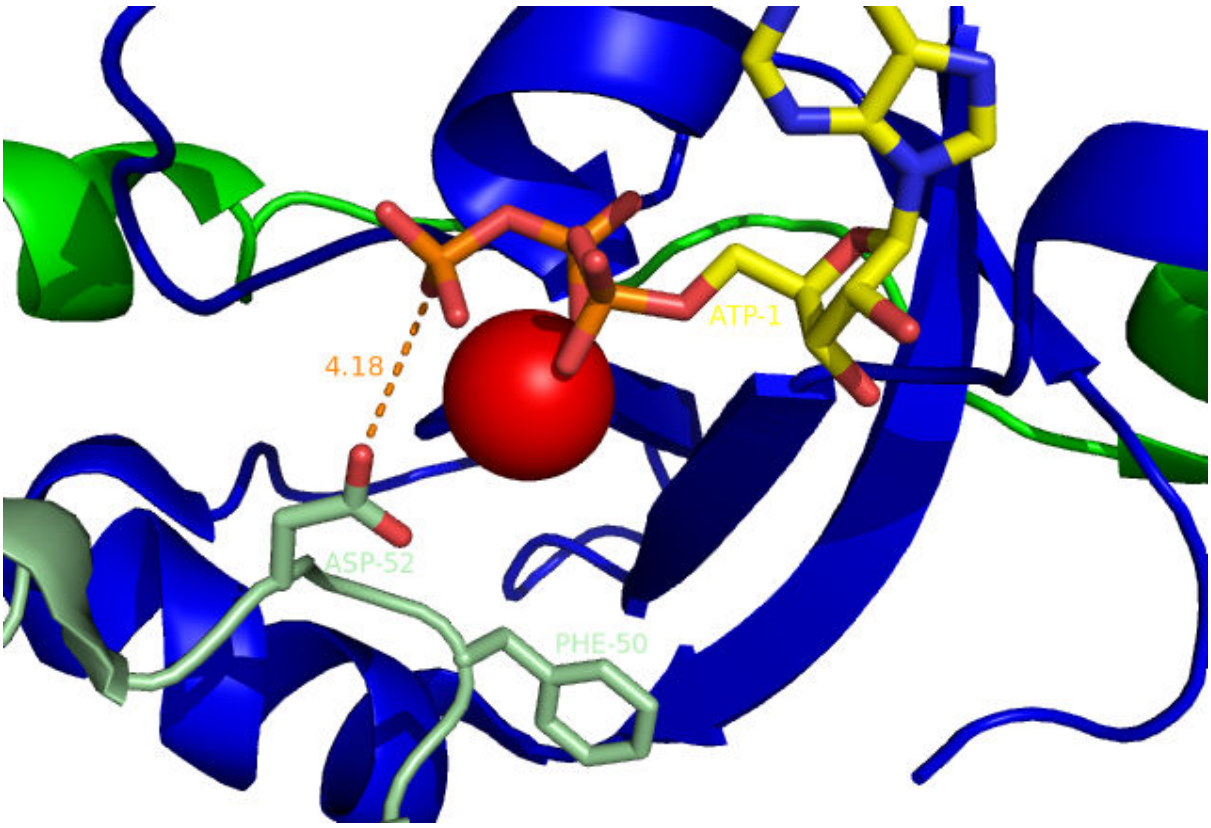

Figure 1.14. Cartoon representation of the ATP-Mg^{2+} interaction site for the PrxI-ET-Srx (PDB: 3HY2) complex showing the distance between the Asp52 and the γ-phosphate of ATP (yellow stick) and the position of the Phe50 residue. The two subunits of the hPrxI homodimer are shown in green and pale green, the Mg^{2+} is shown as a red sphere and the Srx chains shown in blue (figure created using PyMol DeLano Scientific).

1.7. Thioredoxin

Thioredoxin (Trx) is a protein that is ~12 kDa in size and uses two cysteine residues in a conserved CXXC active site sequence to reduce disulfide bridges in target proteins (Holmgren, 1989). The thioredoxin family of proteins all contain a thioredoxin fold and undergo a dithiol-disulfide exchange mechanism to catalyze oxidoreductase reactions (Meyer *et al*., 2009). The first characterized role of the Trx enzyme was to reduce the disulfide bond in the ribonucleotide reductase enzyme. This reduction took place with Trx forming part of a system that moved hydrogen atoms from NADPH through thioredoxin reductase (TrxR) and Trx to reduce the disulfide bond (Eklund *et al*., 1991).

The thioredoxin protein has also been found to be used in a number of other processes such as transcription factor modulation (Matthews *et al*., 1992; Martin, 1995), protein folding (Edman *et al*., 1985), cell growth stimulation

(Gasdaska *et al*., 1995), cell growth inhibition in pregnancy (Clarke *et al*., 1991), and in the reduction of sulfenic and sulfinic acids (Yoshitake *et al*., 1994). It is its ability to reduce the intermolecular disulfide bond that forms between the Cys_P and the Cys_R in hPrxII that will be focused on when discussing the structure and mechanism.

1.7.1. Human thioredoxin

Human thioredoxin (EC 1.8.1.9) is a 105 amino acid protein with a molecular weight ~12 kDa. As part of the catalytic cycle of hTrx the reduced form of the protein (Trx-$(SH)_2$) will reduce Prx from its intermolecular disulfide state (Prx-S_2) down to its reduced state (Prx-$(SH)_2$). This leaves hTrx with a disulfide bond (Trx-S_2) that is then reduced by TrxR which will be discussed later in the chapter (figure 1.15) (Holmgren, 1985).

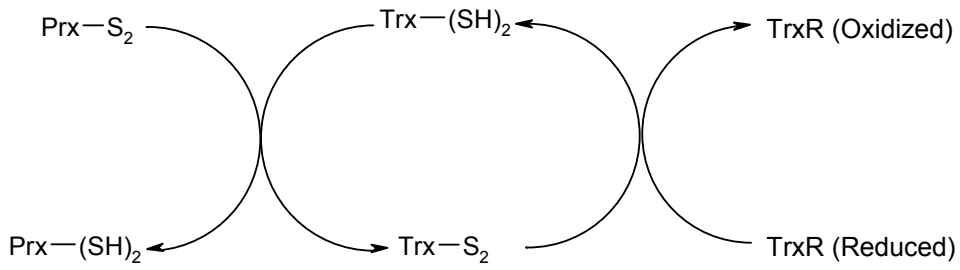

Figure 1.15. The catalytic cycle of hTrx showing the oxidation of the Trx protein as the Prx protein is being reduced, followed by the subsequent reduction of the Trx protein by TrxR. Mechanism recreated from Holmgren (1995).

1.7.1.1. hTrx mechanism

As part of the normal catalytic cycle, Prx will form an intermolecular disulfide that must be reduced by thioredoxin back to its reduced state so that it can restart its catalytic cycle (Wood *et al*., 2003b). For this to happen we must first have binding occurring between the reduced Trx and Prx molecules which is thought to occur via its hydrophobic surface (Holmgren, 1995). The first redox active cysteine residue Cys32 is stabilized to form a thiolate ion by the structural elements discussed below. This intermolecular disulfide bond between Cys_P and Cys_R on PrxII then undergoes nucleophilic attack by the Trx thiolate on Cys32 resulting in the formation of a mixed disulfide species where the two proteins are linked by a disulfide bond. The deprotonated Cys35 then attacks the disulfide bond reducing the PrxII protein and leaving Trx with a disulfide bond between the two redox active cysteines.

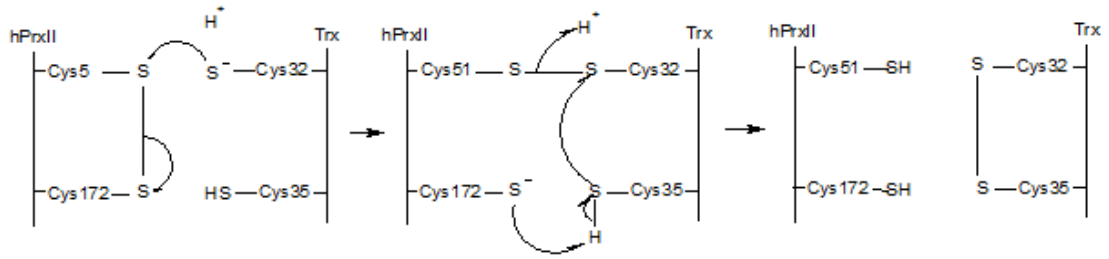

Figure 1.16. The mechanism for the reduction of a target protein by thioredoxin. The thiolate anion on Cys32 attacks the disulfide bond in hPrxII forming a disulfide bond between the two proteins. This disulfide bond is then attacked by the deprotonated Cys35 forming a disulfide bond between the two redox active cysteines on Trx and leaving the Cys_P and Cys_R residues reduced. Mechanism recreated from Holmgren (1995).

1.7.1.2. hTrx structure

hTrx has been crystallized and the structure solved for both the reduced and oxidized form (Weichsel *et al*., 1996), as well as NMR solution structures for the mutated human protein (Qin *et al*., 1994). The Trx structure contains a typical thioredoxin type fold with five-stranded β-sheets surrounded by four α-helices. The conserved active cysteine residues are found to be in the active site motif (CGPC) and are located on a loop region of the protein between the second β-sheet. The second cysteine is located at the start of the second α-helix.

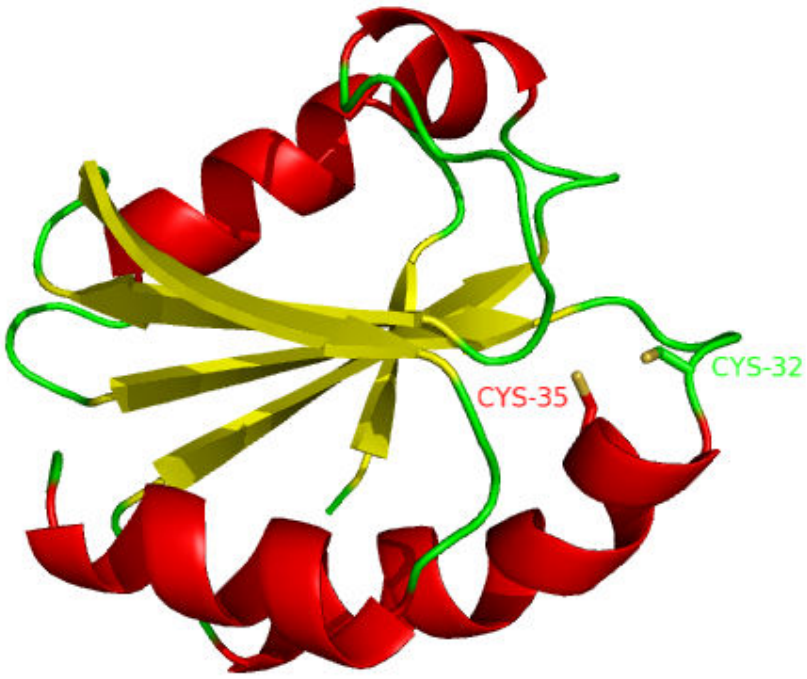

Figure 1.17. Cartoon representation of the reduced crystal structure of recombinant hTrx (PDB: 1ERT). The picture is coloured according to its secondary structure with the five β-sheets (yellow) surrounding four α-helices (red). The loop regions are indicated in green. The picture also shows the two active site cysteines (Cys32 and Cys35) residing between the second β-sheet and the second α-helix (figure created using PyMol DeLano Scientific).

The crystal structures of oxidized, reduced and mutant forms of thioredoxin all show the protein to be in a homodimeric state with a disulfide bond being formed between the two protomers at Cys73. All three forms of the protein showed the same overall structure with differences in the active site (between the reduced and oxidized form) and a difference in the formation of the homodimer (between the mutant and reduced/oxidized form).

1.7.1.2.1. Reduced form of hTrx

The reduced form showed the same overall structure with differences in the active site. In the reduced form the sulfur hydryl groups of the active site cysteine residues align which allows for hydrogen bond formation with the Cys35 as the proton donor and the Cys32 as the proton acceptor. The two cysteine residues are 3.9 Å apart and are at a favourable angle for the hydrogen bond to form (figure 1.18). The significance of this hydrogen bond is

that it may help to reduce the p*K*a of Cys32 from 8.7 down to 6.3 (Weichsel *et al*., 1996). This p*K*a decrease is due to the hydrogen bond's ability to stabilize the thiolate anion. There is also a smaller stabilizing effect caused by a dipole on α-helix two.

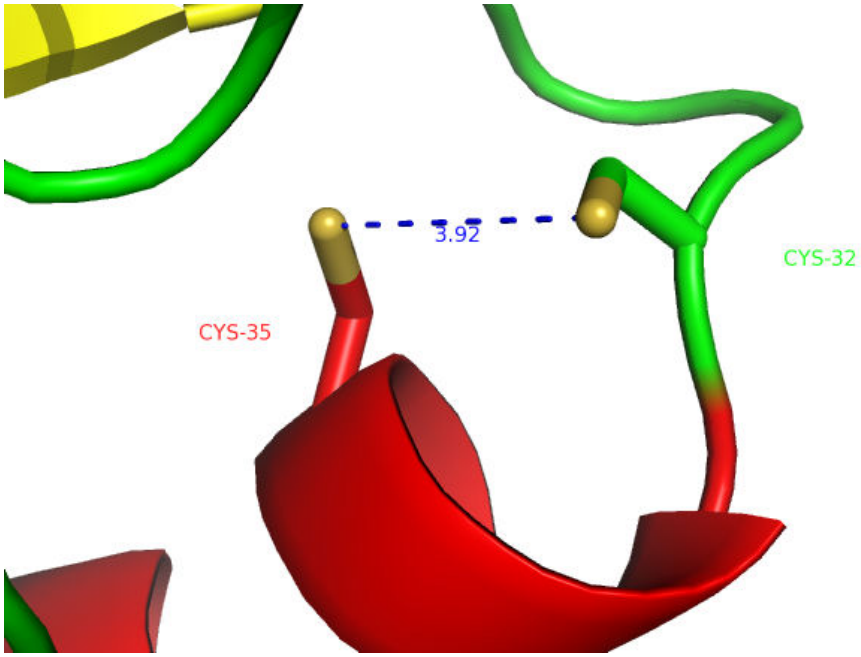

Figure 1.18. Cartoon representation of the orientation and distance between the two redox active cysteine residues in the reduced form of human Trx (PDB: 1ERT). The distance between the two cysteine atoms is ~3.9 Å. The picture is coloured according to secondary structure, showing β-sheets (yellow), α-helices (red) and loop regions in green (figure created using PyMol DeLano Scientific).

Cys32 lies on the surface of the protein whereas Cys35 is almost completely buried. This burial would not favour deprotonation of the sulfur hydryl group (figure 1.19). It is thought that the pKa of this cysteine residue could be increased due to the deprotonation of the Cys32 to a thiolate anion placing a negative charge next to Cys35 (Mossner *et al*., 2000). The crystal structure of the reduced form also revealed a previously unseen hydrogen bond between the sulfur atom on Cys35 and the nitrogen atom of Ala29 (Weichsel *et al*., 1996). With a distance of 3.7 Å between the sulfur and nitrogen atoms, they are at an appropriate distance and are aligned for hydrogen bond formation (Adman *et al*., 1975).

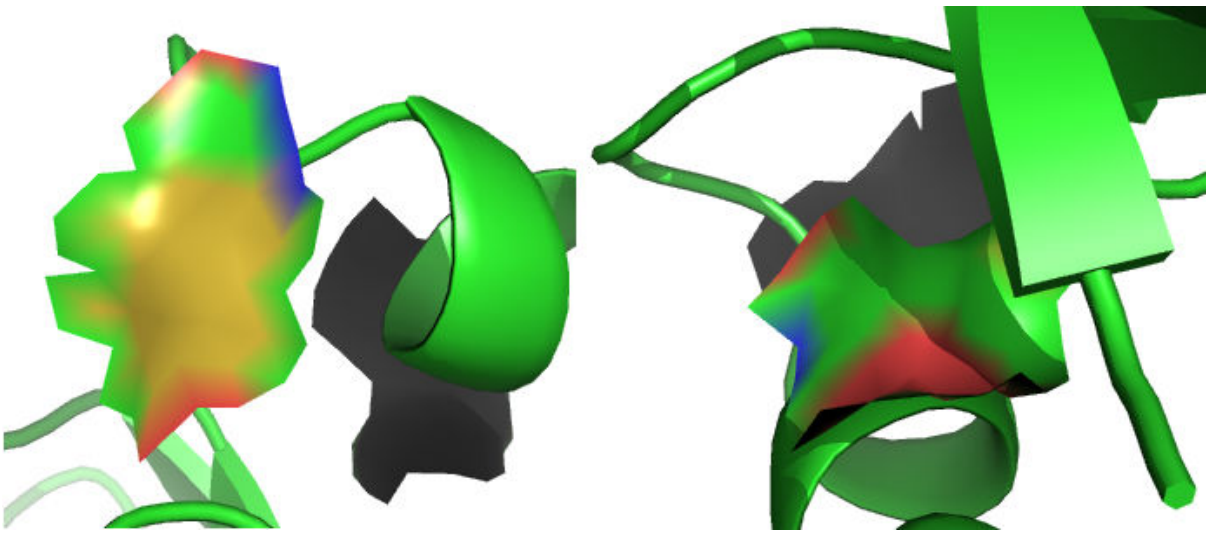

Figure 1.19. The surface representations of both the redox active cysteine residues in the reduced form of human Trx (PDB: 1ERT). The left picture shows Cys32 on the surface of the protein. The right picture shows Cys35 buried under the surface of the protein (figure created using PyMol DeLano Scientific).

1.7.1.2.2. Oxidized hTrx

The oxidized form of the hTrx protein was also crystallized and the conformational changes that allow the formation of the disulfide were studied (Weichsel *et al*., 1996b) (PDB: 1ERU). In general the two structures were very similar with a small difference in the positions of the two redox active cysteines allowing the formation of the disulfide bond (figure 1.20). The Cys32 is brought closer to the Cys35 by movement of the region (Ala29-Cys35) producing a disulfide bond with a bond length of 2.0 Å.

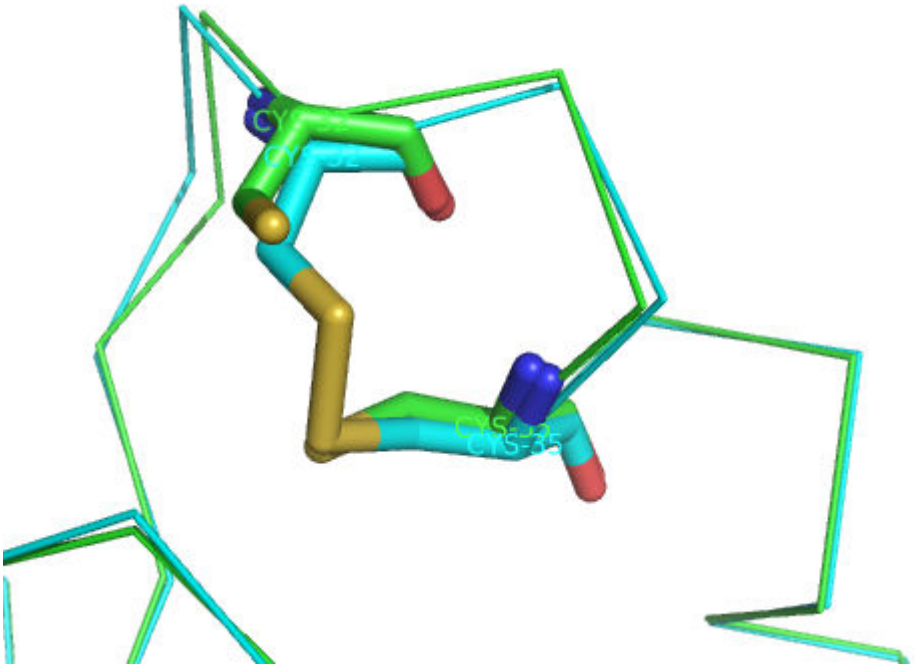

Figure 1.20. Stick representation of the comparison of the position of the active site cysteine residues in both the oxidized and reduced forms of hTrx. The reduced form (PDB: 1ERT) is shown in green with the oxidized form (PDB: 1ERU) shown in blue (figure created using PyMol DeLano Scientific).

The oxidized form of Trx also revealed a set of hydrogen bonds that had been gained from the reduced form and one that had been lost. Additional hydrogen bonds have formed in the oxidized structure between Cys32 and Lys36 and Gly33 and Met37 due to the residues coming closer together. The hydrogen bond between Cys35 and Ala29 has been lost as the residues have moved further apart. It is believed that this hydrogen bond network switch may be one of the factors that allow the reduction and oxidation of thioredoxin to be reversible (Weichsel *et al*., 1996).

1.7.1.2.3. The hTrx dimer

The four crystal structures for hTrx show the protein to be in a homodimeric state with a disulfide bond forming between the Cys73 residues on each subunit. The one exception to this is where the Cys73 has been mutated and replaced with a serine residue. This Ser73 mutant still forms a homodimer but instead forms a hydrogen bond between the two subunits in this position (Weichsel *et al*., 1996). The disulfide bond is maintained and even seen in the crystal grown in the presence of 5 mM DTT which was added to keep the active

Cys in the SH state. It is hypothesized that this is due to the cysteine's being at the "perfect angle" for disulfide bond formation (Weichsel *et al*., 1996). As well as the bond that forms between the residues at position 73 there are also interactions involving a large hydrophobic patch and formation of five hydrogen bonds around the Cys73 residue (Weichsel *et al*., 1996). The hTrx dimeric and monomeric forms have both been identified in solution (Ren *et al*., 1993). The Trx is thought to be active as a monomer and the formation of a Trx dimer is thought to have regulatory role as the dimeric form has been found to be inactive (Holmgren, 1977).

1.7.1.3. hTrx interaction with hPrxII

To date there are no structures solved for the complexes between Trx and Prx. The interactions are thought to occur due to the hydrophobic nature of the reduced form of Trx being able to bind to the Prx protein surface (Holmgren, 1995). A stable complex has been formed between Trx (HvTrxh2 from barley) and barley α-amylase/subtilisin inhibitor (BASI) showing the mixed disulfide species (Maeda *et al*., 2006). The study discovered the interactions that help to stabilize the complex were van der Waals contacts and three intermolecular hydrogen bonds that were made by three structural motifs. These motifs were WCGP (residues 45-48), AMP (residues 87-89) and VGA (residues 104-106) (Maeda *et al*., 2006). A search against the PDB showed similar motifs in the *E. coli* and human reduced forms of the protein as well as a number of other Trx and GST enzymes (Maeda *et al*., 2006). The reduced form of the hTrx protein shows a high similarity to the HvTrxh2 enzyme in these regions and therefore could bind to hPrxII in a similar way.

1.8. Thioredoxin reductase

Thioredoxin reductase (TrxR) (EC 1.8.1.9) is a homodimeric flavo-protein that uses NADPH to catalyze the reduction of the disulfide bond between Cys32 and Cys35 in Trx (Mustacich and Powis, 2000). The mammalian TrxR enzymes are selenocysteine containing enzymes. The selenocysteine is essential for activity and forms part of the active site (Arner *et al*., 1999). Bacteria, plants and archaea have a smaller non-selenocysteine protein (Williams *et al*., 2000). There are three different TrxR proteins in mammalian systems (TrxR1-3) that differ in sequence, length and sub-cellular location (Sun *et al*., 2001). The TrxR that this project will focus on is TrxR1.

1.8.1. Human thioredoxin reductase 1

TrxR1 is located mainly in the cytosol and is the most common form of human thioredoxin reductase (hTrxR). The TrxR1 is a homo-dimeric protein 499 amino acids in length and is ~55 kDa in size (Oblong *et al*., 1993).

1.8.1.1. Mechanism of hTrxR1

The TrxR1 has three elements; a selenocysteine, a redox active disulfide, and a flavin adenine dinucleotide (FAD) molecule that reduces the disulfide bond in Trx. The selenocysteine element is located at the C-terminal end of the protein and is the penultimate residue coded for by a UGA codon (Gladyshev *et al*., 1996). The selenocysteine (Sec, U) is located in a structural motif ($_{496}$Gly-Cys-Sec-Gly$_{499}$) along with a cysteine residue, with the Cys-Sec thought to form the "proper" active site (Zhong and Holmgren, 2000). The second active site has two redox active cysteines in a structural motif ($_{59}$Cys-Val-Asn-Val-Gly-Cys$_{64}$). The two active sites are presented to each other from different chains of the homodimer that is arranged in a head to tail fashion (Fritz-Wolf *et al*., 2007). The mechanism reported in Arner *et al*., (2009) suggests that the first step of the reaction involves the reduction of the bound FAD by NADPH. As part of this reduction the selenenyl sulfide (Se-S) is converted to a highly reactive selenolate anion (Se^-). This selenolate anion attacks the disulfide on the Trx molecule resulting in a mixed disulfide formed between the two. This mixed disulfide is then attacked by the cysteine residue in the active site motif (Cys497) to reproduce the selenenylsulfide. This selenenylsulfide is then converted to the selenolate anion using the second cysteine from the other active site motif (Cys64) starting the cycle once again (Zhong and Holmgren, 2000) (figure 1.21).

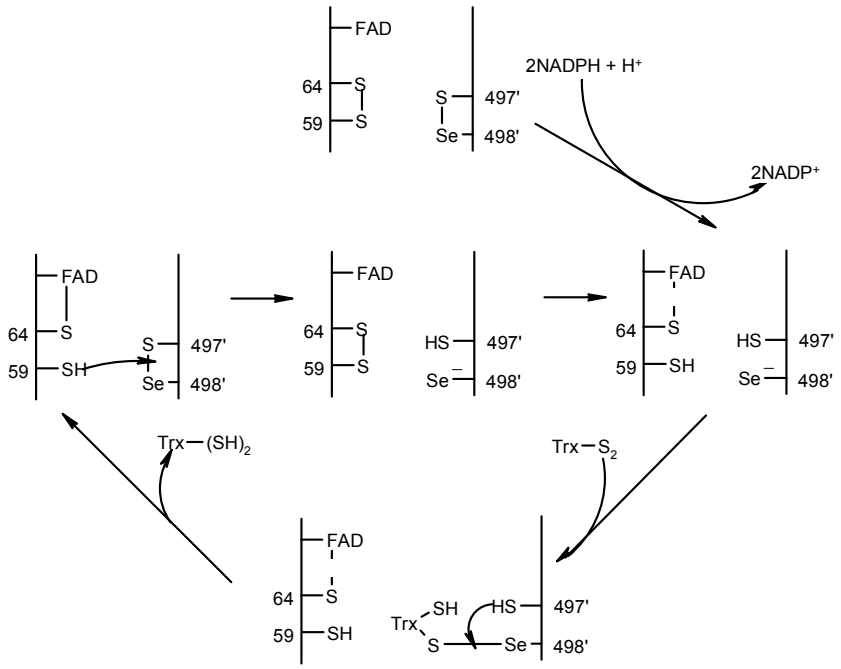

Figure 1.21. The proposed mechanism of Trx reduction by TrxR1. The FAD is reduced by NADPH forming a selenolate anion that is used to attack the disulfide bond on Trx. The enzyme is then recycled by Cys497 reforming the seleneyl sulfide before it is reduced by a thiol on the second active site. Mechanism recreated from Zhong and Holmgren (2000).

1.8.1.2. Structure of hTrxR1

The TrxR1 protein is homodimeric with each chain possessing a FAD and NADPH binding site as well as two redox active sites. The NADPH binding site is located close to the FAD binding site to allow electron transfer between the two molecules. The NADPH molecule binds to the protein through interactions between the phosphate groups and three conserved arginine residues (Arg166, 221 and 226). The FAD binding site lines up the isoalloxazine ring on FAD with the nicotinamide ring in parallel positions to allow for the electron transfer as seen in a number of other enzymes.

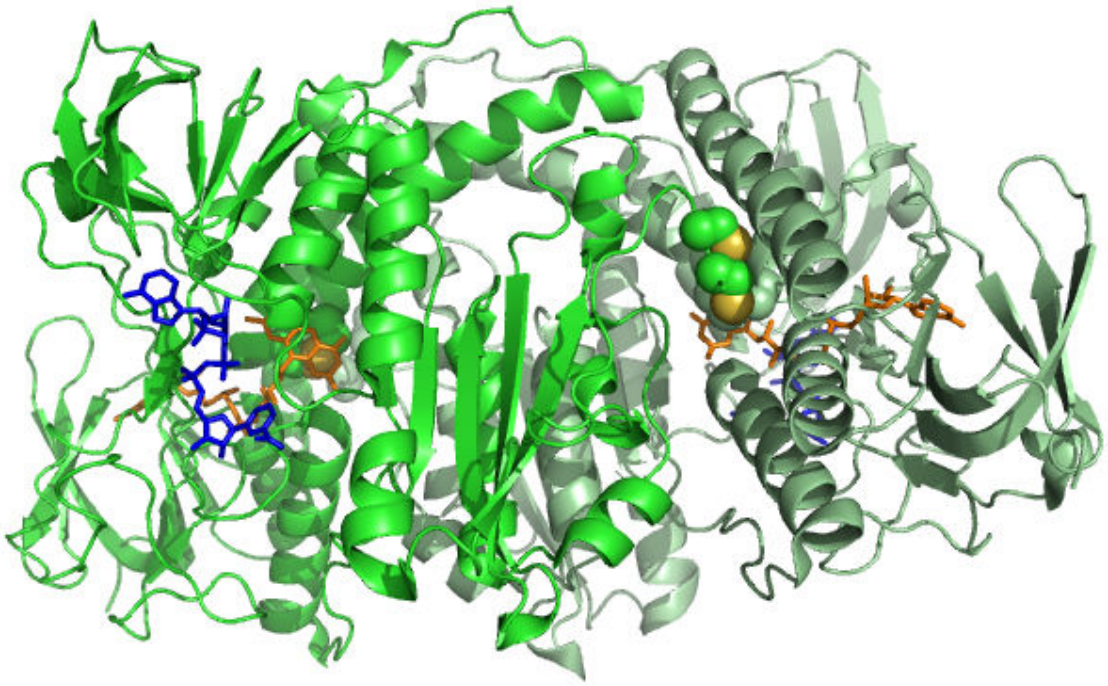

Figure 1.22. Cartoon representation of the structure of TrxR1 (PDB: 2J3N). The different subunits are shown in green and light green. The cysteine residues are shown in sphere mode and the FAD (orange) and NADPH (blue) are shown in stick mode (figure created using PyMol DeLano Scientific).

The redox centre containing the selenocysteine is located on the C-terminal arm of the protein which was shown when the protein was crystallized to be in different states. These different states show a side chain specific switch between the reduced and oxidized form of the second redox active centre ($_{497}CC_{498}$). The switch brings about a change in the orientation of the redox active centre with the cysteine groups in the oxidized state facing inward and would not allow for electron transfer with the Trx. The cysteine groups in the reduced form will face outward allowing them to interact with the Trx molecule.

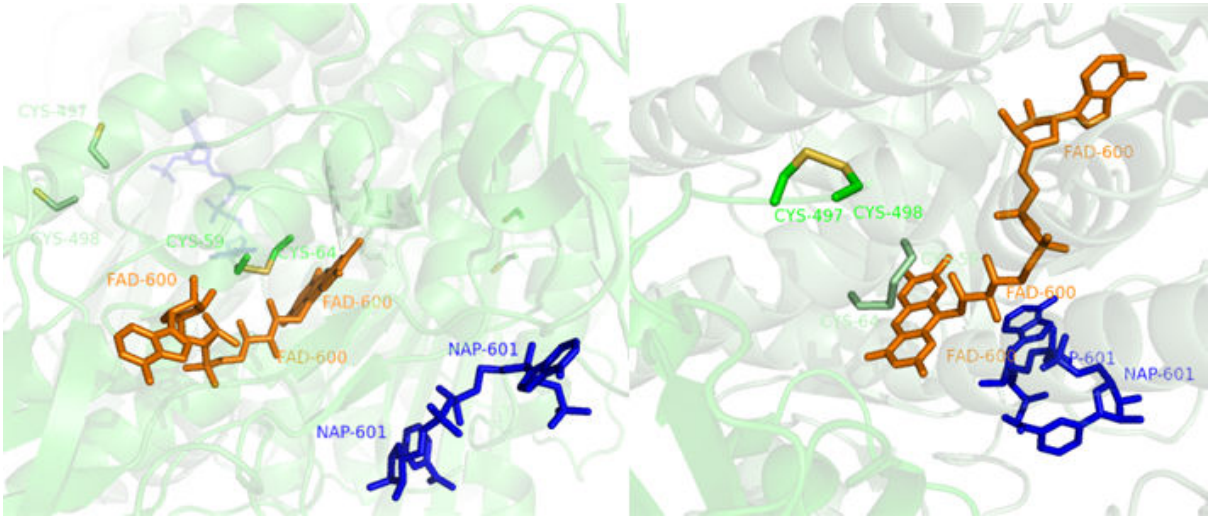

Figure 1.22. Cartoon representation of the structure of the active site residues in both the oxidized (left) and reduced (right) form of TrxR1. The subunits of TrxR1 are shown in green and light green. The Cys residues and the cofactors FAD (orange) and NADPH (blue) are shown in stick mode (figure created using PyMol DeLano Scientific).

1.9. Reconstitution of the Peroxiredoxin system

To form an activity assay for Prx all the enzymes in the normal catalytic cycle must be brought together. The enzymatic activity of hPrxII can be measured by coupling hTrx and TrxR1 in the presence of NADPH. In a typical Prx assay the enzymes in the system are mixed together in μM concentrations and the reaction is initiated by the addition of H_2O_2. The activity is calculated by measuring the decrease in A_{340nm} over a set time frame (usually 3-5 min) and by using the initial rate of reaction expressed in the amount of NADPH oxidized per minute (Kim *et al*., 2005; Cao *et al*., 2007).

1.10. Aims of the project

The aims of this project are:

- The over-expression and purification of stable hPrxII. This will be used along with Trx and TrxR to form a working Prx assay, and also for complex formation and structural studies.
- The over-expression and purification of hPrxII in the disulfide form and subsequent crystallization and structural analysis.
- The formation of a complex between PrxII and Srx. The complex will then be studied using size exclusion chromatography and surface plasmon resonance, and crystallization attempted to obtain a 3D structure.

- The formation of a complex between PrxII and Trx. The complex will then be studied using size exclusion chromatography and surface plasmon resonance, and crystallization attempted to obtain a 3D structure.
- Cloning, over-expression and purification of an active TrxR. This will be used with PrxII and Trx to form a working Prx assay.

2. Cloning, expression and purification of Human Peroxiredoxin II from red blood cells and the effect of a fourth residue mutation

2.1. Introduction

In order to study hPrxII it was essential to have a recombinant protein which could be expressed and purified to high homogeneity. This would negate the need to work with human blood in order to obtain the levels of proteins required for this study. A clone of the hPrxII gene in the pET28a expression vector was obtained from Dr Kirsty Line (University of Exeter). Original attempts to purify the enzyme proved problematic, the recombinant enzyme aggregated very easily during purification, dialysis and concentration. The recombinant protein was also predominantly produced in a different oligomeric state to that of the native enzyme. Native hPrxII is seen mainly in the decameric form with a small amount in the dimeric form, but the opposite was observed for the hPrxII clone. When the sequence information was re-assessed it was noticed that there was a point mutation in the DNA sequence, which resulted in a change of the fourth amino acid of the protein from glycine to valine. Glycine is the smallest amino acid and is very flexible whereas valine is much larger and hydrophobic.

Figure 2.1. Comparison of the Protein sequences for hPrxII (4Gcorrect) and hPrxII (4Vincorrect).

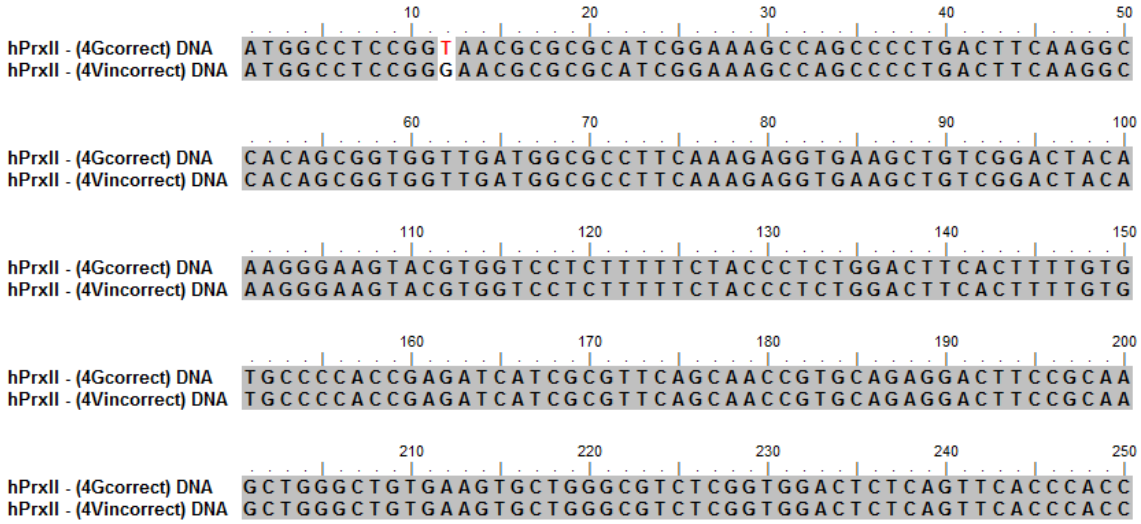

Figure 2.2. Comparison of the first 200 bp of the DNA sequences for hPrxII (4Gcorrect) and hPrxII (4Vincorrect).

In view of the problem with aggregation of the recombinant Prx the decision was taken to re-clone the *hPrxII* gene. This chapter discusses the re-cloning, expression and purification of the hPrxII gene and the resulting effects on the solubility and oligomeric state of the protein.

2.2. Materials and Methods

2.2.1. Cloning of *hPrxII*

PCR was used to generate a DNA fragment which encoded the *hPrxII* gene and the restriction sites *Nde* I and *Not* I. These were incorporated onto the 5' end of the forward and the reverse primer sequences, respectively.

hPrxIIF 5' – AACATATGGCCTCCGGTAACGCGCGCATCG – 3'

hPrxIIR 5' – AAGCGGCCGCTAATTGTGTTTGGA – 3'

The PCR was performed in a total volume of 50 µl containing 200 ng of template DNA, 100 ng of each primer, 200 µM of each dNTP, 2 U Deep Vent Polymerase (New England Biolabs, Beverley, MA), 1 x Deep Vent Buffer and nuclease free water to adjust to the final volume. The PCR cycle consisted of 3 min at 94^{o}C followed by 40 consecutive cycles of denaturation (1 min at 94^{o}C), annealing (1 min at 65^{o}C) and polymerisation (1 min at 72^{o}C). There was also a final extension time of 5 min at 72^{o}C. The DNA was treated with Red Taq Polymerase (Sigma Aldrich) to produce an A overhang (20 min, 72^{o}C) and then separated on a 1% agarose gel. The DNA on the gel was visualized using

ethidium bromide staining and DNA bands visualised by UV. The PCR product of the expected size (747 bp) was purified using a gel extraction kit (Qiagen) according to the manufacturer's instructions. The A overhang was used to ligate the gene into the TOPO TA Cloning vector pCR2.1-TOPO (Invitrogen). The *hPrxII* gene insert was excised from the cloning vector using the restriction enzymes *Nde*I and *Not*I and ligated into pET28a (Novagen) that had been predigested with the previously mentioned restriction enzymes. A 20 µl aliquot of the ligation mixture was transformed (as in methods 2.2.2) into the *E*. *coli* Nova Blue cell line (Novagen). The *E. coli* cells were plated onto Luria Bertani (LB) agar plates containing 50 µg/ml kanamycin. The transformants were verified to contain the *hPrxII* by plasmid DNA isolation, digestion and agarose gel electrophoresis. The recombinant plasmid containing the *hPrxII* gene was sequenced by Eurofins MWG Operon (Ebsberg, Germany).

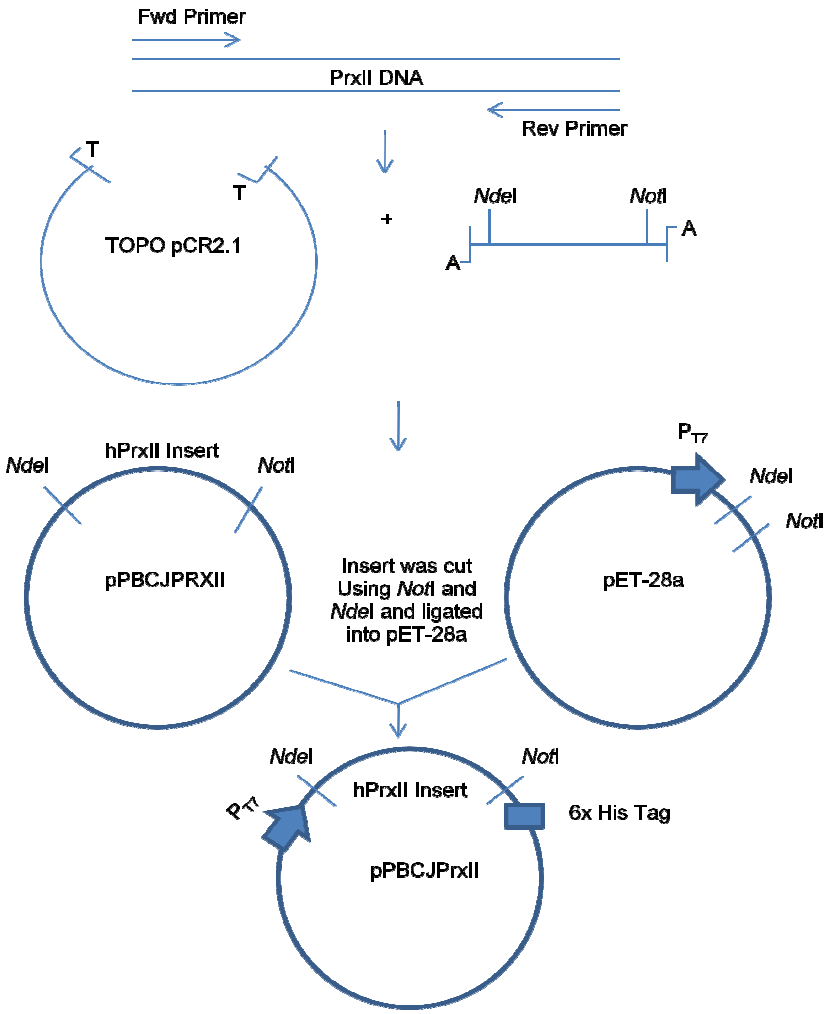

Figure 2.3. The strategy for the cloning of *hPrxII* into the pCR2.1-TOPO vector, followed by subsequent cloning into pET28a to allow for the expression of the protein (figure modified from TOPO Kit manual Invitrogen).

2.2.2. Transformation of hPrxII into an expression cell line

hPrxII DNA was used to transform chemically competent *E. coli* Rosetta Gami 2 (Novagen) cells by addition of 1 µl DNA to ~50 µl of Rosetta Gami 2 cells that were thawed on ice. The reaction was incubated on ice for 30 min followed by heat shock at 42^{o}C for 45 sec. The reaction was cooled on ice for 2 min before the addition of 200 µl of sterile LB medium, followed by incubation in a shaking incubator at 37^{o}C for 1 h before being plated out on a LB agar plate containing kanamycin (50 µg/ml), tetracycline (37.5 µg/ml) and chloroamphenicol (12.5 µg/ml). Colonies were picked, glycerol stocked and the presence of the gene confirmed by DNA sequencing (Geneservice, Oxford).

2.2.3. Expression of recombinant hPrxII

The *hPrxII* gene was cloned incorporating an N-terminal His-tag and expressed under the control of the T7 promoter. The recombinant *hPrxII* gene was transformed into the *E. coli* Rosetta Gami 2 expression cell line and cells (from glycerol stock) containing the pET28a/*hPrxII* construct were used to inoculate 100 ml LB containing kanamycin (50 µg/ml) tetracycline (37.5 µg/ml) and chloroamphenicol (12.5 µg/ml). This starter culture was grown under agitation at 200 rpm overnight at 37^{o}C and 20 ml were used to inoculate 1 L fresh LB medium containing the appropriate antibiotics for selection, and was grown with agitation at 37^{o}C until the optical density OD_{600nm} was approximately 0.8, when isopropyl-β-D-thiogalactopyranoside (IPTG) was added to a final concentration of 1.0 mM and the culture incubated for a further four hours at 37^{o}C. The *E. coli* cells were harvested by centrifugation (20,000 x *g*, 20 min, 4^{o}C) using a Beckman JA-25.50 rotor. The cell pellet was stored at -20^{o}C until further use.

2.2.4. Purification of Recombinant hPrxII

2.2.4.1. Cell lysis

Cell paste was re-suspended at 10% w/v in 100 mM Tris-HCl, pH 7.5, 0.5 M NaCl, 20 mM imidazole. Cells were disrupted by sonication at 10 microns (Soniprep 150, Sanyo) on a program; 30 sec on, 1 min off (x 6 cycles) and the cell debris removed by centrifugation at 20,000 x *g*, 20 min and 4^{o}C using a Beckman JA-25.50 rotor.

2.2.4.2. Purification buffers

Buffer A – 100 mM Tris-HCl, pH 7.5, 0.5 M NaCl, 20 mM imidazole

Buffer B – 100 mM Tris-HCl, pH 7.5, 0.5 M NaCl, 1 M imidazole

Buffer C – 100mM Tris-HCl, pH 7.5, 0.1 M NaCl

2.2.4.3. Nickel affinity chromatography

A HiLoad (GE Healthcare) column containing 50 ml metal chelating cellulose charged with Ni^{2+} (Bioline) was equilibrated with three column volumes of buffer A at a flow rate of 3 ml/min. The sample was then applied to the column via an injection “super loop” (GE Healthcare). Any unbound sample was removed by applying three column volumes of buffer A. Then a six column volume gradient to 100% buffer B was applied to the column, followed by a further two column

volumes of 100% buffer B. Fractions were collected throughout the entire protocol and the absorbance measured at 280 nm. Fractions were analyzed using SDS-PAGE. All columns were run on an ÄKTA Purifier (GE Healthcare).

2.2.4.4. Gel filtration chromatography

A Superdex 200 HiLoad 16/60 (GE Healthcare) gel filtration column (column volume 120 ml) was equilibrated with one column volume of buffer C at a flow rate of 1 ml/min. The sample was loaded and fractions were collected over the elution volume of one column volume and the absorbance measured at 280 nm. Fractions corresponding to protein peaks were analyzed using SDS-PAGE.

The Superdex 200 gel filtration column was calibrated with the protein standards ferritin (440 kDa), β-amylase (200 kDa), alcohol dehydrogenase (158 kDa), albumin (67 kDa), carbonic anhydrase (29 kDa) and cytochrome *c* (12.4 kDa). These standard proteins were applied to the column pre-equilibrated with 10 mM Tris-HCl, pH 8.0 and eluted with the same buffer. The void volume was determined using the protein standard Blue Dextran (2000 kDa). The elution profile (Appendix 7.1) was used to determine an approximate native molecular mass for the proteins using the calculations below.

$$K_{av} = \frac{V_e - V_o}{V_t - V_o}$$

Equation 2.1. Calculation of K_{av}. V_e = elution volume of the protein, V_o = void volume of the column (44 ml), V_t = total volume of the column (122 ml).

A rearrangement of the equation of the line from the calibration is used to calculate the log molecule weight from the K_{av} value.

$$\log MW = \frac{1.0185 - K_{av}}{0.3457}$$

Equation 2.2. Calculation of the log of the molecular weight.

2.2.4.5. Protein concentration

The protein was concentrated using an Amicon Ultrafiltration centrifugal concentrator (10 kDa cut-off PES membrane, Millipore, Cork, Ireland) at 4,000 x *g* and 4^{o}C.

2.2.4.6. SDS-PAGE

Protein was analyzed by SDS-PAGE following a modification of the method of (Laemmli, 1970). A gel containing a 6% stacking gel and a 12.5% separating gel was made and run using a Mini Protean II system (BioRad Labaratories Ltd)

2.2.4.6.1. Stock solutions

10 x SDS PAGE running buffer:-	36 g Tris-HCl, pH 8.8
	12 g SDS
	172.8 g Glycine
	Made up to 2 L with ddH_2O
Solution A:-	Acrylamide (30 %) Bisacrylamide (0.8 %) Solution
Solution B (Separating gel buffer):-	1.5 M Tris-HCl, pH 8.8
Solution C (Stacking gel buffer):-	0.5 M Tris-HCl, pH 6.8
Solution D:-	SDS 10 % w/v
SDS PAGE loading buffer:-	100 mM Tris-HCl, pH 8.0
	2 % β-mercaptoethanol
	4 % SDS w/v
	0.2 % Bromophenol blue w/v
	20 % Glycerol v/v
SDS PAGE non-denaturing loading buffer:-	100 mM Tris-HCl, pH 8.0
	0.2 % Bromophenol blue w/v
	20 % Glycerol v/v
SDS-PAGE Microwave Stain:-	1 g Coomassie Brilliant Blue (G250)
	1 L Methanol
	800 ml ddH_2O
	200 ml Glacial acetic acid

2.2.4.6.2. Preparation of gels

Separating Gels (12.5 %):-	4.2 ml A
	2.5 ml B
	1 ml D
	2.3 ml ddH_2O
Stacking Gel (6%):-	2.0 ml A
	2.5 ml B
	1 ml D
	4.5 ml ddH_2O

100 µl ammonium persulfate (APS) (10% w/v) and 10 µl N,N,N',N',-tetramethylethylenediamine (TEMED) was added to each gel mixture to initiate polymerisation before pouring between the glass plates.

The gel apparatus was assembled according to the manufacturer's instructions. Glass plates were placed in the gel casting apparatus separated by 1 mm spacers. The separating gel was poured between the glass plates to a depth of ~2/3rds and covered with water-saturated isobutanol. Once the gel had polymerized the isobutanol was removed, the gel washed with ddH_2O and blotted dry with filter paper. The stacking gel was then poured on the top of the polymerized separating gel to the top of the glass plates and a comb placed into the top forming the sample wells and the gel was left to polymerize.

2.2.4.6.3. Sample preparation

2 x SDS-PAGE loading buffer was mixed with the protein samples. The SDS buffer denatures the proteins and also adds a negative charge to the protein molecules that is proportional to mass. The loading buffer also contained β-mercaptoethanol to reduce any disulfide bridges within the proteins. The mixture was heated at 100^{o}C for 5 min to ensure the protein was fully denatured before being loaded onto the gel stacking layer. Once fully denatured the protein was capable of travelling through the gel at a distance proportional to its individual subunit molecular weight allowing for determination of molecular weight.

2.2.4.6.4. Sample preparation using non-reducing buffer

2 x non-reducing SDS-PAGE loading buffer was mixed with the protein sample. In this case, the buffer contained no reducing agents and was not heated therefore leaving any disulfide bonds intact. The mixture was left for 5 min at room temperature. The protein was then loaded onto the gel stacking layer.

2.2.4.6.5. SDS-PAGE running

The prepared samples were loaded into the gel wells using a 20 µl Hamilton syringe (Hamilton) additionally 5 µl of a molecular weight marker (Precision Plus Protein Standard 15 – 250 kDa, BioRad Laboratories, Appendix 7.2) was loaded as a molecular weight marker. The gel was run at 200 V for 50 min.

2.2.4.6.6. Gel staining procedure

The SDS-PAGE gel was removed from the gel tank apparatus and placed in the microwave stain solution and heated in the microwave on full power for 3 min. The gel was transferred to 1 L of ddH_2O and heated on full power for 20 min to destain.

2.2.4.7. Protein concentration determination using A280

The protein concentration was calculated by measuring the absorbance at 280 nm. A 200 µl aliquot of the protein solution was placed in a quartz cuvette with a 1 cm path length. The A_{280} measurement was taken in a Biotech UV1101 Photometer (Schimadzu), blanked against a cuvette containing all buffers and reagents apart from the protein. The protein's extinction coefficient was calculated using the protein sequence and the Protparam online bioinformatics tool (Wilkins *et al*., 1999) (www.expasy.ch/tools/protparam.html). The protein concentration was then calculated using Beer-Lambert Law (equation 2.3).

$$A = \varepsilon l c$$

Equation 2.3. Beer-Lambert Law: A is the Absorbance at 280 nm, ε is the extinction coefficient of the protein, *l* is the path length and *c* is the concentration.

2.2.5. Purification of native hPrxII

The method used to isolate and purify the native protein was reproduced from Schroder *et al.*, 1998. The purification of native hPrxII was achieved from out of date blood packs obtained through the Peninsula Medical School (Exeter).

2.2.5.1. Haemolysis and purification buffers

Haemolysis buffer:-	0.625 mM Tris-HCl pH 7.5
	5 mM EDTA
	20 µM Benzamidine (BAM)
	10 µM Phenylmethanesulfonylfluoride (PMSF)
Native hPrxII Purification Buffer A:-	20 mM Tris-HCl pH 7.5
	5 mM EDTA
	20 µM BAM
	10 µM PMSF
Native hPrxII Purification Buffer	20 mM Tris-HCl pH 7.5

B:-	
	5 mM EDTA
	20 µM BAM
	10 µM PMSF
	2 M NaCl
Native hPrxII Purification Buffer C:-	25 mM Tris-HCl pH 7.5
	1 mM EDTA
	20 µM BAM
	10 µM PMSF
	0.1 M NaCl

2.2.5.2. Preparation and haemolysis of erythrocytes

A 200 ml volume of blood was measured and centrifuged at 1,000 x *g,* 40 min and 4^{o}C in a Beckman JA-25.50 rotor to separate the plasma from the red blood cells. The red blood cell layer (bottom) was centrifuged again at 1,000 x *g,* 40 min and 4^{o}C in a Beckman JA-25.50 rotor to completely remove all the sera before haemolysis. The pellet was then suspended in 200 ml of haemolysis buffer and left over night at 4^{o}C. The haemolysate was centrifuged to remove cell debris at 13,700 x *g*, 90 min, and 4^{o}C in a Beckman JA-25.50 rotor.

2.2.5.3. Ion exchange chromatography of native hPrxII

A HiLoad column containing 250 ml of Fast Flow Q Sepharose media (FFQ) (GE Healthcare) was equilibrated with three column volumes of buffer A at a flow rate of 3 ml/min. The sample was loaded onto the column under gravity and unbound sample was eluted with buffer A until the flow through ran clear. The column was then connected to an ÄKTA purifier (GE Healthcare) and an elution was carried out over a six column volume linear gradient of 0–50% buffer B. Fractions were collected throughout the entire protocol and the absorbance measured at 280 nm. Fractions were analyzed using SDS-PAGE.

2.2.5.4. Size exclusion chromatography of native hPrxII

A Superdex 200 HiLoad 16/60 (GE Healthcare) gel filtration column (column volume 120 ml) was equilibrated with one column volume of buffer C at a flow rate of 1 ml/min. The sample was loaded and fractions were collected over the elution volume of one column volume and the absorbance measured at 280 nm. Fractions were analyzed using SDS-PAGE.

2.3. Results

2.3.1. Cloning of *hPrxII* gene

Plasmid DNA encoding *hPrxII* (V4Incorrect) was used as template DNA for PCR and the cloning of *hPrxII* was carried out as described in methods 2.2.1. The amplification of *hPrxII* resulted in a DNA band of the expected size (figure 2.4), which was successfully cloned into the expression vector pET28a. DNA sequencing results showed that the correct wild type *hPrxII* sequence had been obtained.

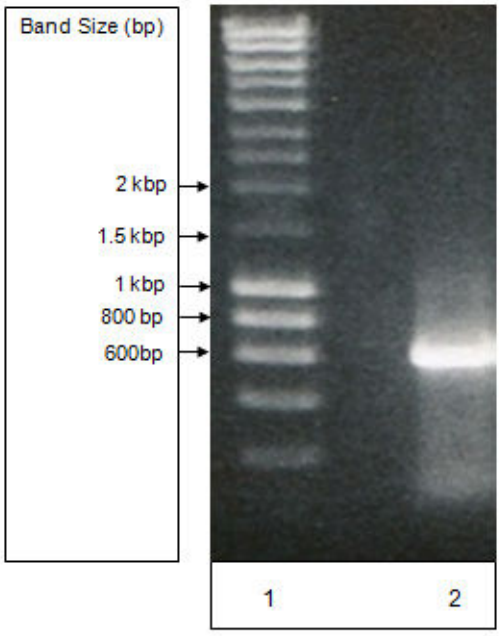

Figure 2.4. 1% agarose gel showing the PCR amplification of the *hPrxII* gene. Lane 1, Marker (Hyperladder 1, BIOLINE (Appendix 7.3)); Lane 2, *hPrxII* PCR band at ~600 bp.

2.3.2. Expression of recombinant hPrxII

The pET28a/*hPrxII* construct was transformed into the *E. coli* strain Rosetta Gami 2. Rosetta Gami 2 was chosen as it aids disulfide bond formation through mutations in the thioredoxin B (*trxB*) and glutathione oxidoreductase (*gor*) genes. As the hPrxII protein contains an intra-molecular disulfide bond in its reaction mechanism, it was thought that the promotion of this oxidation state might aid protein stability. hPrxII protein expression was under the control of the T7 promoter and was induced by IPTG. The over-expression of hPrxII was investigated by induction studies to obtain the best conditions for over-expression. The optimal over-expression was achieved by addition of a final concentration of 1 mM IPTG when the cells had reached an OD_{600nm} of 0.8 with

further incubation for 4 hours at 37°C. The over-expression of hPrxII resulted in soluble protein being produced at the expected size (~24 kDa).

2.3.3. Purification of recombinant hPrxII

One litre of culture produced 2.1 g of cell paste and after cell lysis and centrifugation (as described previously see section 2.2.4.1) the supernatant was purified using nickel affinity chromatography and gel filtration chromatography as described in methods 2.2.4.3 and 2.2.4.4.

2.3.3.1. Nickel Affinity Chromatography

The clarified cell extract was applied to a nickel column as described in methods 2.2.4.3 (figure 2.5). The fractions were analyzed using SDS-PAGE as described in methods 2.2.4.6 (figure 2.6 and 2.7). The fractions containing hPrxII were pooled and concentrated (methods 2.2.4.5) for gel filtration chromatography.

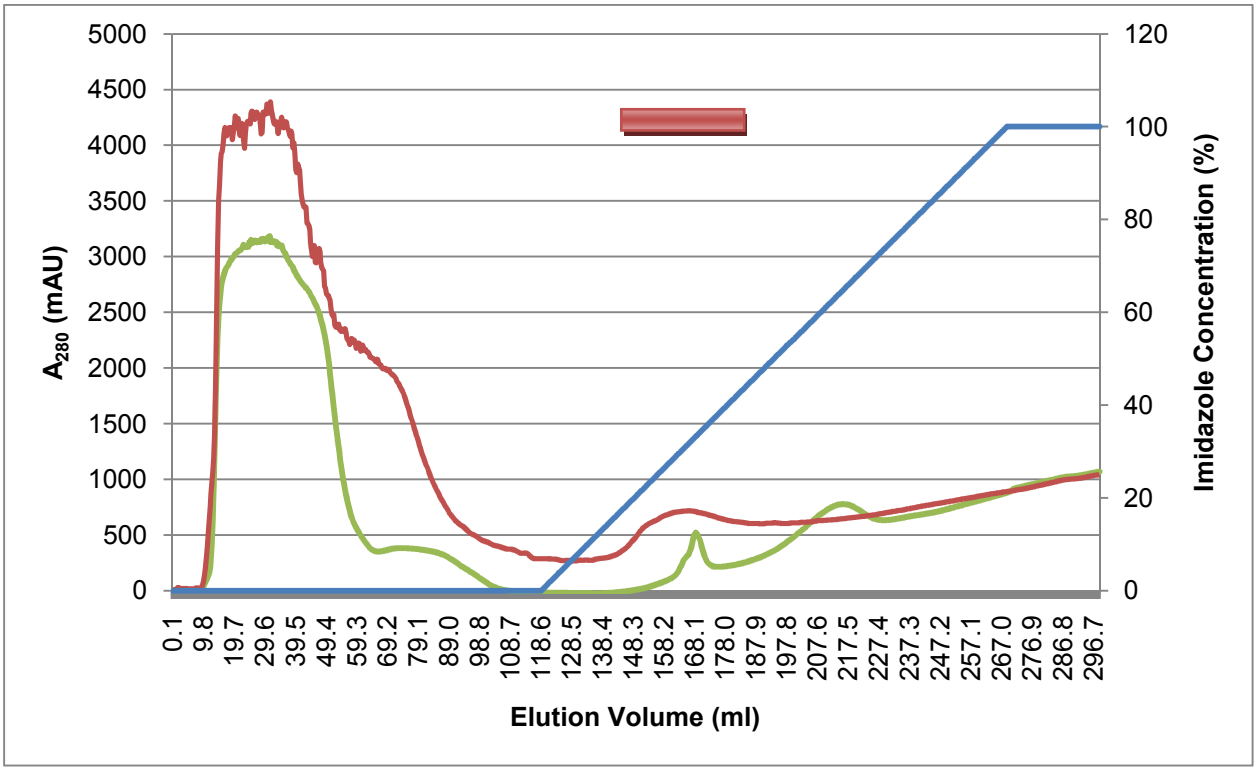

Figure 2.5. Elution profile of hPrxII (4Gcorrect) (red line) and (4Vincorrect) (green line) from nickel affinity chromatography. 10 ml fractions were collected throughout the entire elution. The blue line shows the % imidazole concentration. The fractions that showed a band of the correct size on SDS-PAGE (figure 2.6) are indicated by a red bar.

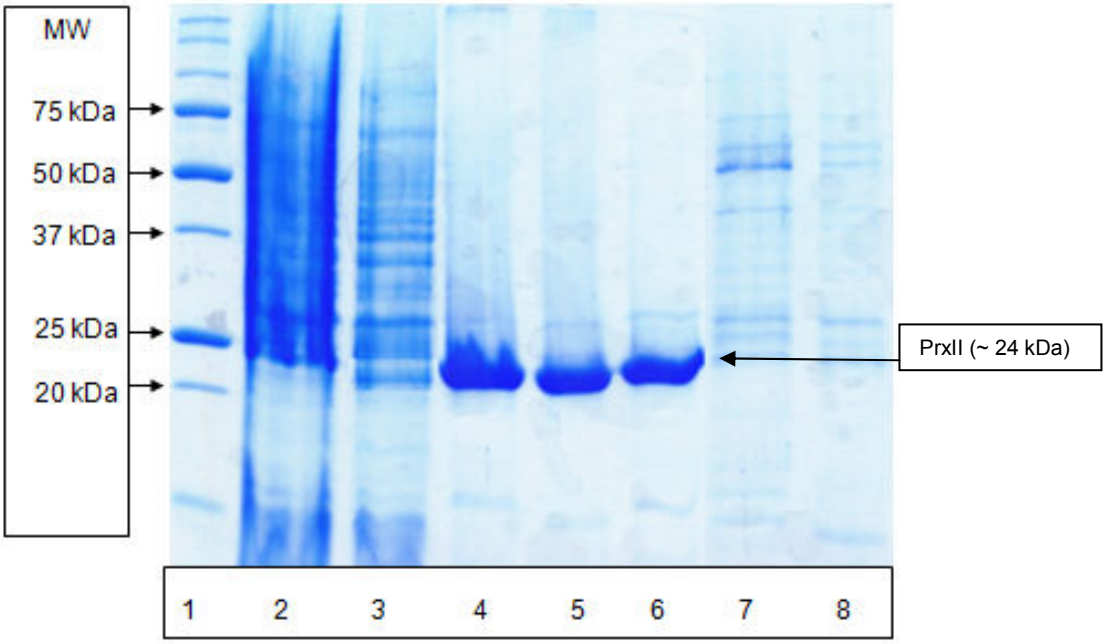

Figure 2.6. SDS-PAGE analysis of the hPrxII (4Vincorrect) nickel affinity column elution. Lane 1, molecular weight marker; Lane 2, sample loaded on to the column; Lane 3, sample from 20 ml; Lane 4, sample from 160 ml; Lane 5, sample from 170 ml; Lane 6, sample from 180 ml; Lane 7, sample from 210 ml; Lane 8, sample from 220 ml.

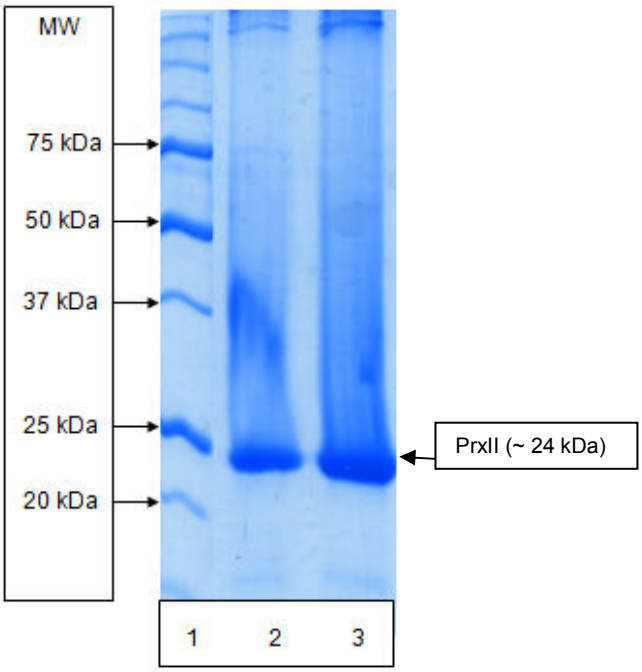

Figure 2.7. SDS-PAGE analysis of the hPrxII (4Gcorrect). Lane 1, molecular weight marker; Lane 2, sample from 160 ml; Lane 3, sample from 170 ml.

2.3.3.2. Gel filtration chromatography

Gel filtration chromatography was used as a final step of the purification and as a tool for the estimation of the molecular weight of the protein. The concentrated protein sample was loaded onto an equilibrated HiLoad 16/60 Superdex 200 and run as described in methods 2.2.4.4. The elution profiles for both hPrxII (4Vincorrect and 4Gcorrect) are shown in figure 2.8. The peak fractions were analyzed by SDS-PAGE and those that contained hPrxII were pooled and concentrated.

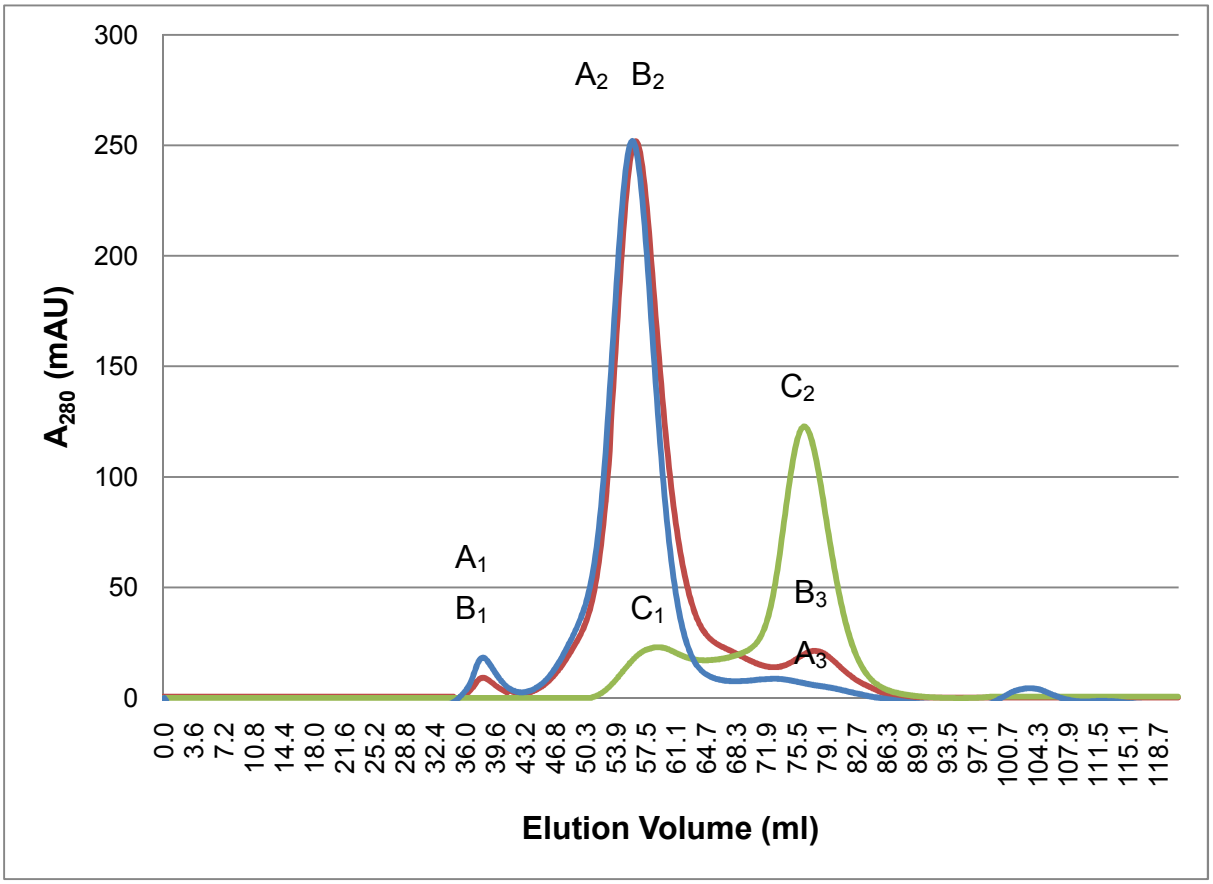

Figure 2.8. The elution profile from the Superdex 200 gel filtration column for hPrxII (4Gcorrect) (red line), hPrxII (4Vincorrect) (green line) and native hPrxII (blue line). Fractions were collected at 1 ml intervals throughout the elution volume. Peak A_1 and B_1 (~38 ml) correspond to the void volume; Peak C_1, A_2 and B_2 (~58 ml) correspond to the decameric form of hPrxII; Peak A_3, B_3 and C_2 (~76 ml) correspond to the dimeric form of hPrxII. The oligomeric state was determined using a calibrated Superdex 200 column (Appendix 7.1).

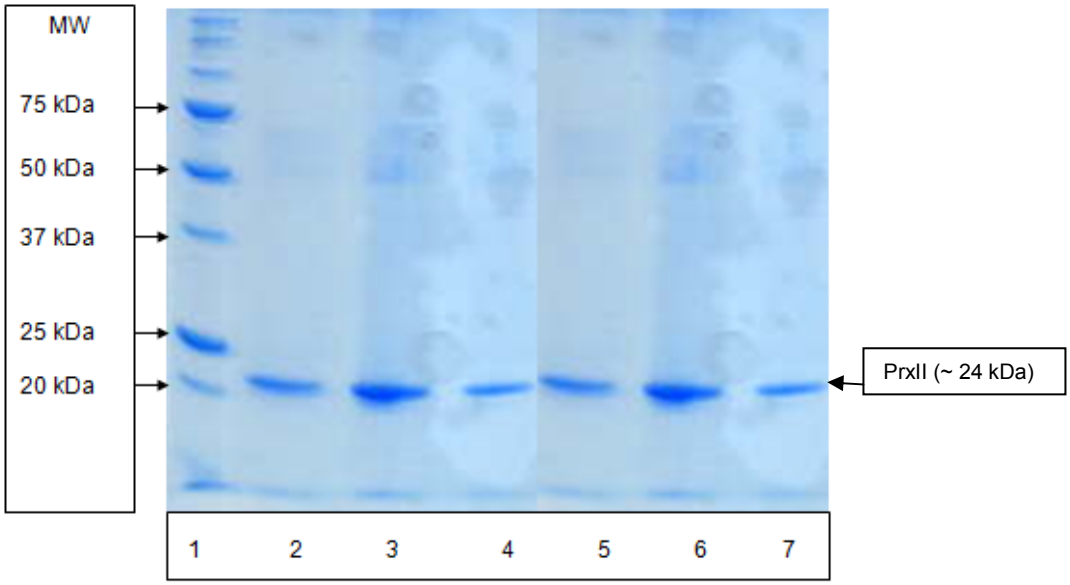

Figure 2.9. SDS-PAGE analysis of peaks from gel filtration chromatography of hPrxII (4Gcorrent), hPrxII (4Vincorrect) and native hPrxII. Lane 1, molecular weight marker; Lane 2, sample from peak A_2; Lane 3, sample from peak B_2; Lane 4, sample from peak C_1; Lane 5, sample from peak C_2; Lane 6, sample from peak A_3; Lane 7, sample from peak B_3.

2.3.3.3. Overview of purification of hPrxII (4Gcorrect) and hPrxII (4Vincorrect)

The purification of both hPrxII proteins was successfully achieved using nickel affinity and gel filtration column chromatography (Superdex 200), however, these proteins showed different properties during purification as well as exhibiting different oligomeric states.

The molecular weight of the hPrxII monomer is known to be ~24 kDa. It was seen that hPrxII (4Vincorrect) is produced mainly in the dimeric form with a small percentage of it being produced in the decameric form, whereas hPrxII (4Gcorrect) is produced mainly in the decameric form with a small percentage of it being produced in the dimeric form. The elution profile for hPrxII (4Gcorrect) is similar to that seen during the purification of the native protein obtained from blood (as seen in figure 2.12).

Both proteins were very different during the purification in terms of stability. hPrxII (4Vincorrect) was very unstable during the purification. The protein would aggregate very quickly between purification steps; this aggregation meant that it was not possible to be concentrate the protein. Ammonium sulfate precipitation

and storage at -20°C would also result in aggregation. hPrxII (4Gcorrect) was much more stable during purification. The protein could be stored at 4°C for 4 days and -20°C for up to a month without aggregation or degradation (confirmed by gel filtration chromatography and SDS-PAGE (data not shown)). The protein was amenable to concentrations in excess of 20 mg/ml.

2.3.4. Purification of native hPrxII

2.3.4.1. Ion exchange chromatography of native hPrxII

The haemolysate was applied to a FFQ column as described in methods 2.2.5.3 producing the trace seen in figure 2.10. The fractions were analyzed using SDS-PAGE as described in methods 2.2.4.6 (figure 2.11).

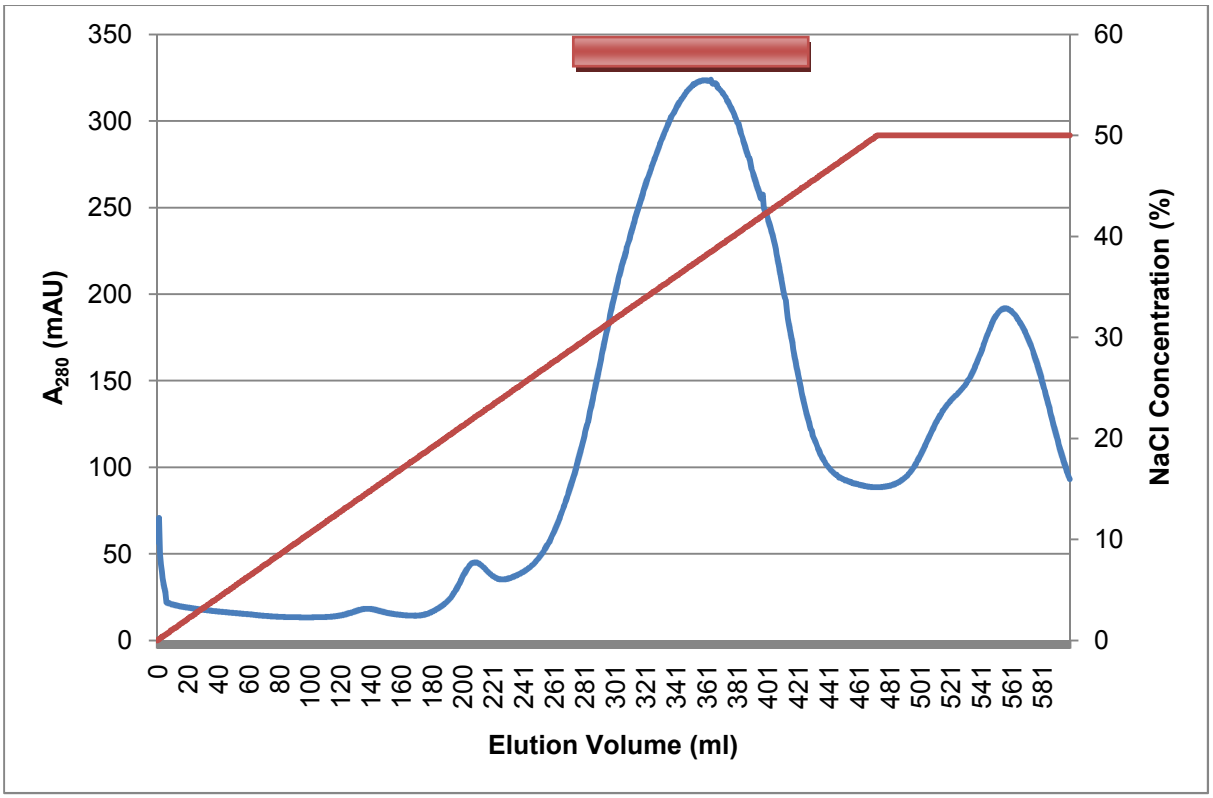

Figure 2.10. Elution profile of native hPrxII (blue line) from ion exchange chromatography. 10 ml fractions were collected throughout the entire elution. The red line shows the NaCl concentration. The fractions that showed a band of the correct size on SDS-PAGE are indicated by the red bar. The second peak showed protein but not hPrxII (SDS-PAGE result not shown).

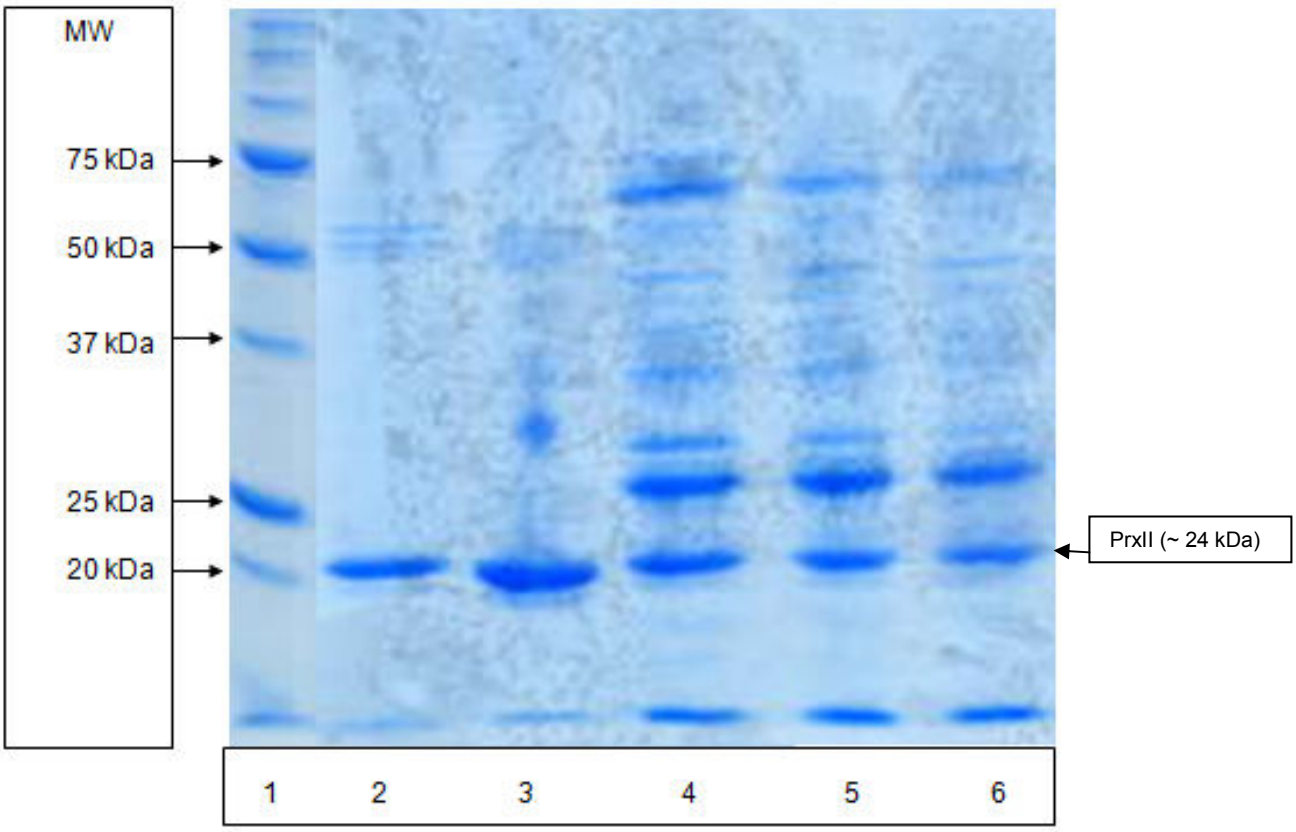

Figure 2.11. SDS-PAGE analysis of peaks from the ion exchange chromatography of native hPrxII. Lane 1, molecular weight marker; Lane 2, sample from column elution (300 ml); Lane 3, sample from column elution (340 ml); Lane 4, sample from column elution (360 ml); Lane 5, sample from column elution (380 ml); Lane 6, sample from column elution (400 ml);.

2.3.4.2. Gel filtration chromatography of native hPrxII

Gel filtration chromatography was used as a final step of the purification and as a tool for estimation of the oligomeric state of the protein. A concentrated protein sample was loaded onto an equilibrated HiLoad 16/60 Superdex 200 (GE Healthcare) and run as described in methods 2.2.4.4.

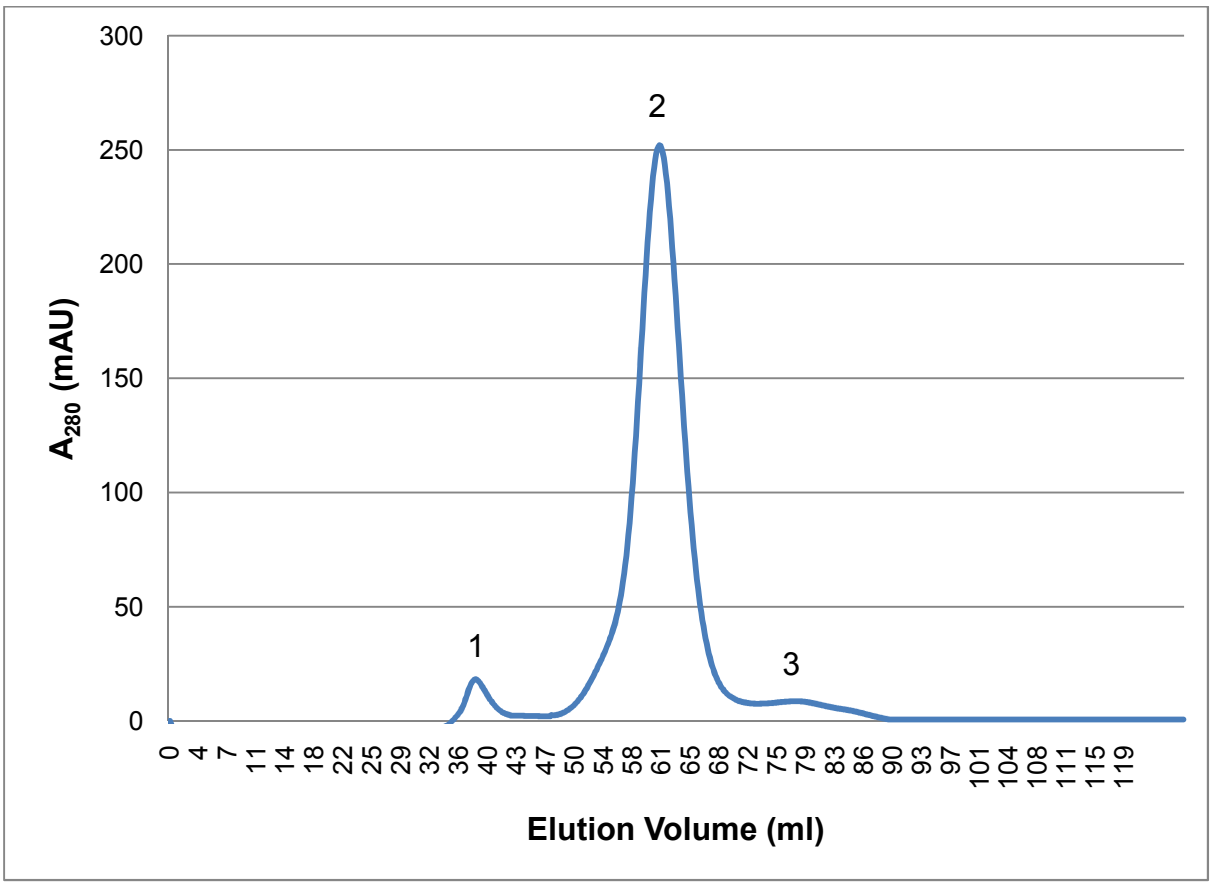

Figure 2.12. The elution profile for native hPrxII from gel filtration chromatography. Peak 1 (36 ml) corresponds to the void volume of the column; Peak 2 (62 ml) corresponds to the decameric form of the protein (~250 kDa); Peak 3 (78 ml) corresponds to the dimeric form of the protein (~48 kDa).

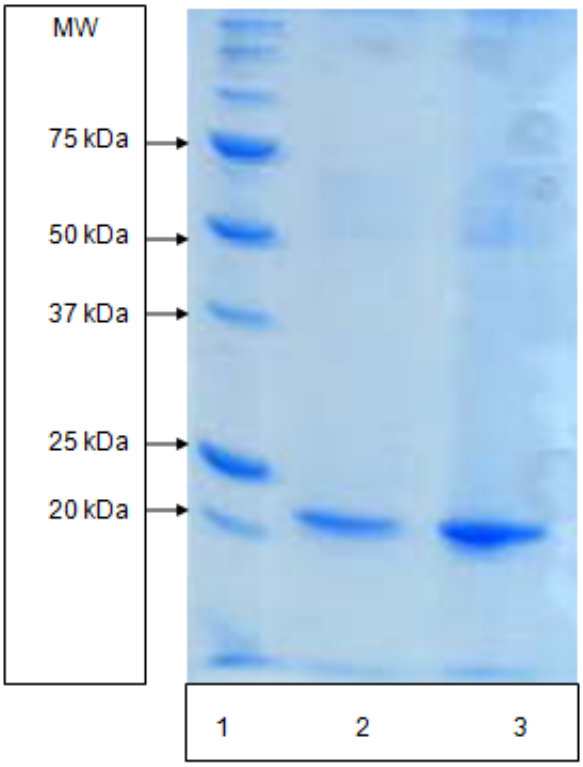

Figure 2.13. SDS-PAGE analysis of the peaks from gel filtration chromatography. Lane 1, molecular weight marker; Lane 2, sample from peak 2 (62 ml); Lane 3, sample from peak 3 (78 ml).

2.3.4.3. Overview of purification of native hPrxII

The purification of native hPrxII was successfully achieved using FFQ Sepharose and gel filtration chromatography. The trace from FFQ chromatography produced two peaks with the first containing the native hPrxII protein. The calibrated gel filtration column showed the protein to be mainly produced in the decameric form. Using this method ~20 mg of protein was purified from 500 ml of blood.

2.4. Discussion

During the early studies on recombinant hPrxII a number of difficulties were encountered during purification and concentration. It was discovered that there was a point mutation in the DNA sequence and consequentially the fourth amino acid in the protein sequence was a valine residue rather than a glycine residue as found in the native enzyme. Glycine is the simplest and smallest amino acid with only a hydrogen atom as the side chain, whereas valine is a branched-chain amino acid with hydrophobic properties. Looking at the two residues it was observed that this mutation might affect the some local properties of the protein chain but the broader changes to solubility and oligomeric state were not predicted. A valine insertion is known to affect the properties of some proteins due to its hydrophobic nature, for example the substitution of a glutamic acid for a valine in haemoglobin is the cause of sickle cell disease (Blouin *et al*., 2000).

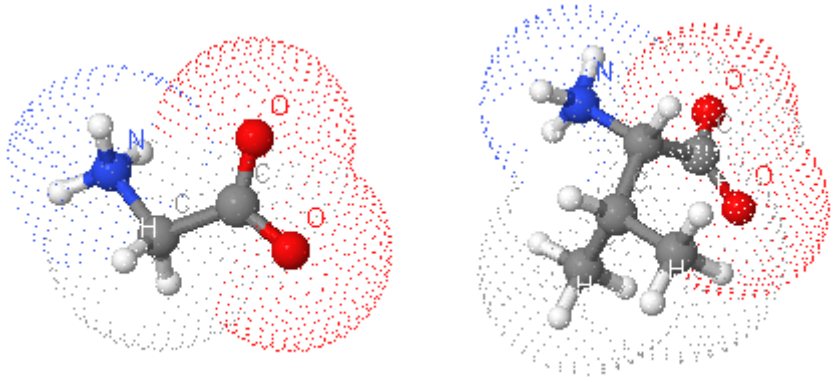

Figure 2.14. Comparison of the structure and the van der Waals surface of glycine and valine.

The mutation was first investigated using the MUpro software (Cheng *et al*., 2006) which can help predict protein stability changes based on single amino acid mutations using the sequence information. Although the MUpro software predicted an increase in stability due to this amino acid change, the software only looks at a single monomer of the protein and not at the active oligomer.

To look at the effects that this mutation might have on the oligomerisation of the protein the 3D structure of the protein (PDB: 1QMV) was analyzed using the

program PyMol (Delano Scientific). The amino acid was changed from a glycine to a valine using the PyMol mutagenesis wizard (Figure 2.15 and Figure 2.16).

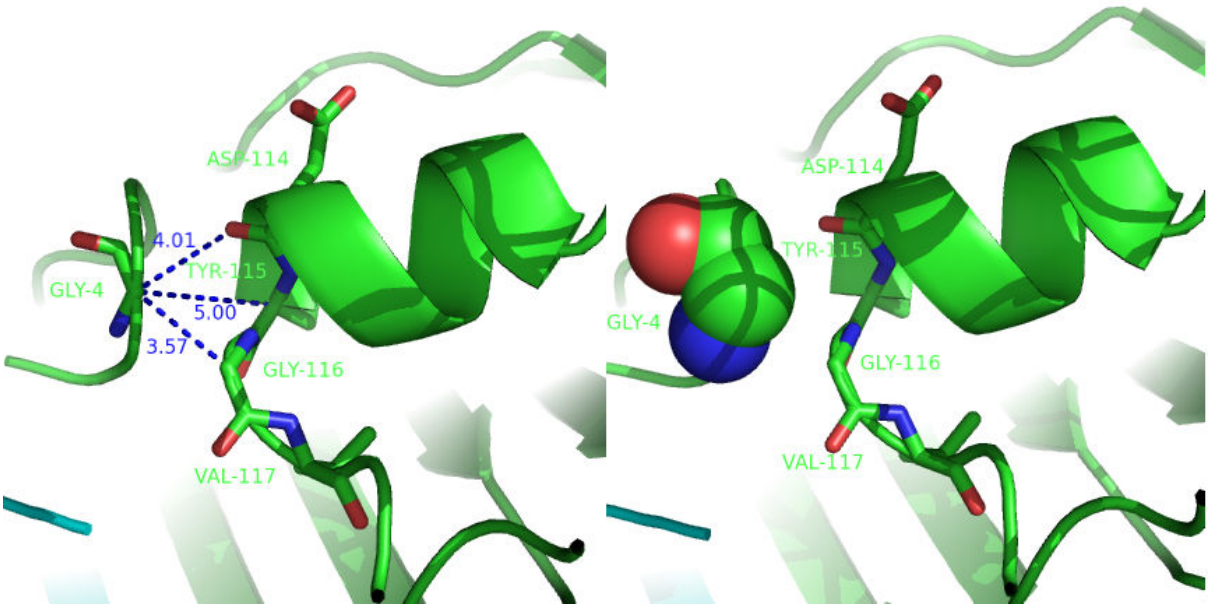

Figure 2.15. Cartoon representation of the location of the fourth residue glycine in relation to helix α4 (of the same subunit) in the native hPrxII and hPrxII (4Gcorrect) enzyme. The fourth residue glycine is shown in stick mode (left hand side) and sphere mode (right hand side) along with 4 residues on helix α4 and the loop associated with it. The glycine residue is ~3.5 – 5 Å away and due to its lack of a side chain will not interact with helix α4. (PDB: 1QMV) (Figure created using PyMol DeLano Scientific).

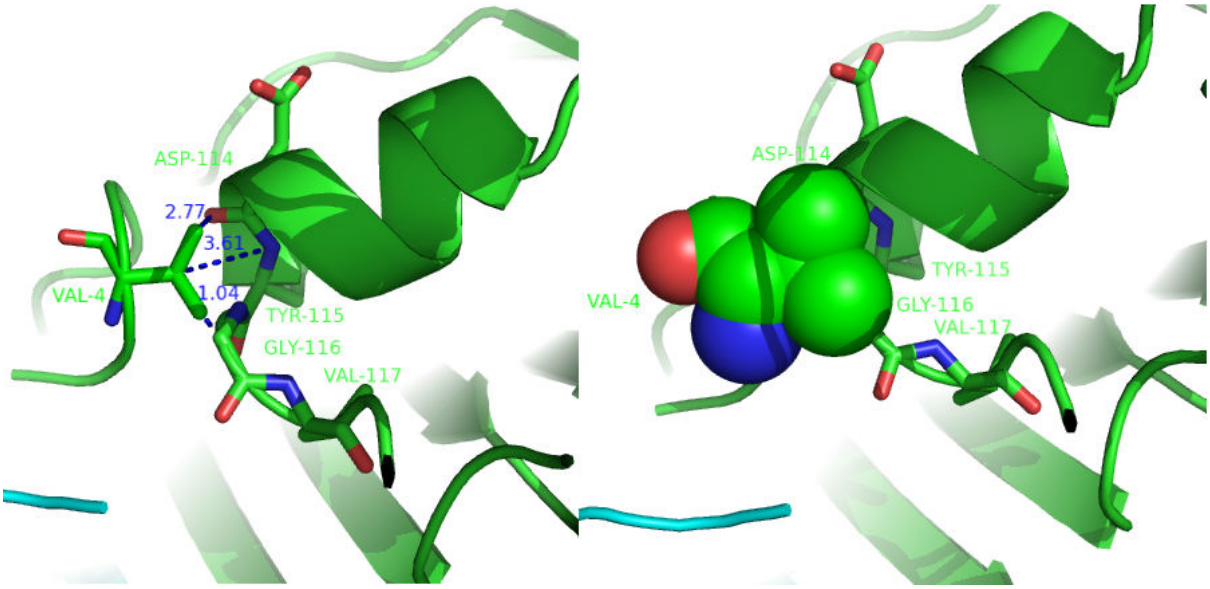

Figure 2.16. Cartoon representation of the location of the fourth residue valine in relation to helix α4 (of the same subunit) in the native hPrxII and hPrxII (4Vincorrect) enzyme. The fourth residue glycine is shown in stick mode (left hand side) and sphere

mode (right hand side) mode along with 4 residues on helix α4 and the loop associated with it. The valine residue can be seen interfering with the helix α4 (of the same subunit), (PDB: 1QMV) (Figure created using PyMol DeLano Scientific).

The fourth residue valine is shown interacting with helix α4 and the loop associated with it. The larger valine molecule is now much closer to the loop and helices and could cause a conformational change pushing the helices further away.

The dimer-dimer interface in the peroxiredoxin decamer has mainly hydrophobic interactions with some water-mediated hydrogen bonding. The major residues that interact to hold the dimers in place are Phe47, Phe81, Thr82, Val107, Arg109 and Asp121 (Figure 2.17) (Schroder *et al.*, 2000).

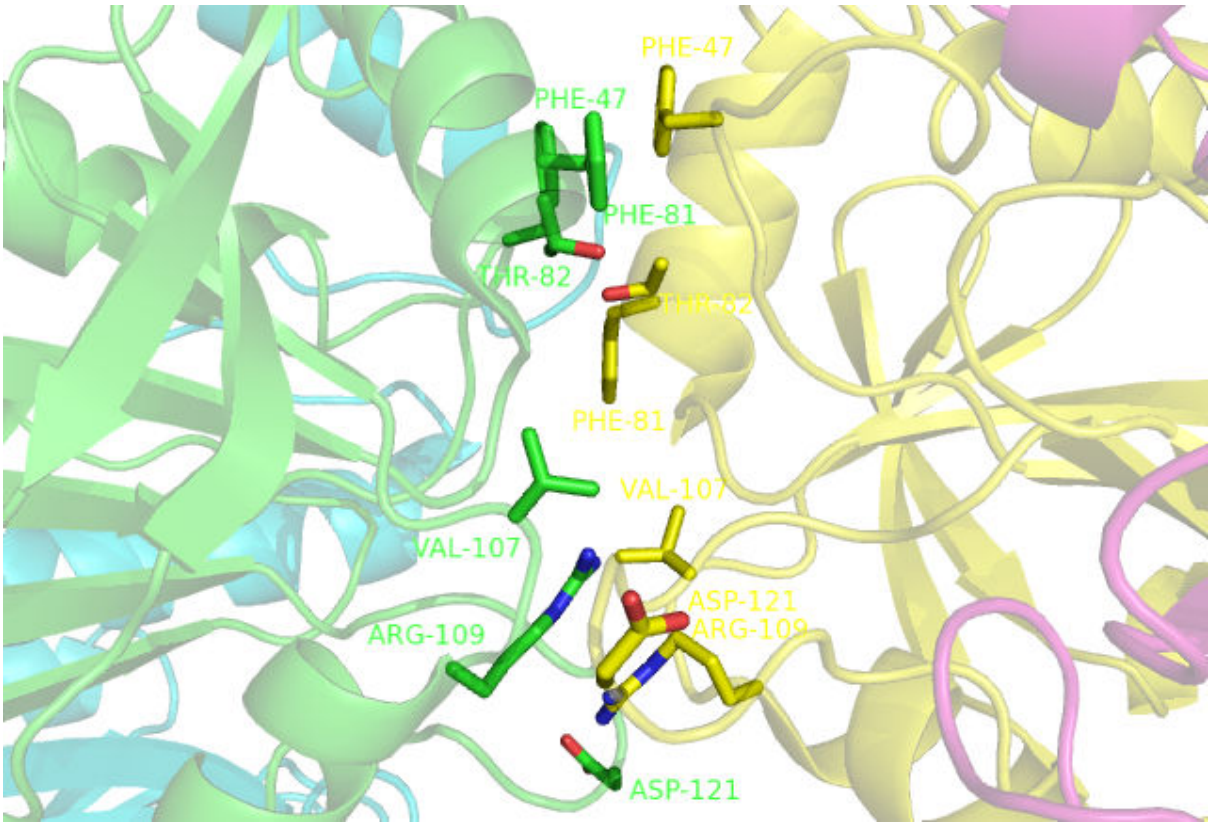

Figure 2.17. Cartoon representation of the interface between two dimers in the native hPrxII decameric structure. The residues in stick mode represent the residues that are involved in the interactions between dimers (PDB: 1QMV). (Figure created in PyMol DeLano Scientific).

Looking at the quaternary structure of the protein, it is seen that the mutated fourth residue is located on a loop region that sits at the bottom of helix α4. It is hypothesized that when the mutation from the small glycine to the bulkier hydrophobic valine is present there is no longer enough space for the relatively larger valine residue to fit in the natural position. This could cause a shift in the position of helix α4 and the attached loop that would lead to a breakdown in the hydrophobic interactions between the dimer:dimer interface residues (Figure 2.18). This theory could be used to explain why the mutant protein produced is mainly in the dimeric form instead of the decameric form, as this conformational change, caused by the mutation, could easily disrupt the dimer:dimer interface while leaving the monomer-monomer interface intact.

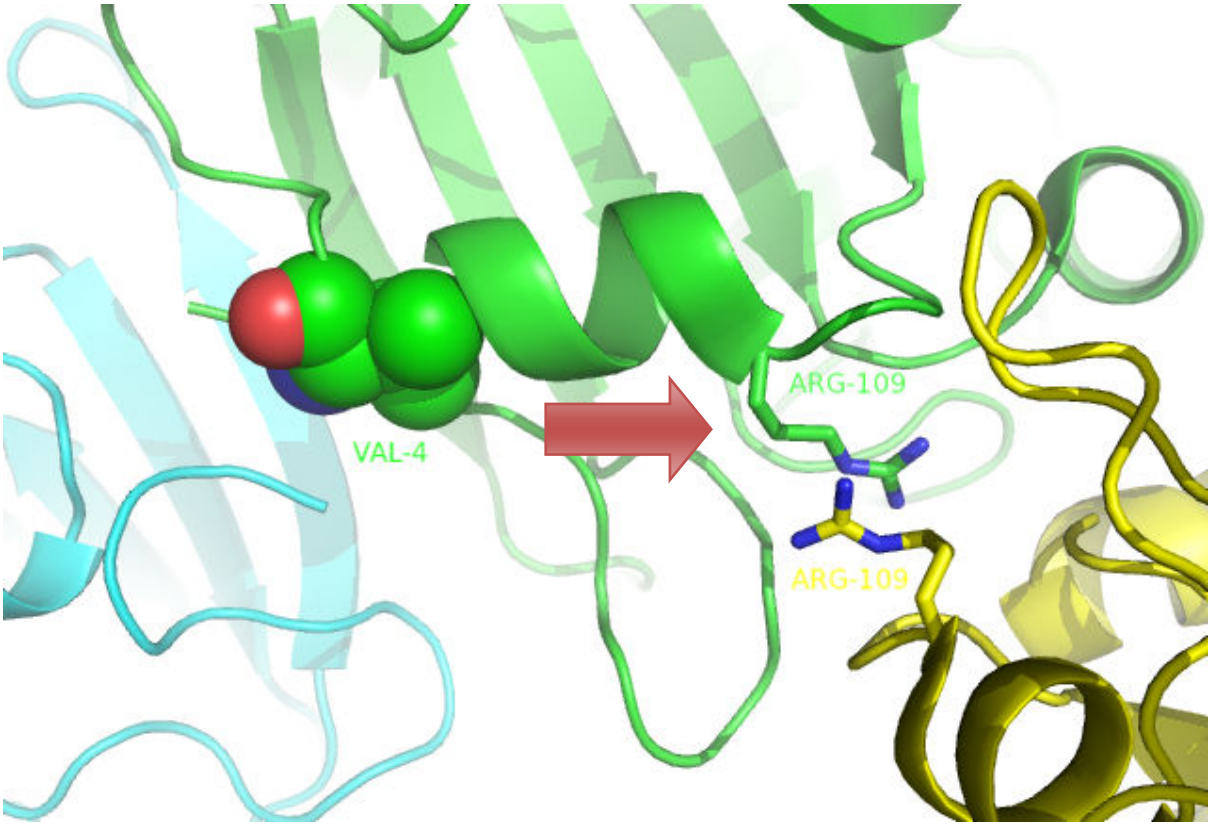

Figure 2.18. Cartoon representation of the potential movement in helix α4 caused by the mutation in the protein sequence to Val4 (sphere mode). The molecule is coloured according to chain and shows the Arg109 (stick) residues involved in the dimer:dimer interface. The arrow represents the proposed direction of the movement of helix α4 (PDB: 1QMV). (Figure created in PyMol DeLano Scientific).

It is hypothesized that the fourth residue valine could cause a movement of α4 in the direction of the dimer:dimer inteface (direction shown by an arrow in figure 2.18). If this conformational change was to occur it could cause a disruption in the dimer:dimer interface at Arg109. This disruption in the dimer:dimer interface could cause the breakup of the decameric structure to dimers.

The conversion of this valine residue back to a glycine caused a change in the protein's behavior during purification. The protein was over-expressed and purified mainly in the decameric form and the protein was able to be concentrated to the concentrations required for crystallization.

3. Crystallization and structure determination of the disulfide state of hPrxII

3.1. Introduction

The crystal structure of a decameric form of hPrxII from erythrocytes was previously determined to 1.7 Å resolution at the University of Exeter (Schroder *et al*., 2000). The structure revealed that hPrxII is a toroid formed from five dimer units. As part of the mechanism of this enzyme, the peroxidatic cysteine (Cys51) forms an intermolecular disulfide bond with the resolving cysteine (Cys172) from another monomer (Wood *et al*., 2003b). In the crystal structure of hPrxII the peroxidatic cysteine is found in the hyper-oxidized sulfinic acid form. In this sulfinic acid form the peroxidatic and resolving cysteine are found to be ~10 Å apart. In order for the intermolecular disulfide to be formed there would have to be some structural movement to allow them to be close enough for the bond to form.

3.1.1. hPrxII disulfide state

The disulfide decamer has been seen in the native protein from both out of date blood packs and fresh blood (Line *et al*., 2009, manuscript in preparation). The oligomeric state of the hPrxII enzymes has been proposed to alternate between the decameric and dimeric forms depending on the oxidation state of the peroxidatic cysteine (Wood *et al*., 2002b). It was hypothesized when looking at the crystal form of the native hPrxII from human erythrocytes that the formation of the disulfide state could result in a breakdown of the dimer-dimer interface (Schroder *et al*., 2000). This would mean that when the disulfide state was formed the hPrxII decamer would break down producing five homodimers.

3.1.2. Producing the protein in the disulfide state

One strategy for the production of proteins in the disulfide state was to place the plasmid in the Rosetta-gami 2 pLysS (DE3) (Novagen) cell line. This cell line is designed to aid disulfide bond formation through mutations in the thioredoxin reductase (*trxB)* and glutathione reductase (*gor)* genes. These mutations prevent the production of thioredoxin B and the glutathione reductase enzymes which are responsible for the reduction of disulfide bonds. A way to induce recombinant enzymes to produce an intermolecular disulfide bond is the addition of the reagent diamide (figure 3.1) to convert the thiol thiolate sulfhydryl

group (XSH) to a disulfide (XSSX) (Kosower *et al*., 1969; Kosower *et al*., 1995). Diamide has also previously been used to form the oxidized disulfide form of the hTrx protein (Andersen *et al*., 1997).

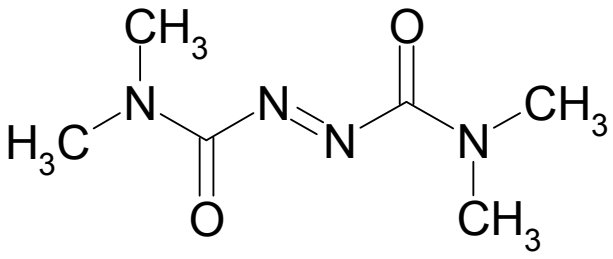

Figure 3.1. The structure of the thiol oxidizing agent diamide.

3.1.3. Protein crystallography

The production of protein crystals can be achieved by allowing the protein to reach a state of super-saturation when being brought out of solution by addition of a precipitant. This can be achieved by the variation of conditions including protein concentration, precipitant concentration and pH. The most common precipitants are ammonium sulfate and polyethylene glycol (PEG).

Crystallization can be further explained by looking at the phase diagram (see figure 3.2). The phase diagram shows the solubility of the protein as a function of the crystallization conditions. This consists of an under-saturated zone in which crystal growth will not occur as the protein is fully dissolved. In the metastable zone crystal growth is most likely and crystals grown are usually stable. The nucleation zone is a zone of lower super-saturation and the zone in which crystals are also known to grow. Proteins going above this zone will precipitate out although crystal growth in this zone is not impossible (Asherie, 2004). As the protein crystal grows the protein concentration in solution will decrease bringing the phase diagram back into the metastable zone.

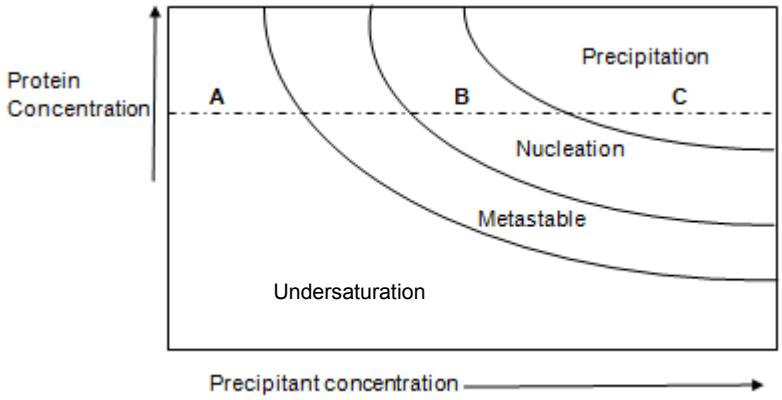

Figure 3.2. The phase diagram showing the solubility of the protein as the precipitant concentration changes. At point A the protein will stay under-saturated. At point B the protein will crystallize and the concentration of the protein in solution drops to saturation as the crystal grows. At point C the protein will precipitate out but crystals may still grow. Figure adapted from Asherie (2004).

There are several different methods of crystallization such as microbatch and vapour-phase diffusion. Microbatch experiments are where the protein and precipitant are mixed directly under oil. In the true microbatch method there is little to no diffusion as H_2O cannot travel through the paraffin oil placed on top of the droplet (Chayen *et al*., 1992; Brumshtein *et al*., 2008). In this method protein crystallization requires that the precipitant concentration is correct for crystal formation. Microbatch crystallization using Al's oil (50/50 paraffin/silicon oil mix) shows some diffusion increasing the concentration of precipitant and protein and is similar in this way to vapor diffusion.

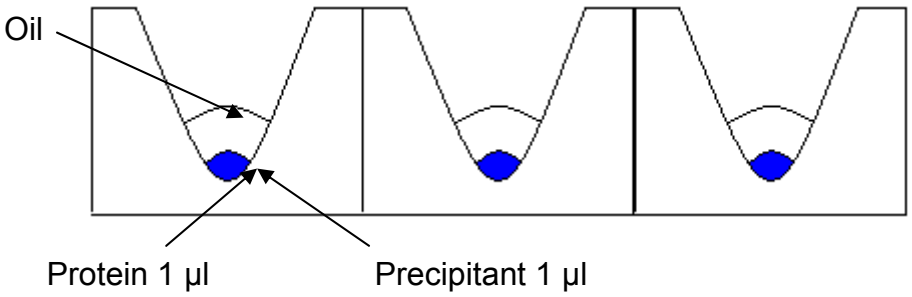

Figure 3.3. The microbatch crystallization setup in a 96 well plate with 1 µl of protein and 1 µl of precipitant mixed directly under oil.

Vapor diffusion consists of a reservoir which contains the precipitating condition that is separated from the protein droplet mixed with a small volume of

precipitant. Water will diffuse from the droplet to the reservoir bringing about equilibrium with the precipitant in the reservoir. This increase in precipitant and protein concentration within the drop can bring the protein into the super-saturation state. As protein crystals begin to grow the solution is brought into the metastable crystal growth zone.

3.1.4. X-ray crystallography

X-rays can be used to determine the 3D structure of a protein. Typically X-rays with a wavelength between 0.5 and 1.6 Å are used as these wavelengths are comparable to the interatomic distances in protein crystals. They also should suitably penetrate and should be scattered strongly enough by the crystals. The X-rays are “shot” onto the crystal and a diffraction pattern is produced according to the different properties of the crystal. The diffraction patterns are used to determine the three dimensional structure of the proteins.

A typical crystal is made up of a regular repeating array of unit cells that amplify the X-ray diffraction patterns. The unit cell is defined by three lengths (*a*, *b*, and *c*) and its three angles (alpha, beta, gamma) and the more unit cells that are present within the crystal the stronger the resulting diffraction. The crystal can be thought of as being divided into a number of planes that run through the unit cell. These planes have various orientations and spacing between them. The diffraction pattern is made up of a number of individual reflections (spots); the spots correspond to the diffraction from the crystal planes.

Bragg’s law (Bragg, 1913) helps us to understand the relationship between the diffraction pattern and the spacing of the crystal planes. Bragg’s law describes the relationship between the reflection angle (θ), the distance between the planes (d) and the wavelength (λ) shown in equation 3.1.

$$n\lambda=2d\sin\theta$$

Equation 3.1. Bragg’s law: n is an integer, λ is the wavelength of the radiation, d is the spacing between the lattice planes and θ is the angle of incidence of the X-ray beam.

Bragg’s law treats all the planes that run through the crystal as mirrors that can reflect the X-rays and these reflections give rise to the reflection spots. The X-rays will add up constructively if they start in phase and arrive at the crystal plane in phase. Constructive diffraction will occur according to Bragg’s law

within a crystal with two planes separated by distance (d) if the difference in path length ($2d\sin\theta$) between the waves is equal to the integer number of wavelengths (figure 3.4).

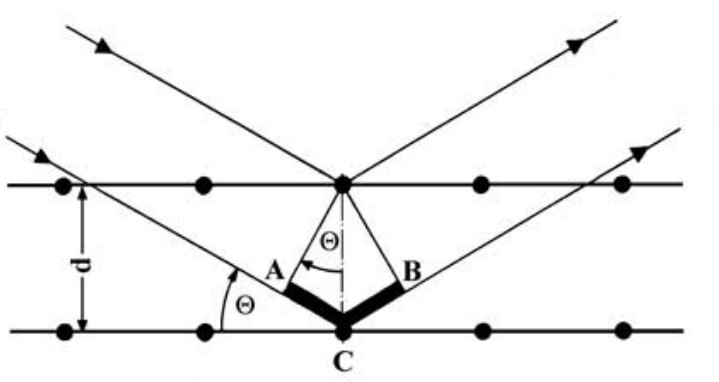

Figure 3.4. Conditions that satisfy Bragg's law. Figure adapted from Asherie (2004).

From this we can observe that the shorter the spacing between the crystal planes then the greater the angle of diffraction. The various lattice planes that divide the crystal across its three dimensions (*a*, *b* and *c*) are described by a set of Miller indices (*h*, *k*, and *l*). A value of the reflection angle (θ) can be calculated using simple trigonometry and from this the spacing (d_{hkl}) can be calculated. This spacing will allow the dimensions of the unit cell to be calculated.

During data collection the crystals were rotated because for a stationary crystal only a limited number of the crystal planes will satisfy Bragg's law and therefore produce a diffraction pattern. Rotating the crystal should allow data to be collected from all the crystal planes. This is better explained by the Ewald's sphere, which describes Bragg's law in three dimensions. Ewald's sphere places the crystal at the centre and has a radius of $1/\lambda$. Each reciprocal lattice point has a position relative to its family of crystal planes, which are located at a vector from the crystal with a length that is inversely proportional to the d spacing. A diffraction spot is produced if the lattice point lies on the surface of the sphere (figure 3.5). When the crystal is rotated so are the reciprocal lattice points. This changes the points that lie on the sphere's surface and this should produce all the required reflections.

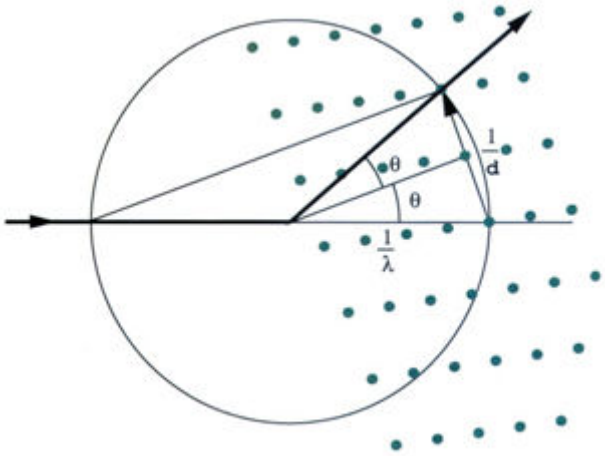

Figure 3.5. Ewald's Sphere. Figure adapted from Dauter (1999)

The X-ray diffraction data is used to calculate the electron density throughout the unit cell. The intensity of each spot is proportional to the amplitude of the diffracted X-ray waves. Phase information is recalculated using other methods, as it is lost during data collection. By combining the amplitude ($|F_h|$) and phase ($i\alpha h$) of the reflections a structure factor (F) can be obtained. The total structure factor (equation 3.2) can be described by all the atomic structure factors (f_j) described by their Miller indices. The structure factor is related to the electron density resulting from the diffracted X-rays by a mathematical Fourier transformation.

$$F_{hkl} = \left| F_h \right| \exp[i\alpha h] = \sum_j f_j \, exp2\pi i(\mathrm{hx_j} + \mathrm{ky_j} + \mathrm{lz_y})$$

Equation 3.2. The structure function equation.

Using the inverse Fourier transform of all the structure factors from each of the Miller indices the electron density for all the positions in the unit cell $\rho(x,y,z)$ can be calculated (equation 3.3).

$$\rho(x,y,z) = \frac{1}{V}\sum_{hkl} \mathrm{F_{hkl}} \exp[-2\pi i\,(\mathrm{hx} + \mathrm{ky} + \mathrm{lz})]$$

Equation 3.3. Calculation of the electron density in a crystal.

The phase information that is lost during data collection can be determined in a number of different ways. One of these is molecular replacement where a

model is used that typically has a sequence homology of 25% or greater to that of the unknown structure. This model is then used to make estimations about the initial phases. Molecular replacement is based upon properties of the Patterson map, which is a Fourier transform of the squared amplitudes with the phases set to zero. Patterson maps are calculated for both the model and the unknown structure. A rotation function is then calculated by rotating the map for the model and scoring for a fit to the map calculated from the diffraction pattern (Crowther and Blow, 1967). The highest score occurs when the structures are in a similar orientation. Next a translation function is used where the model is positioned at all the possible positions within the unit cell of the unknown structure and a statistical correlation of the Patterson functions is calculated for each translational movement. Positions that possess a high correlation are output as positional coordinates (Evans and McCoy, 2008).

If the molecular replacement method is not available then another method must be used to solve the phase problem. Heavy atoms can be bound to specific sites within the molecule that can significantly alter the scattering and the structure factors. The amplitudes of reflections are calculated for the crystals with and without the heavy atom and the differences between the Patterson functions allow calculation of the phases. This technique is known as single or multiple isomorphous replacement.

Multi-wavelength anomalous dispersion (MAD) and single-wavelength anomalous dispersion (SAD) are techniques that typically involve a heavy atom within the crystal. A typical example involves the replacement of the methionine residues with selenomethionine and the phases calculated from the same crystal using multiple data sets collected at different wavelength (MAD) or a single wavelength (SAD). The phases are calculated by using changes in the structure factor amplitudes which are used to locate the heavy atoms.

Once the electron density map has been calculated from the observed amplitudes and the calculated phases, the building of the amino acid chain into the map can begin. A map is created that minimises the bias of the structure factors calculated for the model by subtracting the calculated structure factors from a multiple of the observed amplitudes. This map is referred to as the $2F_o$-F_c map (equation 3.4).

$$p(x,y,z) = \frac{1}{V}\sum_{hkl}(2 \mid \mathrm{F_{obs}} \mid - \mid \mathrm{F_{calc}} \mid) \exp[\mathrm{i}\alpha_{\mathrm{calc}}(\mathrm{h})])$$

Equation 3.4. The electron density $2F_o$-F_c map summation.

The F_o-F_c map is used to highlight regions in which electron density has been observed but has not been accounted for in the model and where the model has been built but no electron density has been observed. These maps allow the protein chain to be built followed by a refinement process. The refinement process involves the structure being adjusted to give the best fit to the data followed by new phase calculation; the phase calculated should improve if the atoms have been placed correctly. This refinement involves the adjustment of the positional coordinates for each atom that is not hydrogen together with their temperature B-factor and their occupancy. The refinement procedure has set bond distances, planarity and angles of groups such as peptide linkages and aromatic rings that allow appropriate models to be built. The accuracy of the model is confirmed by the calculation of R factor. The R factor compares the amplitudes calculated from the model (F_{calc}) with the amplitudes observed from the model (F_{obs}) over a group of reflections (h) (equation 3.5). An R_{free} factor is also calculated using a test set of reflections (typically 2-5%) which are not used in the refinement process.

$$R = \frac{\sum_h \mid\mid F_{obs} \mid - \mid F_{calc} \mid\mid}{\sum_h \mid F_{obs} \mid}$$

Equation 3.5. The R factor equation.

Refinement is stopped when you cannot make the model more consistent with the data in a meaningful way. The structure is then validated using parameters such as bond length and angles as well as stereochemical parameters. The structure is thought to be correct if the parameters fall within expected values (Tronrud, 2007).

This chapter describes the over-expression and purification of the protein in the disulfide decameric state (hPrxII(S-S)), as well as its crystallization and subsequent X-ray structural analysis.

3.2. Materials and methods

3.2.1. Expression of protein in the disulfide state

The recombinant *hPrxII* gene was transformed into the BL21 DE3 (Novagen) cell line as described in 2.2.1 and plated onto an LB agar plate containing kanamycin (50 µg/ml). Induction studies were conducted to find the optimal conditions for producing hPrxII completely in the disulfide state. The BL21 DE3 cells containing the pET28a/hPrxII construct were used to inoculate 100 ml of LB containing kanamycin (50 µg/ml). This starter culture was grown under agitation overnight at 37^{o}C. 20 ml of the starter culture was used to inoculate 1 L LB containing the appropriate selection, and was grown with agitation at 37^{o}C until the OD_{600nm} was approximately 1.0. Induction of hPrxII was carried out using IPTG added to a final concentration of 1.0 mM and addition of diamide to a final concentration of 250 µM. The culture was incubated overnight at 37^{o}C. The cells were then harvested by centrifugation (20,000 x *g*, 20 mins, 4^{o}C) using a Beckman JA-25.50 rotor. The cell pellet was stored at -20^{o}C until further use.

3.2.2. Protein purification of hPrxII(S-S)

3.2.2.1. Cell lysis

The cell paste was re-suspended to 10% w/v in 100 mM Tris-HCl, pH 7.5, 0.5 M NaCl, 20 mM imidazole, 250 µM diamide. Cells were disrupted by sonication as described in section 2.2.4.1.

3.2.2.2. Purification buffers

Buffer A – 100 mM Tris-HCl, pH 7.5, 0.5 M NaCl, 20 mM imidazole, 10 µM diamide

Buffer B – 100 mM Tris-HCl, pH 7.5, 0.5 M NaCl, 1 M imidazole, 10 µM diamide

Buffer C – 100 mM Tris-HCl, pH 7.5, 0.1 M NaCl, 10 µM diamide

3.2.2.3. Nickel affinity and gel filtration chromatography

The nickel affinity chromatography was performed as in methods 2.2.4.3 using a six column volume gradient to 100% buffer B. The fractions from the column elution were analyzed using SDS-PAGE. Size exclusion chromatography was carried out as in methods 2.2.4.4 with fractions collected over one column volume. Fractions containing protein were analyzed using SDS-PAGE (as in

methods 2.2.4.6). The presence of the disulfide state of hPrxII was confirmed using SDS-PAGE analysis loading the protein on to a 12.5 % SDS gel using non-reducing loading buffer. hPrxII(S-S) showed a band ~48 kDa which was double the size of hPrxII (~24 kDa) using reducing buffer.

3.2.3. Western blot analysis

Samples were separated on a 12.5% SDS gel, and the gels were set up to allow the transfer of proteins from the gel onto a nitrocellulose membrane for immunodetection. The blotting apparatus was set up as follows: three layers of 3 mm blotting paper, one layer of nitrocellulose membrane, SDS gel and another three layers of blotting paper. The blotting paper and membrane were presoaked in 1 x transfer buffer (25 mM Tris-HCl pH 7.5, 20 mM glycine). The proteins were transferred from the gel to the membrane at 60 mA for 30 min. The filter membrane was then soaked in 10 – 20 % dried milk diluted in a 1 x wash buffer for 60 min with agitation.

5 x Wash buffer

1 M Tris-HCl pH 7.6	50 ml/L
NaCl	146 g/L
Tween 20	2.5 ml/L

The filter was then washed for 2 x 5 min in a large volume of 1 x wash buffer prior to incubation with rotation overnight at 4^{o}C with the primary antibody for hPrxII (5 µl diluted in 5 ml of 1 x wash buffer). The filter was then washed twice rapidly, followed by a 1 x 15 min wash, then followed by a 2 x 5 min washes in larger volumes of 1 x wash buffer. The filter was incubated with the secondary antibody (1 µl diluted in 5 ml of 1 x wash buffer) with rotation at room temperature for 1 hour. The filter was washed as above and left in buffer until it was developed. The ECL™ Western Blotting System (GE Healthcare) was used to detect the over expressed hPrxII. The prepared filter membrane was drained on blotting paper and soaked briefly in the detection reagent. 4.5 ml of ECL™ detection mix (2.25 ml of solution I plus 2.25 ml of solution II prepared immediately before use) was added and the filter was left to incubate for one minute with agitation in a plastic folder, which was then transferred to a film development box for visualization by autoradiography in a dark room.

3.2.4. Crystallization of hPrxII(S-S)

3.2.4.1. Preparation of proteins

After size exclusion chromatography the fractions containing purified hPrxII(S-S) were concentrated to ~15 mg/ml as in methods 2.2.4.5. The samples were centrifuged at 15,000 x *g* at 4^{o}C for 10 min before being used in crystallization trials to remove any precipitated protein.

3.2.4.2. Initial crystal trials

Microbatch crystallization trials were set up in a Hampton 96 well plate using an Oryx 6 crystallization robot (Douglas Instruments, UK). A range of different commercial screens were used for the microbatch trials including the screens MDL1 and MDL2 (Molecular Dimension Laboratories) (Appendix 7.4), Sigma 8007, Sigma 70437 (Sigma Aldrich) (Appendix 7.5) and JCSG (Molecular Dimensions Laboratories) (Appendix 7.6). The final droplet volume was varied between 1 µl and 2 µl depending on the amount of protein solution available. The droplet contained a 50:50 ratio of protein solution to screen ratio. The droplet was covered with Al's oil (50:50 mix of silicon oil and paraffin). The plates were stored at 18^{o}C and regularly checked for growth of crystals using a light microscope.

3.2.4.3. Optimization of crystal trails

For any conditions that produced crystals optimization was carried out using the X-step optimization software (Douglas Instruments, UK). The X-step software varies the precipitant concentrations, protein concentrations, additive concentrations and pH by +/-30 %. The microbatch method was once again used on the Oryx 6 crystallization robot (Douglas Instruments, UK). The droplet was covered with Al's oil (50:50 mix of silicon oil and paraffin). The plates were stored at 18^{o}C and regularly checked for crystals using a light microscope.

3.2.4.4. Preparing crystals for data collection

Crystals were frozen using a cryo-protectant (0.1 M HEPES Na salt, pH 7.5, 20% PEG 200, 10% PEG 8000, 25% Glycerol). The crystals were removed from the droplet and placed in the cryo-protectant before being frozen directly in liquid nitrogen.

3.2.5. X-Ray data collection

Data were collected on IO3 at the Diamond Synchrotron light source (Oxford, UK) using an ADSC Q315 CCD detector. Data were collected under cryo cooled conditions (100 K in a stream of gaseous nitrogen).

A high resolution dataset was collected at a wavelength of 0.98 Å at a distance of 460.5 mm. 360 frames were collected at an oscillation of 0.5^{o} for each frame.

3.2.6. Structure Determination

3.2.6.1. Data processing

Data was processed using MOSFLM (CCP4) (Evans, 2006), SCALA (CCP4) (Weiss and Hilgenfeld, 1997) and Xia2 (CCP4).

3.2.6.2. Phase determination

Phases were determined using the molecular replacement method performed in MOLREP (Vagin and Teplyakov, 2010).

3.2.6.3. Model building and refinement

Electron density maps were calculated and the structure was fitted to give the best fit to both the $2F_o$-F_c and F_o-F_c maps. Maximum likelihood refinement was performed using REFMAC 5.2 (Murshudov *et al*., 1997) after each session of model building performed in COOT (Emsley and Cowtan, 2004). No solvent molecules were added to the final PDB due to the low resolution.

3.2.6.4. Structure validation

After refinement the quality of the model was checked using the program PROCHECK (Laskowski *et al*., 1993).

3.3. Results

3.3.1. Expression of the protein in the disulfide state

The *hPrxII* gene in the pET28a vector was transformed into the *E. coli* expression strain BL21 DE3. hPrxII protein expression was under the control of the T7 promoter and was induced using IPTG. The over-expression of hPrxII in the disulfide state was investigated by induction studies to obtain the conditions not only for over-expression but to have the protein completely in the disulfide state. The optimal conditions for this were addition of a final concentration of 1 mM IPTG and 250 µM diamide when the cells had reached an OD_{600nm} of 1.0 with further incubation overnight at 37^{o}C. The over-expression of hPrxII resulted

in soluble protein being produced at the expected size (~24 kDa). The presence of the disulfide state was confirmed with a band on SDS-PAGE using native buffer at ~48 kDa.

3.3.2. Protein purification of hPrxII(S-S)

One litre of culture produced 3.0 g of cell paste and after cell lysis (as in methods 2.2.4.1) and centrifugation the supernatant was purified using nickel affinity and gel filtration chromatography as described in methods 2.2.4.3 and 2.2.4.4.

3.3.2.1. Nickel affinity and gel filtration chromatography of hPrxII(S-S)

The clarified cell extract was applied to a nickel column as described in methods 2.2.4.3 producing the trace seen in figure 3.6. The fractions were analyzed using SDS-PAGE (see figure 3.8) as described in methods 2.2.3.6. The fractions containing hPrxII were pooled and concentrated for gel filtration chromatography. Gel filtration chromatography was used as a final step of the purification process and as a tool for the estimation of the molecular weight of the protein. The concentrated protein was loaded on to an equilibrated gel filtration column as in methods 2.2.4.4 (figure 3.7). The peak fractions were analyzed by SDS-PAGE and those that contained hPrxII were pooled and concentrated. The presence that the disulfide had formed was confirmed by SDS-PAGE using non-reducing buffer (figure 3.8). The disulfide form was also confirmed by the use of Western blot analysis (methods 3.2.3) (figure 3.9) as the hPrxII primary antibody will bind to both protein bands on SDS-PAGE ran with native buffer.

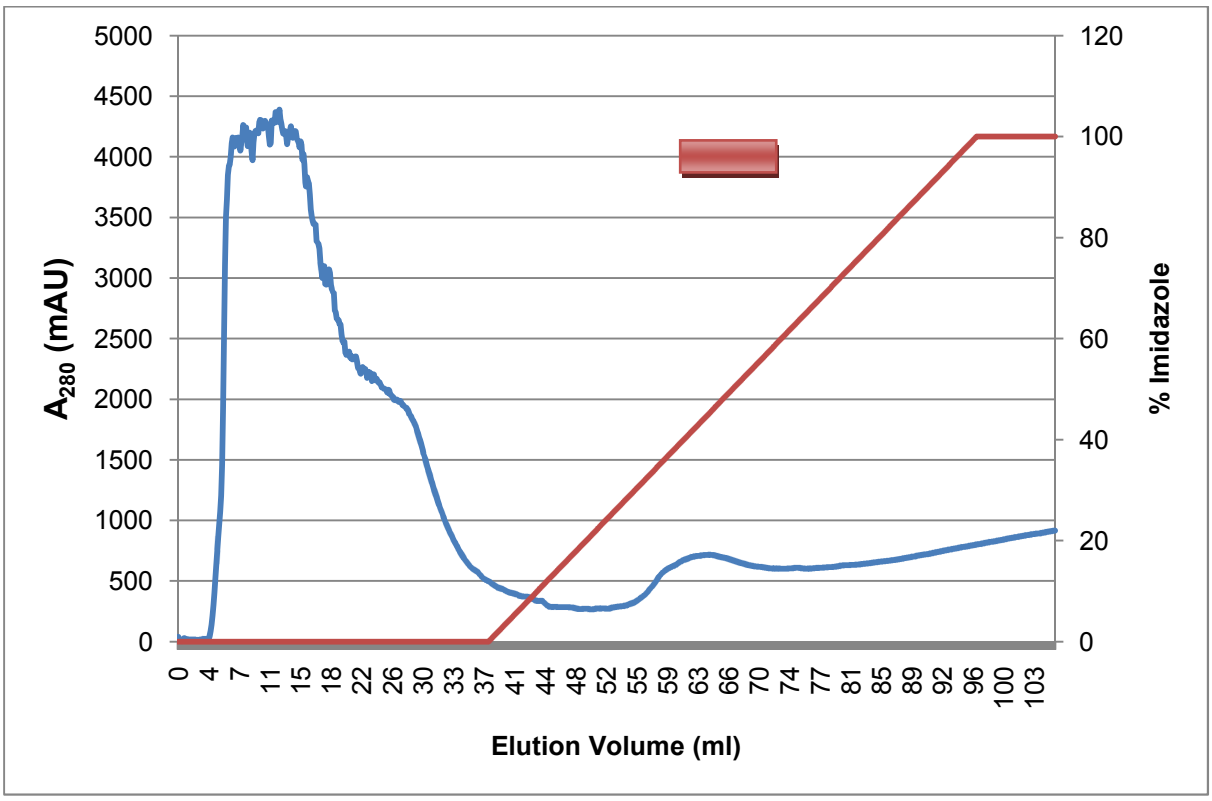

Figure 3.6. Elution profile of hPrxII(S-S) (blue line) from nickel affinity chromatography. 10 ml fractions were collected throughout the entire elution. The red line shows the % imidazole concentration. The fractions that showed a band of the correct size on SDS-PAGE are indicated by the red bar.

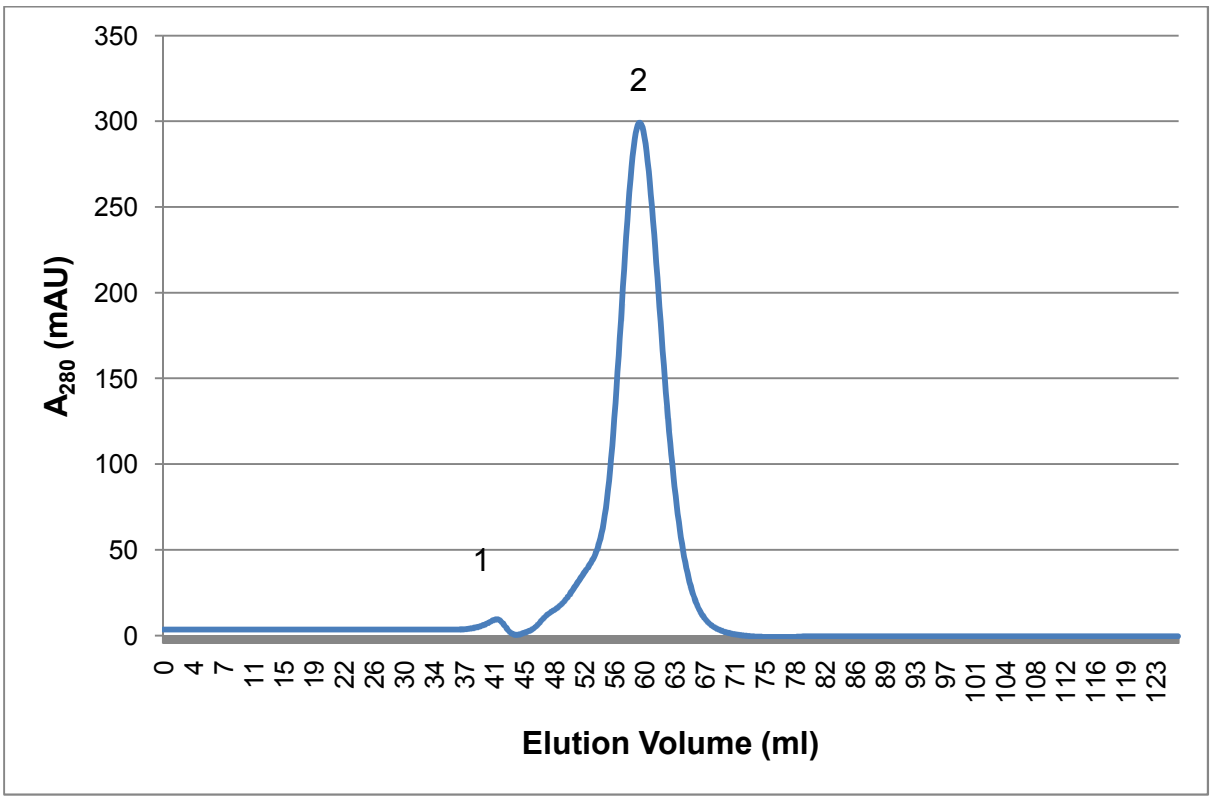

Figure 3.7. Elution profile from the gel filtration column for hPrxII(S-S) (blue line). 1 ml fractions were collected throughout the elution volume. Peak 1 (~42 ml) corresponds to the void volume of the column; Peak 2 (~58 ml) corresponds to the decameric form of hPrxII (250 kDa). The oligomeric state was determined using a calibrated Superdex 200 column (Appendix 7.1.)

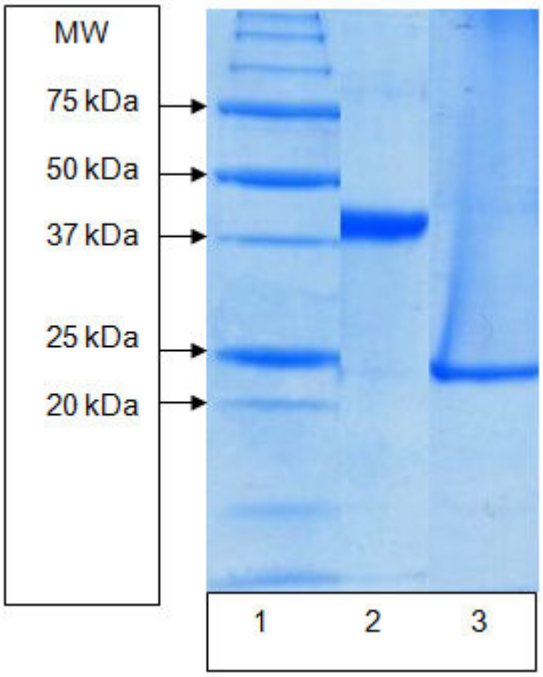

Figure 3.8. SDS-PAGE analysis of the elution from the hPrxII(S-S) gel filtration column. Lane 1, molecular weight marker; Lane 2, sample from peak 2 run on SDS-PAGE using non-reducing buffer; Lane 3, sample from peak 2 run on SDS-PAGE using reducing buffer.

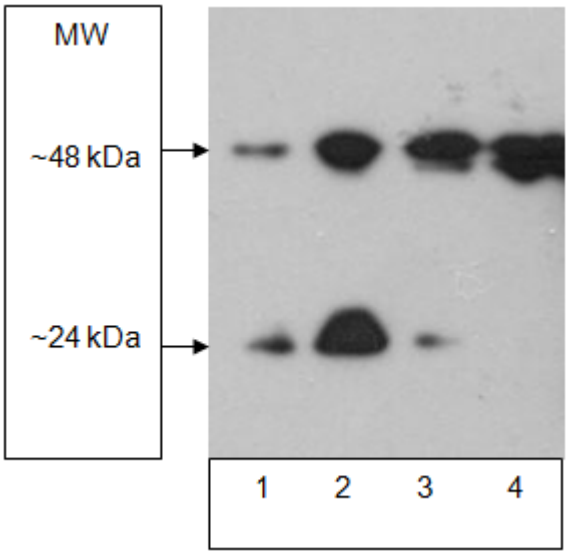

Figure 3.9. Western blotting analysis of hPrxII using non-reducing SDS buffer to show the presence of the intermolecular disulfide bond. Lane 1, analysis of hPrxII from Rosetta-gami 2 pLysS (DE3) cells; Lane 2, analysis of hPrxII from BL21 (DE3) cells; Lane 3, analysis of hPrxII from BL21 (DE3) cells with diamide present at cell lysis; Lane 4, analysis of hPrxII from BL21(DE3) cells with diamide present at induction and in all purification and cell lysis buffers. The molecular weight is predicted based on the marker run on the SDS-PAGE (Marker not shown).

After gel filtration pure hPrxII(S-S) protein was obtained and eluted at ~58 ml from the calibrated gel filtration corresponding to a molecular weight of ~250 kDa suggesting it was present as a decamer.

3.3.3. Crystallization of hPrxII(S-S)

The purified enzyme was concentrated to ~15 mg/ml and microbatch crystallization experiments were carried out using commercial crystal screens (as in methods 3.2.4). Initial results gave crystals produced in 0.1 M HEPES Na Salt pH 7.5, 8% ethylene glycol, 10% PEG 8000 (figure 3.10).

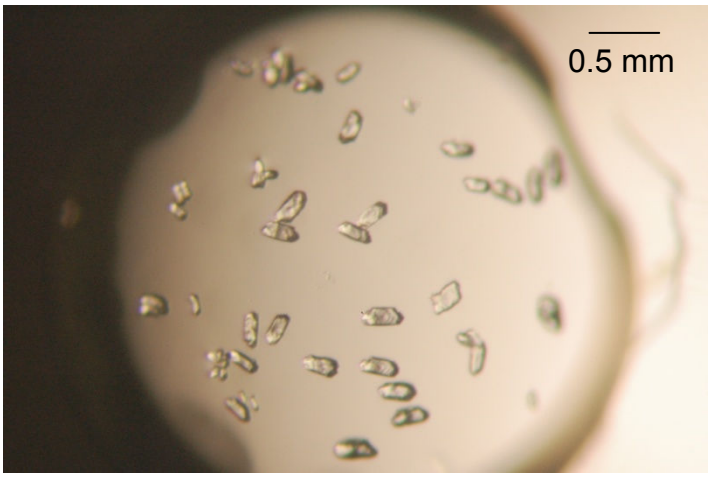

Figure 3.10. hPrxII(S-S) crystals obtained from 0.1 M HEPES Na Salt pH 7.5, 8% ethylene glycol, 10% PEG 8000.

Optimization experiments were carried out around these conditions (as in methods 3.2.4.3) but they failed to yield any crystals and the original crystals were frozen using a cryo-protectant (as in methods 3.2.4.4) and taken to the Diamond Light Source (Oxford, UK)

3.3.4. Structure determination

3.3.4.1. X-ray data collection

Data were collected at the Diamond Light Source (Oxford, UK) as described in methods 3.2.5. Indexing and scaling revealed the crystal belongs to the monoclinic space group $P3_1$ 2 1 or $P3_2$ 2 1. The statistics for the data processing are shown in table 3.1.

Crystal	hPrxII(S-S)
Resolution range (Å)	140-3.3 (3.38 – 3.30)
Space group	$P3_1$ 2 1
Cell parameters	a=b= 211.2, c=217.5 Å α =β=90°, γ = 120°
Solvent content (%) V_M ($Å^3 Da^{-1}$)	82.7 7.11
No. protomers in asymmetric unit	10
No. measured reflections	929861
No. unique reflections	84379
Completeness (%)	100 (100)
Redundancy	11.02 (11.24)
(I)/σ (I)	9.8 (1.8)
Rsym† (%)	0.23 (1.36)

Table 3.1. Data processing statistics for the hPrxII(S-S). Values in parentheses are given for the outer resolution shell.

$R_{sym}=\Sigma_h\Sigma_J|<I_h>-I_J(h)|/\Sigma_h\Sigma_J I(h)$, where I(h) is the intensity of reflection h. Σ_h is the sum over all reflections and Σ_J is the sum over J measurements of the reflection.

3.3.4.2. Structure solution

Molecular replacement studies were carried out with the program MOLREP (Vagin and Teplyakov, 2010) using the original decameric structure of the PrxII (PDB: 1QMV). The solution was found with the full model, however, significant clashes were observed. Residues 165-198 were removed from each model subunit and molecular replacement was successfully performed on the modified decameric model. This work was carried out in collaboration with Dr. M. Isupov at Exeter.

The cross-rotation function was calculated for the decamer with a radius of 60 Å and a resolution range of 40-3.5 Å. The rotation solution had a peak at 12 σ with a noise peak no greater than 3 σ. The translation function was calculated in both possible enantiomorphs of the space group, (*P*3_1 2 1 and *P*3_2 2 1). The solution was found in the $P3_1$ 2 1 enantiomorph with a correlation of 50.3% and an R-factor of 46.6% with a background correlation of 32.9%. The highest

correlation for the other enantiomorph of the space group was calculated at 27%.

3.3.4.3. Model building and validation

Ten fold electron density averaging was carried out on the solution from molecular replacement and was subsequently refined using REFMAC (Murshudov *et al*., 1997) and rebuilt in COOT (Emsley and Cowtan, 2004) using the averaged maps. The LOCAL NCS option of REFMAC (Murshudov *et al*., 1997) was used for further refinement, allowing individual B factors to be assigned to all atoms. Final rounds of model building were done independently for each subunit using the 2Fo-Fc maps. Statistics for the final model are displayed in table 3.2. The Ramachandran plot for the structure is displayed in appendix 7.7.

Crystal	hPrxII(S-S)
Resolution range (Å)	50-3.30
Overall R factor (%)	19.4
R_{free} (5% total data)	21.3
No. protein residues	1705
Residues modeled	**Residues** **(A,B** 1 -174), (**C,D,G,J** 1 – 172), (**E,F,H** 1 – 175), **I** (1 – 173). **S-S BONDS** Cys 172 (E) – Cys 51 (F), Cys 51 (E) – Cys 172 (F) Cys 51 (G) – Cys 172 (H), Cys 172 (A) – Cys 51 (B) Cys 51 (C) – Cys 172 (D), Cys 172 (I) – Cys 51 (J) Cys 172 (C) – Cys 51 (D)
No. solvent molecules (water)	0
No. substrate/cofactor molecules	16 (SO_4)
RMSD bond length (Å)	0.012 (0.022)
RMSD bond angles (^{o})	1.43 (1.99)
Wilson B factor (Å^2)	73.83
Average B factor	
Protein (Å^2)	78.0
REFMAC RMS error (Å)	0.29
Ramachandran analysis (% of residues)	
Most favoured	87.7
Additionally allowed	9.8
Generously allowed	1.9
Disallowed	0.5
G factor	0

Table 3.2. The final X-ray refinement statistics for hPrxII(S-S) structure. Target values are given in parenthesis.

3.4. Discussion

3.4.1. Expression of the protein in the disulfide state

Over-expression of the protein in the disulfide state was attempted in a number of different ways. The protein was originally transformed into the chemically competent Rosetta-gami 2 pLysS (DE3) *E. coli* cell line as it is known to enhance disulfide bond formation in the cytoplasm. The enhanced disulfide bond formation is caused by this strain of *E. coli* having mutations in the *trxB* and *gor* genes. These mutations prevent the production of thioredoxin B and the glutathione reductase enzymes which are responsible for the reduction of disulfide bonds. The purified protein from Rosetta-gami 2 pLysS (DE3) was found to be a mixed species with the protein being expressed in both the disulfide and a non-disulfide state (figure 3.9). hPrxII was then transformed into the BL21 (DE3) cell line and diamide was introduced at cell lysis and at induction and the composition of the purified sample was studied using SDS-PAGE and Western blotting (figure 3.8 and figure 3.9). It was shown that in the BL21 (DE3) cell line without diamide, the protein was expressed in greater levels than in the Rosetta-gami 2 pLysS (DE3), but was still expressed equally in the disulfide and non-disulfide state. When diamide was introduced in the purification and cell lysis buffers, the amount of protein being produced in the disulfide state was greatly improved but to obtain protein crystals suitable for X-ray diffraction data the protein had to be in a completely homogenous state. By introducing diamide at induction and then keeping it present in the cell lysis and all the purification buffers, the protein was produced completely in the disulfide state.

3.4.2. Crystal structure of hPrxII(S-S)

3.4.2.1. Monomer unit

The monomer of the disulfide hPrxII within the decameric structure consists of domain I (residues 1-169) as previously described in the hyperoxidised/thiol form of the enzyme (Schroder *et al*., 2000). Residues 176-202 were not built in the current structure due to poorly defined electron density. The thioredoxin fold is made up of four β strands (β3, β4, β6 and β7) and by four flanking α helices (α1, α2, α4 and α5) as found in the original hPrxII structure. The overall secondary structure of the disulfide Prx monomer is shown in figure 3.11.

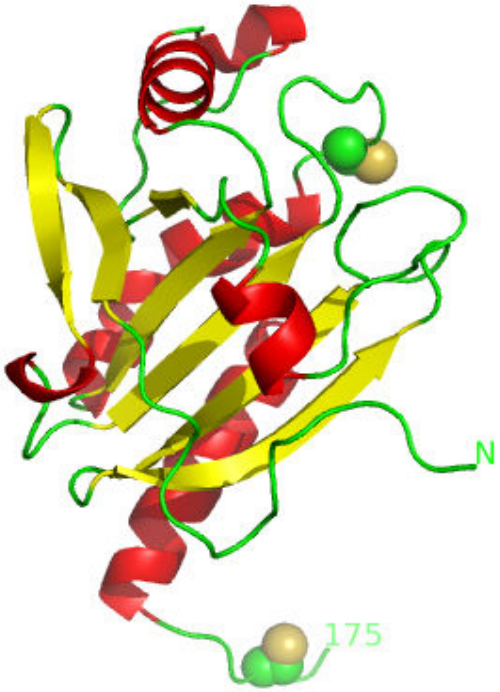

Figure 3.11. Cartoon representation of the overall secondary structure fold of the hPrxII monomer within the decameric structure with the Cys51 and Cys172 residues shown as spheres. The figure is coloured according to secondary structure and the Cys residues are shown as spheres (Figure produced using PyMol DeLano scientific).

3.4.2.2. Dimer structure

The dimer highlighting the formation of the disulfide bond is shown in figure 3.12. The C-terminal region was believed to play a significant role in the dimer interface based on the original findings of the hyper-oxidized/thiol hPrxII structure. Rearrangements of the N and C terminal regions which allow the formation of the disulfide and a comparison to the hyper-oxidized/thiol form of the enzyme are described in section 3.4.2.5.

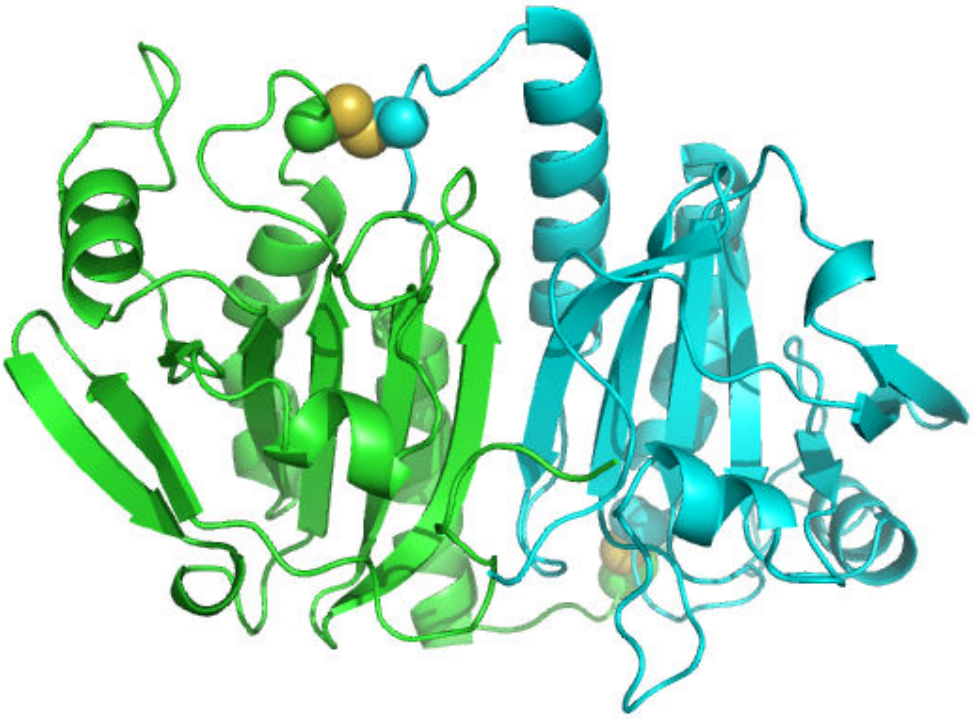

Figure 3.12. Cartoon representation of the hPrxII dimer within the decameric structure highlighting the disulfide as spheres at the dimer interface. The two chains of the homodimer are shown in cyan and green with the disulfides shown in sphere mode (Figure produced using PyMol DeLano scientific).

3.4.2.3. Decameric structure

The disulfide structure of the hPrxII revealed a decamer in the asymmetric unit. Although not all dimers were shown to be in the disulfide state due to poorly defined electron density, this structure still suggests the disulfide state of the enzyme does exist in a decameric form. Figure 3.13 highlights the existence of disulfide bonds on neighbouring dimer subunits. It was originally hypothesized that the disulfide state might only exist as dimers of the protein due to a breakdown in the dimer:dimer interface due to steric clashes induced by disulfide formation. This disulfide structure however provides evidence that the disulfide state exists in the decamer form of the enzyme. The dimer:dimer interface is largely hydrophobic with the interface formed between αH3, its preceding loop region, and the loop regions between β6-β7, β5-α4 and β3-α1 on each neighbouring subunit. In particular Phe47 from one subunit is involved in a hydrophobic cluster with Phe47, Phe81 and Ala85 from the neighbouring dimer as described for the original hPrxII structure. A comparison of the

dimer:dimer interface between this disulfide state and the original hyperoxidised/thiol state is discussed in section 3.4.2.5.

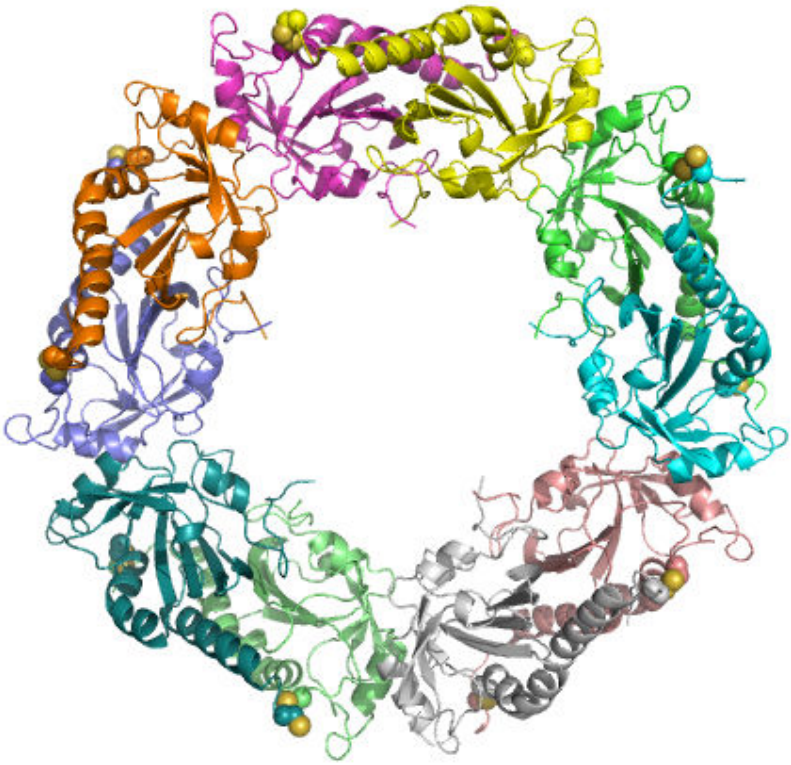

Figure 3.13. Cartoon representation of the decameric structure of hPrxII highlighting the position of the disulfide bonds shown in spheres mode (Figure produced using PyMol DeLano scientific).

3.4.2.4. The active site

The $2F_o$-F_c and F_o-F_c electron density maps revealed the presence of the disulfide bond in the subunits as described in table 3.2 (poor electron density did not allow the other disulfides to be described). Electron density for the disulfide bond is shown in figure 3.14. The disulfide and residues within 5 Å are highlighted in reference to the hPrxII dimer in figure 3.15. A comparison of the active site and Cys binding pockets is discussed in section 3.4.2.5.

(A) (B)

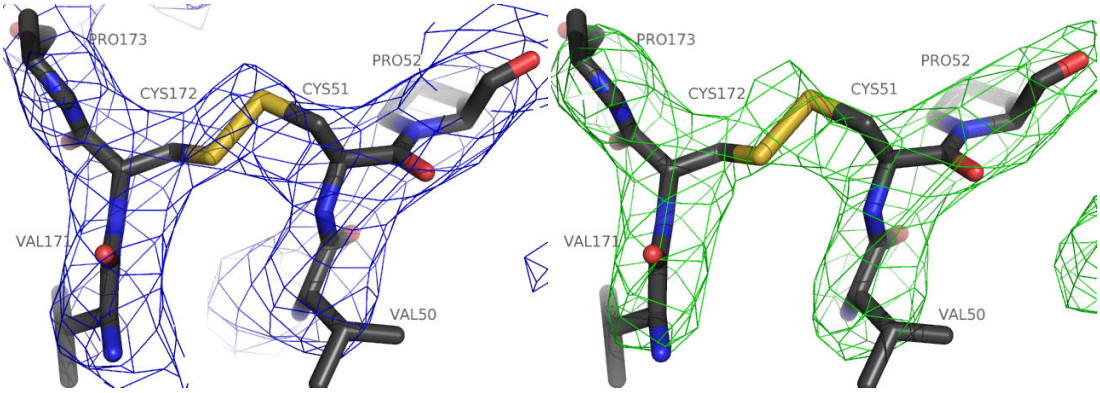

Figure 3.14. A) The $2F_o$-F_c electron density map for the disulfide and surrounding residues. B) The F_o-F_c omit map calculated in the absence of the shown residues.

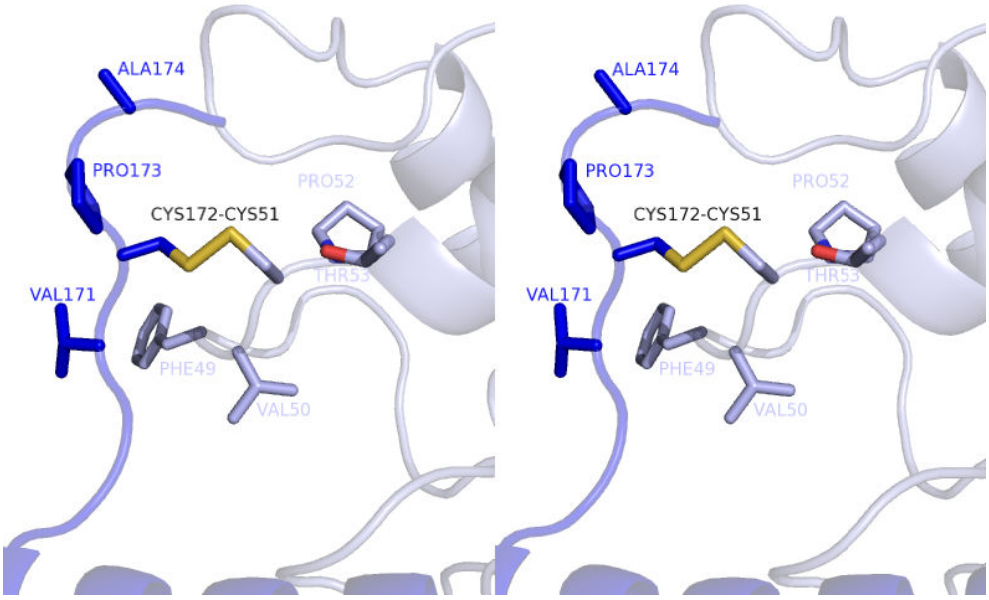

Figure 3.15. Stereo cartoon representation of the hPrxII disulfide bond and surrounding residues in reference to the dimer. The two subunits of the homodimer are coloured in blue and light blue with the disulfide and surrounding residues shown in stick mode (Figure produced using PyMol DeLano scientific).

3.4.2.5. Structural comparison between hPrxII hyper-oxidized/thiol and hPrxII(S-S) crystal structure.

The hPrxII disulfide structure was compared to the previously known form of the structure (PDB: 1QMV) in which Cys51 and Cys172 are in hyper-oxidized and thiol states respectively. The overall composition of the secondary structure of the disulfide form of the enzyme is unchanged. A comparison of the two structures highlights structural changes which occur in loop regions consisting of residues 47-54 and 170-202 as well as at the C terminal region, which occur

to allow for disulfide bond formation. An overall comparison of the monomers is shown in figure 3.16. In the previously known structure it was reported that there was a 10 Å distance between the Cα positions of Cys51 and Cys172 from the neighbouring subunits of the dimer and a 13 Å gap between the sulfur atoms of the two redox active cysteines.

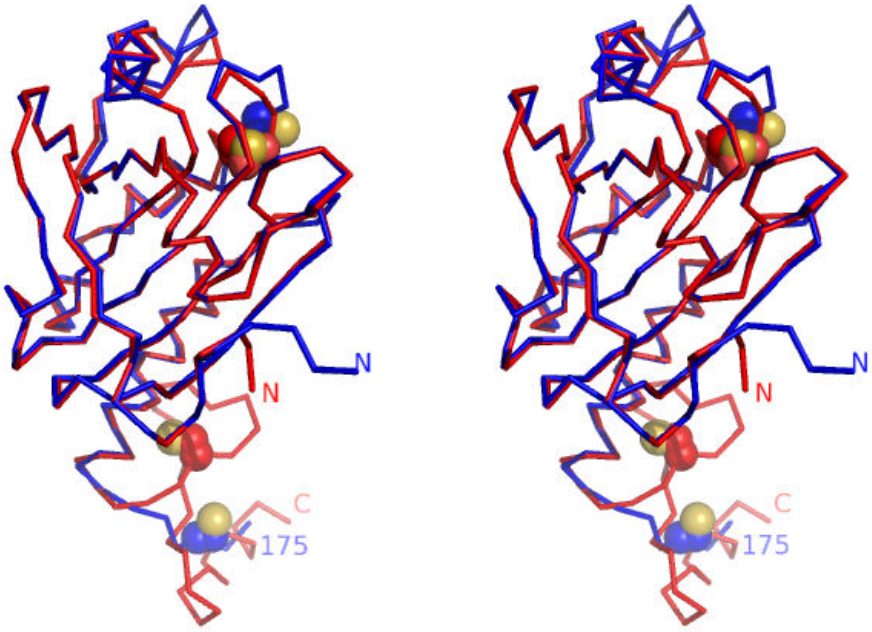

Figure 3.16. Stereo diagram comparison of the original hyper-oxidized/thiol Prx (red) and the hPrxII(S-S) (blue) forms. Cysteines are shown as spheres. (Figure produced using PyMol DeLano scientific).

It was reported previously that Cys51 is buried by residues Tyr43, Pro44, Thr48, Val50, Glu54, Trp86, Arg127 and Arg150 and Val171 from the neighbouring subunit. The disulfide structure reveals an overall movement of the loop consisting of residues 47-54 towards the neighbouring monomer. In particular the side chains of Val50 and Phe49 are displaced from the dimer interface resulting in a 6 Å movement of Cys51 towards the neighbouring subunit. The positions of Tyr43, Pro44, Thr48, Glu54, Trp86, Arg127 and Arg150 are relatively unchanged.

In the neighbouring subunit Cys172 was previously described in the thiol state positioned within a hydrophobic pocket consisting of residues Ala161, Tyr164 and Trp176 and Val148 from the neighbouring subunit. In the disulfide structure large structural movements of the region consisting of residues 170-202 are observed to allow for the formation of this bond. In the thiol state this loop

region folds in towards the neighbouring subunit. However, in the disulfide structure the loop adopts a dramatically different conformation which moves the Cα of Cys172 10 Å. This results in residues 170-175 in the disulfide structure displacing the C terminal αH6 in the hyper-oxidized/thiol structure and adopts a completely different conformation allowing disulfide bond formation. The displaced αH6 C terminal region has not been able to be modelled in the disulfide structure due to poorly defined electron density. The previously described binding pocket of Cys172 in its thiol state is unchanged.

The new conformation of both subunits results in potential hydrogen bonds between the two subunits. These are between the main chain oxygen atom of Phe49 of one subunit to the main chain nitrogen atom of Cys172 of the neighbouring subunit and between the main chain oxygen atom of Glu170 to the main chain nitrogen atom of Val150.

Overall these structural changes allow the cysteine residues to form a disulfide bond on the surface of the dimer which would allow future reduction by Trx, (The C-terminal region has not been defined in the disulfide structure; however there is plenty of room available to suggest this region would not shield the disulfide bond).

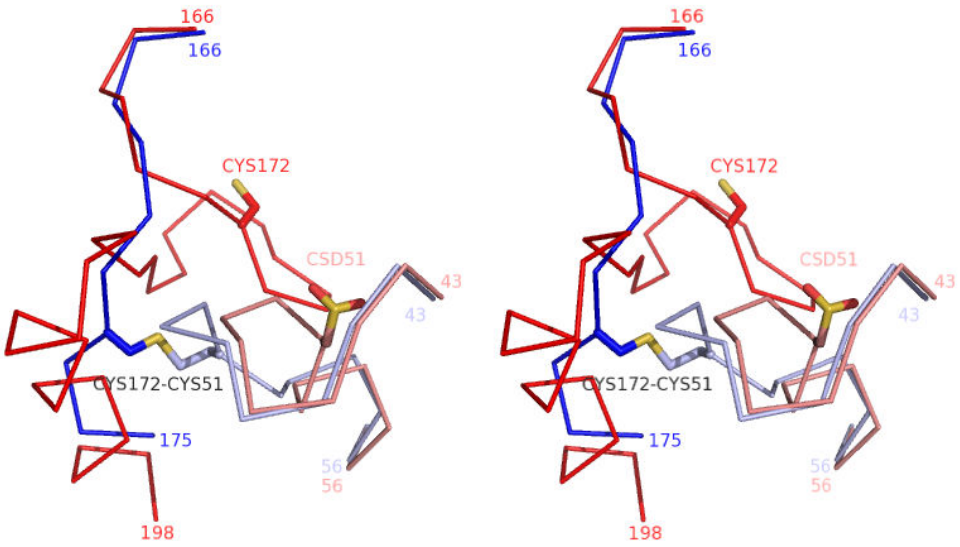

Figure 3.17. Stereo diagram illustrating the differences in secondary structure allowing for the disulfide bond formation. The original hyper-oxidized/thiol Prx structure is displayed in red and light red corresponding to the two subunits of the homodimer. The

disulfide Prx is displayed in blue and light blue corresponding to the two subunits of the homodimer (Figure produced using PyMol DeLano scientific).

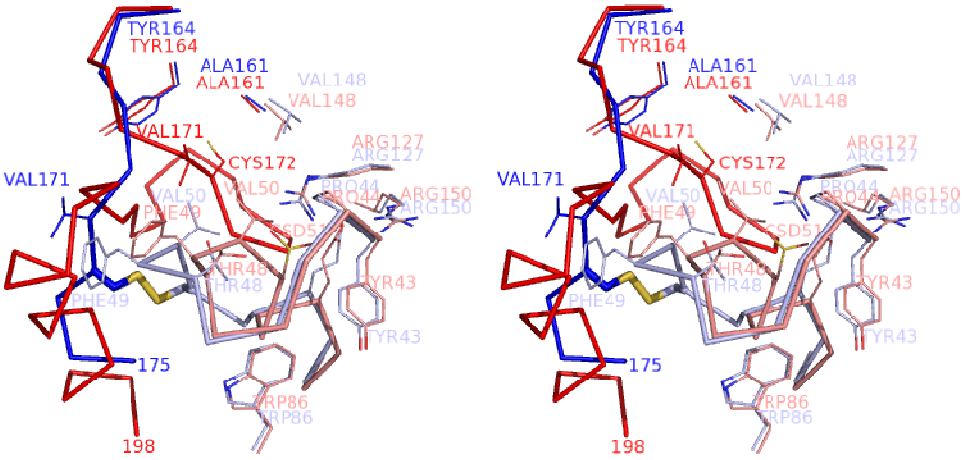

Figure 3.18. Stereo diagram highlighting the differences and similarities for the active site pocket residues around Cys51 and Cys172. The original hyper-oxidized/thiol Prx structure is displayed in red and light red corresponding to the two subunits of the homodimer. The disulfide Prx is displayed in blue and light blue corresponding to the two subunits of the homodimer (Figure produced using PyMol DeLano scientific).

Comparisons of the dimer:dimer interface reveal there are few changes at this interface, apart from the un-modeled C terminus. Figure 3.19 highlights the similarities in the dimer:dimer interface. The only noticeable difference is the position of Phe49 however, the position adopted in the disulfide state does not clash with the neighbouring dimer. Therefore the changes which occur around the active site Cys51-Cys172 bond do not affect the original residues responsible for the dimer:dimer interaction which explains how the disulfide form of hPrxII can exist in the decameric state.

Heme-binding protein 23 (HBP23) (PDB: 1QQ2) is a mammalian two cysteine peroxiredoxin that was found to be in the intermolecular disulfide state with a disulfide bond between Cys52 and Cys173 and shares 77% sequence homology with hPrxII (Hirotsu *et al*., 1999). The structure of the HBP23 protein revealed only the dimer. Based on differences observed between the disulfide HBP23 enzyme and the original hyperoxidised/thiol hPrxII enzyme it was

hypothesized that changes at the dimer: dimer interface upon disulfide formation would cause the breakdown of the decamer.

It was originally suggested in the hPrxII enzyme (based on the disulfide HDP23 structure) that partial unwinding of the active site helix (α1) would cause a change in the position of the side-chain of the Phe47. This would potentially cause a steric clash with the Phe81 from the neighbouring dimer in the hPrxII structure. Figure 3.19 clearly shows there is no movement or clash of these residues in the disulfide decamer interface. It was also suggested movements in residue Trp86 would result in a clash with Ala85 from the neighbouring subunit. (This corresponds to the position of Trp87 observed in HBP23). However, figure 3.19 shows there is no movement of these residues between the two different hPrxII states. The only change observed at the dimer:dimer interface is in the position of Phe49, however, the position of this residue in the disulfide structure would not cause a breakdown of the decamer.

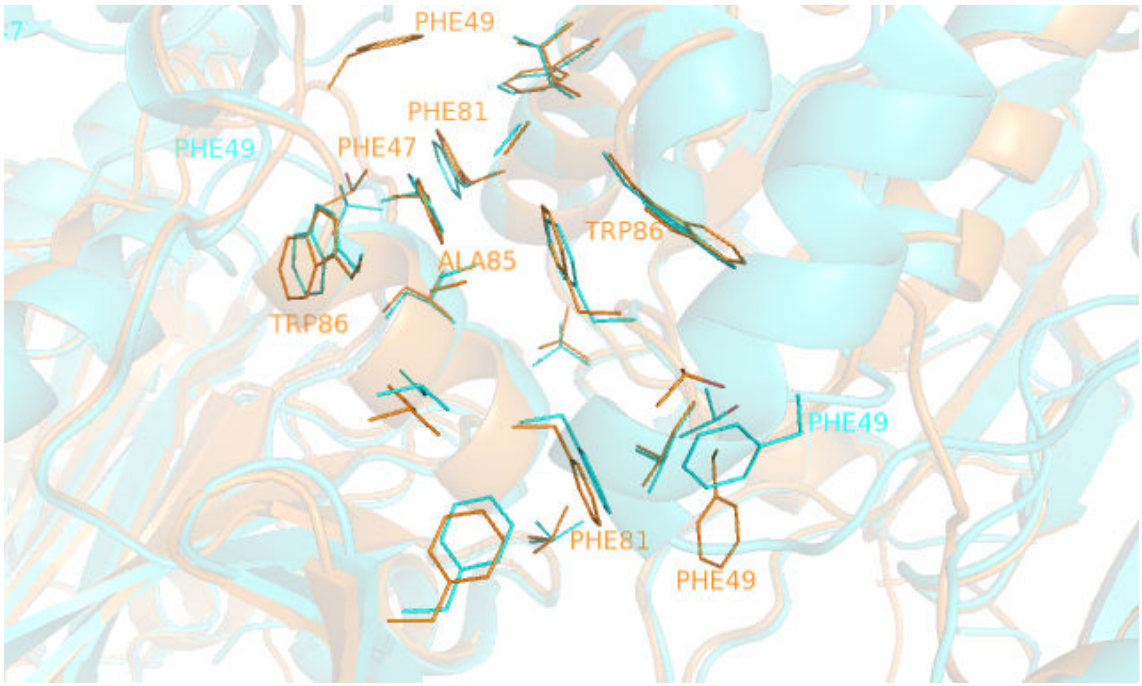

Figure 3.19. Cartoon representation of the dimer:dimer interface for hPrxII(S-S) shown in orange and the original hyperoxidized/thiol hPrxII structure shown in cyan. Residues at the dimer interface are shown as lines (Figure produced using PyMol DeLano scientific).

4. Study of the complexes formed between hPrxII and the proteins it interacts with in the Prx antioxidant system.

4.1. Introduction

4.1.1. The interaction between hPrxII and Srx

During the normal catalytic cycle hPrxII will undergo oxidation converting the peroxidatic cysteine sulfur hydryl group (-SH) to a sulfenic acid (-SOH). Once the sulfenic acid group has been produced the resolving cysteine is thought to reduce the peroxidatic cysteine to its natural state. The attack of the resolving cysteine is thought to be potentially slow due to the distance between the peroxidatic and resolving cysteines, as well as interference from the GGLG and YF motifs restricts access to the peroxidatic cysteine (Wood *et al*., 2003a). This slow mechanism allows the sulfenic acid to become hyper-oxidized to the sulfinic acid form (-SOOH). This form was once thought to be “un-repairable” and was believed to leave the protein inactivated (Chae *et al*., 1994). It has also been suggested that this over-oxidized state is a signal for apoptosis (Zhao *et al*., 2009). A protein was discovered in *S. cerevisae* that was found to repair the hyper-oxidized sulfinic acid form of a yeast peroxiredoxin (Biteau *et al*., 2003a). The protein was found to have a human homologue. The human oxidoreductase hSrx is 14.2 kDa in size and requires both ATP and Mg^{2+} to function.

The structure of the peroxiredoxin-sulfiredoxin complex has been studied using a disulfide link between PrxI and hSrx to mimic the proposed thiosulfinate intermediate (Jonsson *et al*., 2008b) but a complex was unable to be formed between the decameric form of either PrxI or PrxII.

The crystal structure of hPrxII reveals the structure of the hyper-oxidized form to be a stable decameric structure with buried active sites that would provide difficulty for Srx to access the sulfinic acid (Schroder *et al*., 2000). The crystal structure of the hSrx reveals a concave shape to the active site that is hypothesized to be ideally suited to interacting with the convex shape of the PrxII decamer (Jonsson *et al*., 2005). The interaction between decameric PrxII

and hSrx has been studied using molecular modelling (Lee *et al*., 2006), but as yet there is little data on the complex and the stoichiometry of Srx binding.

4.1.2. The interaction between hPrxII and Trx

As part of the normal catalytic cycle of hPrxII an intermolecular disulfide is formed in the reduction of the peroxidatic cysteine. This intermolecular disulfide is then reduced by thioredoxin. The disulfide bond undergoes nucleophilic attack by the thiolate of Cys32 forming a covalently linked mixed disulfide. The second catalytic cysteine (Cys35) then attacks the mixed disulfide leaving the hPrxII reduced and an intermolecular disulfide between the catalytic cysteine residues on Trx (Holmgren, 1995).

4.1.3. Site-directed ligase independent mutagenesis (SLIM) of Srx to ET-Srx

Previous work on the crystallization and the complex formation of Prx and Srx showed that Srx contains a glycine-rich region (35%; 13 of 37 residues) (Jonsson *et al*., 2005; Jonsson *et al* 2008b). In both studies it was an engineered truncated Srx (ET-Srx) with the first 31 residues removed that produced the best crystals.

The optimal way to produce the ET-Srx involved mutating out the undesired residues by using SLIM on the original Srx clone. SLIM is a method for producing mutations in a DNA sequence using PCR (figure 4.1). PCR is performed using four primers, two short primers and two long tailed primers. It is the two tailed primers that contain the desired mutation on complementary overhangs. The PCR reaction will produce four products. Products one and two are identical except for the positions of the tails which are found at opposite ends of the sequence. Product three contains the tail sections on both ends and product four does not possess the tailed portion (therefore no sequence deletion). The PCR product is then denatured and re-annealed forming a stable heteroduplex generated from one strand of product one and one strand of product two. This heteroduplex is stable as the generated strand will form with complementary 5' and 3' overhangs at opposite ends which can form circular DNA. The circular DNA is then transformed into a cloning *E. coli* cell line. SLIM was chosen to create ET-Srx as it can be done in a single tube in a short time frame and has shown to be >95% efficient (Chiu *et al*., 2004).

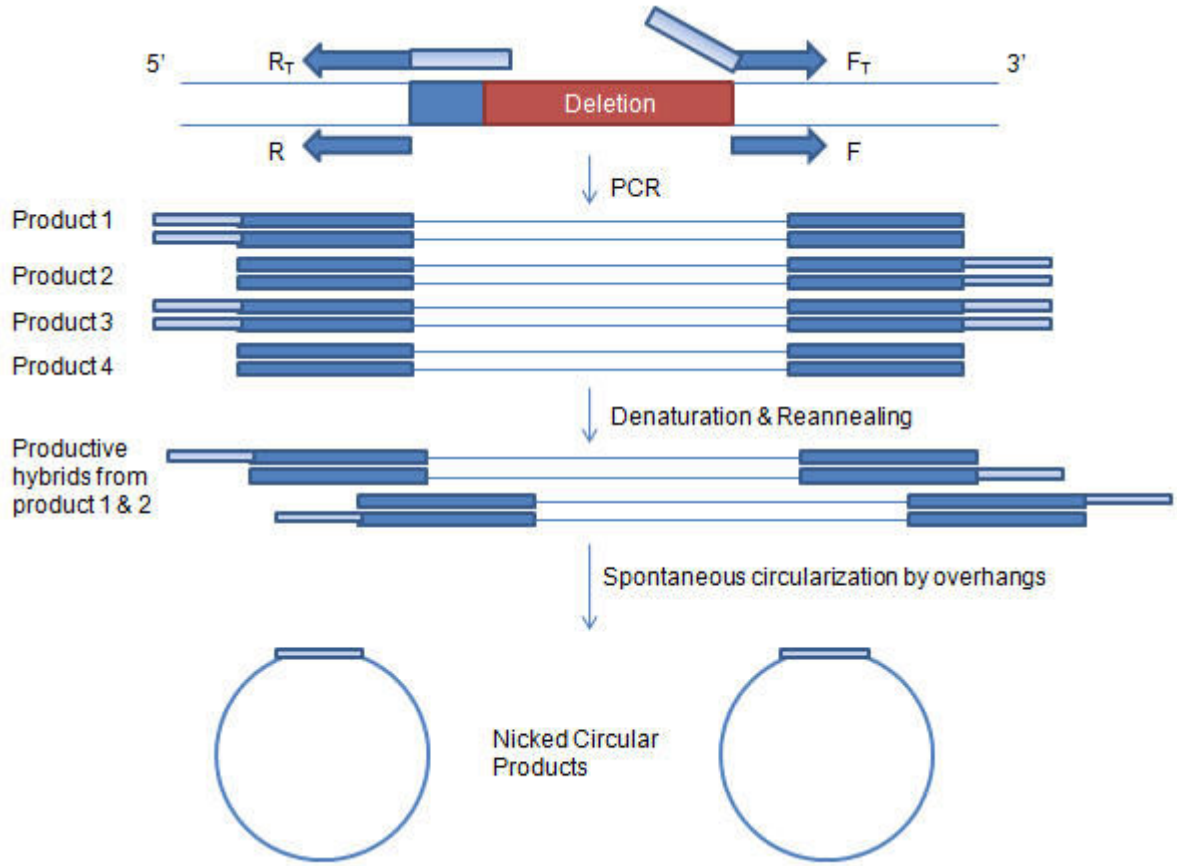

Figure 4.1. The SLIM method for the production of *ET-Srx*. Inverse PCR is performed to remove the DNA region corresponding to the first 31 amino acids. The PCR will produce four products. On denaturation and annealing a heteroduplex will be formed from one strand of product one and one strand of product two. This heteroduplex will have complementary 5' and 3' overhangs that can form stable circular DNA that can then be transformed into chemically competent *E. coli* cells. Figure adapted from Chiu *et al*., (2004).

4.1.4. Site directed mutagenesis

4.1.4.1. Site directed mutagenesis of hPrxII to mPrxII

In order to produce the complex between hPrxII and ET-Srx it was necessary to produce a disulfide linkage using a chemical method. In order to produce the disulfide link between the peroxidatic cysteine (Cys51) and the cysteine on Srx it was necessary to remove the resolving cysteine (Cys172) and the remaining cysteine residue (Cys70).

4.1.4.2. Site directed mutagenesis of Trx to mTrx

In order to produce the complex between mPrxII and Trx the same chemical conjugation reaction was used. In order to recreate the reaction between the

peroxidatic cysteine (Cys51) and Cys32 on Trx it was necessary to remove the second catalytic cysteine residue (Cys35). Trx contains four other cysteine residues but only one of these was chosen to be mutated out as only Cys73 appears on the surface of the protein and so is the only cysteine residue that would react with the chemical conjugating agent.

4.1.5. Chemical conjugation of the proteins

4.1.5.1. Chemical conjugation of mPrxII to ET-Srx

To form stable complexes between mPrxII and ET-Srx it was necessary to form a disulfide bond that mimics the proposed thiosulfinate intermediate (Roussel *et al.*, 2008). In the first part of this procedure 5,5'-dithiobis-(2-nitrobenzoic acid) (DTNB) was added to the mPrxII, this reacted with the peroxidatic cysteine leaving TNB. TNB can then be attacked by the cysteine residue on Srx forming the disulfide linkage between the two and resulting in the release of TNB (figure 4.2). The release of TNB can be followed by monitoring the $A_{412\ nm}$.

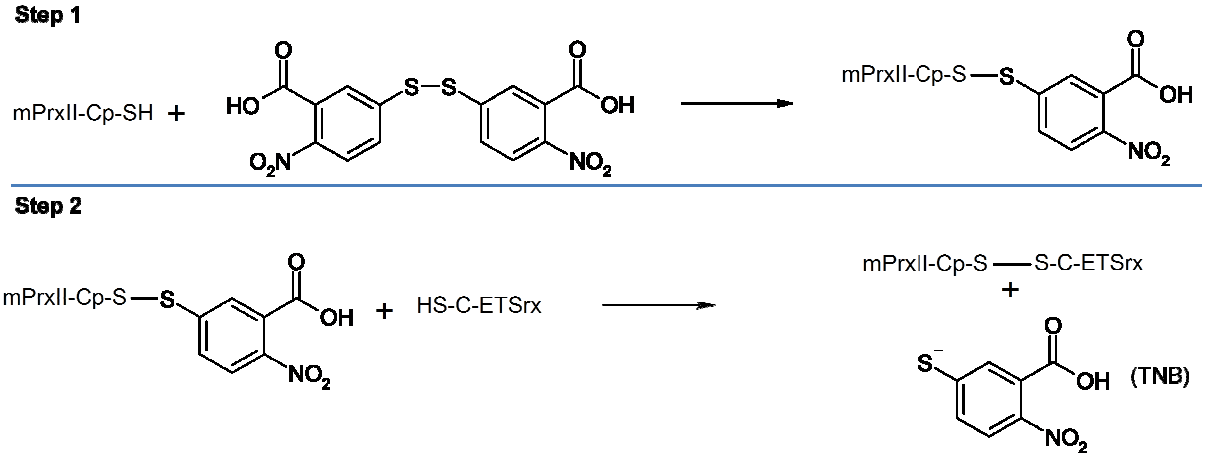

Figure 4.2. The mechanism of conjugation between mPrxII and ET-Srx using DTNB. Step one shows the reaction between mPrxII and DTNB forming a link to the peroxidatic cysteine. Step two shows the ET-Srx replacing the TNB forming the desired complex and releasing the TNB which can be followed at A_{412nm}.

4.1.5.2. Chemical conjugation of mPrxII and Trx

In this case DTNB was used to form the mixed disulfide between the peroxidatic cysteine (Cys51) and the first catalytic cysteine residue on Trx (Cys32). The first step is the same as the above mechanism (figure 4.2) with TNB being added to the peroxidatic cysteine. In this second step the available cysteine residue from Trx replaces the TNB molecule which can be monitored by following the A_{412nm} (figure 4.3).

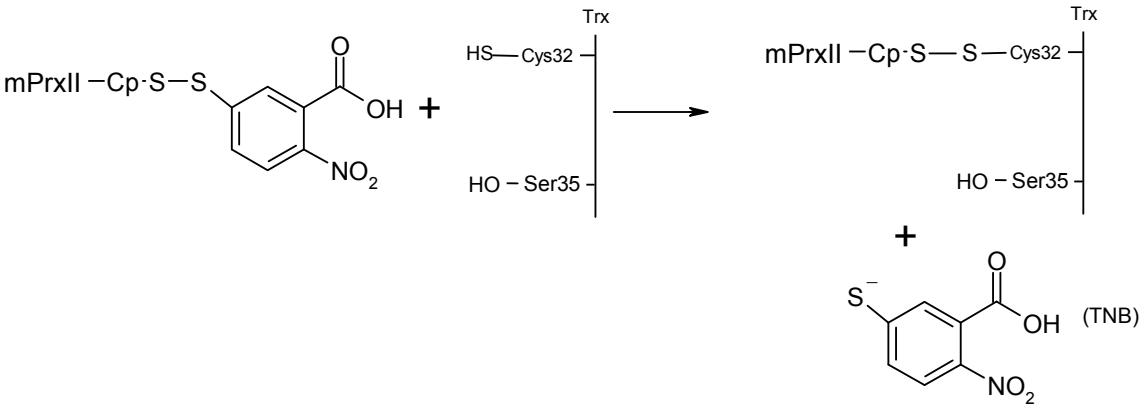

Figure 4.3. The second step of the conjugation reaction with the cysteine residue on Trx replacing the TNB molecule attached to the peroxidatic cysteine of mPrxII. The release of TNB can be monitored by following the A_{412nm}.

4.1.6. Potential interaction with PDCL3

This work was performed in collaboration with Professor Keith Willison (Institute of Cancer Research) and Heather Rada (Institute of Cancer Research). Phosducin-like protein 2 (PLP2) is an ATP-elutable binding partner for the yeast chaperonin-containing TCP-1 (CCT) (McCormack *et al*., 2009). PLP2 has been shown to interact with CCT to help to promote actin folding, with a 30% increase in actin folding with PLP2 compared to without PLP2 (McCormack *et al*., 2009). PDCL3 is the human orthologue of yeast phosducin-like protein 2 (PLP2) (Stirling *et al*., 2007) and a potential interaction with PDCL3 was first identified using electro spray ionization mass spectrometry (ESI-MS). PDCL3 from human colorectal cancer cell extracts and potential binding partners were analyzed by ESI-MS with a very strong signal being shown with PrxI.

4.1.7. Surface plasmon resonance

Surface plasmon resonance (SPR) can be used to measure bimolecular interactions (Homola *et al*., 1999). In this technique polarized light is shone through a prism on to the sensor chip. This sensor chip has a thin layer of gold that acts as a mirror reflecting the light. The angle of incidence of the polarized light is changed and the intensity measured and the intensity passes through a minimum at which point the light will excite surface plasmons. The intensity of the optical field in the waves coming off the surface will decay exponentially with distance from the surface. This will happen at a distance of over 100 nm and means that the SPR angle will change depending on the refractive index (RI) of anything adjacent to the surface (Kooyman, 2008).

An SPR gold chip can have a protein (ligand) covalently linked to the surface and a buffer containing the other protein (analyte) will flow over the chip and the change in RI at the surface can be measured. If the two partner proteins bind or interact with each other there will be a change in the RI and therefore a change in the SPR angle can be observed. SPR is now frequently used to look at protein-protein interactions.

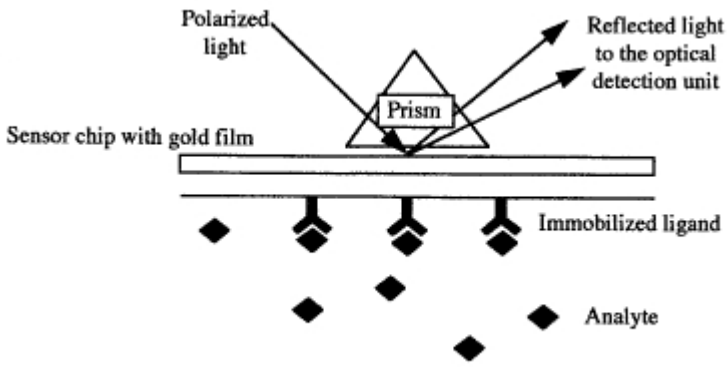

Figure 4.4. The set up of the SPR assay with the prism reflecting light on to the sensor chip gold film surface and the immobilized ligand bound to it interacting with the analyte. Figure modified from Cullen *et al*., (1987).

The typical means of immobilization of the protein to the surface is via amide coupling which consists of three stages: activation, pre-concentration and deactivation. The gold chip is supplied with a layer of carboxylic acids on the surface. During activation of the surface the carboxylic acid group reacts with 1-Ethyl-3-[3-dimethylaminopropyl]carbodiimide (EDC) and is then reacted with N-hydroxysulfosuccinimide (Sulfo-NHS) to form a reactive NHS-ester. Preconcentration is done immediately after activation: the proteins are injected in a condition below their pI so they are positively charged and attracted to the negatively charged surface. Lysine residues containing primary amines will form a stable amide bond to the surface. Unreacted activated carboxyl groups are deactivated in the final step by ethanolamine. Ethanolamine will also remove ligands that are bound electrostatically and not covalently to the surface.

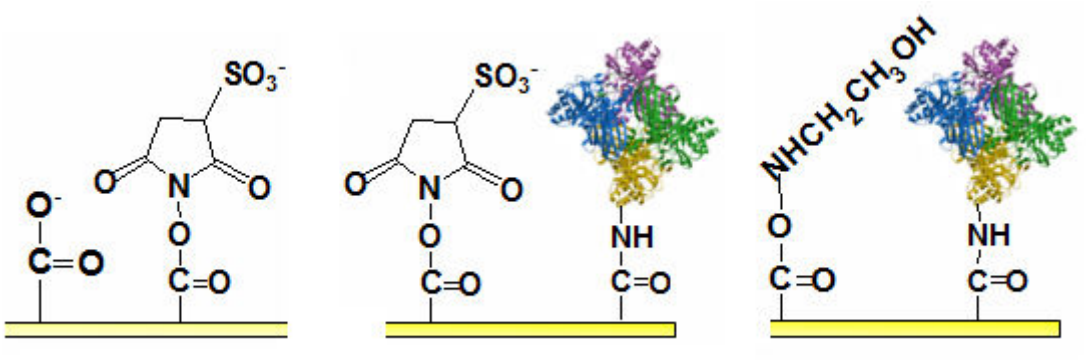

Figure 4.5. The 3 steps for ligand immobilization to the surface of a carboxylic acid coated gold chip. Figure recreated from Kooyman (2008).

There are four steps to an SPR assay that allow reliable results to be obtained. The first step is to achieve a suitable baseline. The sensor surface should be conditioned with a suitable buffer solution to produce a repeatable baseline to which other steps can be compared. In the second step injection of the analyte begins and a shift in RI can be measured that should respond to the association of the analyte to the ligand. This association step should allow the calculation of adsorption kinetics in real time. After a suitable time period injection is switched to a buffer solution that does not contain the analyte and dissociation of the ligand and analyte will occur. Once again in this region dissociation kinetic data should be obtained in real time. The surface is then regenerated for the use in another assay as a solution is injected that will break the specific interaction between the ligand and the analyte while still leaving the ligand covalently bound to the chip surface. A typical cycle will end with buffer injected to reestablish the baseline ensuring no analyte remains bound to the surface of the sensor.

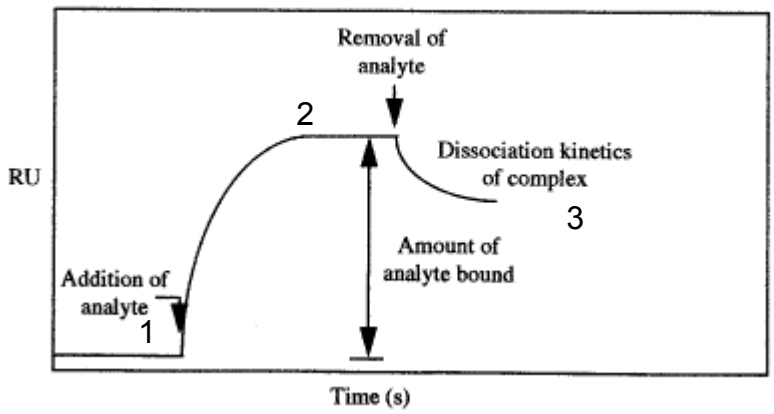

Figure 4.6. A sensogram showing the steps of an SPR assay. Step one shows the baseline; Step two shows association; Step three shows disassociation; after this buffer is injected to re-establish the baseline and check all the analyte has been removed. Figure recreated from Cullen *et al.* (1987).

This chapter will discuss the cloning and over-expression of mPrxII and ET-Srx, as well as the chemical conjugation to produce an mPrxII-ET-Srx complex in order to fully investigate the interactions between hSrx and the decameric form of PrxII. The complex stoichiometry was analyzed using a calibrated gel filtration column and the produced complex was placed into crystallization trials. A potential interaction with PDCL3 was analyzed by native gel electrophoresis and sucrose gradients. Surface plasmon resonance was also attempted to obtain kinetic data on the interactions between the proteins.

4.2. Materials and Methods

4.2.1. Cloning of *ET-Srx*

The original Srx clone was supplied by Dr Kirsty Line, University of Exeter.

4.2.1.1. Primer design

The PCR reaction amplified the entire vector with the deletion incorporated into the oligonucleotide primers. Four primers were designed for this technique.

SRXETF 5’ ATCCACTCGGGCCGCATCGC 3’

SRXETF$_T$ 5’ CCGCGCGCATATG ATCCACTCGGGCCGCATCGC 3’

SRXETR 5’ CACCAGGCCGCTGCTGTGATGATGATGATGATG 3’

SRXETR$_T$ 5'CATATGGCTGCCGCGCGGCACCAGGCCGCTGCTGTGATGATGATGATG ATG 3'

4.2.1.2. SLIM PCR amplification

PCR was carried out to amplify *hSrx* and the expression vector pET28a minus the deletion set by the primers. The PCR was performed in a total volume of 25 µl containing 2.5 µl of 10 x Pfx buffer (Invitrogen, California, USA), 200 µM each dNTP, 1 mM $MgSO_4$, 100 mM betaine, 10 pmol of each primer, 100 pg of the template *hSrx*, 0.5 U *Taq* DNA polymerase (New England Biolabs, Massachusetts, USA), 0.25 U Platinum *Pfx* DNA polymerase (Invitrogen, California, USA) and nuclease free water to adjust to the final volume. The reaction was hot started by heating to 98^{o}C for 2 min, then cooling to 85^{o}C at which point the DNA polymerase mixture was added. The PCR cycle consisted of 30 consecutive cycles of denaturation (15 s at 95^{o}C), annealing (20 s at 50^{o}C) and polymerization (3.5 min at 68^{o}C). The reaction was then subjected to a final extension step of seven minutes at 68^{o}C.

4.2.1.3. SLIM hybridization

The conditions for the hybridization reaction were adapted from Chiu *et al*., (2004). The PCR mixture was diluted in 5 µl of fast enzyme buffer (Fermentas) and mixed with 5 U *Dpn* I. The mixture was incubated for 10 min at 37^{o}C and then denatured by incubating at 99^{o}C for 3 min. Hybridization was performed using two cycles of 65^{o}C for 5 min and 30^{o}C for 15 min. An aliquot of 20 µl from the PCR reaction was used to transform chemically competent *E. coli* One shot TOP10 (Invitrogen, California, USA). The mutation was confirmed by DNA sequencing (Geneservice, Oxford, UK).

4.2.2. Site directed mutagenesis of hPrxII to mPrxII and Trx to mTrx

4.2.2.1. Primer design

Primers were designed using the www.bioinformatics.org/primerx tool. The primers were designed to be between 25-45 base pairs in length, have a melting temperature (T_M) between 75-85^{o}C and GC content between 40-60%.

mPrxII Mutation C172S

mPrxIIFC172S 5' CATGGGGAAGTTAGTCCCGCTGGCTG 3'

mPrxIIRC172S 5' CAGCCAGCGGGACTAACTTCCCCATG 3'

mPrxII Mutation C70S

mPrxIIFC70S 5’ CGCAAGCTGGGCAGTGAAGTGCTGG 3’

mPrxIIRC70S 5’ CCAGCACTTCACCTGCCCAGCTTGCG 3’

mTrx Mutation C35S

mTrxFC35S 5’ CGTGGTGTGGGCCTAGCAAAATGATCAAG 3’

mTrxRC35S 5’ CTTGATCATTTTTGCTAGGCCCACACCACG 3’

mTrx Mutation C73S

mTrxFC73S 5’ GAGTGTGAAGTCAAAAGCATGCCAACATTCC 3’

mTrxRC73S 5’ GGAATGTTGGCATGCTTTTGACTTCACACTC 3’

4.2.2.2. Site directed mutagenesis

The *Trx* DNA was supplied by Dr Kamal Hamidi (University of Exeter). The *hPrxII* and *Trx* DNA was prepared using a mini prep kit (Fermentas) and carried out according to the manufacturer’s instructions. The mutagenesis was carried out following the manufacturer’s instructions using a QuikChange lightning site-directed mutagenesis kit (Stratagene). The mutant DNA was then used to transform chemically competent *E. coli* XL10-Gold ultra-competent cells (Stratagene). The transformation mixtures were spread on LB agar plates containing the appropriate antibiotic selection and incubated at 37^{o}C overnight. A single colony from the mutagenesis reaction was selected and grown overnight in 10 ml LB medium containing the appropriate antibiotic selection and the DNA was extracted and sent for sequencing to confirm the mutation (Geneservice, Oxford, United Kingdom).

4.2.3. Expression of ET-Srx

The ET-Srx/pET28a construct encoded for an N-terminal His-tag and was expressed under the control of the T7 promoter. The recombinant *ET-Srx* gene was transformed into the *E. coli* BL21 (DE3) (Merck Biosciences) expression cell line and these cells were used to inoculate 100 ml LB containing the appropriate antibiotic for selection. The starter culture was grown under agitation at 200 rpm overnight at 37^{o}C and 10 ml used to inoculate fresh 1 L LB medium containing the appropriate antibiotic for selection, and was grown with agitation at 37^{o}C until the OD_{600nm} reached 0.6. IPTG was added to a final concentration of 1.0 mM and the culture incubated for a further 4 hours at 37^{o}C. The *E. coli* cells were harvested by centrifugation (20,000 x *g*, 20 min, 4^{o}C) using a Beckman JA-25.50 rotor. The cell pellet was stored at -20^{o}C until further use.

4.2.4. Expression of mTrx

The mTrx in pET30 Xa/LIC vector encoded for an N-terminal His-tag and was expressed under the control of the T7 promoter. The recombinant *mTrx* gene was transformed into the *E. coli* BL21 (DE3) (Merck Biosciences) expression cell line and these cells were used to inoculate 100 ml LB containing the appropriate antibiotic for selection. The starter culture was grown under agitation at 200 rpm overnight at 37^{o}C and 10 ml was used to inoculate fresh 1 L LB medium containing the appropriate antibiotic for selection, and was grown under agitation at 37^{o}C until the OD_{600nm} reached 0.8. IPTG was added to a final concentration of 1.0 mM and the culture incubated overnight at 37^{o}C. The *E. coli* cells were harvested by centrifugation (20,000 x *g*, 20 min, 4^{o}C) using a Beckman JA-25.50 rotor. The cell pellet was stored at -20^{o}C until further use.

4.2.5. Expression of mPrxII

The mPrxII/pET28a construct encodes for an N-terminal His-tag and was expressed under the control of the T7 promoter. The expression was carried out as in methods 2.2.3 and the pellet stored at -20^{o}C until further use.

4.2.6. Protein purification of ET-Srx and mTrx

4.2.6.1. Cell lysis

The cell paste was re-suspended at 10% w/v in 50 mM Tris-HCl, pH 7.5, 0.5 M NaCl, 20 mM imidazole. Cells were disrupted by sonication as described in 2.2.4.1.

4.2.6.2. Purification buffers

Buffer A – 50 mM Tris-HCl, pH 7.5, 0.5 M NaCl, 20 mM imidazole

Buffer B – 50 mM Tris-HCl, pH 7.5, 0.5 M NaCl, 1 M imidazole

Buffer C – 50 mM Tris-HCl, pH 7.5, 1 M NaCl

4.2.6.3. Nickel affinity chromatography

The nickel affinity chromatography was performed as in methods 2.2.4.3 using a six column volume gradient to 100% buffer B. The fractions containing protein were analyzed using SDS-PAGE as in methods 2.2.4.6.

4.2.6.4. Gel filtration chromatography

The protein fractions were pooled together and concentrated to a 2 ml sample to be loaded onto the GF column using the method described in 2.2.4.5. The

Superdex 200 HiLoad 16/60 (GE Healthcare) was equilibrated with one column volume of buffer C at a flow rate of 1 ml/min. The sample was loaded and fractions were collected over the elution volume (one column volume) and the absorbance measured at 280 nm. The fractions were analyzed using SDS-PAGE as in methods 2.2.4.6.

4.2.7. Protein purification of mPrxII

4.2.7.1. Cell lysis

Cell paste was re-suspended at 10% w/v in 100 mM Tris-HCl, pH 7.5, 0.5 M NaCl, 20 mM imidazole and cell lysis was carried out as in methods 2.2.4.1.

4.2.7.2. Purification buffers

Buffer A – 100 mM Tris-HCl, pH 7.5, 0.5 M NaCl, 20 mM imidazole

Buffer B – 100 mM Tris-HCl, pH 7.5, 0.5 M NaCl, 1 M imidazole

Buffer C – 100 mM Tris-HCl, pH 7.5, 1 M NaCl

4.2.7.3. Nickel affinity and gel filtration chromatography

The nickel affinity chromatography was performed as in methods 2.2.4.3 using a six column volume gradient to 100% buffer B. The fractions containing protein were analyzed using SDS-PAGE as in methods 2.2.4.6. The fractions containing protein were pooled together and concentrated to a 2 ml sample to be loaded on to the GF column using the method described in 2.2.4.5. The fractions were analyzed using SDS-PAGE as in methods 2.2.4.6.

4.2.8. Conjugation of the mPrxII to both mTrx and ET-Srx

The conjugation of mPrxII to ET-Srx was adapted from Jonsson *et al*., (2008b). A similar method has also been used to study the mixed disulfide complexes of Trx (Maeda *et al*., 2006). Once mPrxII had been purified as described above the fractions from GF containing the protein of interest were pooled together and 500 µM 5,5'-dithiobis-(2-nitrobenzoic acid) (DTNB) added. The protein was run down a GF Superdex 200 column to remove excess DTNB and generated TNB. Purified ET-Srx or mTrx was then titrated into the mPrxII solution until no further release of TNB was observed at A_{412nm}. The new complex was then run down a GF Superdex 200 column to remove produced TNB and excess ET-Srx or mTrx.

4.2.9. Crystallization of both complexes

Microbatch crystallization trials were set up in a Hampton 96 well plate using an Oryx 6 crystallization robot (Douglas Instruments, UK). A range of different commercial screens were used for the microbatch trials (as in methods 3.2.4.2). The final droplet volume was varied between 1 µl and 2 µl dependent on the amount of protein solution available. The droplet contained a 50:50 ratio of protein solution to screen ratio. The droplet was covered with Al's oil (50:50 mix of silicon oil and paraffin). The plates were stored at 18^{o}C and regularly checked for crystals using a light microscope.

4.2.10. Interaction with PDCL3

4.2.10.1. Probing the interaction via native gel electrophoresis

Reactions were set up between hPrxII and PDCL3 and between hPrxII and fluorescent labelled PDCL3 (PDCL3*^{568}). Reactions were set up in a 1:1 ratio (1 µg:1 µg) and a 3:1 ratio (3 µg:1 µg) and made up to an overall reaction volume of 10 µl with buffer (20 mM HEPES, 50 mM KCl, pH 8.0). A second round of reactions also took place that contained 1 mM TCEP (reducing agent). The gel was visualized for fluorescence using a Typhoon (Ex-532 nm, Em-610BP30) (Amersham Biosciences) and then Coomassie blue stain.

4.2.10.2. Native SDS-PAGE

The gel was made with a 6% resolving gel and a 3.3% stacking gel.

Resolving Gel	7.5 ml Acrylamide (40%)
	3.7 ml Bis-acrylamide (2 %)
	18.55 ml 1 M Tris (pH8.8)
	25 µl TEMED
	10 µl APS
Stacking Gel	4.0 ml Acrylamide (40%)
	3.0 ml Bis-acrylamide (2 %)
	1 M Tris-HCl pH 8.8
	50 µl TEMED
	15 µl APS

The gels were run using Electrophoresis Buffer (1x): 0.6 g Tris, 2.9 g glycine and ddH_2O to 200 ml. A 10% volume of sample buffer (190 µl Tris-HCl pH 8.8, 1.26 ml glycerol and 50 µl ddH_2O + Bromophenol blue to colour) was added to the sample before running at 90-110 V at 4^oC in a Hoeffer Mini-gel system.

4.2.10.3. Probing the interaction via sucrose gradients

Sucrose gradients were prepared as below and PDCL3*568, incubated with PrxII (1:1 ratio, 50 µg: 50 µg), was applied to the sucrose gradient. The sucrose gradient was made using two buffers.

Buffer A – 20 mM HEPES, pH 8.0, 150 mM KCl, 0.01% LDAO, 15% glycerol, 1 mM TCEP.

Buffer B – 20 mM HEPES, pH 8.0, 150 mM KCl, 0.01% LDAO, 15% glycerol, 1 mM TCEP, 40% sucrose.

10 – 40% sucrose gradient solutions were made in 2.5% steps and stored at -20^oC. Gradients were poured into Beckman Ultra-Clear (13 x 51 mm) centrifuge tubes (Beckman) using 0.4 ml of each solution starting with 40% and decreasing the sucrose solution percentage at each level. Each layer is frozen before the next layer was added and the gradient had a total volume of 5.2 ml. The gradients were centrifuged after addition of 50 µl of sample and tubes spun at 48,000 rpm using a Beckman Coulter Optima L-100 XP ultracentrifuge (Beckman) with an SW55 Ti rotor at 4^oC for 18-19 hours. 600 µl fractions were collected by piercing the bottom of the tubes and collecting drop-wise. This was repeated using three truncations of PDCL3 (1-211, 90-end and 90-226).

4.2.10.4. Identification of potential binding partners for hPrxII

4.2.10.4.1. Confirmation of binding to a Zymo His-Affinity column

First the binding of the PrxII protein to a Zymo His-Affinity column was confirmed. An aliquot of 200 µl fully mixed Zymo His-Affinity gel was placed into two Zymo columns and the columns pulse spun for 5 sec (13,000 rpm max). 50 µl of hPrxII was then added to the top of each column along with 250 µl His-binding buffer (50 mM Na_2HPO_4/ NaH_2PO_4), 300 mM NaCl, 10 mM imidazole, 0.03% Triton-X-100, pH 7.7) to one column and 250 µl *E. coli* post spin lysate to the other. The columns were resuspended and allowed to incubate for ~5 min

followed by a pulse spin for 7 sec (13,000 rpm max). A sample of the flowthrough was taken for SDS-PAGE analysis before being washed three times with 250 µl His-binding buffer followed by a pulse spin for 5 sec (13,000 rpm max). A sample of the first wash was taken for SDS-PAGE analysis. The protein was then eluted from the columns by resuspension with 100 µl His-Elution buffer (50 mM Na_2HPO_4/ NaH_2PO_4, 300 mM NaCl, 250 mM imidazole, pH 7.7) for 1 min followed by a pulse spin for 7 sec (13,000 rpm max) and a sample taken for SDS-PAGE analysis.

4.2.10.4.2. Identification of binding partners using the Zymo His-Affinity column

Adherent human colon carcinoma cells (BE) cell lysate was prepared from six 175 cm^2 flasks of cells lysed in 2 ml HARMS buffer (250 mM sucrose, 10 mM triethanolamine, 10 mM acetic acid, 1 mM EDTA pH 7.45 + complete mini EDTA-free protease inhibitor mix (Roche) with bug buster. The lysate was spun down and the soluble fractions aliquoted into 200 µl samples and snap frozen in liquid nitrogen and stored at -80^oC until further use.

A 100 µl Zymo-His column was run with the addition of 15 µl purified hPrxII diluted with 200 µl of 20 mM HEPES, 50 mM KCl, pH 8.0 buffer and incubated for seven min with mixing. The flowthrough was separated by pulse spin for seven sec (13,000 rpm max). The resin was then resuspended with 100 µl BE cell lysate diluted with 400 µl 20 mM HEPES, 50mM KCl, pH 8.0 buffer and mixed on a roller mixer at 4^oC for 45 min. The flowthrough was then separated by a pulse spin for 10 sec (13,000 rpm max). Three washes were then carried out using 250 µl His-binding buffers and a pulse spin was carried out for five sec. Elution was then carried out by resuspending the resin with 80 µl of His-Elution buffer for two min and the elution sample separated by a pulse spin for seven sec (13,000 rpm max). Samples of the BE cell lysate and the elution from the column were analyzed by SDS-PAGE and the elution sample was sent for analysis by mass spectrometry.

4.2.11. Surface plasmon resonance assay

This work was undertaken in collaboration with Dr Robert Parker (University of Exeter) and run on a SensiQ® Discovery SPR machine. For these experiments a COOH1 (2D surface) chip was used. A second round of experiments was also undertaken using a ProteOn XPR36 (BIORAD) machine in collaboration with

BIORAD and Dr Kamal Hamidi (University of Exeter). For these experiments a GLC (alginate) sensor chip was used.

In all experiments amide coupling immobilization was achieved using EDC and Sulfo-NHS, and capping (or deactivation) was achieved by the injection of ethanolamine. The experiments were designed as below. The proteins were prepared as before (as described in methods 2.2.4) except the final proteins were buffer exchanged into 50 mM Na_2PO_4/ NaH_2PO_4, 0.1 M NaCl, pH 7.5.

4.2.11.1. Interactions between hyperoxidised hPrxII and Srx

Ligand: Srx

Analyte: Prx (SOOH)

Buffer: 50 mM Na_2PO_4/ NaH_2PO_4, 0.1 M NaCl, 1 mM ATP, 1 mM $MgCl_2$, pH 7.5

The ligand was bound to the surface by the injection of 30 µg/ml of ligand. A concentration between 0.1 µM, 75 nm, 50 nM, 25 nM and 10 nM of analyte was injected to test for an interaction between the proteins.

4.2.11.2. Interaction between disulfide hPrxII and Trx

Ligand: Trx

Analyte: Prx (S-S)

Buffer: 50 mM Na_2PO_4/ NaH_2PO_4, 0.1 M NaCl, pH 7.5

The ligand was bound to the surface by the injection of 30 µg/ml of ligand. A concentration between 0.1 µM, 75 nm, 50 nM, 25 nM and 10 nM of analyte was injected to test for an interaction between the proteins.

4.3. Results

4.3.1. Cloning of *ET-Srx*

Plasmid DNA encoding the *hSrx* gene was used as a template for the SLIM reaction. The SLIM PCR amplification of the entire vector minus the deletion set by the primers was carried out as in methods 4.2.1.2. The PCR product underwent hybridization as in methods 4.2.1.3 creating products with complementary 5' and 3' overhangs at opposite termini. These overhangs allowed the DNA to form circular DNA that can then be transformed into chemically competent *E. coli* cells. The transformation yielded eight colonies of

which seven contained the desired mutation. Presence of the mutation was confirmed by DNA sequencing (APPENDIX 7.8) (Geneservice, Oxford, UK).

4.3.2. Site directed mutagenesis of hPrxII to mPrxII

The site-directed mutagenesis of hPrxII to mPrxII was carried out as described in methods 4.2.2.2. The DNA was then transformed into the *E.coli* expression cell line BL21 (DE3) (Merck Biosciences). DNA sequencing (APPENDIX 7.9) (Geneservice, Oxford, UK) was used to confirm the mutation of the cysteine residues at position 172 and position 70 to a serine residue.

4.3.3. Expression of ET-Srx

The pET28a/ET-Srx construct was transformed into the *E. coli* expression strain BL21 (DE3) (Merck Biosciences). ET-Srx protein expression was under the control of the T7 promoter and was induced by IPTG. The over-expression of ET-Srx was investigated by induction studies to obtain the best conditions for over-expression. The optimal over-expression was achieved as described in methods 4.2.3 and the over-expression resulted in soluble protein being produced at the expected size (~13 KDa).

4.3.4. Expression of mTrx

The pET30 Xa/LIC/mTrx construct was transformed into the *E. coli* expression strain BL21 (DE3) (Merck Biosciences). The mTrx protein expression was under the control of the T7 promoter and was induced by IPTG. The over-expression of mTrx was investigated by induction studies to obtain the best conditions for over-expression. The optimal over expression was achieved as described in methods 4.2.4 and the over-expression resulted in soluble protein being produced at the expected size (~12 KDa).

4.3.5. Expression of mPrxII

The pET28a/mPrxII construct was transformed into the *E. coli* expression strain BL21 (DE3) (Merck Biosciences). The mPrxII protein expression was under the control of the T7 promoter and was induced by IPTG. The over-expression of mPrxII was investigated by induction studies to obtain the best conditions for over-expression. The optimal over-expression was achieved as described in methods 4.2.4 and the over-expression resulted in soluble protein being produced at the expected size (~24 KDa).

4.3.6. Purification of ET-Srx and mTrx

One litre of ET-Srx culture produced 1.6 g of cell paste and one litre of mTrx culture produced 2.8 g of cell paste. After cell lysis and centrifugation (as described in methods 2.2.4.1) the supernatant was purified using nickel affinity chromatography and gel filtration chromatography (as described in sections 4.2.5.3 and 4.2.5.4.)

4.3.6.1. ET-Srx nickel affinity chromatography

The clarified cell extract was applied to a nickel column as described in methods 4.2.6.3 producing the trace seen in figure 4.7. The fractions were analyzed using SDS-PAGE as described in methods 2.2.3.6 (figure 4.8). The fractions containing ET-Srx were pooled together and concentrated for gel filtration chromatography (as in methods 4.2.6.4).

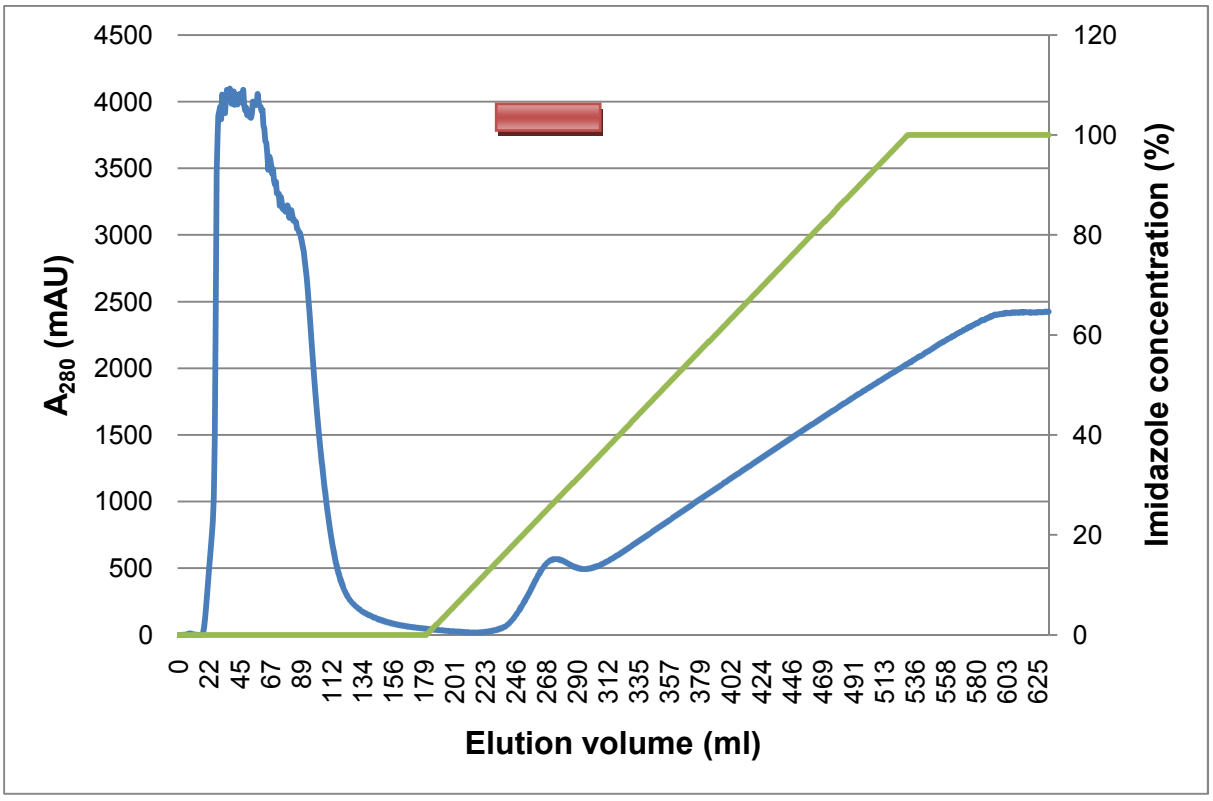

Figure 4.7. Elution profile of ET-Srx (blue line) from nickel affinity chromatography. 10 ml fractions were collected throughout the entire elution. The green line shows the % imidazole concentration. The fractions that showed a band of the correct size on SDS-PAGE are indicated by a red bar.

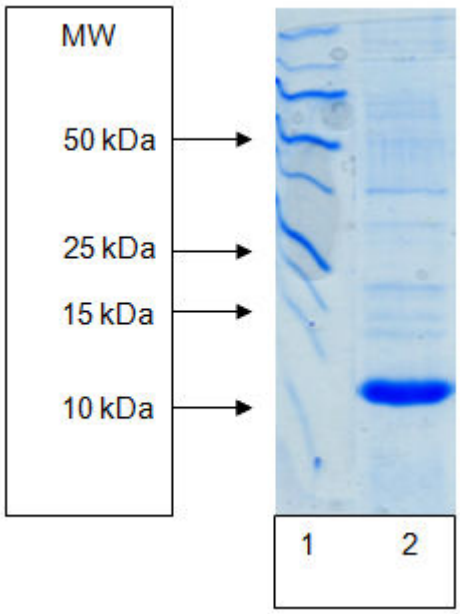

Figure 4.8. SDS-PAGE analysis of the ET-Srx nickel affinity chromatography elution. Lane 1, molecular weight marker; Lane 2, sample from fraction at 270 ml (middle of the elution peak).

4.3.6.2. mTrx nickel affinity chromatography

The clarified cell extract was applied to a nickel column as described in methods 4.2.6.3 producing the trace seen in figure 4.9. The fractions were analyzed using SDS-PAGE as described in methods 2.2.3.6 (figure 4.10). The fractions containing mTrx were pooled together and concentrated for gel filtration chromatography.

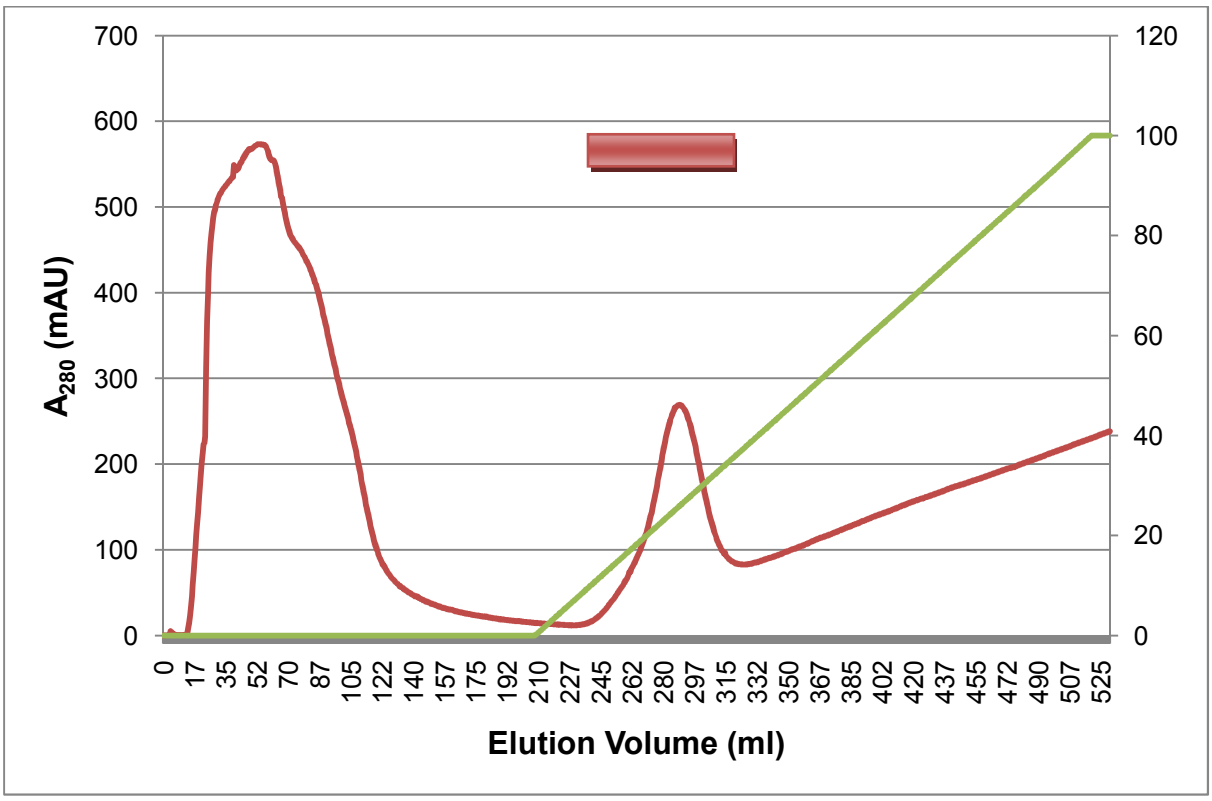

Figure 4.9. Elution profile of mTrx (red line) from nickel affinity chromatography. 10 ml fractions were collected throughout the entire elution. The green line shows the % imidazole concentration. The fractions that showed a band at the correct size on SDS-PAGE are indicated by a red bar.

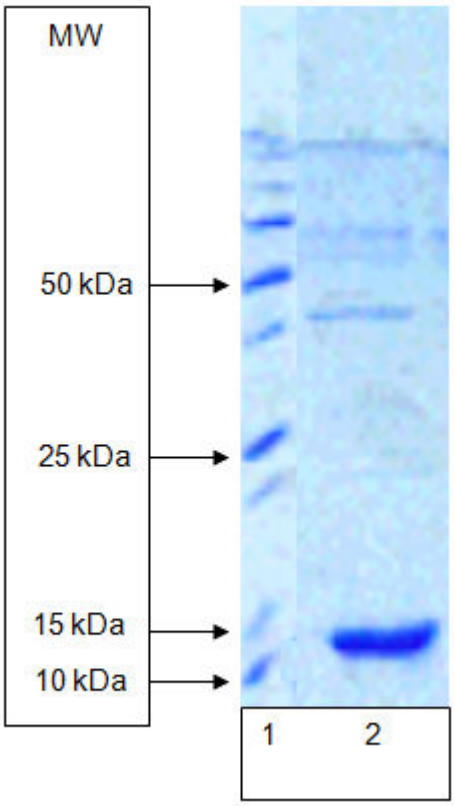

Figure 4.10. SDS-PAGE analysis of the mTrx nickel affinity chromatography elution. Lane 1, molecular weight marker; Lane 2, sample from middle of peak from nickel affinity chromatography (~290 ml).

4.3.6.3. ET-Srx gel filtration chromatography

Gel filtration chromatography was used as a final step of the purification and as a tool for the estimation of the oligomeric state of the protein. The concentrated protein sample was loaded onto a Superdex 200 column and run as described in methods 4.2.6.4, the elution profile of which can be seen in figure 4.11. The peak fractions were analyzed by SDS-PAGE (figure 4.12) and those that contained ET-Srx were pooled and concentrated. Pure ET-Srx protein was obtained and eluted at ~93 ml from the calibrated gel filtration corresponding to a molecular weight of ~13 kDa suggesting it was present as a monomer.

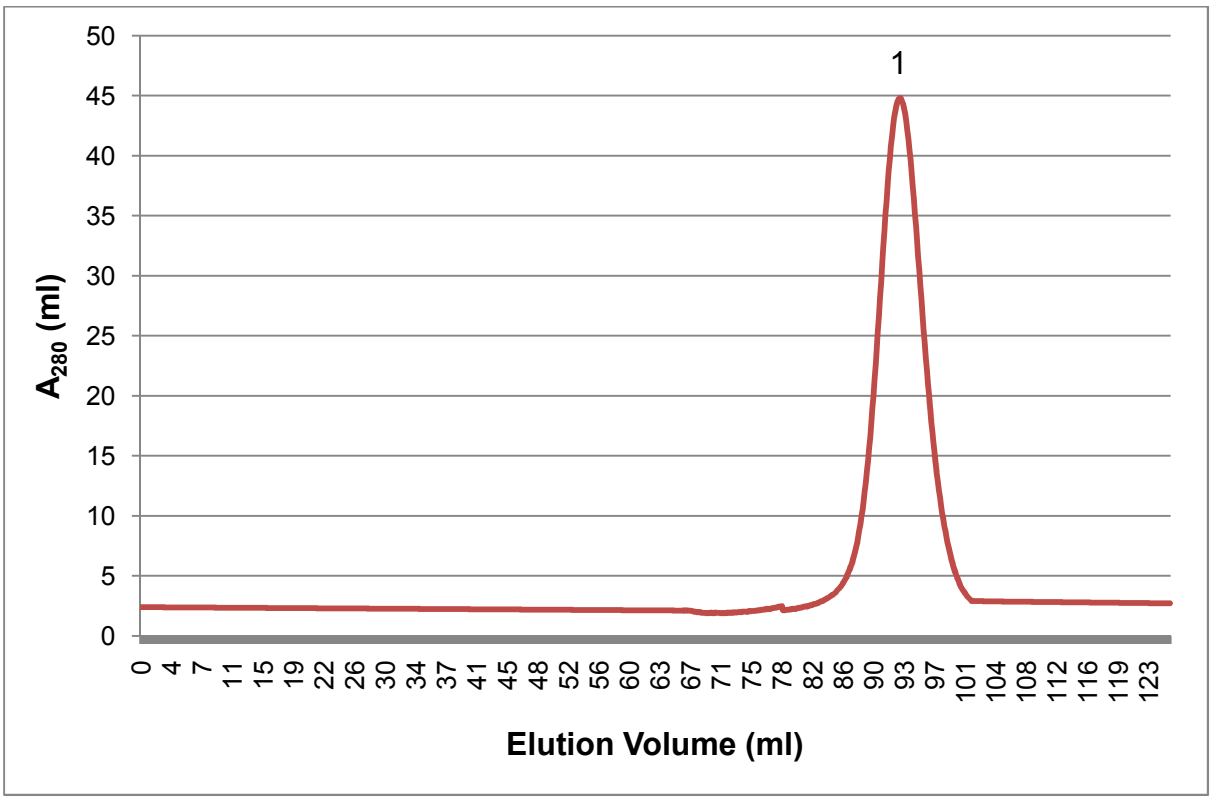

Figure 4.11. Elution profile from the gel filtration column for ET-Srx (red line). 1 ml fractions were collected throughout the elution volume. Peak 1 (92 ml) corresponds to the monomeric ET-Srx (~13 kDa). The molecular weight was determined using a calibrated Superdex 200 column (Appendix 7.1).

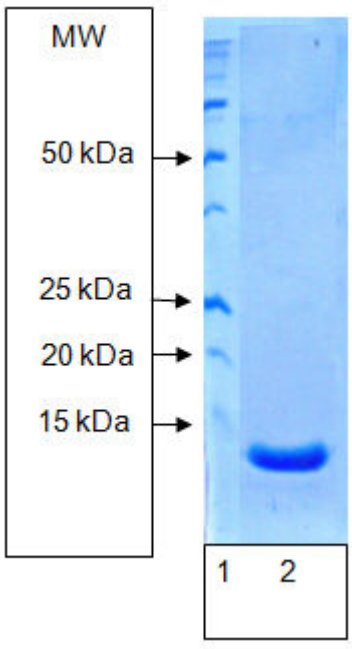

Figure 4.12. SDS-PAGE analysis of the elution from the ET-Srx gel filtration column. Lane 1, molecular weight marker; Lane 2, sample from peak 1 (~93 ml).

4.3.6.4. mTrx gel filtration chromatography

Gel filtration chromatography was used as a final step of the purification and as a tool for the estimation of the oligomeric state of the protein. During the first gel filtration run the protein eluted at 86 ml which corresponds to a MW of ~24 kDa suggesting it was present as a dimer whereas Trx is functionally active as a monomer (as discussed in section 1.7). The protein was then incubated with a final concentration of 5 mM DTT to break any potential disulfide bonds between monomeric units and then loaded onto a Superdex 200 column and run as described in methods 4.2.6.4. The elution profile can be seen in figure 4.13. The peak fractions were analyzed by SDS-PAGE (figure 4.14) and those that contained mTrx were pooled and concentrated. After treatment with DTT pure Trx protein was obtained and the protein eluted at ~93 ml, corresponding to a molecular weight of ~12 kDa, suggesting it was present as a monomer.

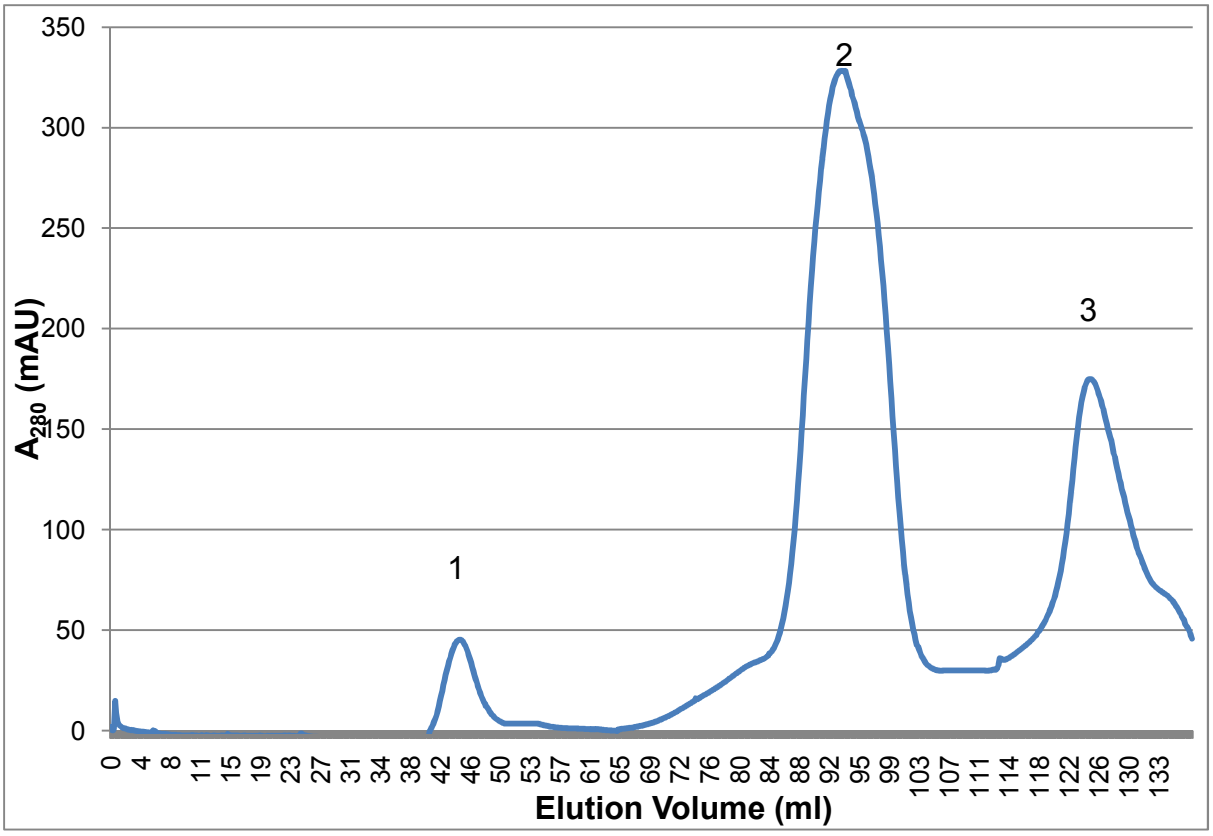

Figure 4.13. Elution profile of mTrx (blue line) from gel filtration chromatography. Fractions were collected at 1 ml intervals throughout the elution volume. Peak 1 (~44 ml) corresponds to the void volume; Peak 2 (~93 ml) corresponds to the monomeric Trx (12 kDa); Peak 3 (~125 ml) corresponds to the DTT used to separate the Trx dimer.

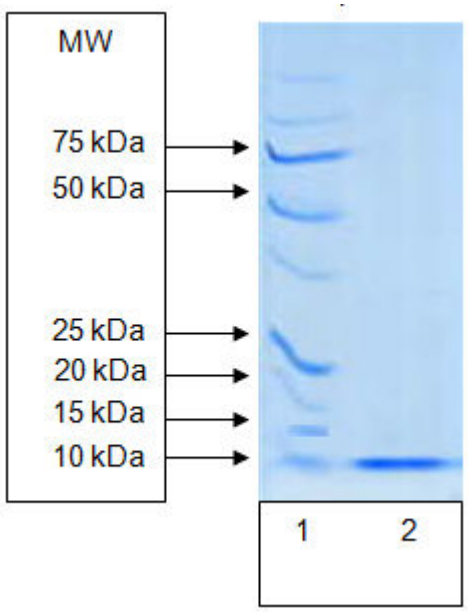

Figure 4.14. SDS-PAGE analysis of the mTrx gel filtration chromatography elution. Lane 1, molecular weight marker; Lane 2, sample from peak 2 (~93 ml) corresponding to a MW of ~12 kDa.

4.3.7. Purification of mPrxII

One litre of culture produced 2.2 g of cell paste and after cell lysis and centrifugation (as described in methods 2.2.4.1) the supernatant was purified using nickel affinity chromatography and gel filtration chromatography (as described in sections 4.2.6.3).

4.3.7.1. Nickel affinity and gel filtration chromatography

The clarified cell extract was applied to a nickel column as described in methods 4.2.7.3 producing the trace seen in figure 4.15. The fractions were analyzed using SDS-PAGE as described in methods 2.2.3.6 (figure 4.16). The fractions containing ET-Srx were pooled together and concentrated for gel filtration chromatography and the column ran as in methods 4.2.7.3 producing the trace seen in figure 4.17. The fractions were analyzed using SDS-PAGE as described in methods 2.2.3.6 (figure 4.18). Pure mPrxII protein was obtained and eluted at ~58 ml from the calibrated gel filtration corresponding to a molecular weight of ~250 kDa suggesting it was present as a decamer.

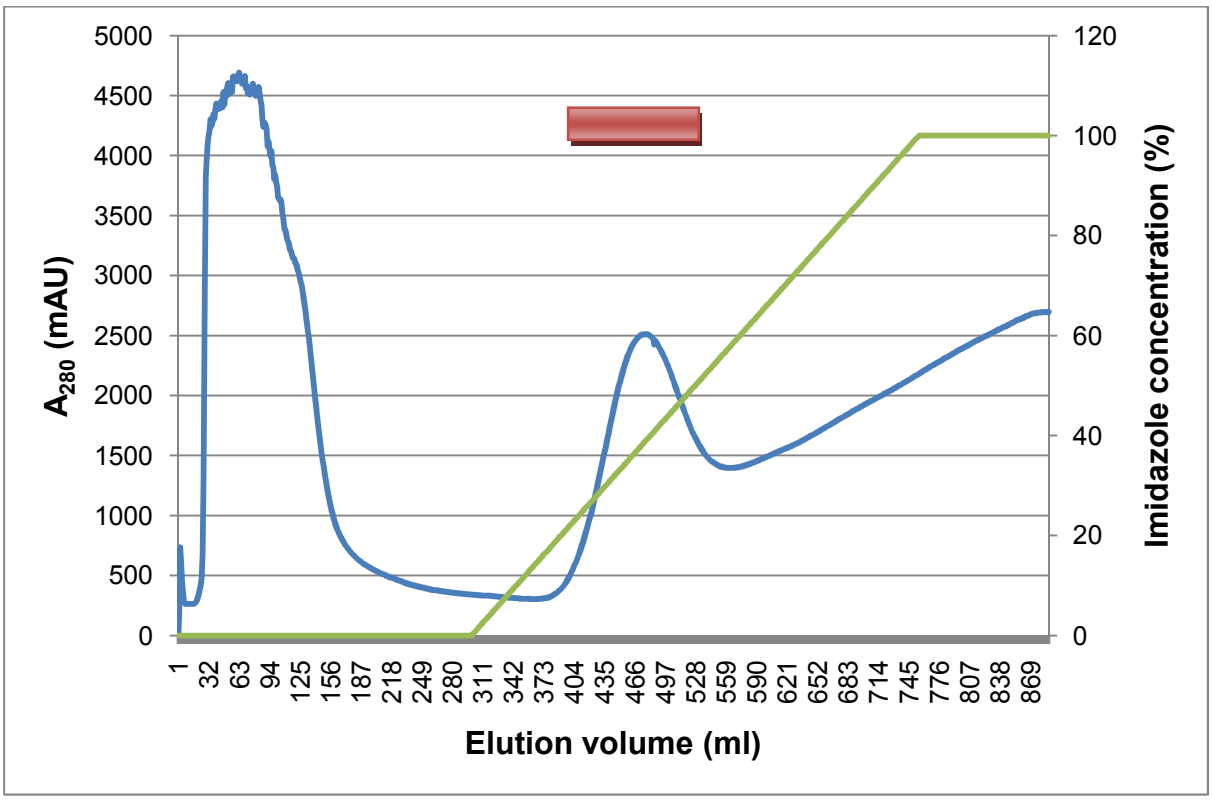

Figure 4.15. Elution profile of mPrxII from nickel affinity chromatography (blue line). Fractions were collected at 10 ml intervals throughout the entire elution. The green line shows the % imidazole concentration. The fractions that showed a band of the correct size on SDS-PAGE are indicated by a red bar.

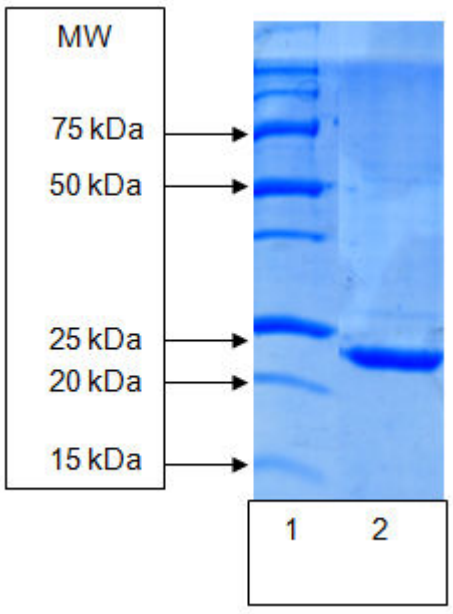

Figure 4.16. SDS-PAGE analysis of peak fractions from mPrxII nickel column. Lane 1, molecular weight marker; Lane 2, sample from the middle of the peak from the nickel chromatography elution (~460 ml)

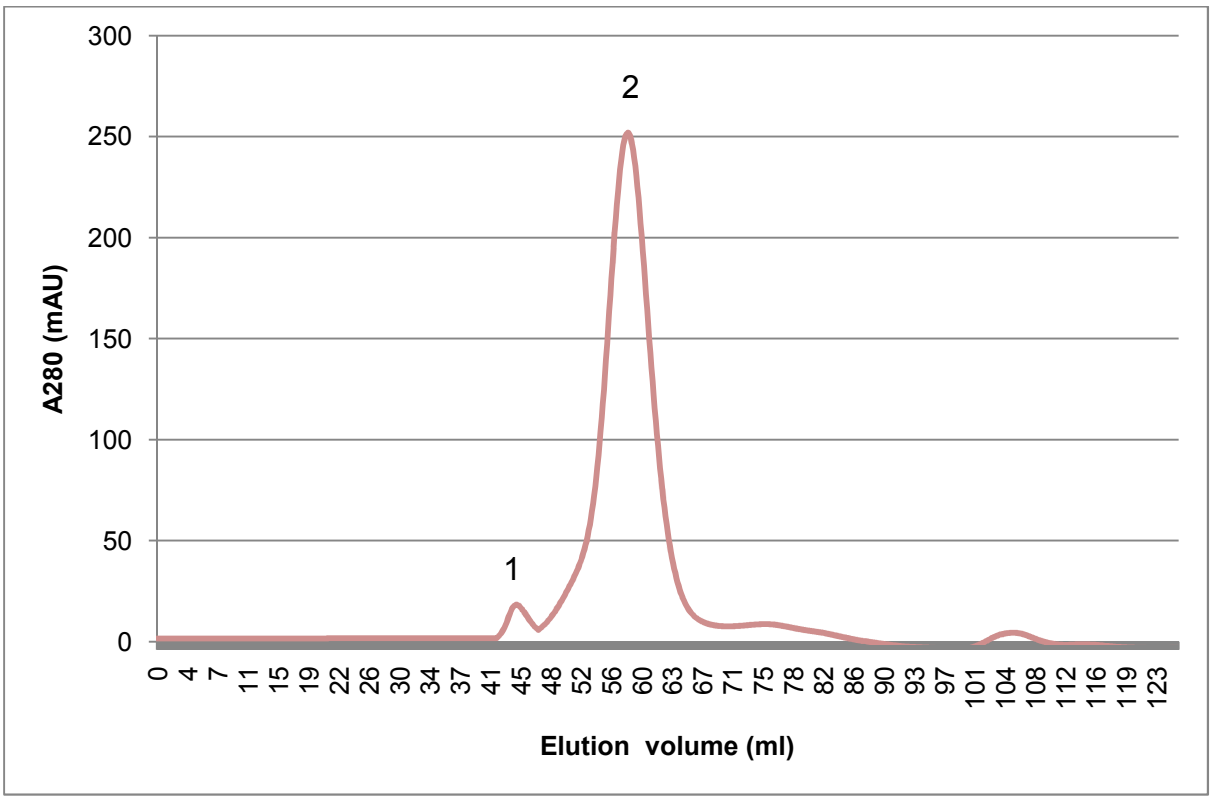

Figure 4.17. Elution profile of mPrxII from gel filtration chromatography. Peak 1 corresponds to the void volume (~44 ml); Peak 2 corresponds to the decameric form (~250 kDa) of the protein (~56 ml).

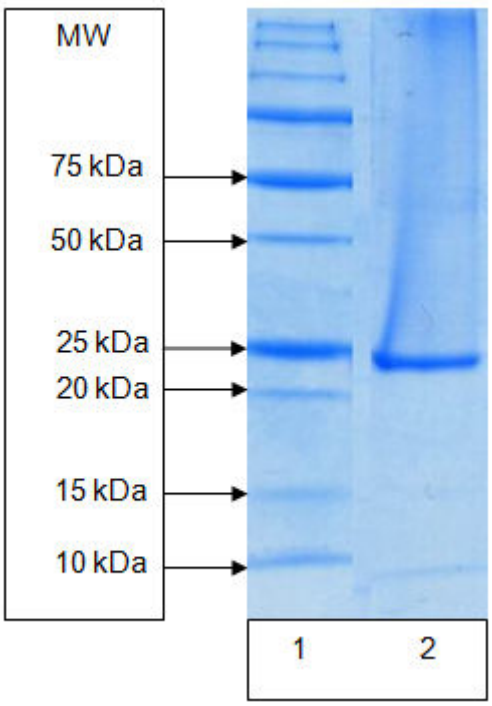

Figure 4.18. SDS-PAGE analysis of peak fraction from mPrxII gel filtration column. Lane 1, molecular weight marker; Lane 2, sample from peak 2 (~56 ml).

4.3.8. Conjugation of mPrxII to ET-Srx

Conjugation of mPrxII to ET-Srx was carried out as in methods 4.2.8. In the first step the free peroxidatic cysteine on mPrxII was reacted with DTNB. The formation of the mPrxII-TNB complex was confirmed by the addition of dithiothreitol and monitoring the release of TNB by measuring A_{412nm}. After this step the protein-DTNB mix was run down the GF column to remove excess DTNB before the addition of ET-Srx. The second step was to react the mPrxII-TNB with ET-Srx. As the ET-Srx has a higher affinity to the peroxidatic cysteine the complex was formed replacing the TNB. This was confirmed by watching the release of the TNB at A_{412nm}. After each step the proteins were run down a Superdex 200 column as in methods 4.2.6.4 the trace of which can be seen in figure 4.19.

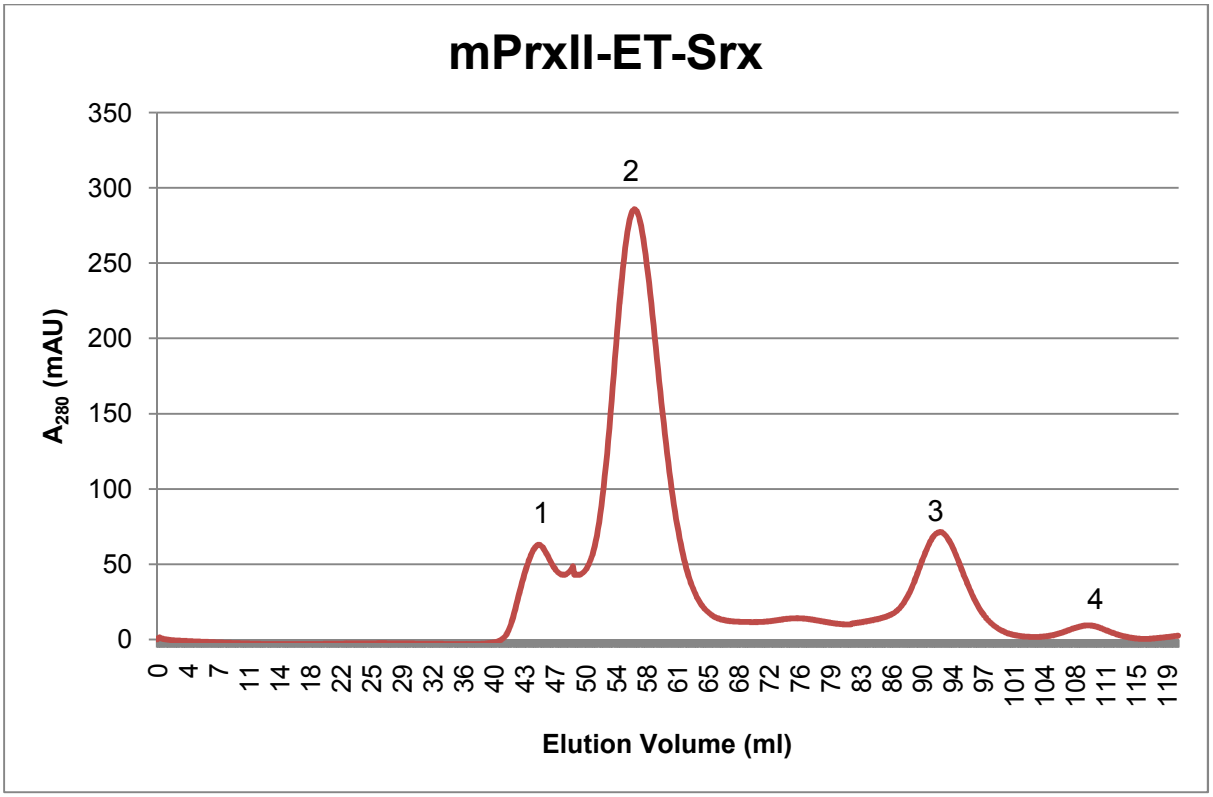

Figure 4.19. The elution profile from the gel filtration column for mPrxII-ET-Srx (red line). Peak 1 corresponds to the void volume (~44 ml); Peak 2 corresponds to the mPrxII-ET-Srx complex (~56 ml); Peak 3 corresponds to Srx (~92 ml); Peak 4 corresponds to TNB produced in the conjugation reaction.

The gel filtration elution of ET-Srx produced a peak at ~92 ml. The molecular weight of this peak can be estimated using a calibration curve from the

Superdex 200 column (appendix 7.1). This estimates the molecular weight at ~13 kDa which corresponds to the monomeric truncated protein. The gel filtration elution of mPrxII produced a peak at ~58 ml. The molecular weight is estimated at ~245 kDa which corresponds to the decameric form of mPrxII. Once this protein had been reacted with DTNB the elution volume decreased to ~56 ml and the molecular weight was estimated at slightly above that expected for the decameric protein. A small peak was also seen at the very end of the column corresponding to un-reacted DTNB and produced TNB. This complex was then reacted with ET-Srx and the elution volume increased to ~55 ml. The molecular weight was estimated at ~300 kDa. SDS-PAGE analysis of the peak at ~56 ml showed the presence of both mPrxII and ET-Srx (figure 4.20).

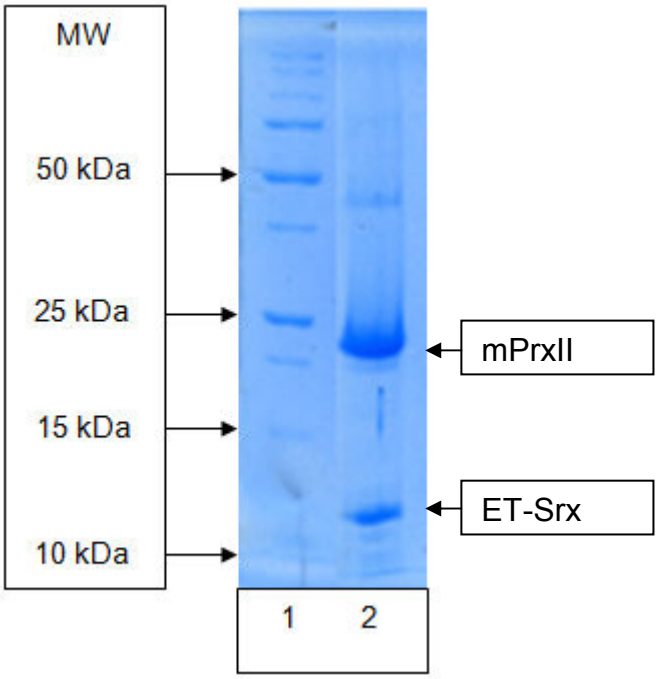

Figure 4.20. SDS-PAGE analysis of peak 2 from the gel filtration column elution of mPrxII-Et-Srx. Lane 1 molecular weight marker; Lane 2, sample from peak 2, this shows a band at the size of mPrxII (~25 kDa) and a band at the size of ET-Srx (~13 kDa).

Using the calibration curve from the gel filtration column the presence of the decameric form of the protein (~245 kDa) it is evident that there is ~65 kDa of ET-Srx attached to the mPrxII. This would indicate that we are seeing five molecules of ET-Srx reacting with one mPrxII decamer.

4.3.9. Conjugation of mPrxII to mTrx

Conjugation of mPrxII to mTrx was carried out as in methods 4.2.8. In the first step the free peroxidatic cysteine on mPrxII was reacted with DTNB. The formation of the mPrxII-TNB complex was confirmed by the addition of dithiothreitol and monitoring the release of TNB by meaduring A_{412nm}. The second step was to react the mPrxII-TNB with mTrx. As the mTrx has a higher affinity to the peroxidatic cysteine the complex was formed replacing the TNB. This was confirmed by watching the release of TNB at A_{412nm}. After each step the proteins were run down a Superdex 200 column as in methods 4.2.6.4, the trace of which can be seen in figure 4.21.

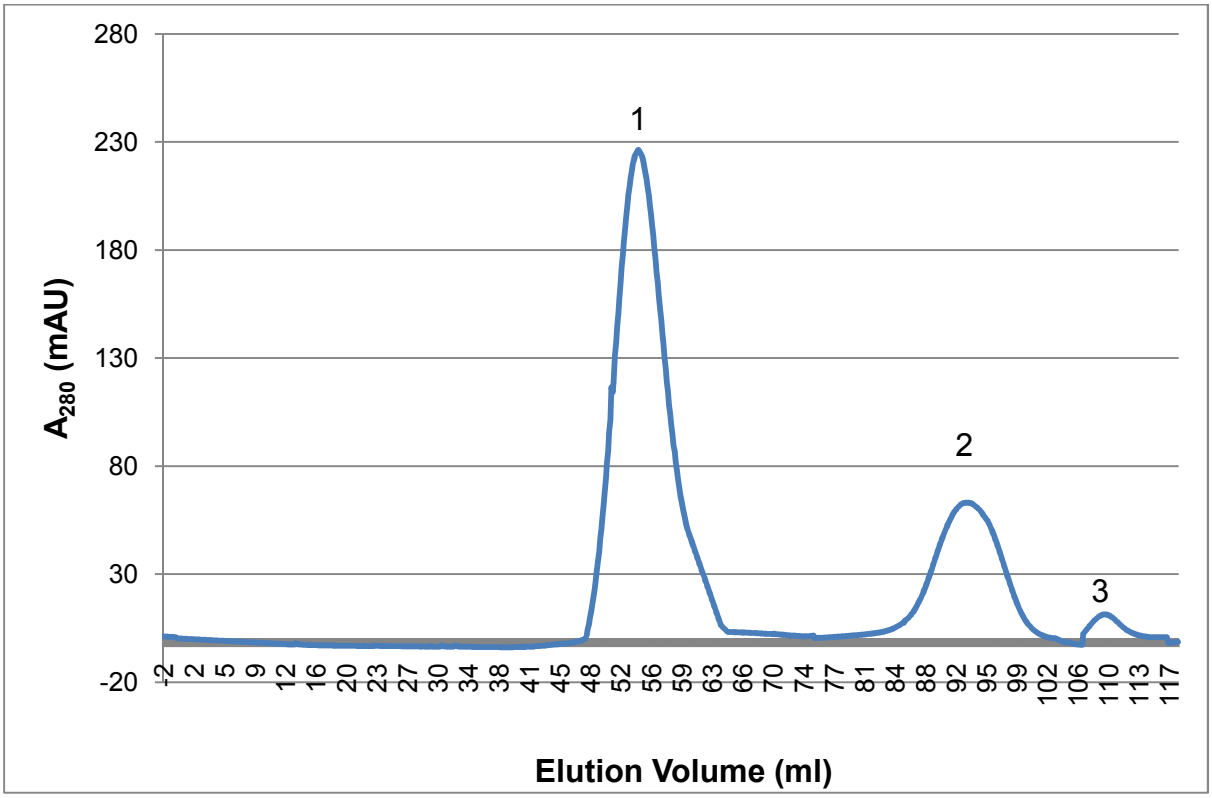

Figure 4.21. The elution profile from the gel filtration column for mPrxII-mTrx (blue line). Peak 1 corresponds to the mPrxII-mTrx complex (~54 ml); Peak 2 corresponds to un-reacted mTrx (~93 ml). Peak 3 corresponds to TNB released as part of the reaction (~110 ml).

The gel filtration elution of the mTrx produced a peak at ~93 ml. The molecular weight of this peak is estimated at ~12 kDa which corresponds to the

monomeric form of the Trx protein. The gel filtration elution of mPrxII produced a peak at ~58 ml. The molecular weight is estimated at ~250 kDa which corresponds to the decameric form of mPrxII. Once this protein had been reacted with DTNB the elution volume decreased to ~55 ml and the molecular weight was estimated at slightly above that expected for the decameric protein. A small peak was also seen at the very end of the column corresponding to un-reacted DTNB and produced TNB. This complex was then reacted with mTrx and the elution volume decreased to ~54 ml. The molecular weight was estimated at ~367 kDa. SDS-PAGE analysis of the peak at ~54 ml showed the presence of both mPrxII and mTrx (figure 4.22.).

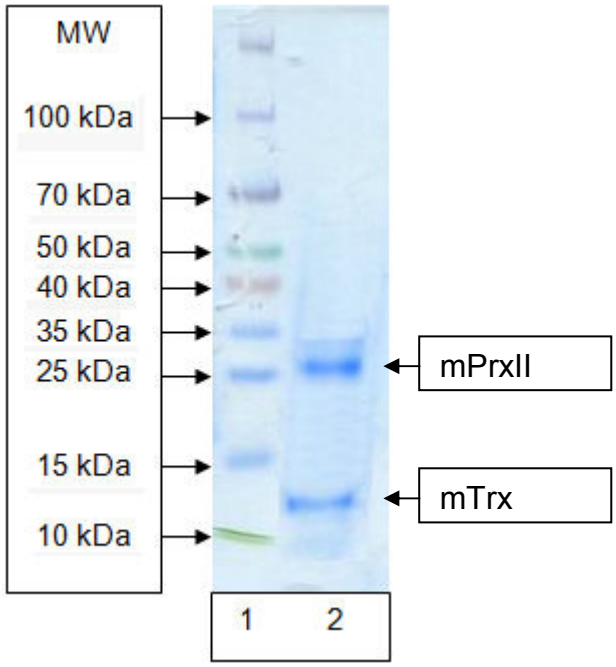

Figure 4.22. SDS-PAGE analysis of peak 2 from the gel filtration column elution of mPrxII-mTrx. Lane 1 molecular weight marker (Spectra™ multicolour broad range protein ladder (Fermentas) (appendix 7.10); Lane 2, sample from peak 2, showing a band at the size of mPrxII (~25 kDa) and a band at the size of mTrx (~12 kDa).

Using the calibration curve from the gel filtration column and the presence of the decameric form of the protein (~245 kDa) it is evident that there is ~120 kDa of mTrx attached to the mPrxII. This would indicate that we are seeing 10 molecules of mTrx reacting with one mPrxII decamer.

4.3.10. Interaction with PDCL3

4.3.10.1. Probing the interaction via native gel electrophoresis

The hPrxII was run on a native gel with PDCL3 and PDCL3*[568] as in methods 4.2.10.1 (figure 4.23). The hPrxII was also run on a native gel in the presence of a reducing agent (TCEP) with PDCL3 and PDCL3*[568] as in methods 4.2.10.1 and the fractions analyzed using SDS-PAGE (gel not shown). The gels were also visualized on a Typhoon (Ex-532nm, Em-610BP30) (figure 4.24).

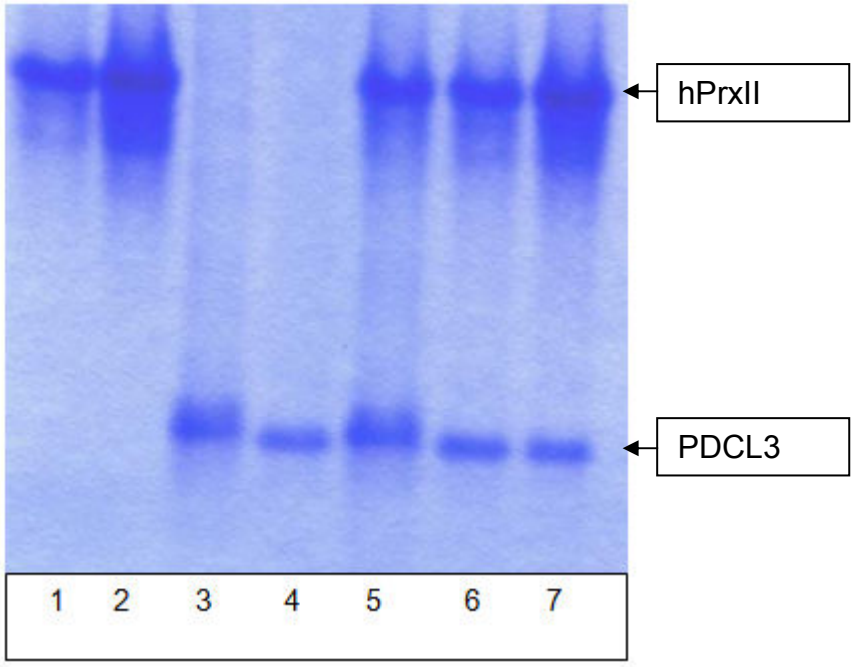

Figure 4.23. Native gel analysis of complex formation between hPrxII and PDCL3. Lane 1, 1 µg PrxII; Lane 2, 3 µg PrxII Lane 3, 1 µg PDCL3; Lane 4, 1 µg PDCL3*[568]; Lane 5, 1 µg PrxII + 1 µg PDCL3; Lane 6, 1 µg PrxII + 1 µg PDCL3*[568]; Lane 7, 3 µg PrxII + 1 µg PDCL3*[568].

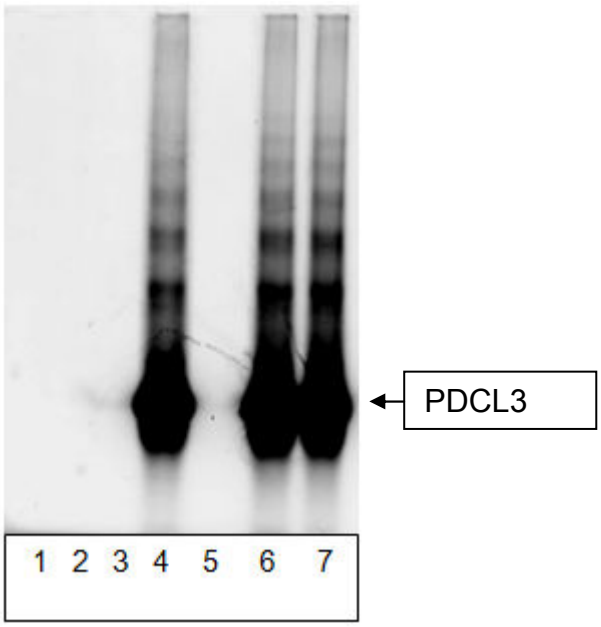

Figure 4.24. Fluorescence image of complex formation between hPrxII and PDCL3. Lane 1, 1 µg PrxII; Lane 2, 3 µg PrxII Lane 3, 1 µg PDCL3; Lane 4, 1 µg PDCL3*^{568}; Lane 5, 1 µg PrxII + 1 µg PDCL3; Lane 6, 1 µg PrxII + 1 µg PDCL3*^{568}; Lane 7, 3 µg PrxII + 1 µg PDCL3*^{568}.

It was confirmed that hPrxII ran well on a native gel with a sharp band obtained with both with a fresh and samples after snap freezing in liquid nitrogen and stored at -80^{o}C overnight. Addition of TCEP did affect the running of hPrxII showing some slight smearing, but this did not break down the hPrxII decamer. No shifting was seen in any of the lanes containing both hPrxII and either PDCL3 and PDCL3*^{568}.

4.3.10.2. Probing the interaction via sucrose gradients

The interaction between hPrxII and PDCL3 was best analysed using sucrose gradients rather than the slightly dissociative conditions of the native gel system. An interaction was observed between hPrxII and PDCL3 in fractions 6 and 7 from the sucrose gradient (Figures 4.25 and 4.26). The complex was estimated to migrate at ~ 200 – 300 kDa. This estimates the binding ratio to be 10:1 (PDCL3: hPrxII(decamer)). When the sucrose gradients were run with the three truncated forms of the PDCL3 (1-211, 90-end and 90-226) no interaction was seen between the two protein fragments that start at residue 90 suggesting the interaction site was located on the N-terminus.

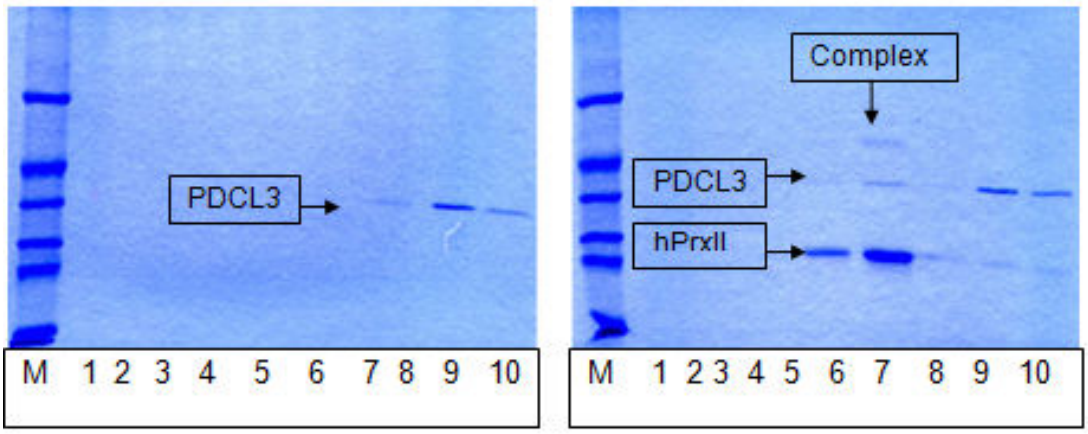

Figure 4.25. SDS-PAGE analysis of hPrxII interacting with PDCL3 on a sucrose gradient. M is the Sigma SDS 7 molecular weight marker (Appendix 7.12) and the numbers correspond to the fraction collected from sucrose gradient (as in methods 4.2.10.3). The gel on the left is PDCL3 run without hPrxII, the gel on the right is run with hPrxII.

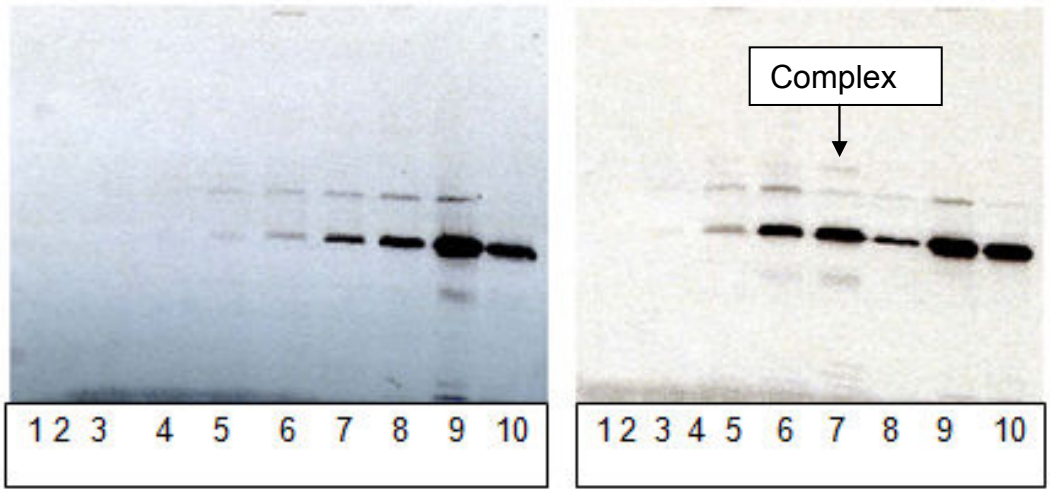

Figure 4.26. Fluorescence image hPrxII interacting with PDCL3*[568] on a sucrose gradient with only PDCL3*[568] being visualised. The numbers correspond to the fraction collected from the sucrose gradient (as in methods 4.2.10.3). The gel on the left is PDCL3 run without hPrxII, the gel on the right is run with hPrxII.

4.3.10.3. Identification of potential binding partners for hPrxII

4.3.10.3.1. Confirmation of binding to a Zymo His-Affinity column

The hPrxII binding to the Zymo His-Affinity was confirmed as in methods (4.2.10.4.1) and the fractions analyzed by SDS-PAGE (figure 4.27). Both proteins (PrxII and PrxII + *E.coli* lysate) behaved identically on the Zymo columns, binding without any problem.

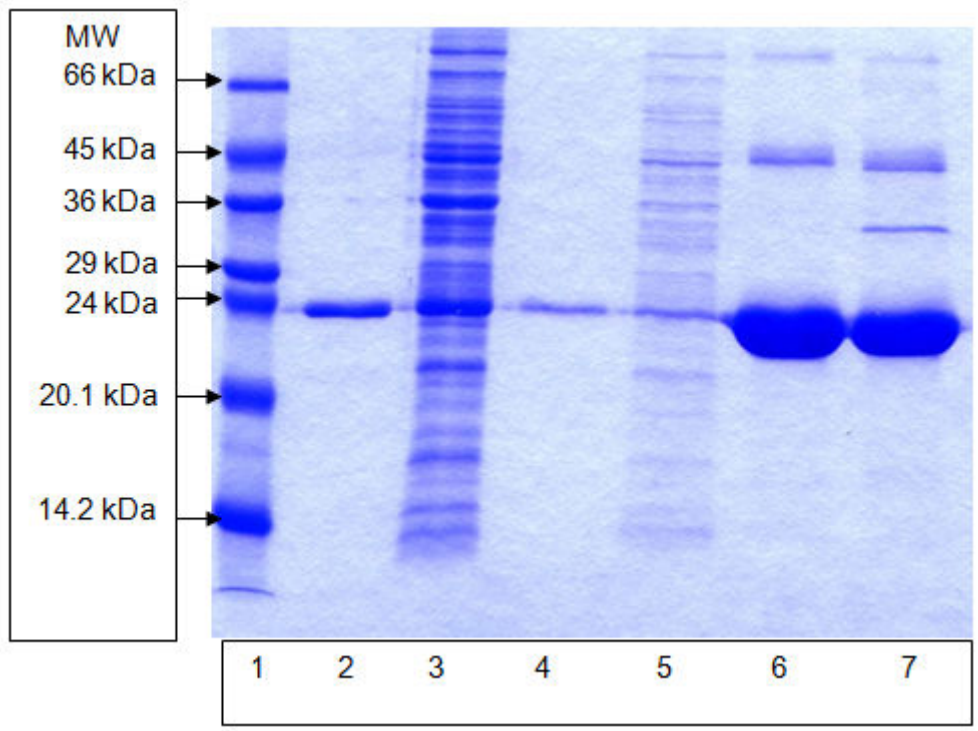

Figure 4.27. SDS-PAGE analysis of hPrxII binding to the Zymo His-Affinity column. Lane 1, Sigma SDS 7 molecular weight marker (Sigma)(Appendix 7.12); Lane 2, post resin lysate (-); Lane 3, post resin lysate (+); Lane 4, wash 1 (-); Lane 5, wash 1 (+); Lane 6, elution (-); Lane 7, elution (+). (-) is without *E. coli* lysate added, (+) is with *E. coli* lysate added.

4.3.10.3.2. Identification of binding partners using the Zymo His-Affinity column

The hPrxII was bound to the Zymo His-Affinity column and the BE cell lysate was run over it as in methods 4.2.10.4.2. SDS-PAGE analysis of the elution confirmed that some proteins had been pulled down by the hPrxII attached to the column (figure 4.28). The elution sample was sent for mass spectrometry sequencing to identify the proteins content using trypsin digestion and comparison of the fragment pattern against known protein fingerprints. These results are still awaiting analysis.

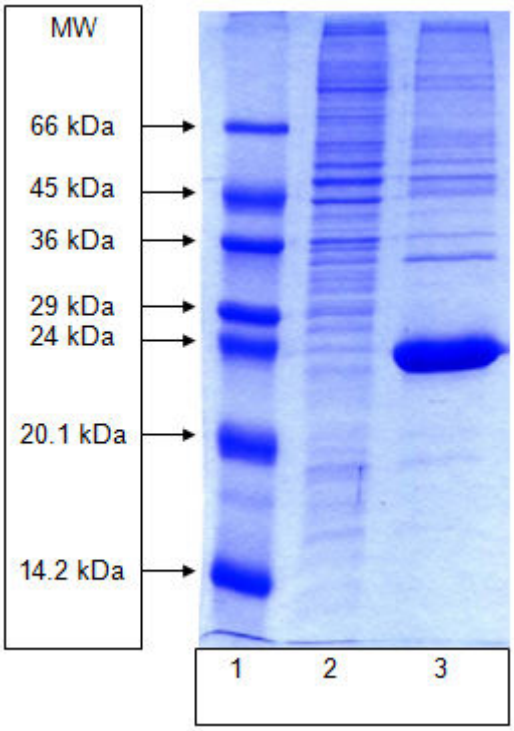

Figure 4.28. SDS-PAGE analysis of hPrxII pull down from the BE cell lysate from the Zymo His-Affinity column. Lane 1, Sigma SDS 7 molecular weight marker (Sigma) (Appendix 7.12); Lane 2, BE cell lysate; Lane 3, elution 1 sample.

4.3.11. Surface plasmon resonance assay results

In all assays (both BIORAD and “in house”) the ligand was found to bind to the surface of the chip in varying amounts but within the amounts needed to allow for data to be collected (figure 4.29). No results were obtained for these assays due to non specific binding (figure 4.30) dominating the signal or due to a lack of an interaction being observed between the ligand and the analyte (data not shown). Potential reasons for this are discussed below.

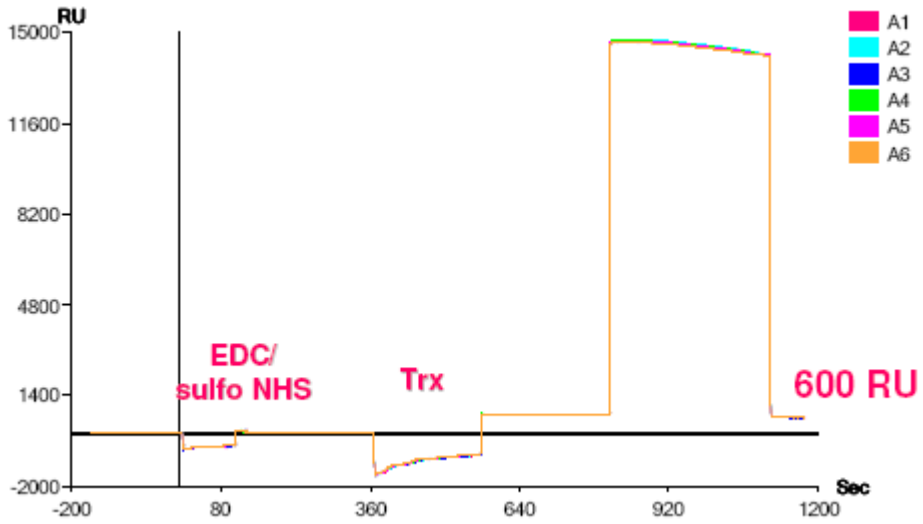

Figure 4.29. Typical sensogram for the immobilization of the ligand to the carboxylic acid surface of the gold chip.

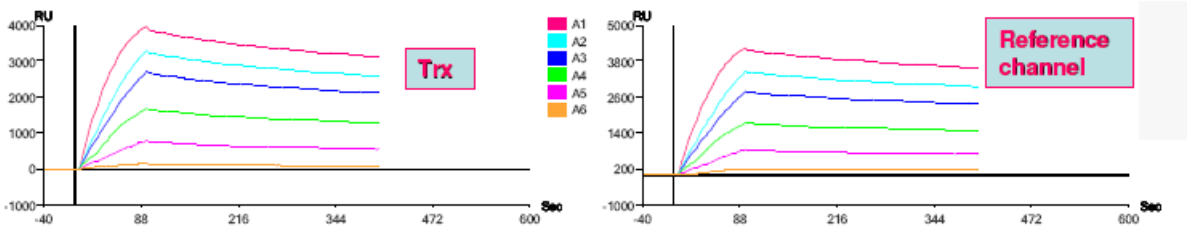

Figure 4.30. Typical sensogram showing non-specific binding in the assay between the ligand with injection of the analyte (association) followed by injection of buffer (disassociation) and the typical sensogram of the reference channel.

4.4. Discussion

Both sets of complex formation binding stoichiometry results are based upon the elution volumes from a calibrated Superdex 200 gel filtration column (Appendix 7.1). Size-exclusion chromatography separates a protein based on its Stokes radius (Irvine, 2001), which is based on the molecular weight and shape. Prx has been seen to elute at the volume expected for the mass of the decameric state of the protein despite its toroidal shape. The binding of Trx and Srx to the decameric hPrxII is assumed to not affect the overall shape on complex formation.

4.4.1. The mPrxII-ET-Srx Complex

Both proteins were purified in a state required to form the complex. The hPrxII was over-expressed and purified in the decameric form and remained in the

decameric form throughout complex formation and Srx was over-expressed and purified as its functionally active monomer.

The Prx/Srx complex has been studied previously by both crystallography and molecular modelling. To date only the crystal structure of hPrxI-Srx complex (PDB: 2RII) has been described (Jonsson *et al*., 2008; Jonsson *et al*., 2009). This complex was achieved with hPrxI in its homodimeric form and the complex contained one PrxI dimer and two Srx monomers. From this structure it would be easy to postulate that the PrxII decamer would be able to accommodate 10 Srx proteins around it.

The SDS PAGE results described in this chapter show that the second peak on the gel filtration column ~56 ml contains both the mPrxII and ET-Srx protein. Using a calibration curve for the Superdex 200 column the size of the complex was estimated to be ~310 kDa taking into account both the ~245 kDa size of the decameric mPrxII protein and the ~65 kDa of ET-Srx attached to it this is assuming that the stokes radius does not change too much. This would equate to five ET-Srx proteins attached to hPrxII suggesting that in this form and under these conditions, each individual dimer in the decamer is able to bind one ET-Srx molecule.

The crystal structure of the decameric form of the protein previously studied in Exeter (PDB: 1QMV) shows the protein has two active sites per homodimer and that the Cys_P in all of the active sites of the decamer is present in the sulfinic acid form. Previous work on modelling of the hPrxII decamer in complex with the Srx protein had suggested that the hPrxII was able to form an interaction with Srx at each of the active sites resulting in a 10:1 ratio of Srx to PrxII (decamer). The model shows Srx bound to all 10 potential sites in the PrxII molecule because there should be no steric reason why the PrxII molecule should not be able to be reduced by 10 Srx molecules at once. The model however does not take into account any potential allosteric effects that might be caused by the interaction of the two proteins. The complex formation as seen from the results in this chapter suggests that out of the ten available sites on mPrxII only five show an interaction with Srx.

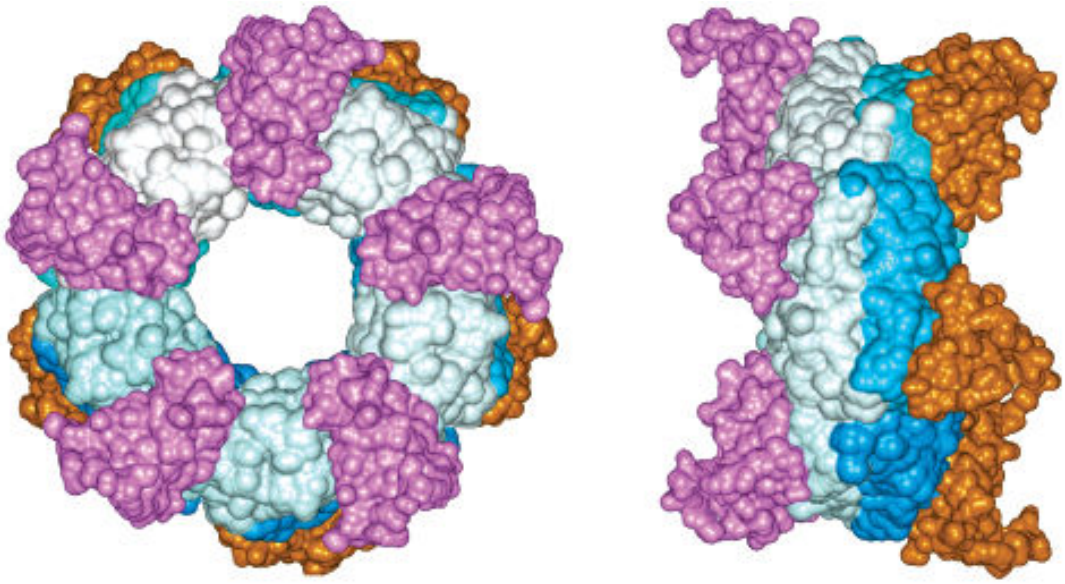

Figure 4.31. The axial (left) and side (right) view of the surface of the model produced in Lee *et al*., (2006). The Prx monomers are shown in light blue and dark blue while the Srx monomers are shown in purple and orange. The model shows no contact between the Srx monomers suggesting that all available sites could show an interaction.

The first crystal structure reporting the interactions between a Prx and Srx (PDB: 2RII) (Jonsson *et al*., 2008b) shows a large movement in the C-terminal of Prx, which could potentially be the cause of the "closing off" of one of the active sites. The structure was analyzed by aligning five copies of the dimeric complex (PDB: 2RII) to the five dimers in the decameric hPrxII structure (PDB: 1QMV) and the differing residues mutated in PyMol Delano Scientific.

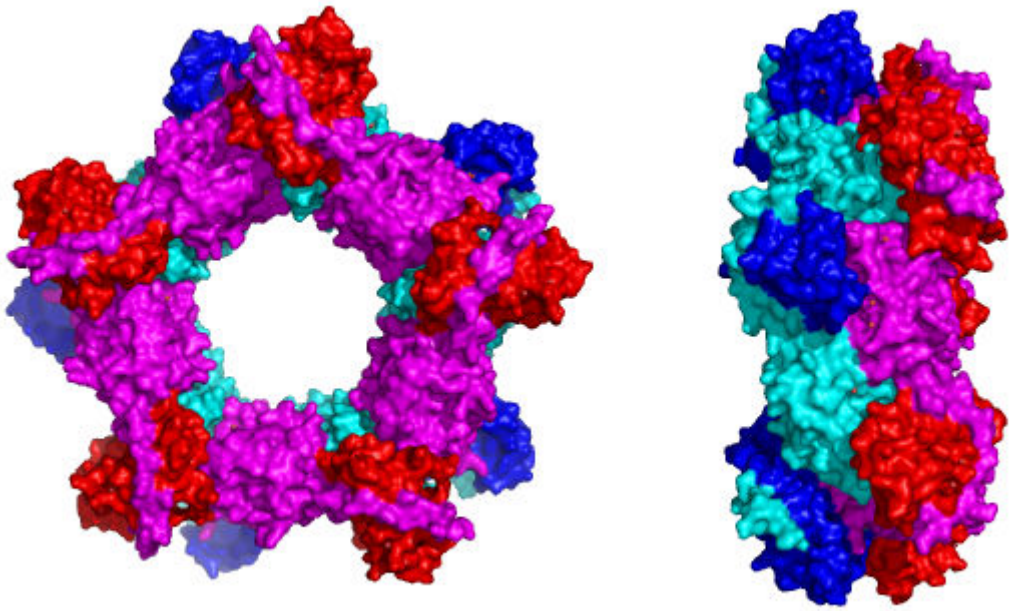

Figure 4.32. The axial (left) and side (right) view of the surface of the complex between hPrxI and Srx (PDB: 2RII) superimposed on to the decameric structure of hPrxII (PDB: 1QMV). Srx molecules are shown in red and blue with the individual monomers of the hPrx shown in cyan and magenta. The “backside” interaction can be seen between the hPrxI monomer and a Srx molecule (figure created using PyMol DeLano Scientific).

Looking at the surface view of this model it is possible that the surface of an Srx protein attached to one homodimer can interfere with the surface of a Prx of the neighbouring homodimer within the decamer. One explanation for the binding ratio could be that to stop the surface interference between the Srx and the Prxs on adjacent homodimers only one active site at each homodimer allows an Srx protein to bind. This could also help to explain why no X-ray diffracting crystals have been produced from this complex if different active sites are used. If this were the case it would be difficult to produce a protein complex of sufficient homogeneity required to obtain X-ray quality crystals.

4.4.2. The mPrxII-mTrx Complex

Both proteins were purified in a state required to form the complex. The hPrxII was over-expressed and purified in the decameric form and remained in the decameric form throughout complex formation (as mentioned previously). The mTrx originally formed a previously reported homodimer (Weichsel *et al*., 1996) even though it lacked the Cys73 required to form the disulfide usually

accountable for this. The previous structure paper (Weichsel *et al*., 1996) shows that the Trx molecule forms hydrogen bonds between the mutated Ser73 residues. In the study reported here this interaction was broken and did not re-form when the protein was stored for 3 months at -20^{o}C (data not shown).

Looking at the results from gel filtration chromatography the complex between mPrxII and mTrx has an estimated molecular mass of ~370 kDa. The mPrxII decamer is ~250 kDa in size leaving ~120 kDa unaccounted for. This would indicate that there are 10 molecules of mTrx interacting with one mPrxII decamer. To better understand this potential interaction, the way in which Trx binds to the PrxII is discussed to give a better understanding into why a 10:1 ratio is seen where a potential 5:1 ratio was observed with Srx.

The interaction between thioredoxin and its target proteins has been researched before in three major studies. The first two were NMR structural determinations of two disulfide bonded complexes between a mutant form of the hTrx and some short synthetic peptide fragments derived from the transcription factors NF-kB and Ref-1 (Qin *et al*., 1995; Qin *et al*., 1996) and the third was a crystal structure of a mutant HvTrxh2 from barley and one of its protein substrates, barley α-amylase/subtilisin inhibitor (BASI) (Maeda *et al*., 2006).

It is understood from the early work on the Trx structure that there is a switch in the hydrophobic surface of the protein around the redox active cysteine residues between the oxidized and reduced form of the protein (Qin *et al*., 1994). The Prx molecule could bind to the hydrophobic region around the oxidized Trx cysteines and this suggests a mechanism for recognition of the oxidized form over the reduced form. The crystal structure of the BASI/Trx complex revealed three regions that make up specific loops that can then bind via hydrophobic interactions and hydrogen bonds, to the outside of the substrate molecule. These three regions were $_{45}$WCGP$_{48}$, $_{87}$AMP$_{89}$ and $_{104}$VGA$_{106}$. These structural loop regions are highly conserved in the Trx proteins and correspond well to three regions in hTrx (PDB: 1ERT), $_{45}$WCGP$_{48}$, $_{87}$**C**MP$_{89}$ and $_{104}$**S**GA$_{106}$ (residues in bold differ from the BASI/Trx complex).

The crystal structure of the disulfide state of hPrxII that was determined in Chapter 3 was used to model the interaction between hPrxII and Trx, using the ClusPro2 Server (Comeau *et al*., 2004). The obtained model revealed a slight

rearrangement of the residues around the disulfide bond that allowed a bond to be formed between Cys35 of the Trx molecule and Cys52 of the hPrxII molecule. This rearrangement was localized to the disulfide area and did not cause any major structural movements in the rest of the protein.

The model does suggest that the Trx molecule will interact with both subunits in a hPrxII dimer but not interact near the dimer: dimer interface. The model suggests that the mixed disulfide complex is held together by hydrophobic interactions in the binding motifs mentioned above as well as hydrogen bonds between Trp31 and Arg91 (Subunit 1), Gly33 and Phe49 (Subunit 1), Cys73 and Gly175 (Subunit 2), Met74 and Thr53 (Subunit 1), Ser90 and Tyr164 (Subunit 2), and Ala92 and Val171 (Subunit 2).

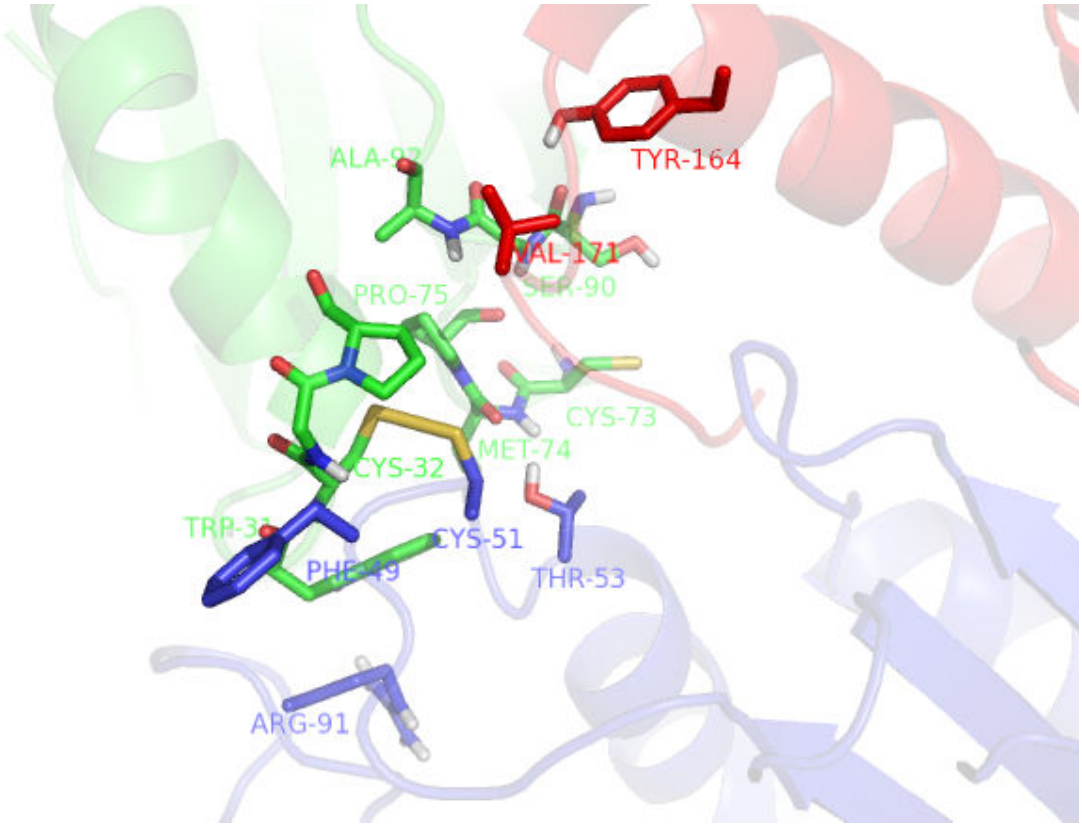

Figure 4.33. Cartoon representation of the potential disulfide between hPrxII (Cys51) and Trx (Cys32) (shown in yellow) from the model created from the hPrxII(S-S) and reduced Trx (PDB: 1ERT) structures. The binding motif residues are shown in green with interacting residues from the two hPrxII subunits shown in blue and red, respectively (figure created using PyMol DeLano Scientific).

The interaction of Trx from the model suggests that the 10 Trx molecules would be able to interact with the decameric form of the protein at once without interfering with either the dimer:dimer interactions or with each other. This agrees with the 10:1 ratio that can be seen in the covalent complex of mPrxII/mTrx. The fact that all 10 Trx molecules are seen bound to the PrxII enzyme in the covalent complex does not necessarily mean that in the real cellular situation this would occur.

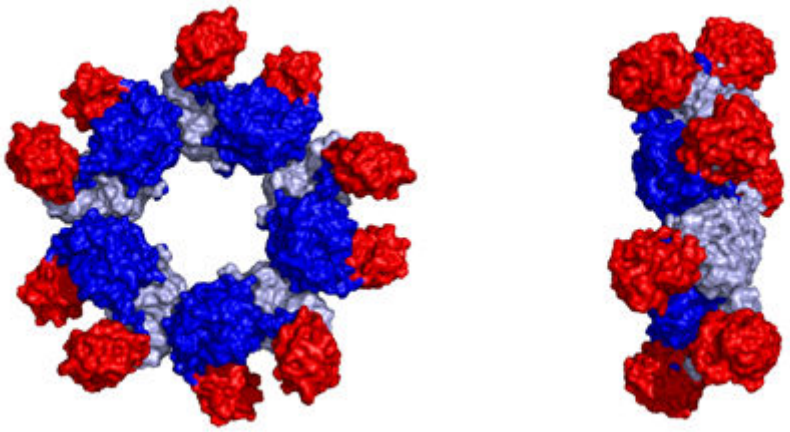

Figure 4.34. Surface representation of the model of Trx interacting at all 10 active sites of decameric form of hPrxII S-S. The hPrxII subunits are shown in blue and light blue with Trx molecules shown in red (figure created using PyMol DeLano Scientific).

It is possible that Trx molecules would associate and dissociate, with the actual number interacting with PrxII at any one time relating to the oxidative pressures within the cell. This oxidative pressure would govern how many PrxII active sites are being oxidized at any one time and control the rate of oxidation.

4.4.3. Interaction with PDCL3

The native gel electrophoresis studies of the complexes were unable to yield any results even though a potential interaction had been flagged during the ESI-MS studies (Professor Keith Willison, Personal Communication). It is possible that the native gels were unable to yield any results as the complexes were too transient to be analyzed on the gel. The complex was then analyzed using a sucrose gradient, a much “softer” technique which showed a positive result. The PDCL3^{*568} was shown to interact with hPrxII forming a complex ~ 250 – 300 kDa in size. This would suggest that the ratio of binding would be 10:1 (PDCL3:

hPrxII(decamer)). The sucrose gradients run with the two truncations of PDCL3 missing the first 90 residues showed no interaction suggesting the binding site is on the N-terminus. The third truncation (1-211) was shown to be prone to aggregation and it was shown that hPrxII may prefer binding to the aggregates over the monomeric form (Professor Keith Willison, Personal Communication). This interaction is under further investigation although it is believed that hPrxII may have a chaperone type function in its interaction with PDCL3.

4.4.4. Surface plasmon resonance

4.4.4.1. Interactions between hyperoxidised hPrxII and Srx

The immobilized Srx and Trx proteins were inactive and did not show any interaction with the hPrxII. It is suggested that the loss of activity was due to the immobilization process.

The hPrxII enzymes were checked to be in the correct oxidation state for the reaction to occur before injected into the SPR machine. The hPrxII interacting with Trx was shown to be solely in the disulfide state and was prepared in exactly the same manner as the hPrxIIS-S that was crystallized. The hPrxII interacting with Srx was reduced with DTT and hyperoxidised with H_2O_2 and confirmed to contain no disulfide bonds using SDS-PAGE. The Srx and Trx were checked to be in their functional monomeric state and were reduced with DTT prior to the assay.

The proteins could have been bound to the gold surface restricting access to their active site. Both Trx and Srx were analysed to determine the position of their lysine residues (Pymol DeLano Scientific). Trx has six surface accessible lysine residues that would preferentially bind with the activated carboxylic acid surface but none of these are located at the active site or in the previosuly postulated binding domains between Trx and its target protein (Maeda *et al*., 2006). Srx has four surface accessible lysine residues so would bind to the surface of the chip. The recent structure of the essential repair embrace (Jonsson *et al*., 2008) that occurs in the hPrxI-ET-Srx complex shows the C-terminal arm of hPrxI interacting with ET-Srx along the site of these surface lysine residues. If the protein was bound to the SPR chip by these residues the C-terminal arm of PrxII would not be able to interact with the Srx and could result in the complex not being observed. One way to solve this could be to mutate those residues and introduce some other lysine residues on the surface

of Srx that do not show any interaction with the hPrxII. Another solution could be to tag the proteins with a biotin tag or His-tag and immobilize the proteins via this interaction instead of amide coupling. As both of the proteins are His-tagged, one of the proteins would have to have its tag removed or be cloned without a His-tag. The problem of non-specific binding needs to be addressed and could possibly be due to the denaturation of the protein during amide coupling. Another explanation for the non-specific binding could be electrostatic interaction with the chip surface as it was partially removed upon the addition of NaCl.

5. The cloning and over-expression of an active human thioredoxin reductase

5.1. Introduction

5.1.1. Thioredoxin reductase

Thioredoxin reductase is part of a family of homodimeric flavoproteins that are known to reduce thioredoxin as part of the peroxiredoxin peroxide scavenging system. Thioredoxin reductase 1 (TrxR1) is the major form of thioredoxin reductase and is found mainly in the cytoplasm. TrxR1 is a selenoprotein containing a selenocysteine which is essential for the activity of the enzyme. The selenocysteine forms part of the TrxR1 active site at the C-terminal end in a Cys-Sec-Gly-COOH motif (Arner, 2009).

5.1.2. Selenocysteine and selenocysteine incorporation

Selenocysteine is the 21st amino acid and has the same structure as cysteine except the sulfur group has been replaced by selenium (figure 5.1) to form a selenol group. Selenocysteine has a lower p*K*a and a higher reducing potential complared to cysteine (Stadtman, 1996).

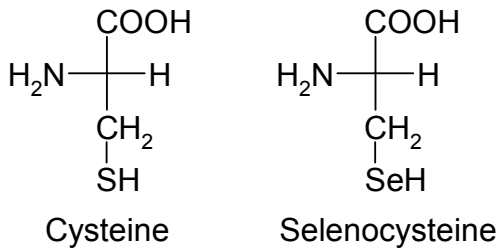

Figure 5.1. The chemical structure of the amino acids cysteine and selenocysteine. Selenocysteine has the sulfur atom replaced by a selenium atom.

Selenocysteine containing proteins are difficult to reproduce in an *E. coli* expression system as secondary structural elements and genes that aide selenocysteine incorporation are missing.

5.1.2.1. Selenocysteine insertion sequence

A selenocysteine insertion sequence (SECIS) is required to incorporate a selenocysteine in place of the stop codon UGA. The SECIS used in this project is a minimal SECIS and is an mRNA element that forms a stem-loop structure. It was adapted from the SECIS found in the *E. coli* selenoprotein formate

dehydrogenase (Jormakka *et al*., 2003). The minimal SECIS is made up of 17 nucleotides which form the mini upper-stem-loop structure; these nucleotides must be located 11 nucleotides away from the UGA codon that will encode for the selenocysteine (Liu *et al*., 1998) (figure 5.2).

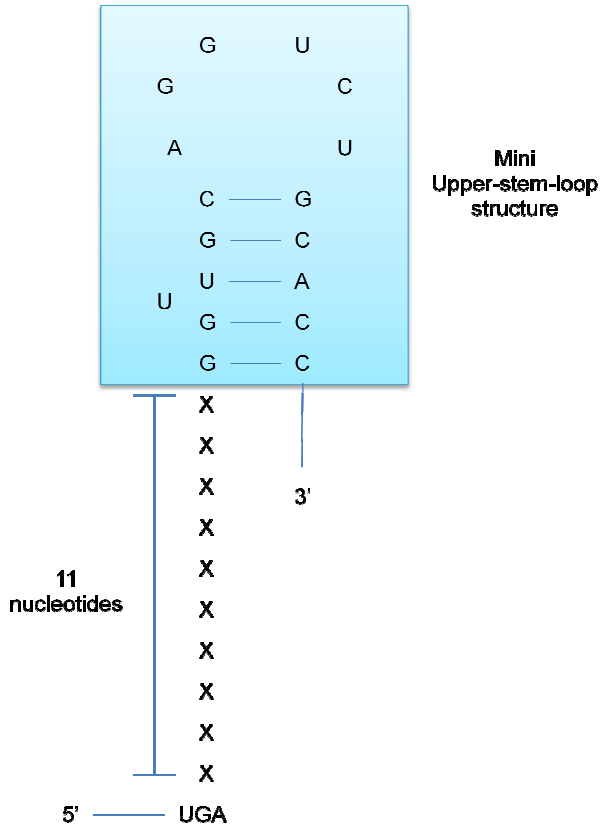

Figure 5.2. The structure and sequence of the minimal SECIS developed from *E. coli* formate dehydrogenase. The UGA codon that will encode for the selenocysteine is located 11 nucleotides away from the 17 nucleotide upper-stem-loop structure.

The SECIS aids incorporation of the selenocysteine at the UGA codon as the stem-loop region will bind to the selenocysteine specific elongation factor (SelB) protein. The SelB protein binds to the *selC* gene product which is the selenocysteine-specific tRNA ($tRNA^{Sec}$). The $tRNA^{Sec}$ is originally charged with a seryl residue but is converted to selenocysteinyl by selenocysteine synthase, an oligomer of the *selA* gene product. The *selABC* genes are important elements in the incorporation of a selenocysteine residue (Arner *et al*., 1999).

5.1.2.2. Co-expression with the selA, selB and selC genes and the use of a double stop codon

As well as the SECIS it has been shown that the co-expression of the hTrxR proteins with the *selA*, *selB* and *selC* genes greatly increases the amount of

selenocysteine inserted and therefore the activity of the protein (Arner *et al*., 1999). The pSUABC plasmid contains all three genes in a specially designed pSU vector supplying the relevant tRNA, tRNA synthase and the recognition factor for translation of the UGA SeCys codon (Cao *et al*., 2007). A double stop codon is also incorporated on the 3' end of the TrxR1 open reading frame as it has been shown to promote a higher level of SeCys incorporation in recombinant TrxR1 (Arner *et al*., 1999).

5.2. Materials and Methods

5.2.1. Cloning of *hTrxR1*

TrxR1 was cloned using the ligation-independent cloning (LIC) vector system (Merck Biosciences). PCR was used to amplify the gene with vector specific overhangs. The vector specific overhangs were created by pre-treating the vector with T4 DNA polymerase and dGTP. The gene with the overhangs attached was then annealed to the vector allowing the vector plus insert to be transformed into an *E. coli* expression cell line for protein expression and purification (see figure 5.3).

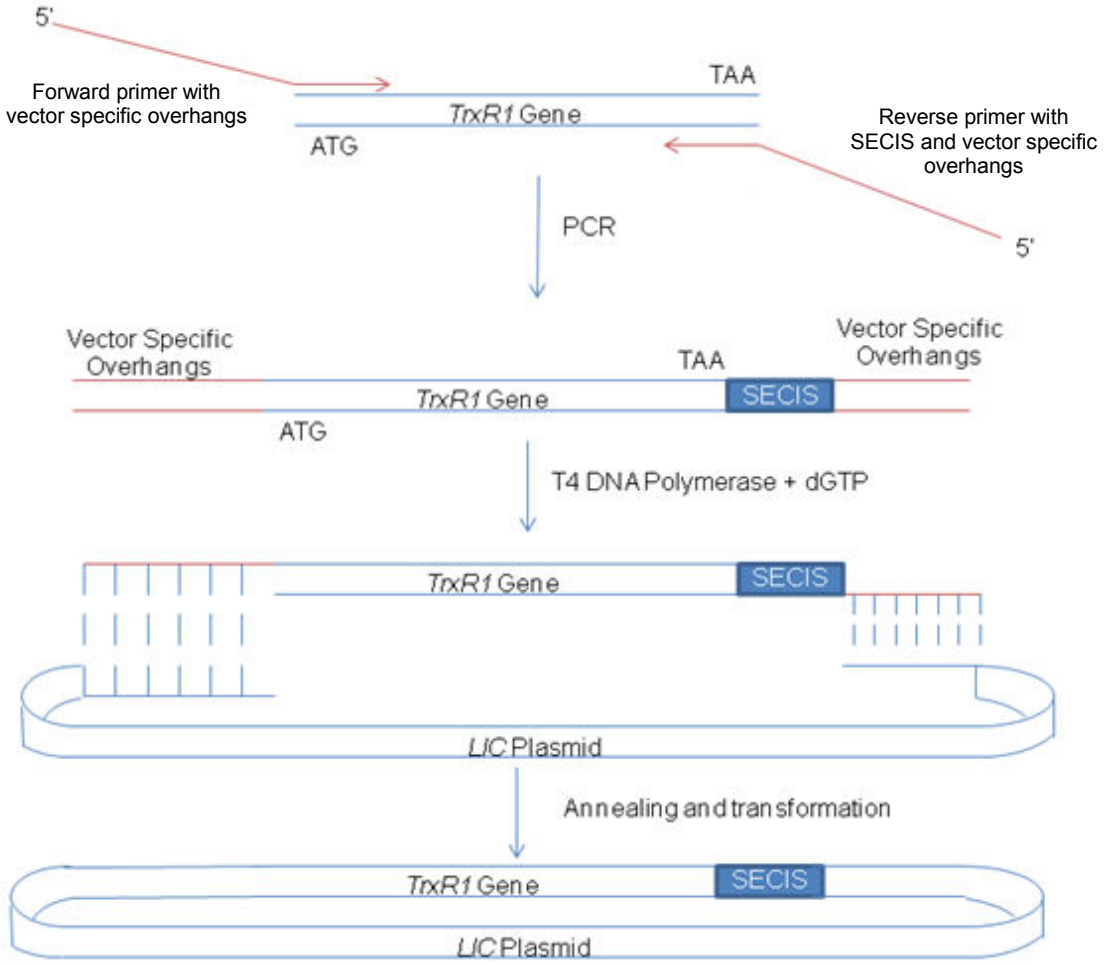

Figure 5.3. The strategy for the cloning of *TrxR1* gene into the pET30 Xa/LIC vector to allow for expression of the protein (adapted from LIC Manual, Novagen).

5.2.1.1. Primer sequences

TrxR1F 5' GGTATTGAGGGTCGCATGAACGGCCCTGAAGATC 3'

TrxR1R 5'AGAGGAGAGTTAGAGCCGGTGCAGACCTGCAACCGATTATTAACCTCAGC AGCCAGC 3'

Underlined are the vector specific overhangs for the pET30 Xa/LIC vector. The SECIS sequence is shown in red.

5.2.1.2. PCR of hTrxR1

An image clone was purchased from Open Biosystems which contained *Homo sapiens* TrxR1 in the pCMV-SPORT6 vector and was used as the template for the PCR reaction. The PCR was performed in a total volume of 50 µl containing 200 ng of template DNA, 100 ng of each primer, 200 µM dNTP solution mix, 1 U Deep Vent Polymerase (New England Biolabs, Beverley, MA), 1x Deep Vent Buffer and nuclease free water to adjust to the final volume. The PCR cycle consisted of an initial denaturation step of 5 min at 95^{o}C and 30 consecutive

cycles of denaturation (30 sec at 95°C), annealing (30 sec at 65°C) and polymerisation (1.5 min at 72°C). There was also a final extension time of five min at 72°C. A 1% agarose gel was run to confirm a DNA product of the correct size and the PCR product was purified using a gel extraction kit (Qiagen) according to the manufacturer's instructions. The purified PCR product was eluted using TlowE® buffer (10 mM Tris-HCl, 0.1 mM EDTA, pH 8.0).

5.2.1.3. T4 DNA polymerase treatment of the hTrxR1 insert

The purified PCR product was treated with T4 DNA Polymerase to generate the vector compatible overhangs. The reaction was performed in a total volume of 20 µl containing 0.2 pmol of the purified PCR product in TlowE® buffer, 1x T4 DNA polymerase buffer, 2.5 mM dGTP, 5 mM DTT, 1 U T4 DNA Polymerase (LIC qualified, Merck Biosciences) and nuclease free water to adjust to the final volume. The reaction was incubated at 22°C for 30 min followed by enzyme inactivation by incubation at 75°C for 20 min. The prepared insert was then stored at -20°C before the annealing reaction took place.

5.2.1.4. Annealing the vector and prepared insert

The annealing reaction takes place in a final volume of 4 µl containing 1 µl pET30 Xa/LIC vector, 2 µl T4 DNA Polymerase treated *hTxrR1* insert (0.02 pmol) this was then incubated at 22°C for five min before addition of 1 µl EDTA (6.25 mM) and further incubation at 22°C for 5 min. 1 µl of the annealing reaction was used to transform chemically competent *E. coli* NovaBlue cell line (as described in methods 2.2.2) (Merck Biosciences). The *E. coli* cells were plated onto LB agar plates containing the appropriate antibiotic for selection. The transformants were verified to contain *hTrxR1* gene by plasmid DNA isolation, digestion and agarose gel electrophoresis. The recombinant plasmid containing the *hTrxR1* gene was sequenced by Geneservice (Oxford, United Kingdom).

5.2.2. Expression of recombinant hTrxR1

The TrxR1 DNA was used to transform the chemically competent expression cell line BL21 (DE3)-pLysS (Invitrogen) as previously described in methods 2.2.2. The pET30 Xa/LIC vector encodes for an N-terminal poly histidine tag and features a T7*lac* promoter to control expression of the target protein.

Expression trials on the TrxR1 protein showed poor expression and production of insoluble protein under conditions previously used for expression of proteins (as in methods 2.2.3), so new conditions based on previous work on expressing thioredoxin reductases were used (Cao *et al*., 2007). The protein was expressed in a new modified rich LB media (recipe shown below).

Modified rich LB media:-

0.5 % w/v NaCl
1.2 % w/v Bactotryptone
2.4 % w/v Yeast extract
4 % v/v Glycerol
0.5 % w/v K_2HPO_4
0.0142 % w/v Na_2SO_4

BL21 (DE3)-pLysS cells containing the TrxR1 plasmid were used to inoculate 100 ml of modified rich LB media containing the appropriate antibiotic for selection. This starter culture was grown under agitation at 200 rpm overnight at 37^{o}C and 10 ml was used to inoculate 1 L fresh modified rich LB media containing the appropriate antibiotic selection, and grown under agitation at 37^{o}C until the OD_{600nm} reached 0.6. At this point the temperature was reduced to 15^{o}C and left for 30 min before the addition of 0.3 mM IPTG and 1 µM sodium selenite and the culture incubated for a further 18 hours at 15^{o}C. The cells were then harvested by centrifugation (20,000 x *g*, 20 min, 4^{o}C) using a Beckman JA-10 rotor. The cell pellet was stored at -20^{o}C until further use.

5.2.2.1. Co-expression with pSUABC

The protein was also co-expressed with the *selA*, *selB* and *selC* genes that were kindly donated in one plasmid (pSUABC) by Professor Elias Arner (Department of Medical Biochemistry and Biophysics, Karolinska Institute). The pSUABC component was placed into the pLysS cell line and used to inoculate 100 ml modified rich LB media containing chloroamphenicol and kanamycin. The starter culture was grown under agitation at 200 rpm overnight at 37^{o}C. 10 ml was then used to inoculate 1 L of fresh modified rich LB media that was then also inoculated by 10 ml of TrxR1 starter culture. The rest of the over-expression procedure was carried out as described previously (see methods 5.2.2).

5.2.3. Purification of recombinant TrxR1

Cell lysis was carried out as described in methods 2.2.4.1.

5.2.3.1. Purification buffers

Buffer A – 20 mM HEPES, pH 8.0, 0.5 M NaCl, 20 mM imidazole

Buffer B – 20mM HEPES, pH 8.0, 0.5 M NaCl, 1 M imidazole

Buffer C – 20mM HEPES, pH 8.0, 0.1 M NaCl

5.2.3.2. Nickel affinity and gel chromatography

The nickel affinity chromatography was performed as in methods 2.2.4.3 using a six column volume gradient to 100 % buffer B with the fractions containing protein analyzed using SDS-PAGE as described in methods 2.2.4.6. The protein was loaded on a Superdex 200 column (GE Healthcare) using the method described in 2.2.4.5. The Superdex 200 column was equilibrated with one column volume at a flow rate of 1 ml/min. The sample was loaded and fractions collected over one column volume and the fractions were analyzed using SDS-PAGE as in methods 2.2.4.6.

5.2.4. TrxR1 DTNB assay

The activity of TrxR1 was determined by measuring the DTNB reductase activity. The assay was performed at 25^{o}C in a final volume of 2 ml containing 1 µg TrxR1 and 1.5 mM DTNB and made up to volume with 100 mM Tris-HCl, pH 7.5, 2 mM EDTA. The reaction was started by the addition of 0.2 mM NADPH and the change in A_{412nm} was measured over 10 min. The activity of the protein was expressed as µmol/min/mg of protein and was calculated using the formula below.

Activity (µmol/min) = (ΔA_{412} x 1000)/ 13.6 /min

Equation 5.1. The activity of the protein in µmol/min is determined by measuring the ΔA_{412} over the 10 min time period and using the equation above. 13.6 is the extinction coefficient of TNB.

5.2.5. Reconstitution of the PrxII pathway

An assay to measure the activity of the hPrxII pathway was performed at 25^{o}C in a final volume of 1 ml containing 100 µM NADPH, 2 µM hTrx, 1 µM TrxR1 and 0.5 µM hPrxII and made up to volume with 50 mM Tris-HCl, pH 7.5. The

reaction was started by the addition of 0.1 mM H_2O_2 and the change in A_{340nm} was measured over 180 seconds.

5.3. Results

5.3.1. Cloning of *TrxR1*

An IMAGE clone was purchased from Open Biosystems encoding for the *TrxR1* gene and was used as a template for PCR, which was carried out as described in methods 5.2.1. The amplification of the *TrxR1* gene resulted in a DNA band of the correct size (~1.5 kbp) which was successfully cloned into the expression vector pET30 Xa/LIC. DNA sequencing results show that the correct *TrxR1* sequence had been obtained and also show the presence of the SECIS, the double stop codon and the 3' end of the gene (Appendix 7.11) (Figure 5.4).

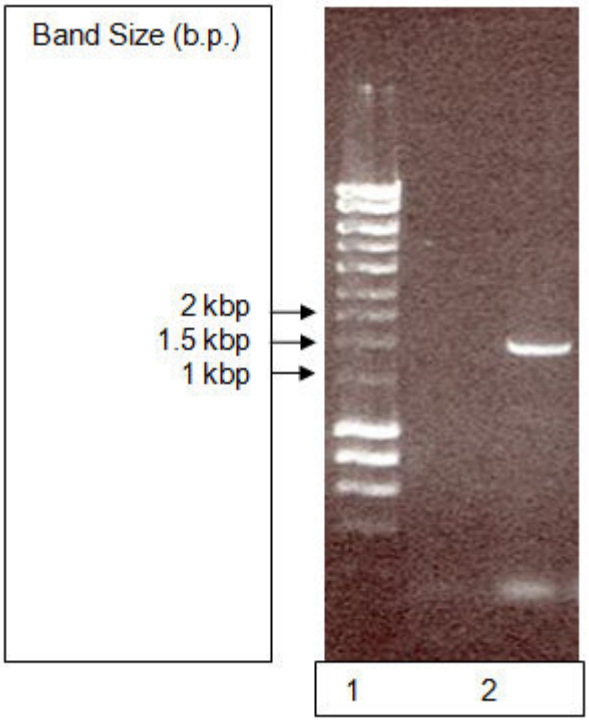

Figure 5.4. 1 % agarose gel showing the PCR amplification of the *TrxR1* gene. Lane 1, marker (Hyperladder 1, BIOLINE, (Appendix 7.3)); Lane 2, *TrxR1* PCR band at ~1.5 kbp.

5.3.2. Expression of recombinant TrxR1

The pET30 Xa/LIC/TrxR1 construct was transformed into the *E. coli* expression strain BL21 (DE3)-pLysS. TrxR1 protein expression was under the control of the T7 promoter and induced using IPTG. The over-expression of TrxR1 was investigated by induction studies to obtain the best conditions for over-

expression. The optimal over-expression was achieved by addition of a final concentration 0.3 mM IPTG when the cells had reached an OD_{600nm} of 0.6 with further incubation for 16 hours at 15°C. 1 µM sodium selenite was also added at induction as a source of selenium for the selenocysteine. The over-expression of TrxR1 resulted in soluble protein being produced at the expected size (~61 kDa). The protein was also co-expressed with the pSUABC component. When over-expressed with this component the amount of TrxR1 produced was not affected. This was confirmed by observing the strength of a band on SDS-PAGE as well as the calculation of total protein using A_{280}.

5.3.3. Purification of recombinant TrxR1

One litre of culture produced 1.7 g of cell paste and after cell lysis (methods 2.2.4.1) and centrifugation the supernatant was purified using nickel affinity and gel filtration chromatography as described in methods 5.2.3.2.

5.3.3.1. Nickel affinity and gel filtration chromatography

The clarified cell extract was applied to a nickel column as described in methods 5.2.3.2 (figure 5.5). The fractions were analyzed using SDS-PAGE (data not shown) as described in methods 2.2.3.6. The fractions containing TrxR1 were pooled and concentrated (methods 2.2.4.5), in preparation for gel filtration chromatography.

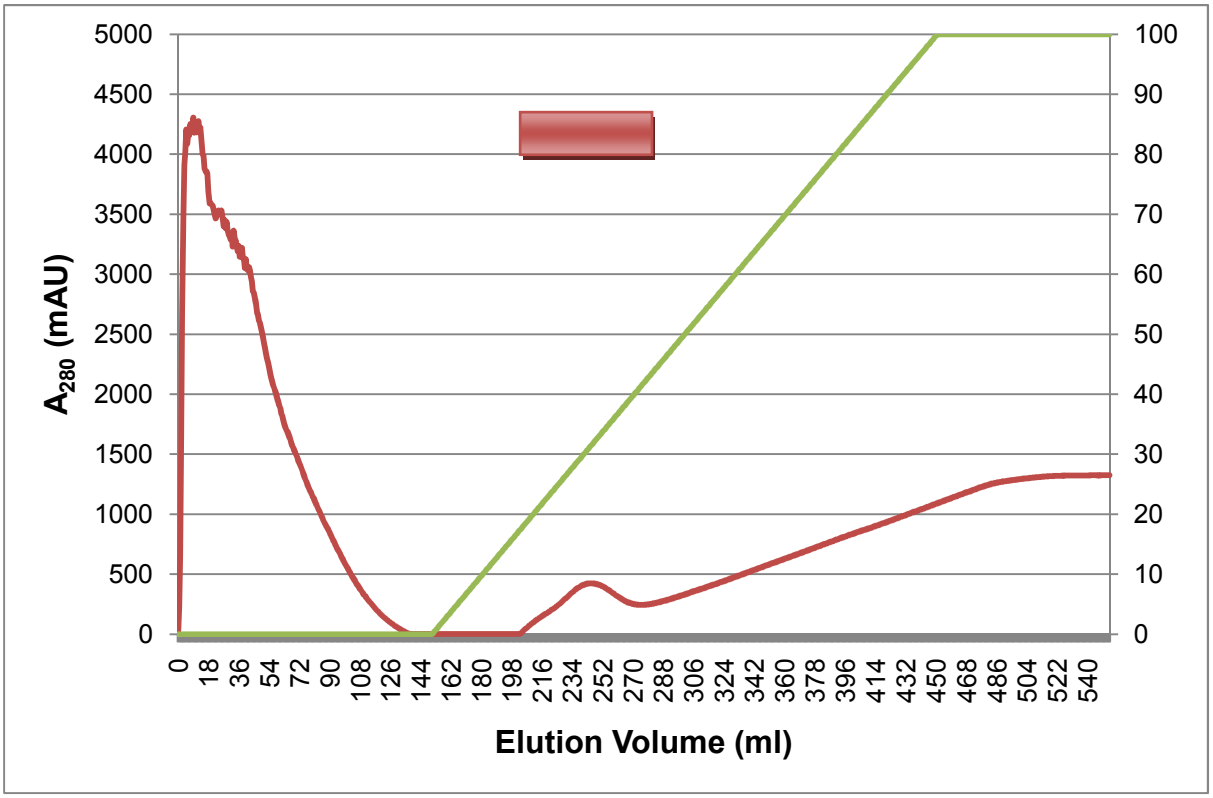

Figure 5.5. Elution profile of TrxR1 (red line) from nickel affinity chromatography. 10 ml fractions were collected throughout the entire elution volume. The green line shows the % imidazole concentration. The fractions that showed a band of the correct size on SDS-PAGE (result not shown) are indicated by the red bar.

Gel filtration was used as a final step of the purification process and the use of a calibrated gel filtration column allowed the size and therefore the oligomeric state of the protein to be estimated. The concentrated protein sample was loaded onto the gel filtration column as described in methods 5.2.3.2 (figure 5.6). The peak fractions were analyzed by SDS-PAGE (figure 5.7) and those that contained TrxR1 were pooled and concentrated (as in methods 2.2.4.5).

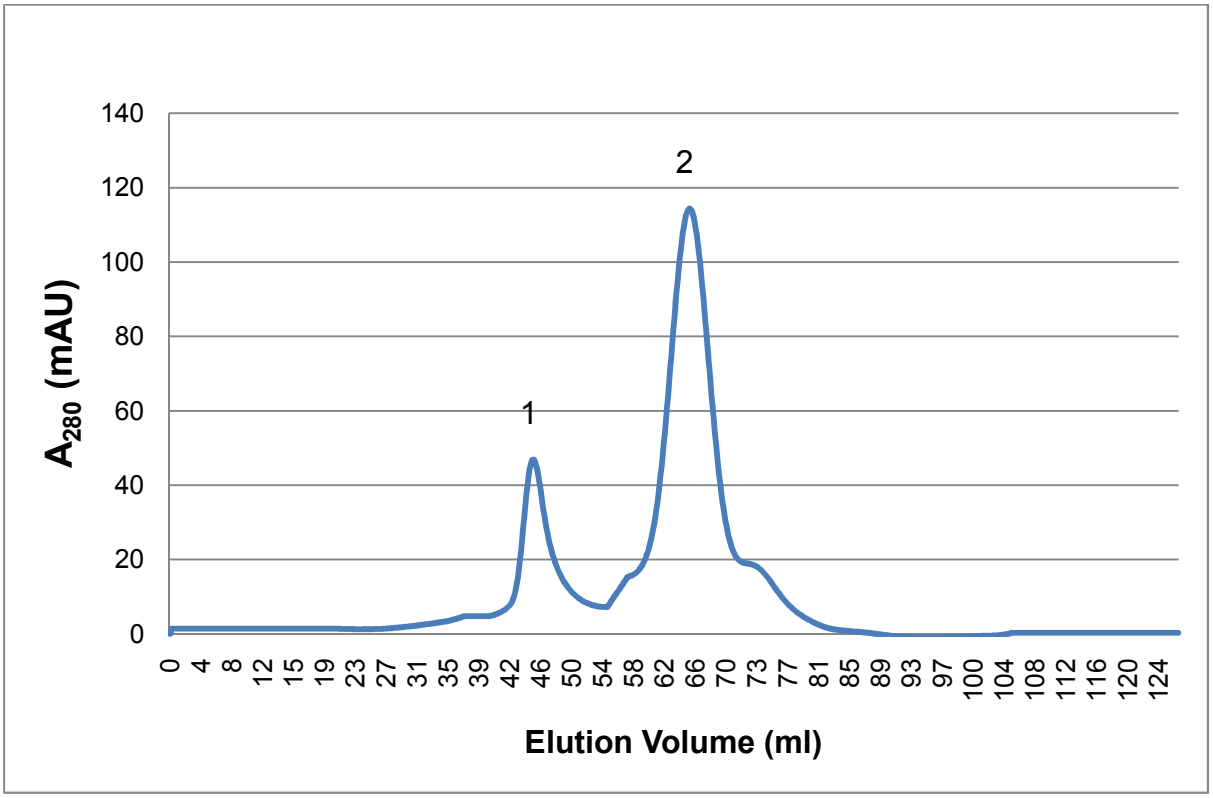

Figure 5.6. Elution profile of TrxR1 (blue line) from a calibrated HiLoad 16/60 Superdex 200 gel filtration column. 1 ml fractions were collected throughout the elution volume. Peak 1 corresponds to the columns void volume (~44 ml); Peak 2 contained the dimeric form of TrxR1 (~66 ml) (~128 kDa).

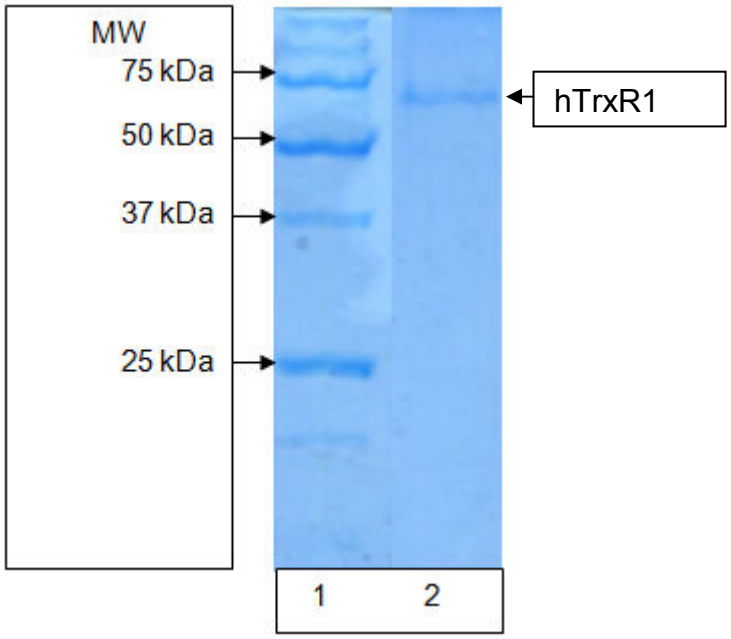

Figure 5.7. SDS-PAGE analysis of the peak from gel filtration chromatography showing the purified TrxR1. Lane 1, molecular weight marker (Precision Plus Protein Standard, BioRad Laboratories); Lane 2, sample of TrxR1 after gel filtration chromatography (elution volume ~66 ml).

5.3.4. TrxR1 DTNB activity assay

The activity assay was carried out with both TrxR1 co-expressed with pSUABC and without pSUABC. The assay was also carried out without the presence of the TrxR1 enzyme as a control (figure 5.8).

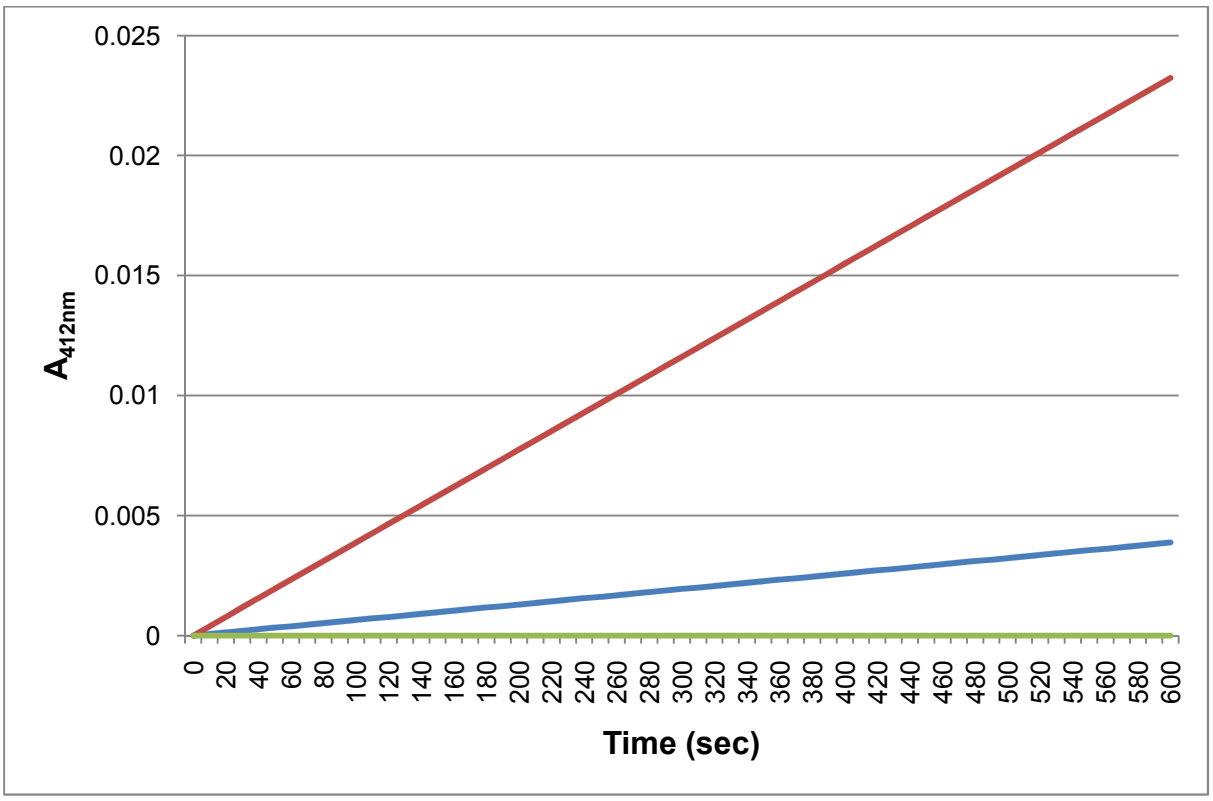

Figure 5.8. DTNB activity assay run over a period of ten minutes from when the NADPH was added. The green line shows the assay run with TrxR1 that did not possess the C-terminal SECIS element. The blue line shows the assay run with TrxR1 that possessed the SECIS element but was not co-expressed with pSUABC. The red line shows the assay run with TrxR1 that possessed the SECIS element and was co-expressed with the pSUABC component.

The TrxR1 expressed without pSUABC showed an activity of 1.42 µmol/min but when pSUABC was co-expressed the activity showed a six fold increase to 8.54 µmol/min. The TrxR1 cloned without the SECIS was shown to have no activity at all. The protein over-expressed without the pSUABC plasmid was unable to incorporate the selenocysteine and may have read the stop codon used to code for the selenocysteine to terminate the gene missing the last three residues.

5.3.5. Reconstitution of the PrxII pathway

The reconstitution of the PrxII pathway in this case proved unsuccessful and was not finished due to time constraints.

5.4. Discussion

5.4.1. Activity of hTrxR1

An active thioredoxin reductase recombinant protein was successfully cloned and over-expressed allowing the completion of the PrxII pathway and therefore

the production of a working assay. TrxR1 that was co-expressed with the pSUABC component was found to have activity of 8.54 µmol/min, although this is fivefold less than that observed for some native thioredoxin reductases (Goratov and Stadtman, 1998). It is however comparable to literature values obtained from other recombinant forms of TrxR1 (Arner *et al*., 1999; Cao *et al*., 2007).

It can be seen from the assay that the minimal SECIS adapted from SECIS from *E. coli* formate dehydrogenase is essential for the insertion of a selenocysteine as removal of the SECIS results in no activity being observed. It is postulated that this is due to the lack of a SECIS causing the protein to be terminated at the position of the UGA codon instead of using it as the site of selenocysteine insertion. The presence of a double stop codon as part of the SECIS element before the main part of the stem-loop structure shows that the SECIS only needs to be present in the mRNA and its translation is not required for the insertion of a selenocysteine.

The other major element required for the insertion of the selenocysteine and therefore the activity of TrxR1 was the co-expression of the protein with the pSUABC component. This co-expression greatly increased the activity of this over-expressed TrxR1. The co-expression of the pSUABC component seemed to have no effect on the amount of TrxR1 produced (the same band intensity was seen on a SDS-PAGE and the same total protein calculated using A_{280}) but had a six fold increase on the activity of the protein in the DTNB assay. This result reiterates the importance between the ratio of the mRNA SECIS and the *selA*, *B* and *C* genes in producing an active TrxR1 (Tormay *et al*., 1996). The protein over-expressed without these genes was unable to incorporate the selenocysteine and may have read the stop codon used to code for the selenocysteine to terminate the gene missing the last three residues.

5.4.2. Reconstitution of the PrxII pathway

Due to the late stage in the project at which TrxR1 was cloned and over-expressed in its active form the assay for the entire pathway was unable to be formed. The cloning of the TrxR1 proved to be very problematic. The SECIS presence in traditional primers yielded no results with traditional PCR methods as the Loop-Stem structure resulted in the SECIS being added backwards or not at all. The failure in getting the whole pathway assay to be functional could

be down to a number of different reasons but it is suggested that the major problems could be the activity of the proteins hPrxII and Trx as their activity has not been determined.

The hPrxII protein could possibly not be active in its current form. Either all of the protein is being converted to the sulfinic acid form (as seen in the structure (Schroder *et al*., 2000)) or the disulfide decamer is unable to be reduced by Trx. The hPrxII protein was reduced with DTT (and the DTT removed by gel filtration chromatography) prior to the assay being run, but this does allow for the hyper-oxidation to re-occur although it is unlikely that this would result in the inactivation of all the PrxII (Jonsson *et al*., 2008). If the PrxII was all in the hyperoxidised state this would mean that the Trx could not act upon the sulfinic acid moiety and so would leave the protein inactive in this assay as Srx is the only known protein to be able to reduce the sulfinic acid form (Biteau *et al*., 2003). Although it has been shown previously that the disulfide decamer and the Trx protein interact this has only been shown using chemical methods and the *in vivo* relationship has not been demonstrated. It could be the case that the Trx is unable to reduce the disulfide decameric state suggesting the protein is inactive in this form. Once again this is unlikely as although the interaction was shown chemically, the disulfide decameric structure of the protein observed above shows no structural reason as to why the Trx protein would be unable to reduce it.

The Trx protein has not been tested for activity as all of the assays require the TrxR1 enzyme. The activity of this protein would have to be tested to confirm it is not a broken link in the chain. The Trx protein does seem to purify well with no degradation, although the protein does originally form a dimer that is then reduced back to its functional monomer (Weichsel *et al*., 1996) chemically. Gel filtration of the protein used just before the assay was run still showed the Trx to be present as a monomer. It is likely that the problem lies in the assay itself as due to time constraints this assay was run only twice and although following a protocol that yielded results for a mitochondrial PrxIII (Cao *et al*., 2007), the assay would have to be modified to achieve results.

6. Summary and further work

6.1. Summary

hPrxII was originally cloned with a point mutation in the fourth residue leading to an amino acid change of glycine to valine. The hPrxII protein was unstable during purification and was unable to be purified and concentrated to satisfactory concentrations. The re-cloning of this protein with the correct residue allowed purification of this protein to homogeneity using nickel and gel filtration chromatography. This correction in the amino acid sequence also resulted in a shift in the oligomeric state of the protein with the protein being produced in the same oligomeric state as the native protein.

The hPrxII protein was over-expressed in the decameric state with a disulfide bond between the peroxidatic and the resolving cysteines. The hPrxII(S-S) was purified to homogeneity using nickel and gel filtration column chromatography and diffraction quality crystals obtained. Structural analysis of the enzyme resulted in the 3.3 Å resolution structure of the disulfide form of the enzyme. The structure was solved using molecular replacement using the native hPrxII (PDB: 1QMV) as a model and revealed a disulfide bond between the peroxidatic (Cys52) and resolving (Cys171) cysteines but lacked the C-terminus of the protein (due to poorly defined electron density). The structure revealed a movement in the loop region consisting of residues 47-54 resulting in a 6 Å movement of Cys52 towards the neighbouring monomer within the homodimer. In the neighbouring subunit a large structural movement in the region consisting of residues 170-202 is observed to form the disulfide bond. The residues 170-175 displace the C-terminal αH6 in the hyperoxidized/thiol structure which results in a 10 Å movement in the Cα of Cys172. The structure also revealed that the rearrangements needed to bring the two redox active cysteines together did not result in the breakdown of the dimer:dimer interface and revealed the protein to be decameric in structure contrary to what was postulated when the original native structure was solved. There was only one observed change in the residues involved in the dimer:dimer interface which occurred at Phe47. It was shown that the movement of this residue would not have resulted in the breakdown of the dimer:dimer interface.

An engineered truncation of Srx and a mutant Prx (C70S/C172S) were purified to homogeneity using nickel and gel filtration chromatography. The ET-Srx lacked the first 31 residues of the amino acid sequence removing a glycine rich region that is thought to be problematic in the crystallization of the complex. A covalent complex was then formed between the two cysteine residues using the chemical conjugating agent DTNB. Size exclusion chromatography revealed the binding stoichiometry of this complex to be a 5:1 ratio of Srx to hPrxII decamer. Modelling of the known structure of a highly similar complex reveals that a large conformational change that occurs upon binding could result in the need for co-operation between the two active sites on the hPrxII homodimer. This could result in only one active site being used per homodimer hence the 5:1 ratio. The complex was also studied using SPR but no meaningful results were obtained from these experiments. One of the reasons behind this could be due to C-terminal embrace that is seen when the two proteins interact. The Srx protein was attached to the carboxylic acid surface of the gold chip by amide coupling (through lysine residues). The largest group of surface accessible lysine residues appears along the site of this interaction meaning that tethering to the surface by these residues may have left the protein unable to interact with hPrxII. Also it was suspected that the protein was denatured by the amide coupling procedure. Crystal dishes were put down using the mPrxII-ET-Srx complex but unfortunately to date have yielded no crystals. If the Srx molecule is able to bind to only one active site in the homodimer this could result in a lack of homogeneity in the sample preventing crystallisation.

A mutant Trx (C46S/C73S) and mutant Prx (C70S/C172S) were purified to homogeneity using nickel and gel filtration chromatography. A covalent complex was then formed between the two cysteine residues using the chemical conjugating agent DTNB. Size exclusion chromatography revealed the binding stoichiometry of this complex to be a 10:1 ratio of Trx to hPrxII decamer. The previously obtained disulfide structure of hPrxII was used to model the interaction with Trx. The model showed interaction between the hPrxII(S-S) and Trx at three conserved binding motifs. The binding in these regions consisted of hydrogen bonds and hydrophobic interactions. The minimal conformational change in the hPrxII protein is postulated to be the reason why binding can be observed at all 10 redox active centers in the hPrxII decamer. The complex was

also studied using SPR but no meaningful results were obtained from these experiments. The reasons for this are unclear and would require further investigation. Crystal dishes were put down using the mPrxII-mTrx complex but unfortunately to date have yielded no crystals.

Whilst working with Professor Willison (Institute of Cancer Research) an interaction was confirmed between hPrxII and PDCL3 using sucrose gradients. The nature of the hPrxII/PDCL3 interaction suggests a chaperone function for hPrxII.

The selenocysteine containing *TrxR1* was cloned with a minimal SECIS attached to the 3' end of the DNA sequence that allowed over-expression and purification of the active enzyme. The activity of this enzyme was increased when co-expressed with a plasmid containing the *selA*, *selB* and *selC* genes. When co-expressed with this plasmid a six-fold increase in activity was observed from 1.42 µmol/min to 8.54 µmol/min with the TrxR1 over-expressed without the SECIS showing no activity at all. The reconstitution of the hPrxII pathway was never achieved due to the time constraints of the PhD. Two preliminary experiments were carried out to obtain an active pathway without success. The activity of TrxR1 has been demostrated with an assay but hPrxII or Trx could be inactive providing a break in the chain needed for the assay to function. Further work is required to optimise the system.

6.2. Further work

There are a number of ways in which the work contained within this thesis can be taken forward with most of the further work focusing on the interaction between hPrxII, Srx and Trx. Now that the individual component enzymes are available a working hPrxII assay needs to be developed.

The investigation into the hPrxII-Srx and hPrxII-Trx complex could be continued with extensive investigation into the structure, binding stoichiometry and binding kinetics. Since there is no structure of either of the hPrxII-Srx and hPrxII-Trx complexes published, the complexes remain an interesting target for structural biology. Further studies could be undertaken to grow diffraction quality crystals, with the aim of solving these structures. Structural studies on the complexes could provide a greater insight into the mechanisms for binding between the two proteins as well as a further understanding of the interaction between

decameric hPrxII and the two reducing enzymes. Of particular interest would be the location of the C-terminal arm that is missing from the hPrxII(S-S) structure and performs a large structural movement in the hPrxI-ET-Srx complex structure. Another analytical tool for obtaining a structure for this complex could be to use biological small angle X-ray scattering (SAXS). SAXS has the advantage that a structure can be obtained without the need for a crystalline sample. Obtaining greater information on the structure of the hPrxII-Srx complex may help to understand any co-operation between the redox active sites in binding Srx and help to understand the 1:5 ratio observed from size exclusion chromatography.

There is still little information on the binding stoichiometry of these complexes as well as the kinetics of association and dissociation. Further evidence of the binding stoichiometry could be obtained using cryo-electron microscopy (cryo-EM). Pictures have been obtained of the toroidal shape of hPrxII using TEM and it would be interesting to see if the presence of the Srx/Trx protein can be seen attached to the hPrxII toroid. The binding stoichiometry could also be analyzed further using analytical techniques such as ultracentrifugation and sucrose gradients. Information on this binding stoichiometry would help to provide an understanding into the mechanism of complex formation and may provide information of the biological relevance of the decameric form of the protein.

Further development of the SPR assays could be continued to obtain kinetic data on these complexes. Extensive work must go into the design of these experiments to remove the issue of non-specific binding. Non-specific binding was identified as an electrostatic interaction and was partially removed by the addition of NaCl to the buffer. Future work could include changing different experimental conditions, or by altering the chemical layer through which the ligand and the gold interact. The proteins must be tested to see if amide coupling is rendering them inactive and if so an alternative to amide coupling can be used, such as binding to the gold surface through a tag attached to the protein, such as biotin or the His-tag. Binding through the His-tag would require removal of the His-tag from one of the proteins. Data obtained from these SPR studies would help to further understand the interactions between these proteins.

Now that all the proteins in the Prx pathway have been cloned, over-expressed and purified, formation of an assay for these proteins can be carried out. Formation of a working assay would allow the reaction of the hPrxII to be studied further. Information could be obtained on the range of concentrations of H_2O_2 at which hPrxII is functional. The assay could also be used to allow for studies into the effect of different inhibitors on the hPrxII and particular the interaction with Srx which could be used in cancer therapy to stimulate apotosis. Additionally, mutagenesis studies of key residues could investigate how different structural changes within hPrxII could alter its activity.

7. Appendix

7.1. Superdex 200 gel filtration column calibration

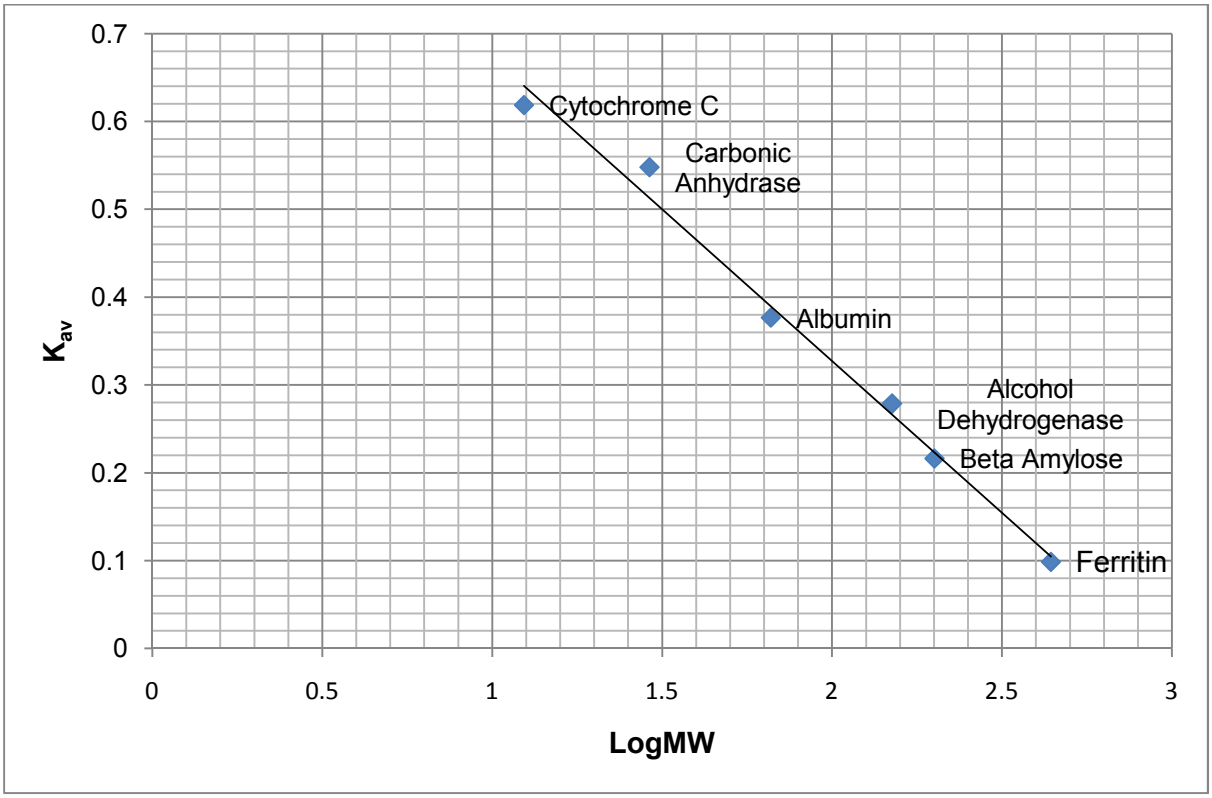

7.2. BioRad Precision Plus Protein Standard 15 – 250 kDa

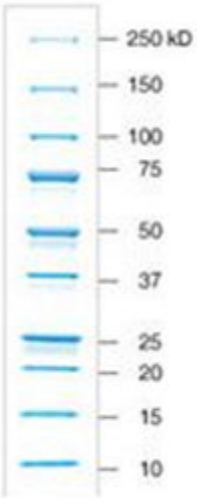

7.3. Hyperladder I (BIOLINE)

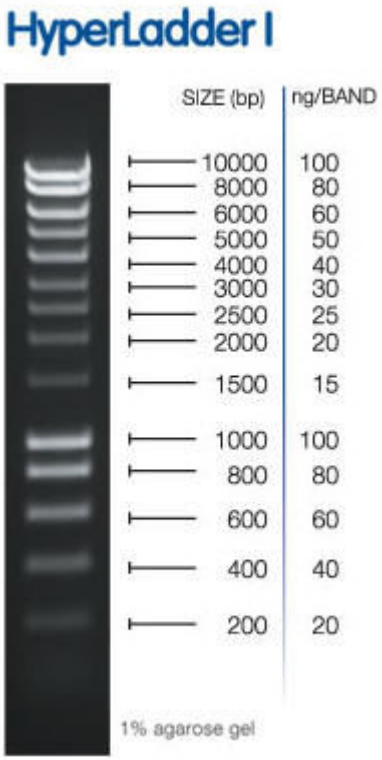

7.4. MDL 1 & 2 Crystal screen (Molecular Dimensions Laboratories)

7.4.1. MD1-01

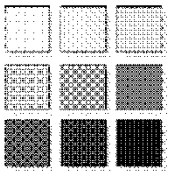

moleculardimensions.com

Structure Screen 1 **MD1-01**

Tube #	Salt	Buffer	pH	Precipitant
1	0.02 M calcium chloride	0.1 M sodium acetate	4.6	30 % v/v MPD
2	0.2 M ammonium acetate	0.1 M sodium acetate	4.6	30 % w/v PEG 4K
3	0.2 M ammonium sulfate	0.1 M sodium acetate	4.6	25 % w/v PEG 4K
4	None	0.1 M sodium acetate	4.6	2.0 M sodium formate
5	None	0.1 M sodium acetate	4.6	2.0 M ammonium sulfate
6	None	0.1 M sodium acetate	4.6	8 % w/v PEG 4K
7	0.2 M ammonium acetate	0.1 M tri-sodium citrate	5.6	30 % w/v PEG 4K
8	0.2 M ammonium acetate	0.1 M tri-sodium citrate	5.6	30 % v/v MPD
9	None	0.1 M tri-sodium citrate	5.6	20 % v/v 2-propanol, 20%w/v PEG 4K
10	None	0.1 M tri-sodium citrate	5.6	1.0 M ammonium dihydrogen phosphate
11	0.2 M calcium chloride	0.1 M sodium acetate	4.6	20 % v/v 2-propanol
12	None	0.1 M sodium cacodylate	6.5	1.4 M sodium acetate
13	0.2 M tri-sodium citrate	0.1 M sodium cacodylate	6.5	30 % v/v 2-propanol
14	0.2 M ammonium sulfate	0.1 M sodium cacodylate	6.5	30 % w/v PEG 8K
15	0.2 M magnesium acetate	0.1 M sodium cacodylate	6.5	20 % w/v PEG 8K
16	0.2 M magnesium acetate	0.1 M sodium cacodylate	6.5	30 % v/v MPD
17	None	0.1 M imidazole	6.5	1.0 M sodium acetate
18	0.2 M sodium acetate	0.1 M sodium cacodylate	6.5	30 % w/v PEG 8K
19	0.2 M zinc acetate	0.1 M sodium cacodylate	6.5	18 % w/v PEG 8K
20	0.2 M calcium acetate	0.1 M sodium cacodylate	6.5	18 % w/v PEG 8K
21	0.2 M tri-sodium citrate	0.1 M Na HEPES	7.5	30 % v/v MPD
22	0.2 M magnesium chloride	0.1 M Na HEPES	7.5	30 % v/ v 2-propanol
23	0.2 M calcium chloride	0.1 M Na HEPES	7.5	28 % v/v PEG 400
24	0.2 M magnesium chloride	0.1 M Na HEPES	7.5	30 % v/v PEG 400
25	0.2 M tri-sodium citrate	0.1 M Na HEPES	7.5	20 % v/v 2-propanol
26	None	0.1 M Na HEPES	7.5	0.8 M K/Na tartrate
27	None	0.1 M Na HEPES	7.5	1.5 M lithium sulfate
28	None	0.1 M Na HEPES	7.5	0.8 M sodium dihydrogen phosphate/ 0.8 M K dihydrogen phosphate
29	None	0.1 M Na HEPES	7.5	1.4 M tri-sodium citrate
30	None	0.1 M Na HEPES	7.5	2 % v/v PEG 400, 2.0 M ammonium sulfate
31	None	0.1 M Na HEPES	7.5	10 % v/v 2-propanol, 20% w/v PEG 4K
32	None	0.1 M Tris	8.5	2.0 M ammonium sulfate
33	0.2 M magnesium chloride	0.1 M Tris	8.5	30 % w/v PEG 4K
34	0.2 M tri-sodium citrate	0.1 M Tris	8.5	30 % v/v PEG 400
35	0.2 M lithium sulfate	0.1 M Tris	8.5	30 % w/v PEG 4K
36	0.2 M ammonium acetate	0.1 M Tris	8.5	30 % v/v 2-Propanol
37	0.2 M sodium acetate	0.1 M Tris	8.5	30 % w/v PEG 4K
38	None	0.1 M Tris	8.5	8 % w/v PEG 8K
39	None	0.1 M Tris	8.5	2.0 M ammonium dihydrogen phosphate
40	None	None	-	0.4 M K/Na Tartrate
41	None	None	-	0.4 M ammonium dihydrogen phosphate
42	0.2 M ammonium sulfate	None	-	30 % w/v PEG 8K
43	0.2 M ammonium sulfate	None	-	30 % w/v PEG 4K
44	None	None	-	2.0 M ammonium sulfate
45	None	None	-	4.0 M sodium formate
46	0.05 M potassium dihydrogen phosphate	None	-	20 % w/v PEG 8K
47	None	None	-	30 % w/v PEG 1.5K
48	None	None	-	0.2 M magnesium formate
49	1.0 M lithium sulfate	None	-	2 % w/v PEG 8K
50	0.5 M lithium sulfate	None	-	15 % w/v PEG 8K

Abbreviations: Na HEPES; 2-(4-(2-Hydroxyethyl)-1-piperazinyl)ethanesulfonic Acid Sodium Salt, **MPD;** 2,4-methyl pentanediol, **PEG;** Polyethylene glycol (1.5K, 4K and 8K correspond to the molecular weight, in thousands of Daltons, of PEG), **Tris**; 2-Amino-2-(hydroxymethyl)propane-1,3-diol.

Manufacturer's safety data sheets are available upon request.

3

7.4.2. MD1-02

moleculardimensions.com

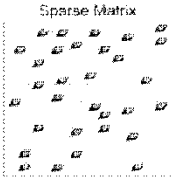

Structure Screen 2 **MD1-02**

Tube No.	Salt	Buffer	pH	Precipitant
1	0.1 M sodium chloride	0.1 M Bicine	9.0	30 % v/v PEG 550 MME
2	None	0.1 M Bicine	9.0	2.0 M magnesium chloride
3	None	0.1 M Bicine	9.0	2 % v/v 1,4-Dioxane/10 % w/v PEG 20,000
4	0.2 M magnesium chloride	0.1 M Tris	8.5	3.4 M 1,6-hexanediol
5	None	0.1 M Tris	8.5	25 % v/v tert-butanol
6	0.01 M nickel chloride	0.1 M Tris	8.5	1.0 M lithium sulfate
7	1.5 M ammonium sulfate	0.1 M Tris	8.5	12 % v/v glycerol
8	0.2 M ammonium dihydrogen phosphate	0.1 M Tris	8.5	50 % v/v MPD
9	None	0.1 M Tris	8.5	20 % v/v ethanol
10	0.01 M nickel chloride	0.1 M Tris	8.5	20 % w/v PEG 2000 MME
11	0.5 M ammonium sulfate	0.1 M Na HEPES	7.5	30 % v/v MPD
12	None	0.1 M Na HEPES	7.5	10 % w/v PEG 6000, 5% v/v MPD
13	None	0.1 M Na HEPES	7.5	20 % v/v Jeffamine M-600
14	0.1 M sodium chloride	0.1 M Na HEPES	7.5	1.6 M ammonium sulfate
15	None	0.1 M Na HEPES	7.5	2.0 M ammonium formate
16	0.05 M cadmium sulfate	0.1 M Na HEPES	7.5	1.0 M sodium acetate
17	None	0.1 M Na HEPES	7.5	70 % v/v MPD
18	None	0.1 M Na HEPES	7.5	4.3 M sodium chloride
19	None	0.1 M Na HEPES	7.5	10 % w/v PEG 8000, 8 % v/v ethylene glycol
20	None	0.1 M MES	6.5	1.6 M magnesium sulfate
21	0.1 M potassium phosphate + 0.1 M sodium phosphate	0.1 M MES	6.5	2.0 M sodium chloride
22	None	0.1 M MES	6.5	12 % w/v PEG 20,000
23	1.6 M ammonium sulfate	0.1 M MES	6.5	10 % v/v Dioxane
24	0.05 M caesium chloride	0.1 M MES	6.5	30 % v/v Jeffamine M-600
25	0.01 M cobalt chloride	0.1 M MES	6.5	1.8 M ammonium sulfate
26	0.2 M ammonium sulfate	0.1 M MES	6.5	30 % w/v PEG 5000 MME
27	0.01 M zinc sulfate	0.1 M MES	6.5	25 % v/v PEG 550 MME
28	None	0.1 M Na HEPES	7.5	20 % w/v PEG 10,000
29	0.2 M potassium sodium tartrate	0.1 M Na citrate	5.6	2.0 M ammonium sulfate
30	0.5 M ammonium sulfate	0.1 M Na citrate	5.6	1.0 M lithium sulfate
31	0.5 M sodium chloride	0.1 M Na citrate	5.6	4 % v/v polyethyleneimine
32	None	0.1 M Na citrate	5.6	35 % v/v tert-butanol
33	0.01 M ferric chloride	0.1 M Na citrate	5.6	10 % v/v Jeffamine M-600
34	0.01 M manganese chloride	0.1 M Na citrate	5.6	2.5 M 1,6-hexanediol
35	None	0.1 M Na acetate	4.6	2.0 M sodium chloride
36	0.2 M sodium chloride	0.1 M Na acetate	4.6	30 % v/v MPD
37	0.01 M cobalt chloride	0.1 M Na acetate	4.6	1.0 M 1,6-hexanediol
38	0.1 M cadmium chloride	0.1 M Na acetate	4.6	30 % v/v PEG 400
39	0.2 M ammonium sulfate	0.1 M Na acetate	4.6	30 % w/v PEG 2000 MME
40	2.0 M sodium chloride	None	None	10 % w/v PEG 6000
41	0.01 M CTAB	None	None	0.5 M sodium chloride, 0.1 M magnesium chloride
42	None	None	None	25 % v/v ethylene glycol
43	None	None	None	35 % v/v dioxane
44	2.0 M ammonium sulfate	None	None	5 % v/v 2-propanol
45	None	None	None	1.0 M imidazole pH 7.0
46	None	None	None	10 % w/v PEG 1000, 10 % w/v PEG 8000
47	1.5 M sodium chloride	None	None	10 % v/v ethanol
48	None	None	None	1.6 M sodium citrate pH 6.5
49	15 % w/v polyvinylpyrolidone	None	None	None
50	2.0 M urea	None	None	None

Abbreviations:
Bicine; N,N-Bis(2-hydroxyethyl)glycine, **CTAB**; cetyltrimethylammonium bromide, **Na HEPES**; 2-(4-(2-Hydroxyethyl)-1-piperazinyl)ethanesulfonic Acid Sodium Salt, **MES**; 2-(N-morpholino)ethanesulfonic acid, **MME**; Monomethylether, **MPD;** 2,4-methyl pentanediol, **PEG**; Polyethylene glycol, **Tris**; 2-Amino-2-(hydroxymethyl)propane-1,3-diol,

7.5. Sigma crystal screens

7.5.1. Sigma 8007 Crystal Screen (Sigma)

SIGMA

82009 Crystallization Basic Kit for Proteins Observation Sheet

Sample description: _____ Date: _____
concentration: _____ Incubation Temperature: _____
buffer: _____ Reservoir Volume: _____
1 Drop contains : Crystallization Reagent_____ul Sample_____ul Additive (name)_____(volume)_____ul

	precipitate without birefringent and edges	**precipitates shows birefringent or has edges**
1 drop is clear	3 mostly clear drop	7 spherulites or small structures maybe edges
2 drop contains non-protein particles	4 fully precipitated dark colour	8 crystal grown 1 D
	5 gelatinous protein precipitate	9 crystal grown 2 D
	6 phase separation	10 crystal grown 3 D

No.	Fluka No.	Reagent composition	Date:	Date:	Date:	Date:	Date:
1.	89754	Ca-chloride 0.02M, Na-acetate (pH 4.6) 0.1M, 2-Methyl-2,4-pentanediol 30%					
2.	78016	K-,Na-tartrate 0.4M					
3.	77104	NH_4-dihydrogenphosphate 0.4M					
4.	84653	TRIS-HCl (pH 8.5) 0.1M, NH_4-sulfate 2.0M					
5.	77103	Na-citrate 0.2M, HEPES Na-salt (pH 7.5) 0.1M, 2-Methyl-2,4-pentanediol 30%					
6.	78760	Mg-chloride 0.2M, TRIS-HCl (pH 8.5) 0.1M, PEG 4000 30%					
7.	70114	Na-cacodylate (pH 6.5) 0.1M, Na-acetate 1.4M					
8.	85887	Na-citrate 0.2M, Na-cacodylate (pH 6.5) 0.1M, 2-Propanol 30%					
9.	73374	NH_4-acetate 0.2M, Na-citrate (pH 5.6) 0.1M, PEG 4000 30%					
10.	76028	NH_4-acetate 0.2M, Na-acetate (pH 4.6) 0.1M, PEG 4000 30%					
11.	78993	Na-citrate (pH 5.6) 0.1M, NH_4-dihyrogenphosphate 1.0M					
12.	73682	Mg-chloride 0.2M, HEPES Na-salt (pH 7.5) 0.1M, 2-Propanol 30%					
13.	76018	Na-citrate 0.2M, TRIS-HCl (pH 8.5) 0.1M, PEG 400 30%					
14.	79052	Ca-chloride 0.2M, HEPES Na-salt (pH 7.5) 0.1M, PEG 400 28%					
15.	86686	NH_4-sulfate 0.2M, Na-cacodylate (pH 6.5) 0.1M, PEG 8000 30%					
16.	86445	HEPES Na-salt (pH 7.5) 0.1M, Li-sulfate 1.5M					
17.	89786	Li-sulfate 0.2M, TRIS-HCl (pH 8.5) 0.1M, PEG 4000 30%					
18.	88518	Mg-acetate 0.2M, Na-cacodylate pH (6.5) 0.1M, PEG 8000 20%					
19.	88512	NH_4-acetate 0.2M, TRIS-HCl (pH 8.5) 0.1M, 2-Propanol 30%					
20.	82406	NH_4-sulfate 0.2M, Na-acetate (pH 4.6) 0.1M, PEG 4000 25%					
21.	87924	Mg-acetate 0.2M, Na-cacodylate (pH 6.5) 0.1M, 2-Methyl-2,4-pentanediol 30%					
22.	88543	Na-acetate 0.2M, TRIS-HCl (pH 8.5) 0.1M, PEG 4000 30%					
23.	73642	Mg-chloride 0.2M, HEPES Na-salt (pH 7.5) 0.1M, PEG 400 30%					
24.	92644	Ca-chloride 0.2M, Na-acetate (pH 4.6) 0.1M, 2-Propanol 20%					
25.	70377	Imidazole (pH 6.5) 0.1M, Na-acetate 1M					
26.	88530	NH_4-acetate 0.2M, Na-citrate (pH 5.6) 0.1M, 2-Methyl-2,4-pentanediol 30%					
27.	92465	Na-citrate 0.2M, HEPES Na-salt (pH 7.5) 0.1M, 2-Propanol 20%					
28.	96345	Na-acetate 0.2M, Na-cacodylate pH (6.5) 0.1M, PEG 8000 30%					
29.	93268	HEPES Na-salt (pH 7.5) 0.1M, K-,Na-tartrate 0.8M					
30.	71907	NH_4-sulfate 0.2M, PEG 8000 30%					
31.	80677	NH_4-sulfate 0.2M, PEG 4000 30%					
32.	76399	NH_4-sulfate 2M					
33.	73932	Na-formiate 4M					
34.	76728	Na-acetate (pH 4.6) 0.1M,Na-formiate 2M					
35.	71835	HEPES Na-salt (pH 7.5) 0.1M, K-dihydrogenphosphate 0.8M, Na-dihydrogenphosphate 0.8M					
36.	80526	TRIS-HCl (pH 8.5) 0.1M, PEG 8000 8%					
37.	77436	Na-acetate (pH 4.6) 0.1M, PEG 4000 8%					
38.	73931	HEPES Na-salt (pH 7.5) 0.1M, Na-citrate 1.4M					
39.	80346	HEPES Na-salt (pH 7.5) 0.1M, PEG 400 2%, NH_4-sulfate 2.0M					
40.	73933	Na-citrate (pH 5.6) 0.1M, 2-Propanol 20%, PEG 4000 20%					
41.	80565	HEPES Na-salt (pH 7.5) 0.1M, 2-Propanol 10%, PEG 4000 20%					
42.	80806	K-dihydrogenphosphate 0.05M, PEG 8000 20%					
43.	78225	PEG 1500 30%					
44.	73934	Mg-formiate 0.2M					
45.	82409	Zn-acetate 0.2M, Na-cacodylate (pH 6.5) 0.1M, PEG 8000 18%					
46.	91113	Ca-acetate 0.2M, Na-cacodylate (pH 6.5) 0.1M, PEG 8000 18%					
47.	91633	Na-acetate (pH 4.6) 0.1M, NH_4-sulfate 2.0M					
48.	85934	TRIS-HCl (pH 8.5) 0.1M, NH_4-dihydrogenphosphate 2.0M					
49.	91114	Li-sulfate 1.0M, PEG 8000 2%					
50.	88862	Li-sulfate 0.5M, PEG 8000 15%					

Industriestrasse 25
CH-9471 Buchs
E-mail: Flukatec@eurnotes.sial.com
Fax: ++41 81 755 2815

7.5.2. Sigma 70437 Crystal Screen (Sigma)

70437 Crystallization Extension Kit for Proteins Observation Sheet

Sample description: _____ Date: _____
concentration: _____ Incubation Temperature: _____
buffer: _____ Reservoir Volume: _____
1 Drop contains : Crystallization Reagent_____ul Sample_____ul Additive (name)_____(volume)_____ul

1 drop is clear
2 drop contains non-protein particles

precipitate without birefringent and edges
3 mostly clear drop
4 fully precipitated dark colour
5 gelatinous protein precipitate
6 phase separation

precipitates shows birefringent or has edges
7 spherulites or small structures maybe edges
8 crystal grown 1 D
9 crystal grown 2 D
10 crystal grown 3 D

No.	Fluka No.	Name	Date:	Date:	Date:	Date:	Date:
1.	88716	Na-chloride 2M, PEG 6000 10%					
2.	83935	Na-chloride 0.5M, Mg-chloride 0.01M, CTAB 0.01M					
3.	72526	Ethylene glycol 25%					
4.	75691	Dioxane 35%					
5.	70293	NH_4-sulfate 2M, 2-Propanol 5%					
6.	95514	Imidazole (pH 7.0) 1M					
7.	93593	PEG 1000 10%, PEG 8000 10%					
8.	92982	Na-chloride 1.5M, Ethanol 10%					
9.	93471	Na-chloride 2M, Na-acetate (pH 4.6) 0.1M					
10.	93714	Na-chloride 0.2M, Na-acetate (pH 4.6) 0.1M, 2-Methyl-2,4-pentanediol 30%					
11.	96346	Co-chloride 0.01M, Na-acetate (pH 4.6) 0.1M, 1,6-Hexanediol 1M					
12.	95958	Cd-chloride 0.1M, Na-acetate (pH 4.6) 0.1M, PEG 400 30%					
13.	92913	NH_4-sulfate 0.2M, Na-acetate (pH 4.6) 0.1M, PEG MME 2000 30%					
14.	96765	K-,Na-tartrate 0.2M, NH_4-sulfate 2M, Na-citrate (pH 5.6) 0.1M					
15.	92347	Li-sulfate 1M, NH_4-sulfate 0.5M, Na-citrate (pH 5.6) 0.1M					
16.	94832	Na-chloride 0.5M, Na-citrate (pH 5.6) 0.1M, Polyethylenimin 2%					
17.	94839	Na-citrate (pH 5.6) 0.1M, tert.-Butanol 35%					
18.	71228	Fe(III)-chloride 0.01M, Na-citrate (pH 5.6) 0.1M, Jeffamine M-600 10%					
19.	80557	Na-citrate (pH 5.6) 0.1M, 1,6-Hexanediol 2.5M					
20.	80094	Mg-sulfate 1.6M, MES (pH 6.5) 0.1M					
21.	77583	Na-chloride 2M, Ka-,Na- dihydrogenphosphate each 0.1M, MES (pH 6.5) 0.1M					
22.	79975	MES (pH 6.5) 0.1M, PEG 20'000 12%					
23.	80095	NH_4-sulfate 1.6M, MES (pH 6.5) 0.1M, Dioxane 10%					
24.	72873	Cs-chloride 0.05M, MES (pH 6.5) 0.1M, Jeffamine M-600 30%					
25.	72874	Co-chloride 0.01M, NH_4-sulfate 1.8M, MES (pH 6.5) 0.1M					
26.	79688	NH_4-sulfate 0.2M, MES (pH 6.5) 0.1M, PEG MME 5000 30%					
27.	74616	Zn-sulfate 0.01M, MES (pH 6.5) 0.1M, PEG MME 550 25%					
28.	73894	Na-citrate (pH 6.5) 1.6M					
29.	80386	NH_4-sulfate 0.5M, HEPES Na-salt (pH 7.5) 0.1M, 2-Methyl-2,4-pentanediol 30%					
30.	80060	HEPES Na-salt (pH 7.5) 0.1M, 2-Methyl-2,4-pentanediol 5%, PEG 6000 10%					
31.	79976	HEPES Na-salt (pH 7.5) 0.1M, Jeffamine M-600 20%					
32.	79687	NH_4-sulfate 1.6M, Na-chloride 0.1M, HEPES Na-salt (pH 7.5) 0.1M					
33.	91476	NH_4-formate 2.0M, HEPES Na-salt (pH 7.5) 0.1M					
34.	89718	Na-acetate 1.0M, Cd-sulfate 0.05M, HEPES Na-salt (pH 7.5) 0.1M					
35.	86953	HEPES Na-salt (pH 7.5) 0.1M, 2-Methyl-2,4-pentanediol 70%					
36.	82238	Na-chloride 4.3M, HEPES Na-salt (pH 7.5) 0.1M					
37.	90196	HEPES Na-salt (pH 7.5) 0.1M, Ethylene glycol 8%, PEG 8000 10%					
38.	82217	HEPES Na-salt (pH 7.5) 0.1M, PEG 10'000 20%					
39.	82208	Mg-chloride 0.2M, TRIS-HCl (pH 8.5) 0.1M, 1,6-Hexanediol 3.4M					
40.	86261	TRIS-HCl (pH 8.5) 0.1M, tert.-Butanol 25%					
41.	81935	Li-sulfate 1M, Ni(II)-chloride 0.01M, TRIS-HCl (pH 8.5) 0.1M					
42.	82237	NH_4-sulfate 1.5M, TRIS-HCl (pH 8.5) 0.1M, Glycerol 12%					
43.	80925	NH_4-phosphate 0.2M, TRIS-HCl (pH 8.5) 0.1M, 2-Methyl-2,4-pentanediol 50%					
44.	88438	TRIS-HCl (pH 8.5) 0.1M, Ethanol 20%					
45.	88439	Ni(II)-chloride 0.01M, TRIS-HCl (pH 8.5) 0.1M, PEG MME 2000 20%					
46.	91229	Na-chloride 0.1M, Bicine (pH 9.0) 0.1M, PEG MME 550 20%					
47.	95633	Mg-chloride 2M, Bicine (pH 7.5) 0.1M					
48.	80106	Bicine (pH 9.0) 0.1M, Dioxane 2%, PEG 20'000 10%					
49.	79924	Mg-chloride 0.1 M, TRIS-HCl (pH 8.5) 0.1M, PEG 20000 15%					
50.	80105	PEG 20000 20 %					

Industriestrasse 25
CH-9471 Buchs
E-mail: Flukatec@eurnotes.sial.com
Fax: ++41 81 755 2815

7.6. JCSG Crystal Screen (Molecular Dimensions Laboratories)

7.6.1. Box 1

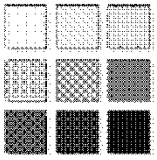

moleculardimensions.com

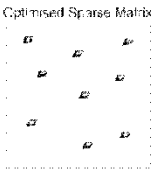

JCSG-*plus* **Box 1 of 2** **MD1-37**

Tube No.	Salt	Buffer	pH	Precipitant
1.1	0.2 M lithium sulfate	0.1 M sodium acetate	4.5	50 % v/v PEG 400
1.2	None	0.1 M sodium citrate	5.5	20 % w/v PEG 3000
1.3	0.2 M di-ammonium hydrogen citrate	None	-	20 % w/v PEG 3350
1.4	0.02 M calcium chloride	0.1 M sodium acetate	4.6	30 % v/v MPD
1.5	0.2 M magnesium formate	None	-	20 % w/v PEG 3350
1.6	0.2 M lithium sulfate	0.1 M phosphate/citrate	4.2	20 % w/v PEG 1000
1.7	None	0.1 M CHES	9.5	20 % w/v PEG 8000
1.8	0.2 M ammonium formate	None	-	20 % w/v PEG 3350
1.9	0.2 M ammonium chloride	None	-	20 % w/v PEG 3350
1.10	0.2 M potassium formate	None	-	20 % w/v PEG 3350
1.11	0.2 M ammonium dihydrogen phosphate	0.1 M Tris	8.5	50 % v/v MPD
1.12	0.2 M potassium nitrate	None	-	20 % w/v PEG 3350
1.13	None	0.1 M citrate	4.0	0.8 M ammonium sulfate
1.14	0.2 M sodium thiocyanate	None	-	20 % w/v PEG 3350
1.15	None	0.1 M Bicine	9.0	20 % w/v PEG 6000
1.16	None	0.1 M HEPES	7.5	10 % w/v PEG 8000/ 8 % v/v Ethylene glycol
1.17	None	0.1 M sodium cacodylate	6.5	40 % v/v MPD/ 5 % w/v PEG 8000
1.18	None	0.1 M phosphate/citrate	4.2	40 % v/v Ethanol/ 5 % w/v PEG 1000
1.19	None	0.1 M sodium acetate	4.6	8 % w/v PEG 4000
1.20	0.2 M magnesium chloride	0.1 M Tris	7.0	10 % w/v PEG 8000
1.21	None	0.1 M citrate	5.0	20 % w/v PEG 6000
1.22	0.2 M magnesium chloride	0.1 M sodium cacodylate	6.5	50 % v/v PEG 200
1.23	None	None	6.5	1.6 M tri-sodium citrate
1.24	0.2 M tri-potassium citrate	None	-	20 % w/v PEG 3350
1.25	0.2 M sodium chloride	0.1 M phosphate/citrate	4.2	20 % w/v PEG 8000
1.26	1.0 M lithium chloride	0.1 M Na citrate	4.0	20 % w/v PEG 6000
1.27	0.2 M ammonium nitrate	None	-	20 % w/v PEG 3350
1.28	None	0.1 M Na HEPES	7.0	10 % w/v PEG 6000
1.29	None	0.1 M Na HEPES	7.5	0.8 M sodium dihydrogen phosphate 0.8 M potassium dihydrogen phosphate
1.30	None	0.1 M phosphate/citrate	4.2	40 % v/v PEG 300
1.31	0.2 M zinc acetate	0.1 M sodium acetate	4.5	10 % w/v PEG 3000
1.32	None	0.1 M Tris	8.5	20 % v/v Ethanol
1.33	None	0.1 M Na/K phosphate	6.2	25 % v/v 1,2-propanediol 10 % v/v Glycerol
1.34	None	0.1 M Bicine	9.0	10 % w/v PEG 20,000/ 2% v/v Dioxane
1.35	None	0.1 M sodium acetate	4.6	2.0 M ammonium sulfate
1.36	None	None	-	10 % w/v PEG 1000/ 10 % w/v PEG 8000
1.37	None	None	-	24 % w/v PEG 1500/ 20 % v/v Glycerol
1.38	0.2 M magnesium chloride	0.1 M Na HEPES	7.5	30 % v/v PEG 400
1.39	0.2 M sodium chloride	0.1 M Na/K phosphate	6.2	50 % v/v PEG 200
1.40	0.2 M lithium sulfate	0.1 M sodium acetate	4.5	30 % w/v PEG 8000
1.41	None	0.1 M HEPES	7.5	70 % v/v MPD
1.42	0.2 M magnesium chloride	0.1 M Tris	8.5	20 % w/v PEG 8000
1.43	0.2 M lithium sulfate	0.1 M Tris	8.5	40 % v/v PEG 400
1.44	None	0.1 M Tris	8.0	40 % v/v MPD
1.45	0.17 M ammonium sulfate	None	-	25.5 % w/v PEG 4000/ 15 % v/v Glycerol
1.46	0.2 M calcium acetate	0.1 M sodium cacodylate	6.5	40 % v/v PEG 300
1.47	0.14 M calcium chloride	0.07 M sodium acetate	4.6	14 % v/v 2-propanol/ 30 % v/v Glycerol
1.48	0.04 M potassium dihydrogen phosphate	None	-	16 % w/v PEG 8000/ 20 % v/v Glycerol

7.6.2. Box 2

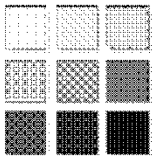

moleculardimensions.com

JCSG-*plus* **Box 2 of 2** **MD1-37**

Tube	Salt	Buffer	pH	Precipitant
2.1	None	0.1 M sodium cacodylate	6.5	1.0 M tri-sodium citrate
2.2	0.2 M sodium chloride	0.1 M sodium cacodylate	6.5	2.0 M ammonium sulfate
2.3	0.2 M sodium chloride	0.1 M HEPES	7.5	10 % v/v 2-propanol
2.4	0.2 M lithium sulfate	0.1 M Tris	8.5	1.26 M ammonium sulfate
2.5	None	0.1 M CAPS	10.5	40 % v/v MPD
2.6	0.2 M zinc acetate	0.1 M imidazole	8.0	20 % w/v PEG 3000
2.7	0.2 M zinc acetate	0.1 M sodium cacodylate	6.5	10 % v/v 2-propanol
2.8	None	0.1 M sodium acetate	4.5	1.0 M di-ammonium hydrogen phosphate
2.9	None	0.1 M MES	6.5	1.6 M magnesium sulfate
2.10	None	0.1 M Bicine	9.0	10 % w/v PEG 6000
2.11	0.16 M calcium acetate	0.08 M sodium cacodylate	6.5	14.4 % w/v PEG 8000/ 20 % v/v glycerol
2.12	None	0.1 M imidazole	8.0	10 % w/v PEG 8000
2.13	0.05 M caesium chloride	0.1 M MES	6.5	30 % v/v Jeffamine M-600
2.14	None	0.1 M Na Citrate	5.0	3.2 M ammonium sulfate
2.15	None	0.1 M Tris	8.0	20 % v/v MPD
2.16	None	0.1 M HEPES	7.5	20 % v/v Jeffamine M-600
2.17	0.2 M magnesium chloride	0.1 M Tris	8.5	50 % v/v ethylene glycol
2.18	None	0.1 M Bicine	9.0	10 % v/v MPD
2.19	None	None	7.0	0.8 M succinic acid
2.20	None	None	7.0	2.1 M DL-malic acid
2.21	None	None	7.0	2.4 M sodium malonate
2.22	1.1 M sodium malonate	0.1 M HEPES	7.0	0.5 % v/v Jeffamine ED-2001
2.23	1.0 M succinic acid	0.1 M HEPES	7.0	1 % w/v PEG 2000 MME
2.24	None	0.1 M HEPES	7.0	30 % v/v Jeffamine M-600
2.25	None	0.1 M HEPES	7.0	30 % v/v Jeffamine ED-2001
2.26	0.02 M magnesium chloride	0.1 M HEPES	7.5	22 % w/v polyacrylic acid 5100 sodium salt
2.27	0.01 M cobalt chloride	0.1 M Tris	8.5	20 % w/v polyvinylpyrrolidone K15
2.28	0.2 M tri-methylamine N-oxide	0.1 M Tris	8.5	20 % w/v PEG 2000 MME
2.29	0.005 M cobalt chloride 0.005 M cadmium chloride 0.005 M magnesium chloride 0.005 M nickel chloride	0.1 M HEPES	7.5	12 % w/v PEG 3350
2.30	0.2 M sodium malonate	None	7.0	20 % w/v PEG 3350
2.31	0.1 M succinic acid	None	7.0	15 % w/v PEG 3350
2.32	0.15 M DL - malic acid	None	7.0	20 % w/v PEG 3350
2.33	0.1 M potassium thiocyanate	None	-	30 % w/v PEG 2000 MME
2.34	0.15 M potassium bromide	None	-	30 % w/v PEG 2000 MME
2.35	None	0.1 M Bis Tris	5.5	2.0 M ammonium sulfate
2.36	None	0.1 M Bis Tris	5.5	3.0 M sodium chloride
2.37	None	0.1 M Bis Tris	5.5	0.3 M magnesium formate
2.38	1.0 M ammonium sulfate	0.1 M Bis Tris	5.5	1 % w/v PEG 3350
2.39	None	0.1 M Bis Tris	5.5	25 % w/v PEG 3350
2.40	0.2 M calcium chloride	0.1 M Bis Tris	5.5	45 % v/v MPD
2.41	0.2 M ammonium acetate	0.1 M Bis Tris	5.5	45 % v/v MPD
2.42	0.1 M ammonium acetate	0.1 M Bis Tris	5.5	17 % w/v PEG 10000
2.43	0.2 M ammonium sulfate	0.1 M Bis Tris	5.5	25 % w/v PEG 3350
2.44	0.2 M sodium chloride	0.1 M Bis Tris	5.5	25 % w/v PEG 3350
2.45	0.2 M lithium sulfate	0.1 M Bis Tris	5.5	25 % w/v PEG 3350
2.46	0.2 M ammonium acetate	0.1 M Bis Tris	5.5	25 % w/v PEG 3350
2.47	0.2 M magnesium chloride	0.1 M Bis Tris	5.5	25 % w/v PEG 3350
2.48	0.2 M ammonium acetate	0.1 M HEPES	7.5	45 % v/v MPD

Abbreviations: Bis Tris; Bis-(2-hydroxyethyl)imino-tris(hydroxymethyl)methane, **CAPS**; N-Cyclohexyl-3-aminopropanesulfonic acid, **CHES**; 2-(N-Cyclohexylamino)ethane Sulfonic Acid, **HEPES;** 2-(4-(2-Hydroxyethyl)-1-piperazinyl)ethanesulfonic Acid, **Na HEPES**; 2-(4-(2-Hydroxyethyl)-1-piperazinyl)ethanesulfonic Acid Sodium Salt, **MES**; 2-(N-morpholino)ethanesulfonic acid, **MPD;** 2,4-methyl pentanediol, **PEG**; Polyethylene glycol, **Tris**; 2-Amino-2-(hydroxymethyl)propane-1,3-diol.

Manufacturer's safety data sheets are available upon request.

7.7. Ramachandran plot for the hPrxII(S-S) structure

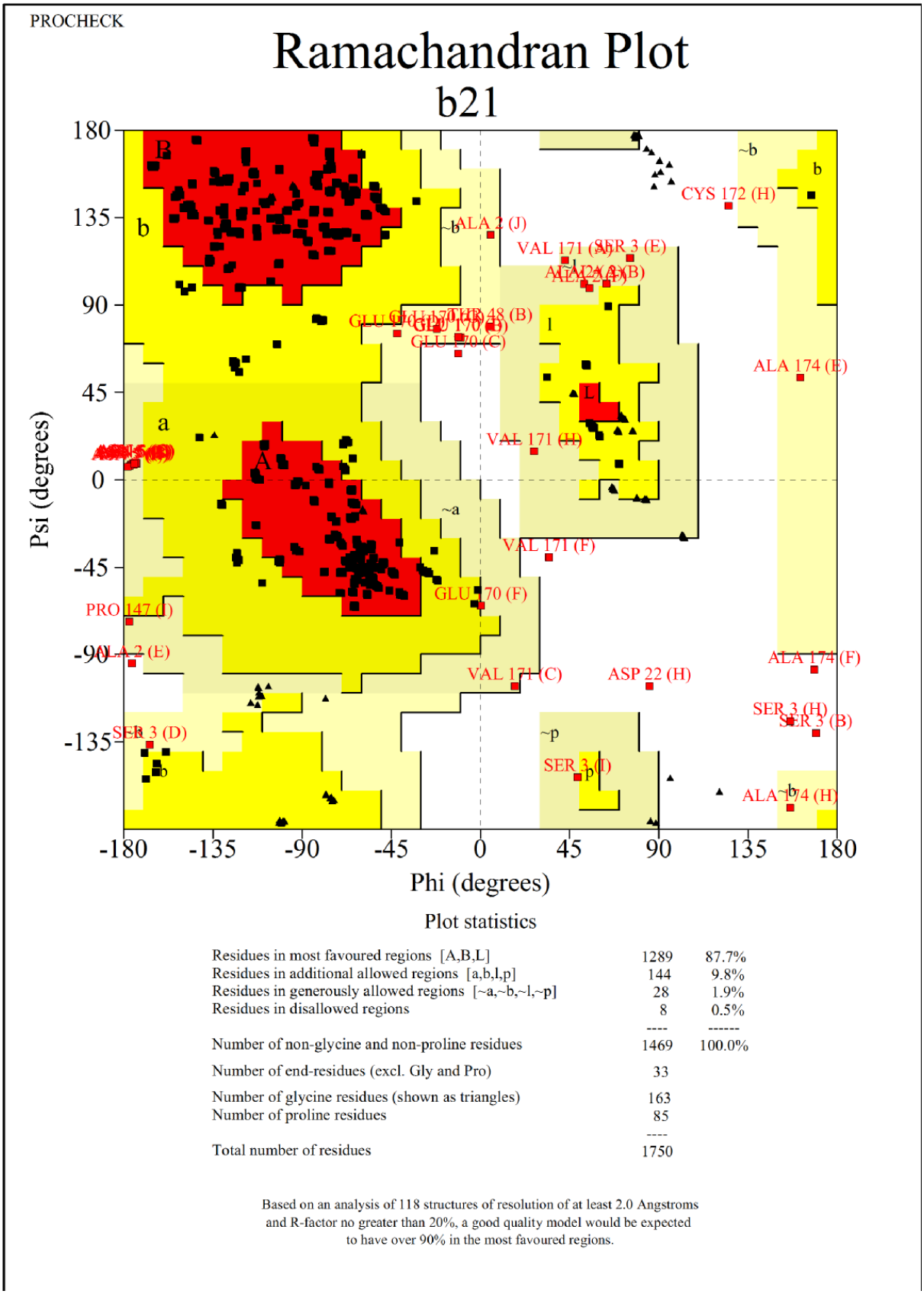

Plot statistics

Residues in most favoured regions [A,B,L]	1289	87.7%
Residues in additional allowed regions [a,b,l,p]	144	9.8%
Residues in generously allowed regions [~a,~b,~l,~p]	28	1.9%
Residues in disallowed regions	8	0.5%
Number of non-glycine and non-proline residues	1469	100.0%
Number of end-residues (excl. Gly and Pro)	33	
Number of glycine residues (shown as triangles)	163	
Number of proline residues	85	
Total number of residues	1750	

Based on an analysis of 118 structures of resolution of at least 2.0 Angstroms and R-factor no greater than 20%, a good quality model would be expected to have over 90% in the most favoured regions.

7.8. ET-Srx mutation

7.8.1. DNA sequence

3’ATGGGCAGCAGCCATCATCATCATCATCACAGCAGCGGCCTGGTGCCGC
GCGGCAGCCATATGATCCACTCGGGCCGCATCGCCGCGGTGCACAACGT
GCCGCTGAGCGTGCTCATCCGGCCGCTGCCGTCCGTGTTGGACCCCGCC
AAGGTGCAGAGCCTCGTGGACACGATCCGGGAGGACCCAGACAGCGTGC
CCCCCATCGATGTCCTCTGGATCAAAGGGGCCCAGGGAGGTGACTACTTC
TACTCCTTTGGGGGCTGCCACCGCTACGCGGCCTACCAGCAACTGCAGC
GAGAGACCATCCCCGCCAAGCTTGTCCAGTCCACTCTCTCAGACCTAAGG
GTGTACCTGGGAGCATCCACACCAGACTTGCAGTAG 5’

7.8.2. Protein sequence

MGLRAGGTLGRAGAGRGAPEGPGPSGGAQGGSIHSGRIAAVHNVPLSVLIRP
LPSVLDPAKVQSLVDTIREDPDSVPPIDVLWIKGAQGGDYFYSFGGCHRYAAY
QQLQRETIPAKLVQSTLSDLRVYLGASTPDLQ

7.9. mPrxII mutation

7.9.1. DNA sequence (Mutation in bold)

ATGGCCTCCGGTAACGCGCGCATCGGAAAGCCAGCCCCTGACTTCAAGG
CCACAGCGGTGGTTGATGGCGCCTTCAAAGAGGTGAAGCTGTCGGACTAC
AAAGGGAAGTACGTGGTCCTCTTTTTCTACCCTCTGGACTTCACTTTTGTG
TGCCCCACCGAGATCATCGCGTTCAGCAACCGTGCAGAGGACTTCCGCAA
GCTGGGC**TCA**GAAGTGCTGGGCGTCTCGGTGGACTCTCAGTTCACCCAC
CTGGCTTGGATCAACACCCCCCGGAAAGAGGGAGGCTTGGGCCCCCTGA
ACATCCCCCTGCTTGCTGACGTGACCAGACGCTTGTCTGAGGATTACGGC
GTGCTGAAAACAGATGAGGGCATTGCCTACAGGGGCCTCTTTATCATCGA
TGGCAAGGGTGTCCTTCGCCAGATCACTGTTAATGATTTGCCTGTGGGAC
GCTCCGTGGATGAGGCTCTGCGGCTGGTCCAGGCCTTCCAGTACACAGA
CGAGCATGGGGAAGTT**TCA**CCCGCTGGCTGGAAGCCTGGCAGTGACACG
ATTAAGCCCAACGTGGATGACAGCAAGGAATATTTCTCCAAACACAATTAG

Protein sequence (Mutation in bold)

MASGNARIGKPAPDFKATAVVDGAFKEVKLSDYKGKYVVLFFYPLDFTFVCPT
EIIAFSNRAEDFRKLG**S**EVLGVSVDSQFTHLAWINTPRKEGGLGPLNIPLLADV
TRRLSEDYGVLKTDEGIAYRGLFIIDGKGVLRQITVNDLPVGRSVDEALRLVQA
FQYTDEHGEV**S**PAGWKPGSDTIKPNVDDSKEYFSKHN

7.10. Spectra™ multicolour broad range protein ladder (Fermentas)

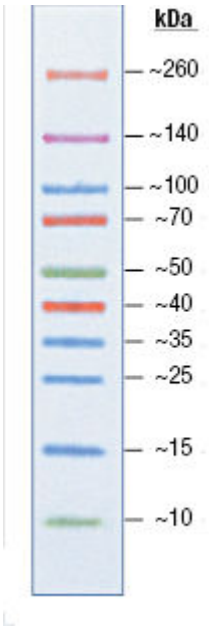

7.11. hTrxR1

7.11.1. DNA sequence (SECIS in bold)

atgaacggccctgaagatcttcccaagtcctatgactatgaccttatcatcattggaggtggctcaggaggtctg
gcagctgctaaggaggcagcccaatatggcaagaaggtgatggtcctggactttgtcactcccacccctcttg
gaactagatggggtcttggaggaacatgtgtgaatgtgggttgcatacctaaaaaactgatgcatcaagcagc
tttgttaggacaagccctgcaagactctcgaaattatggatggaaagtcgaggagacagttaagcatgattgg
gacagaatgatagaagctgtacagaatcacattggctctttgaattggggctaccgagtagctctgcgggaga
aaaaagtcgtctatgagaatgcttatgggcaatttattggtcctcacaggattaaggcaacaaataataaaggc
aaagaaaaaatttattcagcagagagatttctcattgccactggtgaaagaccacgttacttgggcatccctggt
gacaaagaatactgcatcagcagtgatgatcttttctccttgccttactgcccgggtaagaccctggttgttggag
catcctatgtcgctttggagtgcgctggatttcttgctggtattggtttagacgtcactgttatggttaggtccattcttct
tagaggatttgaccaggactggccaacaaaattggtgaacacatggaagaacatggcatcaagtttataaga
cagttcgtaccaattaaagttgaacaaattgaagcagggacaccaggccgactcagagtagtagctcagtcc
accaatagtgaggaaatcattgaaggagaatataatacggtgatgctggcaataggaagagatgcttgcaca
agaaaaattggcttagaaaccgtaggggtgaagataaatgaaaagactggaaaaatacctgtcacagatga
agaacagaccaatgtgccttacatctatgccattggcgatatattggaggataaggtggagctcaccccagttg
caatccaggcaggaagattgctggctcagaggctctatgcaggttccactgtcaagtgtgactatgaaaatgtt
ccaaccactgtatttactcctttggaatatggtgcttgtggcctttctgaggagaaagctgtggagaagtttgggga
agaaaatattgaggtttaccatagttacttttggccattggaatggacgattccgtcaagagataacaacaaatg
ttatgcaaaaataatctgtaatactaaagacaatgaacgtgttgtgggctttcacgtactgggtccaaatgctgg
agaagttacacaaggctttgcagctgcgctcaaatgtggactgaccaaaaagcagctggacagcacaattg

gaatccaccctgtctgtgcagaggtattcacaacattgtctgtgaccaagcgctctggggcaagcatcctccag
gctggctgctgaggttaataa**tcggttgcaggtctgcacc**

7.11.2. Protein sequence

MNGPEDLPKSYDYDLIIIGGGSGGLAAAKEAAQYGKKVMVLDFVTPTPLGTRW
GLGGTCVNVGCIPKKLMHQAALLGQALQDSRNYGWKVEETVKHDWDRMIEA
VQNHIGSLNWGYRVALREKKVVYENAYGQFIGPHRIKATNNKGKEKIYSAERF
LIATGERPRYLGIPGDKEYCISSDDLFSLPYCPGKTLVVGASYVALECAGFLAGI
GLDVTVMVRSILLRGFDQDMANKIGEHMEEHGIKFIRQFVPIKVEQIEAGTPGR
LRVVAQSTNSEEIIEGEYNTVMLAIGRDACTRKIGLETVGVKINEKTGKIPVTDE
EQTNVPYIYAIGDILEDKVELTPVAIQAGRLLAQRLYAGSTVKCDYENVPTTVFT
PLEYGACGLSEEKAVEKFGEENIEVYHSYFWPLEWTIPSRDNNKCYAKIICNTK
DNERVVGFHVLGPNAGEVTQGFAAALKCGLTKKQLDSTIGIHPVCAEVFTTLS
VTKRSGASILQAGCUG**STOPSTOP**

7.12. Sigma SDS 7 molecular weight marker

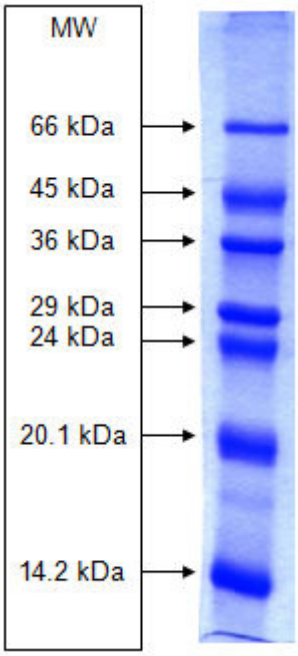

Reference List

Adman,E., K.D.Watenpaugh, and L.H.Jensen., (1975). NH---S hydrogen bonds in *Peptococcus aerogenes* ferredoxin, *Clostridium pasteurianum* rubredoxin, and Chromatium high potential iron protein. *Proc. Natl. Acad. Sci.*, **72**:4854-4858.

Akerman,S.E., and S.Muller., (2005). Peroxiredoxin-linked detoxification of hydroperoxides in *Toxoplasma gondii*. *J. Biol. Chem.*, **280**:564-570.

Alayash,A.I., R.P.Patel, and R.E.Cashon., (2001). Redox reactions of hemoglobin and myoglobin: biological and toxicological implications. *Antioxid. Redox. Signal*., **3**:313-327.

Alfonso-Prieto,M., X.Biarnes, P.Vidossich, and C.Rovira., (2009). The molecular mechanism of the catalase reaction. *J. Am. Chem. Soc.*, **131**:11751-11761.

Allison,W.S., (1976). Formation and reaction of sulfenic acids in proteins. *Acc. Chem. Res.,* **9**:293-299.

Alphey,M.S., C.S.Bond, E.Tetaud, A.H.Fairlamb, and W.N.Hunter., (2000). The structure of reduced tryparedoxin peroxidase reveals a decamer and insight into reactivity of 2Cys-peroxiredoxins. *J. Mol. Biol*., **300**:903-916.

Andersen,J.F., D.A.Sanders, J.R.Gasdaska, A.Weichsel, G.Powis, and W.R.Montfort. 1997. Human thioredoxin homodimers: regulation by pH, role of aspartate 60, and crystal structure of the aspartate 60 --> asparagine mutant. *Biochemistry*, **36**:13979-13988.

Arner,E.S., (2009). Focus on mammalian thioredoxin reductases--important selenoproteins with versatile functions. *Biochim. Biophys. Acta*., **1790**:495-526.

Arner,E.S., H.Sarioglu, F.Lottspeich, A.Holmgren, and A.Bock., (1999). High-level expression in *Escherichia coli* of selenocysteine-containing rat thioredoxin reductase utilizing gene fusions with engineered bacterial-type SECIS elements and co-expression with the *selA*, *selB* and *selC* genes. *J. Mol. Biol*., **292**:1003-1016.

Asherie,N., (2004). Protein crystallization and phase diagrams. *Methods*, **34**:266-272.

Barranco-Medina,S., J.J.Lazaro, and K.J.Dietz., (2009). The oligomeric conformation of peroxiredoxins links redox state to function. *FEBS Lett*., **583**:1809-1816.

Barranco-Medina,S., S.Kakorin, J.J.Lazaro, and K.J.Dietz., (2008). Thermodynamics of the dimer-decamer transition of reduced human and plant 2-cys peroxiredoxin. *Biochemistry*, **47**:7196-7204.

Battin,E.E., and J.L.Brumaghim., (2009). Antioxidant activity of sulfur and selenium: a review of reactive oxygen species scavenging, glutathione peroxidase, and metal-binding antioxidant mechanisms. *Cell Biochem. Biophys*., **55**:1-23.

Baynes,J.W., and S.R.Thorpe., (1999). Role of oxidative stress in diabetic complications: a new perspective on an old paradigm. *Diabetes*, **48**:1-9.

Bernier-Villamor,L., E.Navarro, F.Sevilla, and J.J.Lazaro., (2004). Cloning and characterization of a 2-Cys peroxiredoxin from *Pisum sativum*. *J. Exp. Bot*., **55**:2191-2199.

Bienert,G.P., A.L.Moller, K.A.Kristiansen, A.Schulz, I.M.Moller, J.K.Schjoerring, and T.P.Jahn., (2007). Specific aquaporins facilitate the diffusion of hydrogen peroxide across membranes. *J. Biol. Chem*., **282**:1183-1192.

Biteau,B., J.Labarre, and M.B.Toledano., (2003). ATP-dependent reduction of cysteine-sulphinic acid by *S. cerevisiae* sulphiredoxin. *Nature*, **425**:980-984.

Blouin,M.J., H.Beauchemin, A.Wright, P.M.De, M.Sorette, A.M.Bleau, B.Nakamoto, C.N.Ou, G.Stamatoyannopoulos, and M.Trudel., (2000). Genetic correction of sickle cell disease: insights using transgenic mouse models. *Nat. Med*., **6**:177-182.

Bonda,D.J., X.Wang, G.Perry, A.Nunomura, M.Tabaton, X.Zhu, and M.A.Smith., (2010). Oxidative stress in Alzheimer disease: a possibility for prevention. *Neuropharmacology*, **59**:290-294.

Bragg,W.L., (1913). The structure of crystals as indicated by their x-ray diffraction patterns. *Proc. Roy. Soc*., **A89**:248-277.

Brumshtein,B., H.Greenblat, A.Futerman, I.Silman, and J.Sussman., (2008). Control of the rate of evapouration in protein crystallization by the "microbatch under oil" method. *J. Appl. Cryst*., **41**:969-971

Bulaj,G., T.Kortemme, and D.P.Goldenberg., (1998). Ionization-reactivity relationships for cysteine thiols in polypeptides. *Biochemistry*, **37**:8965-8972.

Butterfield,D.A., T.Koppal, B.Howard, R.Subramaniam, N.Hall, K.Hensley, S.Yatin, K.Allen, M.Aksenov, M.Aksenova, and J.Carney., (1998). Structural and functional changes in proteins induced by free radical-mediated oxidative stress and protective action of the antioxidants N-tert-butyl-alpha-phenylnitrone and vitamin E. *Ann. N. Y. Acad. Sci*., **854**:448-462.

Cao,Z., A.W.Roszak, L.J.Gourlay, J.G.Lindsay, and N.W.Isaacs., (2005). Bovine mitochondrial peroxiredoxin III forms a two-ring catenane. *Structure* **13**:1661-1664.

Cao,Z., D.Bhella, and J.G.Lindsay., (2007). Reconstitution of the mitochondrial PrxIII antioxidant defence pathway: general properties and factors affecting PrxIII activity and oligomeric state. *J. Mol. Biol*. **372**:1022-1033.

Cha,M.K., and I.H.Kim., (1995). Thioredoxin-linked peroxidase from human red blood cell: evidence for the existence of thioredoxin and thioredoxin reductase in human red blood cell. *Biochem. Biophys. Res. Commun*., **217**:900-907.

Chae,H.Z., H.J.Kim, S.W.Kang, and S.G.Rhee., (1999b). Characterization of three isoforms of mammalian peroxiredoxin that reduce peroxides in the presence of thioredoxin. *Diabetes Res Clin. Pract*., **45**:101-112.

Chae,H.Z., S.J.Chung, and S.G.Rhee., (1994). Thioredoxin-dependent peroxide reductase from yeast. *J. Biol. Chem*., **269**:27670-27678.

Chae,H.Z., S.W.Kang, and S.G.Rhee., (1999a). Isoforms of mammalian peroxiredoxin that reduce peroxides in presence of thioredoxin. *Methods Enzymol*., **300**:219-226.

Chayen,N.E., P.D.Shaw Stewart, and D.M.Blow., (1992). Microbatch crystallization under oil -- a new technique allowing many small-volume crystallization trials. *Journal of Crystal Growth*, **122**:176-180.

Cheng, J., Randall, A., and Baldi, P., (2006). Prediction of Protein Stability Changes for Single-Site Mutations Using Support Vector Machines. *Proteins*, **62[4]**:1125-1132.

Chiu,J., P.E.March, R.Lee, and D.Tillett., (2004). Site-directed, Ligase-Independent Mutagenesis (SLIM): a single-tube methodology approaching 100% efficiency in 4 h. *Nucleic Acids Res*., **32**:170-174.

Clarke,F.M., C.Orozco, A.V.Perkins, I.Cock, K.F.Tonissen, A.J.Robins, and J.R.Wells., (1991). Identification of molecules involved in the 'early pregnancy factor' phenomenon. *J. Reprod. Fertil*., **93**:525-539.

Comeau,S.R., D.W.Gatchell, S.Vajda, and C.J.Camacho., (2004). ClusPro: an automated docking and discrimination method for the prediction of protein complexes. *Bioinformatics*., **20**:45-50.

Commoner,B., J.Townsend, and G.E.Pake., (1954). Free radicals in biological materials. *Nature*, **174**:689-691.

Crowther,R.A., and D.M.Blow., (1967). A method for positioning a known molecule in an unknown crystal structure. *Acta. Cryst*., **23**:544-548.

Cullen,D.C., R.G.Brown, and C.R.Lowe., (1987). Detection of immuno-complex formation via surface plasmon resonance on gold-coated diffraction gratings. *Biosensors*, **3**:211-225.

Dauter,Z. 1999. Data-collection strategies. *Acta. Cryst*., **D55**:1703-1717.

Deisseroth,A., and A.L.Dounce., (1970). Catalase: Physical and chemical properties, mechanism of catalysis, and physiological role. *Physiol Rev*., **50**:319-375.

Dietz,K.J., (2003). Plant peroxiredoxins. *Annu. Rev. Plant Biol*., **54**:93-107.

Dougherty,H.W., S.J.Sadowski, and E.E.Baker., (1978). A new iron-containing superoxide dismutase from *Escherichia coli*. *J. Biol. Chem*., **253**:5220-5223.

Dubbs,J.M., and S.Mongkolsuk., (2007). Peroxiredoxins in bacterial antioxidant defense. *Subcell. Biochem.*, **44**:143-193.

Edman,J.C., L.Ellis, R.W.Blacher, R.A.Roth, and W.J.Rutter., (1985). Sequence of protein disulphide isomerase and implications of its relationship to thioredoxin. *Nature*, **317**:267-270.

Eklund,H., F.K.Gleason, and A.Holmgren., (1991). Structural and functional relations among thioredoxins of different species. *Proteins*, **11**:13-28.

Ellis,R.J., and A.P.Minton., (2006). Protein aggregation in crowded environments. *Biol. Chem.*, **387**:485-497.

Ellis,R.J., and S.M.van der Vies., (1991). Molecular chaperones. *Annu. Rev. Biochem.*, **60**:321-347.

Emsley,P., and K.Cowtan., (2004). Coot: model-building tools for molecular graphics. *Acta Crystallogr. D. Biol. Crystallogr.*, **60**:2126-2132.

Engelhardt,R., and H.Arnold., (1975). Membrane characteristics, membrane transport and erythrocyte function. *Verh. Dtsch. Ges. Inn. Med.*, **81**:754-763.

Epp,O., R.Ladenstein, and A.Wendel., (1983). The refined structure of the selenoenzyme glutathione peroxidase at 0.2-nm resolution. *Eur. J. Biochem.*, **133**:51-69.

Evans,P., (2006). Scaling and assessment of data quality. *Acta Crystallogr. D. Biol. Crystallogr.*, **62**:72-82.

Evans,P., and A.McCoy., (2008). An introduction to molecular replacement. *Acta Crystallogr. D. Biol. Crystallogr.*, **64**:1-10.

Flohe,L., H.Budde, K.Bruns, H.Castro, J.Clos, B.Hofmann, S.Kansal-Kalavar, D.Krumme, U.Menge, K.Plank-Schumacher, H.Sztajer, J.Wissing, C.Wylegalla, and H.J.Hecht., (2002). Tryparedoxin peroxidase of Leishmania donovani: molecular cloning, heterologous expression, specificity, and catalytic mechanism. *Arch. Biochem. Biophys.*, **397**:324-335.

Freidman,M., (1973). The chemistry and biochemistry of the sulfhydryl group in amino acids, peptides and proteins. Oxford: Pergamon Press.

Fritz-Wolf,K., S.Urig, and K.Becker., (2007). The structure of human thioredoxin reductase 1 provides insights into C-terminal rearrangements during catalysis. *J. Mol. Biol*., **370**:116-127.

Gasdaska,J.R., M.Berggren, and G.Powis., (1995). Cell growth stimulation by the redox protein thioredoxin occurs by a novel helper mechanism. *Cell Growth Differ*., **6**:1643-1650.

Gatenby,A.A., (1992). Protein folding and chaperonins. *Plant Mol. Biol*., **19**:677-687.

Gerschman,R., D.L.Gilbert, S.W.Nye, P.Dwyer, and W.O.Fenn., (1954). Oxygen poisoning and x-irradiation - A mechanism in common. *Science*, **119**:623-626.

Gilgun-Sherki,Y., E.Melamed, and D.Offen., (2004). The role of oxidative stress in the pathogenesis of multiple sclerosis: the need for effective antioxidant therapy. *J. Neurol*., **251**:261-268.

Gladyshev,V.N., K.T.Jeang, and T.C.Stadtman., (1996). Selenocysteine, identified as the penultimate C-terminal residue in human T-cell thioredoxin reductase, corresponds to TGA in the human placental gene. *Proc. Natl. Acad. Sci*., **93**:6146-6151.

Gorlatov,S.N., and T.C.Stadtman., (1998). Human thioredoxin reductase from HeLa cells: selective alkylation of selenocysteine in the protein inhibits enzyme activity and reduction with NADPH influences affinity to heparin. *Proc. Natl. Acad. Sci*., **95**:8520-8525.

Hall,A., P.A.Karplus, and L.B.Poole., (2009). Typical 2-Cys peroxiredoxins--structures, mechanisms and functions. *FEBS J*., **276**:2469-2477.

Halliwell,B., (1999). Antioxidant defence mechanisms: from the beginning to the end (of the beginning). *Free Radic. Res*., **31**:261-272.

Halliwell,B., and J.M.C.Gutteridge., (1999). Free radicals in biology and medicine. Oxford University Press, Oxford United Kingdom.

Halliwell,B., and C.E.Cross., (1994). Oxygen-derived species: their relation to human disease and environmental stress. *Environ. Health Perspect*., **102** Suppl 10:5-12.

Hamann,M., T.Zhang, S.Hendrich, and J.A.Thomas., (2002). Quantitation of protein sulfinic and sulfonic acid, irreversibly oxidized protein cysteine sites in cellular proteins. *Methods Enzymol*., **348**:146-156.

Harris,J.R., (1969). Some negative contrast staining features of a protein from erythrocyte ghosts. *J. Mol. Biol*., **46**:329-335.

Harris,J.R., and I.Naeem., (1981). Further studies on the characterization of cylindrin and torin, two extrinsic proteins of the erythrocyte membrane. *Biochimica et Biophysica Acta (BBA) - Protein Structure*, **670**:285-290.

Harris,J.R., E.Schroder, M.N.Isupov, D.Scheffler, P.Kristensen, J.A.Littlechild, A.A.Vagin, and U.Meissner., (2001). Comparison of the decameric structure of peroxiredoxin-II by transmission electron microscopy and X-ray crystallography. *Biochim. Biophys. Acta*., **1547**:221-234.

Hartl,F.U., and J.Martin., (1995). Molecular chaperones in cellular protein folding. *Curr. Opin. Struct. Biol*., **5**:92-102.

Hirotsu,S., Y.Abe, K.Okada, N.Nagahara, H.Hori, T.Nishino, and T.Hakoshima., (1999). Crystal structure of a multifunctional 2-Cys peroxiredoxin heme-binding protein 23 kDa/proliferation-associated gene product. *Proc. Natl. Acad. Sci*., **96**:12333-12338.

Ho,Y.S., Y.Xiong, W.Ma, A.Spector, and D.S.Ho., (2004). Mice lacking catalase develop normally but show differential sensitivity to oxidant tissue injury. *J. Biol. Chem*., **279**:32804-32812.

Hofmann,B., H.J.Hecht, and L.Flohe., (2002). Peroxiredoxins. *Biol. Chem*., **383**:347-364.

Holmgren,A., (1977). Bovine thioredoxin system. Purification of thioredoxin reductase from calf liver and thymus and studies of its function in disulfide reduction. *J. Biol. Chem*., **252**:4600-4606.

Holmgren,A., (1985). Thioredoxin. *Annu. Rev. Biochem*., **54**:237-271.

Holmgren,A., (1989). Thioredoxin and glutaredoxin systems. *J. Biol. Chem*., **264**:13963-13966.

Holmgren,A., (1995). Thioredoxin structure and mechanism: conformational changes on oxidation of the active-site sulfhydryls to a disulfide. *Structure*, **3**:239-243.

Homola,J., S.S.Yee, and G.Gauglitz., (1999). Surface plasmon resonance sensors: review. *Sensors and Actuators B: Chemical*, **54**:3-15.

Irvine,G.B., (2001). Determination of molecular size by size-exclusion chromatography (gel filtration). *Curr. Protoc. Cell Biol*., Chapter 5:Unit.

Jacob,C., A.L.Holme, and F.H.Fry., (2004). The sulfinic acid switch in proteins. *Org. Biomol. Chem*., **2**:1953-1956.

Jeong,W., S.J.Park, T.S.Chang, D.Y.Lee, and S.G.Rhee., (2006). Molecular mechanism of the reduction of cysteine sulfinic acid of peroxiredoxin to cysteine by mammalian sulfiredoxin. *J. Biol. Chem*., **281**:14400-14407.

Jocelyn,P.C., (1972). Biochemistry of the SH group. Academic Press, London.

Johnson,R.M., G.Goyette, Jr., Y.Ravindranath, and Y.S.Ho., (2000). Red cells from glutathione peroxidase-1-deficient mice have nearly normal defenses against exogenous peroxides. *Blood*, **96**:1985-1988.

Jonsson,T.J., and W.T.Lowther., (2007). The peroxiredoxin repair proteins. *Subcell. Biochem*., **44**:115-141.

Jonsson,T.J., L.C.Johnson, and W.T.Lowther., (2008a). Structure of the sulphiredoxin-peroxiredoxin complex reveals an essential repair embrace. *Nature*, **451**:98-101.

Jonsson,T.J., L.C.Johnson, and W.T.Lowther., (2009a). Protein engineering of the quaternary sulfiredoxin.peroxiredoxin enzyme.substrate complex reveals the molecular basis for cysteine sulfinic acid phosphorylation. *J. Biol. Chem*., **284**:33305-33310.

Jonsson,T.J., M.S.Murray, L.C.Johnson, and W.T.Lowther., (2008b). Reduction of cysteine sulfinic acid in peroxiredoxin by sulfiredoxin proceeds directly through a sulfinic phosphoryl ester intermediate. *J. Biol. Chem*., **283**:23846-23851.

Jonsson,T.J., M.S.Murray, L.C.Johnson, L.B.Poole, and W.T.Lowther., (2005). Structural basis for the retroreduction of inactivated peroxiredoxins by human sulfiredoxin. *Biochemistry*, **44**:8634-8642.

Jormakka,M., B.Byrne, and S.Iwata., (2003). Formate dehydrogenase--a versatile enzyme in changing environments. *Curr. Opin. Struct. Biol*., **13**:418-423.

Kim,J.A., S.Park, K.Kim, S.G.Rhee, and S.W.Kang., (2005). Activity assay of mammalian 2-cys peroxiredoxins using yeast thioredoxin reductase system. *Anal. Biochem*., **338**:216-223.

Klaunig,J.E., L.M.Kamendulis, and B.A.Hocevar., (2010). Oxidative stress and oxidative damage in carcinogenesis. *Toxicol. Pathol*., **38**:96-109.

Konig,J., K.Lotte, R.Plessow, A.Brockhinke, M.Baier, and K.J.Dietz., (2003). Reaction mechanism of plant 2-Cys peroxiredoxin. Role of the C terminus and the quaternary structure. *J. Biol. Chem*., **278**:24409-24420.

Konig,J., M.Baier, F.Horling, U.Kahmann, G.Harris, P.Schurmann, and K.J.Dietz., (2002). The plant-specific function of 2-Cys peroxiredoxin-mediated detoxification of peroxides in the redox-hierarchy of photosynthetic electron flux. Proc. Natl. Acad. Sci., **99**:5738-5743.

Kooyman,R.P.H., (2008). Handbook of Surface Plasmon Resonance. The Royal Society of Chemistry, The Royal Society of Chemistry

Kosower,N.S., and E.M.Kosower., (1995). Diamide - An Oxidant Probe for Thiols. Academic Press Inc, San Diego.

Kosower,N.S., E.M.Kosower, B.Wertheim, and W.S.Correa., (1969). Diamide, a new reagent for the intracellular oxidation of glutathione to the disulfide. *Biochem. Biophys. Res. Commun*., **37**:593-596.

Kristensen,P., D.E.Rasmussen, and B.I.Kristensen., (1999a). Properties of thiol-specific anti-oxidant protein or calpromotin in solution. Biochem. *Biophys. Res. Commun*., **262**:127-131.

Laemmli,U.K., (1970). Cleavage of structural proteins during the assembly of the head of bacteriophage T4. *Nature*, **227**:680-685.

Laskowski,R.A., M.W.MacArthur, D.S.Moss, and J.M.Thornton., (1993). PROCHECK: a program to check the stereochemical quality of protein structures. *J. Appl. Cryst*., **26**:283-291.

Lee,D.Y., S.J.Park, W.Jeong, H.J.Sung, T.Oho, X.Wu, S.G.Rhee, and J.M.Gruschus., (2006). Mutagenesis and modelling of the peroxiredoxin (Prx) complex with the NMR structure of ATP-bound human sulfiredoxin implicate aspartate 187 of Prx I as the catalytic residue in ATP hydrolysis. *Biochemistry*, **45**:15301-15309.

Lee,W., K.Choi, J.Riddell, C.Ip, D.Ghosh, J.Park, and Y.Park., (2007). Human Peroxiredoxin 1 and 2 Are Not Duplicate Proteins. *J. Biol. Chem*., **282**:22011-22022.

Line,K., Oligomeric state of human erthrocyte peroxiredoxin II. *Blood*., Manuscript in preparation

Link,A.J., K.Robison, and G.M.Church., (1997). Comparing the predicted and observed properties of proteins encoded in the genome of *Escherichia coli* K-12. *Electrophoresis*, **18**:1259-1313.

Liochev,S.I., and I.Fridovich., (2010). Mechanism of the peroxidase activity of Cu, Zn superoxide dismutase. *Free Radic. Biol. Med*., **48**:1565-1569.

Little,C., and P.J.O'Brien., (1969). Mechanism of peroxide-inactivation of the sulphydryl enzyme glyceraldehyde-3-phosphate dehydrogenase. *Eur. J. Biochem*., **10**:533-538.

Liu,Z., M.Reches, I.Groisman, and H.Engelberg-Kulka., (1998). The nature of the minimal 'selenocysteine insertion sequence' (SECIS) in *Escherichia coli*. *Nucleic Acids Res*., **26**:896-902.

Logan,C., and S.G.Mayhew., (2000). Cloning, overexpression, and characterization of peroxiredoxin and NADH peroxiredoxin reductase from *Thermus aquaticus*. *J. Biol. Chem*., **275**:30019-30028.

Low,F.M., M.B.Hampton, A.V.Peskin, and C.C.Winterbourn., (2007). Peroxiredoxin 2 functions as a noncatalytic scavenger of low-level hydrogen peroxide in the erythrocyte. *Blood*, **109**:2611-2617.

Low,F.M., M.B.Hampton, and C.C.Winterbourn., (2008). Peroxiredoxin 2 and peroxide metabolism in the erythrocyte. *Antioxid. Redox. Signal*., **10**:1621-1630.

Maeda,K., P.Hagglund, C.Finnie, B.Svensson, and A.Henriksen., (2006). Structural basis for target protein recognition by the protein disulfide reductase thioredoxin. *Structure*, **14**:1701-1710.

Mapp,P.I., M.C.Grootveld, and D.R.Blake., (1995). Hypoxia, oxidative stress and rheumatoid arthritis. *Br. Med. Bull*., **51**:419-436.

Marnett,L.J., (2000). Oxyradicals and DNA damage. *Carcinogenesis*, **21**:361-370.

Martin,J.L., (1995). Thioredoxin--a fold for all reasons. *Structure*, **3**:245-250.

Mates,J.M., C.Perez-Gomez, and d.C.Nunez, I., (1999). Antioxidant enzymes and human diseases. *Clin. Biochem*., **32**:595-603.

Matsumura,T., K.Okamoto, S.Iwahara, H.Hori, Y.Takahashi, T.Nishino, and Y.Abe., (2008). Dimer-oligomer interconversion of wild-type and mutant rat 2-Cys peroxiredoxin: disulfide formation at dimer-dimer interfaces is not essential for decamerization. *J. Biol. Chem*., **283**:284-293.

Matthews,J.R., N.Wakasugi, J.L.Virelizier, J.Yodoi, and R.T.Hay., (1992). Thioredoxin regulates the DNA binding activity of NF-kappa B by reduction of a disulphide bond involving cysteine 62. *Nucleic Acids Res*., **20**:3821-3830.

McArdle,A., and M.J.Jackson., (2000). Exercise, oxidative stress and ageing. *J. Anat*., **197** Pt 4:539-541.

McCord,J.M., and I.Fridovich., (1969). Superoxide dismutase. An enzymic function for erythrocuprein (hemocuprein). *J. Biol. Chem*., **244**:6049-6055.

McCormack,E.A., G.M.Altschuler, C.Dekker, H.Filmore, and K.R.Willison., (2009). Yeast phosducin-like protein 2 acts as a stimulatory co-factor for the folding of actin by the chaperonin CCT via a ternary complex. *J. Mol. Biol*., **391**:192-206.

Meissner,U., E.Schroder, D.Scheffler, A.G.Martin, and J.R.Harris., (2007). Formation, TEM study and 3D reconstruction of the human erythrocyte peroxiredoxin-2 dodecahedral higher-order assembly. *Micron*, **38**:29-39.

Meyer,Y., B.B.Buchanan, F.Vignols, and J.P.Reichheld., (2009). Thioredoxins and glutaredoxins: unifying elements in redox biology. *Annu. Rev. Genet*., **43**:335-367.

Miranda-Vizuete,A., A.E.Damdimopoulos, and G.Spyrou., (2000). The mitochondrial thioredoxin system. *Antioxid. Redox. Signal*., **2**:801-810.

Montemartini,M., H.M.Kalisz, H.J.Hecht, P.Steinert, and L.Flohe., (1999). Activation of active-site cysteine residues in the peroxiredoxin-type tryparedoxin peroxidase of Crithidia fasciculata. *Eur. J. Biochem*., **264**:516-524.

Moon,J.C., Y.S.Hah, W.Y.Kim, B.G.Jung, H.H.Jang, J.R.Lee, S.Y.Kim, Y.M.Lee, M.G.Jeon, C.W.Kim, M.J.Cho, and S.Y.Lee., (2005). Oxidative stress-dependent structural and functional switching of a human 2-Cys peroxiredoxin isotype II that enhances HeLa cell resistance to H_2O_2-induced cell death. *J. Biol. Chem*., **280**:28775-28784.

Moore,R.B., and S.K.Shriver., (1994). The cDNA sequence for calpromotin indicates that it plays a significant role in the proliferation and differentiation of hematopoietic-cells. *Blood*, **84**:573.

Moore,R.B., M.V.Mankad, S.K.Shriver, V.N.Mankad, and G.A.Plishker., (1991). Reconstitution of $Ca(^{2+})$-dependent K^+ transport in erythrocyte membrane vesicles requires a cytoplasmic protein. *J. Biol. Chem*., **266**:18964-18968.

Morgan,B.A., and E.A.Veal., (2007). Functions of typical 2-Cys peroxiredoxins in yeast. *Subcell. Biochem*., **44**:253-265.

Mossner,E., H.Iwai, and R.Glockshuber., (2000). Influence of the pKa value of the buried, active-site cysteine on the redox properties of thioredoxin-like oxidoreductases. *FEBS Letters*, **477**:21-26.

Murshudov,G.N., A.A.Vagin, and E.J.Dodson., (1997). Refinement of macromolecular structures by the maximum-likelihood method. *Acta Crystallogr. D. Biol. Crystallogr.* **53**:240-255.

Mustacich,D., and G.Powis., (2000). Thioredoxin reductase. *Biochem. J*., **346** Pt 1:1-8.

Niki,E., (2009). Lipid peroxidation: physiological levels and dual biological effects. *Free Radic. Biol. Med*., **47**:469-484.

Oblong,J.E., P.Y.Gasdaska, K.Sherrill, and G.Powis., (1993). Purification of human thioredoxin reductase: properties and characterization by absorption and circular dichroism spectroscopy. *Biochemistry*, **32**:7271-7277.

Peshenko,I.V., and H.Shichi., (2001). Oxidation of active center cysteine of bovine 1-Cys peroxiredoxin to the cysteine sulfenic acid form by peroxide and peroxynitrite. *Free Radic. Biol. Med*., **31**:292-303.

Peskin,A.V., F.M.Low, L.N.Paton, G.J.Maghzal, M.B.Hampton, and C.C.Winterbourn., (2007). The high reactivity of Peroxiredoxin 2 with H_2O_2 is not reflected in its reaction with other oxidants and thiol reagents. *J. Biol. Chem*. **282**:11885-11892.

Poole,L.B., P.A.Karplus, and A.Claiborne., (2004). Protein sulfenic acids in redox signaling. *Annu. Rev. Pharmacol. Toxicol*., **44**:325-347.

Qin,J., G.M.Clore, and A.M.Gronenborn., (1994). The high-resolution three-dimensional solution structures of the oxidized and reduced states of human thioredoxin. *Structure*, **2**:503-522.

Qin,J., G.M.Clore, W.M.Kennedy, J.R.Huth, and A.M.Gronenborn., (1995). Solution structure of human thioredoxin in a mixed disulfide intermediate complex with its target peptide from the transcription factor NFKB. *Structure*, **3**:289-297.

Qin,J., G.M.Clore, W.M.Kennedy, J.R.Huth, and A.M.Gronenborn., (1996). The solution of human thioredoxin complexed with its target from Ref-1 reveals peptide chain reversal. *Structure*, **4**:613-620.

Raha,S., and B.H.Robinson., (2000). Mitochondria, oxygen free radicals, disease and ageing. *Trends Biochem. Sci*., **25**:502-508.

Ren,X., M.Bjornstedt, B.Shen, M.L.Ericson, and A.Holmgren., (1993). Mutagenesis of structural half-cystine residues in human thioredoxin and effects on the regulation of activity by selenodiglutathione. *Biochemistry*, **32**:9701-9708.

Rhee,S.G., (2006). Cell signaling. H_2O_2, a necessary evil for cell signaling. *Science*, **312**:1882-1883.

Roussel,X., G.Bechade, A.Kriznik, D.A.Van, S.Sanglier-Cianferani, G.Branlant, and S.Rahuel-Clermont., (2008). Evidence for the formation of a covalent thiosulfinate intermediate with peroxiredoxin in the catalytic mechanism of sulfiredoxin. *J. Biol. Chem*., **283**:22371-22382.

Salmeen,A., J.N.Andersen, M.P.Myers, T.C.Meng, J.A.Hinks, N.K.Tonks, and D.Barford. (2003). Redox regulation of protein tyrosine phosphatase 1B involves a sulphenyl-amide intermediate. *Nature*, **423**:769-773.

Sayed,A.A., and D.L.Williams., (2004). Biochemical characterization of 2-Cys peroxiredoxins from Schistosoma mansoni. *J. Biol. Chem*. **279**:26159-26166.

Schroder,E., (1998). Porcine natural-killer-enhancing factor-B: oligomerisation and identification as a calpain substrate in vitro. *Biochim. Biophys. Acta*., **1383**:279-291.

Schroder,E., J.A.Littlechild, A.A.Lebedev, N.Errington, A.A.Vagin, and M.N.Isupov., (2000). Crystal structure of decameric 2-Cys peroxiredoxin from human erythrocytes at 1.7 Å resolution. *Structure*, **8**:605-615.

Seo,M.S., S.W.Kang, K.Kim, I.C.Baines, T.H.Lee, and S.G.Rhee., (2000). Identification of a new type of mammalian peroxiredoxin that forms an intramolecular disulfide as a reaction intermediate. *J. Biol. Chem*., **275**:20346-20354.

Shau,H., L.H.Butterfield, R.Chiu, and A.Kim., (1994). Cloning and sequence analysis of candidate human natural killer-enhancing factor genes. *Immunogenetics*, **40**:129-134.

Stadtman,T.C., (1996). Selenocysteine. *Annu. Rev. Biochem*., **65**:83-100.

Stirling,P.C., M.Srayko, K.S.Takhar, A.Pozniakovsky, A.A.Hyman, and M.R.Leroux., (2007). Functional interaction between phosducin-like protein 2

and cytosolic chaperonin is essential for cytoskeletal protein function and cell cycle progression. *Mol. Biol. Cell*., **18**:2336-2345.

Stone,J.R., (2004). An assessment of proposed mechanisms for sensing hydrogen peroxide in mammalian systems. *Arch. Biochem. Biophys*., **422**:119-124.

Storz,G., L.A.Tartaglia, and B.N.Ames., (1990). Transcriptional regulator of oxidative stress-inducible genes: direct activation by oxidation. *Science*, **248**:189-194.

St-Pierre,J., J.A.Buckingham, S.J.Roebuck, and M.D.Brand., (2002). Topology of superoxide production from different sites in the mitochondrial electron transport chain. *J. Biol. Chem*., **277**:44784-44790.

Sun,Q.A., F.Zappacosta, V.M.Factor, P.J.Wirth, D.L.Hatfield, and V.N.Gladyshev., (2001). Heterogeneity within animal thioredoxin reductases. Evidence for alternative first exon splicing. *J. Biol. Chem*., **276**:3106-3114.

Tormay,P., A.Sawers, and A.Bock., (1996). Role of stoichiometry between mRNA, translation factor SelB and selenocysteyl-tRNA in selenoprotein synthesis. *Mol. Microbiol.,* **21**:1253-1259.

Tosatto,S.C., V.Bosello, F.Fogolari, P.Mauri, A.Roveri, S.Toppo, L.Flohe, F.Ursini, and M.Maiorino., (2008). The catalytic site of glutathione peroxidases. *Antioxid. Redox. Signal*., **10**:1515-1526.

Tronrud,D.E., (2007). Introduction to macromolecular refinement. *Methods Mol. Biol*., **364**:231-254.

Turrens,J.F., (2003). Mitochondrial formation of reactive oxygen species. *J. Physiol*., **552**:335-344.

Vagin,A., and A.Teplyakov., (2010). Molecular replacement with MOLREP. *Acta Crystallogr. D. Biol. Crystallogr*., **66**:22-25.

Valko,M., C.J.Rhodes, J.Moncol, M.Izakovic, and M.Mazur., (2006). Free radicals, metals and antioxidants in oxidative stress-induced cancer. *Chem. Biol. Interact*., **160**:1-40.

van Montfort,R.L., M.Congreve, D.Tisi, R.Carr, and H.Jhoti., (2003). Oxidation state of the active-site cysteine in protein tyrosine phosphatase 1B. *Nature*, **423**:773-777.

Wanders,R.J., S.Ferdinandusse, P.Brites, and S.Kemp., (2010). Peroxisomes, lipid metabolism and lipotoxicity. *Biochim. Biophys. Acta*., **1801**:272-280.

Weichsel,A., J.R.Gasdaska, G.Powis, and W.R.Montfort., (1996). Crystal structures of reduced, oxidized, and mutated human thioredoxins: evidence for a regulatory homodimer. *Structure*, **4**:735-751.

Weiss,M., and R.Hilgenfeld. 1997. On the use of the merging R factors as a quality indicator for X-ray data. *J. Appl. Cryst*., **30**:203-205.

Wilkins,M.R., E.Gasteiger, A.Bairoch, J.C.Sanchez, K.L.Williams, R.D.Appel, and D.F.Hochstrasser., (1999). Protein identification and analysis tools in the ExPASy server. *Methods Mol. Biol*., **112**:571-601.

Williams,C.H., L.D.Arscott, S.Muller, B.W.Lennon, M.L.Ludwig, P.F.Wang, D.M.Veine, K.Becker, and R.H.Schirmer., (2000). Thioredoxin reductase two modes of catalysis have evolved. *Eur. J. Biochem*., **267**:6110-6117.

Winterbourn,C.C., (1995). Toxicity of iron and hydrogen peroxide: the Fenton reaction. *Toxicol. Lett*., **82**:969-974.

Woo,H.A., S.W.Kang, H.K.Kim, K.S.Yang, H.Z.Chae, and S.G.Rhee., (2003). Reversible oxidation of the active site cysteine of peroxiredoxins to cysteine sulfinic acid. Immunoblot detection with antibodies specific for the hyperoxidized cysteine-containing sequence. *J. Biol. Chem*., **278**:47361-47364.

Wood,Z.A., E.Schroder, H.J.Robin, and L.B.Poole., (2003b). Structure, mechanism and regulation of peroxiredoxins. *Trends Biochem. Sci*., **28**:32-40.

Wood,Z.A., L.B.Poole, and P.A.Karplus., (2003a). Peroxiredoxin evolution and the regulation of hydrogen peroxide signaling. *Science*, **300**:650-653.

Wood,Z.A., L.B.Poole, R.R.Hantgan, and P.A.Karplus., (2002). Dimers to doughnuts: redox-sensitive oligomerization of 2-cysteine peroxiredoxins. *Biochemistry*, **41**:5493-5504.

Yoshitake,S., H.Nanri, M.R.Fernando, and S.Minakami., (1994). Possible differences in the regenerative roles played by thioltransferase and thioredoxin for oxidatively damaged proteins. *J. Biochem.*, **116**:42-46.

Zhao,W., G.C.Fan, Z.G.Zhang, A.Bandyopadhyay, X.Zhou, and E.G.Kranias., (2009). Protection of peroxiredoxin II on oxidative stress-induced cardiomyocyte death and apoptosis. *Basic Res. Cardiol.*, **104**:377-389.

Zhong,L., and A.Holmgren., (2000). Essential role of selenium in the catalytic activities of mammalian thioredoxin reductase revealed by characterization of recombinant enzymes with selenocysteine mutations. *J. Biol. Chem.*, **275**:18121-18128.

Zhou,C., Y.Huang, and S.Przedborski., (2008). Oxidative stress in Parkinson's disease: a mechanism of pathogenic and therapeutic significance. *Ann. N. Y. Acad. Sci.*, **1147**:93-104.